

August 2019

A Study in Molecular Recognition: Synthesis of a **B**-sheet Mimic & Quantitation of Metal Ions in Aqueous Solutions Through Solid Supported Semi-selective Chemosensors

Tyler G. Fenske
University of Wisconsin-Milwaukee

Follow this and additional works at: <https://dc.uwm.edu/etd>

 Part of the [Organic Chemistry Commons](#), and the [Polymer Chemistry Commons](#)

Recommended Citation

Fenske, Tyler G., "A Study in Molecular Recognition: Synthesis of a B-sheet Mimic & Quantitation of Metal Ions in Aqueous Solutions Through Solid Supported Semi-selective Chemosensors" (2019). *Theses and Dissertations*. 2182.

<https://dc.uwm.edu/etd/2182>

This Dissertation is brought to you for free and open access by UWM Digital Commons. It has been accepted for inclusion in Theses and Dissertations by an authorized administrator of UWM Digital Commons. For more information, please contact open-access@uwm.edu.

A STUDY IN MOLECULAR RECOGNITION: SYNTHESIS OF A β -SHEET MIMIC &
QUANTITATION OF METAL IONS IN AQUEOUS SOLUTIONS THROUGH SOLID
SUPPORTED SEMI-SELECTIVE CHEMOSENSORS

by

Tyler Fenske

A Dissertation Submitted in
Partial Fulfillment of the
Requirements for the Degree of

Doctor of Philosophy

in Chemistry

at

University of Wisconsin Milwaukee

August 2019

ABSTRACT

A STUDY IN MOLECULAR RECOGNITION: SYNTHESIS OF A β -SHEET MIMIC & QUANTITATION OF METAL IONS IN AQUEOUS SOLUTIONS THROUGH SOLID SUPPORTED SEMI-SELECTIVE CHEMOSENSORS

by

Tyler Fenske

The University of Wisconsin – Milwaukee, 2019
Under the Supervision of Professor Alan W. Schwabacher

From the hydrophobic effect, which is responsible for the organization of amphipathic molecules into cellular membranes, to the highly specific hydrogen binding patterns found in DNA base pairs that keeps our genetic material “zipped up”, non-covalent and reversible interactions are critical to properly functioning biological processes. Molecular recognition is an area of study that seeks to better understand these observed phenomena. In a general sense, association of “Host” and “Guest” molecules are based on ionic forces, hydrophobic interactions, cation- π effects, π - π stacking, conformational restriction, and many others. This dissertation will primarily focus on two projects that have an emphasis on studying molecular recognition.

The first major project details the synthesis of a molecule that mimics the hydrogen bonding array of a β -sheet. β -sheets, secondary protein structures found ubiquitously in nature, are composed of peptide strands that associate through hydrogen bonds between an amide carbonyl on one strand to an amide -NH on an adjacent strand. As peptide strands begin to fold into a β -strand it pre-organizes the hydrogen bond donors and acceptors on the other edge allowing for the β -strand to

propagate into a β -sheet. While this propagation is beneficial in the efficient folding of proteins, it makes it difficult for scientists to study this phenomenon in solution apart from the other complexities that exist in protein structures. Chemists have addressed this issue by creating synthetic mimics that simulate the hydrogen bonding array found in β -sheets along only one edge, greatly simplifying the observable phenomena and allowing them to study these effects in greater detail in solution.

Based on the work of previous chemists I have developed a synthetic β -sheet mimic that can replace 3 amino acids in a peptide, has fluorescent properties, and can be incorporated by solid phase synthetic methods into peptides. Using a quinolone as a fluorescent core, I have synthesized a 3,6-diaminoquinol-4-one that has the same hydrogen bonding array. Preliminary studies appear to show association with itself in organic solvents. Additionally, I have developed synthetic schemes towards a pyrido[2,g]quinolone that would retain the same hydrogen binding array with a higher degree of conformational restriction and presumed fluorescent properties. This synthetic work will allow for future graduate students to study these hydrogen bonding interactions.

The second major project in this dissertation details the work I have done on a hydrogel solid support. This work was done to enable the development of a real-time continuously monitoring sensor for the detection and quantitation of metal ions in aqueous solution.

Specific azo dyes have long been known to show a shift in their absorbance spectrum with the addition of metal ions. When used as soluble molecules they are difficult to reuse due to their strong association to the metal ions. I have developed

various hydrogel polymers with covalently attached azo dyes capable of metal ion diffusion in aqueous solutions. Optimization of these hydrogels has been achieved by variation of composition, crosslink-density, co-solvent selection and glass derivatization allowing for a robust attachment to a rigid backing. These hydrogels are optically transparent, allow for removal of the metals with acidic media, and demonstrate sufficient mechanical strength to allow them to be easily moved between analyte solutions. Two separate type of polymers have been developed to allow for either alkylation or acylation reactions to produce the covalent linkage of dye to hydrogel, each with its own advantages.

With others in my research group and in collaboration with a local Milwaukee company, we have shown the azo-dyes covalently tethered to these hydrogels retain their optical properties and can be used for the identification and quantitation of aqueous metal species when incorporated into a flow cell. They are stable to hundreds of binding and release cycles and months of use, at least.

©Copyright by Tyler Fenske, 2019
All Rights Reserved

TABLE OF CONTENTS

ABSTRACT	ii
LIST OF FIGURES.....	vii
LIST OF ABBREVIATIONS.....	xii
ACKNOWLEDGEMENTS	xiii
Chapter 1: Molecular Recognition	1
Introduction.....	1
Metal Ions Chelators.....	2
Organic Host-Guest Systems	4
Chapter 2: Synthesis of a β-Sheet Mimic	7
Background	7
Synthesis towards a pyrido[2,g]quinolone	11
Alternative Routes Towards the pyrido[2,g]quinolone.....	17
Synthesis of a 3,6-diaminoquinolone as a β -sheet mimic.....	19
Examination of the Binding Properties of the β -Sheet Mimic.....	24
Proposed Future Direction.....	27
Experimental Details: Compounds 2, 3a, 4-8, 11-14, 17, 19-23, 25-27	28
Chapter 3: Development of a Metal Ion Chemosensor	44
Introduction.....	44
Instrument Design and Function.....	45
Preliminary Work on Hydrogel Solid Support.....	51
Optimization of Hydrogels.....	53
Development Towards a more Amino Terminated Monomer	60
Derivatization of Glass.....	63
Modifications to Polymer Mold.....	67
Formation of a Versatile Amino Terminated Hydrogel	70
Perturbation Moieties & Dye Preparation.....	74
Amino Terminated Polymer as a Versatile Assembly	76
Spectral Interpretation of Chemosensing Hydrogels (MABA(TEG)-co-HEMA).....	79
Experimental Details: Compounds 28b, 29b, 30-36, 37a, 37b, 38, 39; Polymer Preparation	83
Chapter 4: Synthesis of β,γ-dehydroarginine for Enzymatic Studies of MppP	96
Introduction.....	96
Biosynthesis of Enduracididine	97
Retrosynthetic Analysis and Work Done by Robert Hoppe.....	99
Synthesis of β,γ -dehydro-L-arginine	101
Experimental Details: Compounds 40-46	108
References	114
APPENDIX: COMPOUND CHARACTERIZATION SPECTRA	128
CURRICULUM VITAE	174

LIST OF FIGURES

<i>Figure 1. Equilibrium equation showing host-guest complex formation (Top) and the equations for the association (k_a) and disassociation (k_d) constants (Bottom).....</i>	<i>1</i>
<i>Figure 2. The structure of EDTA (Left) and general representation of the complex formed from EDTA and a metal cation (Right).....</i>	<i>2</i>
<i>Figure 3. Equilibrium equation for 18-crown-6 forming a complex with a metal cation.</i>	<i>3</i>
<i>Figure 4. A general representation of cyclodextrins (Left) and the most common form α-cyclodextrin (Right).....</i>	<i>4</i>
<i>Figure 5. Structure of one of Dougherty's macrocyclic receptors comprised of aromatic moieties.</i>	<i>6</i>
<i>Figure 6. A peptide organized into a β-sheet shown as a structural (Left) and ribbon (Right) diagram.....</i>	<i>8</i>
<i>Figure 7. Kemp's 2,8-diaminoepindolidione</i>	<i>8</i>
<i>Figure 8. Nowick's Fmoc*-Hao-OH and its dimeric form with dimerization constants in D_2O and $CDCl_3$.....</i>	<i>9</i>
<i>Figure 9. Nowick's scheme for the synthesis of Fmoc*-Hao-OH.....</i>	<i>9</i>
<i>Figure 10. Our synthetic target (Top-Right) based on Nowicks Fmoc*-Hao-OH (Top-Left)</i>	<i>10</i>
<i>Figure 11. Formation of symmetrical bisenamine 2.....</i>	<i>11</i>
<i>Figure 12. Thermocyclization of bisenamine 2.....</i>	<i>12</i>
<i>Figure 13. Synthetic progress towards the pyrido[2,g]quinol-4-one 10.</i>	<i>13</i>
<i>Figure 14. Synthesis of ethyl nitroacetate 11 and ethyl 2-nitro-3-ethoxyacrylate 12.</i>	<i>15</i>

Figure 15. Attempted cyclization conditions to obtain pyrido[2,g]quinolone 9 from nitroenamine 8	16
Figure 16. Nitroenoether 12 fails to yield quinolone 14 using standard cyclization conditions.	16
Figure 17. Formation of a dimethyl diaminoterephthalate from DMSS.....	17
Figure 18. Alternative scheme beginning with all bonds to central ring already formed.	18
Figure 19. Target modification to a 3,6-diaminoquinol-4-one core.	19
Figure 20. Desired target using a 3,6-diaminoquinol-4-one core.....	20
Figure 21. Full scheme to obtain β -sheet mimic 24 and β -sheet mimic precursor 27	20
Figure 22. Fluorescent dimerization of 27	24
Figure 23. Non linearity observed in fluorescence of 27 at 430 nm with narrow-band excitation.	25
Figure 24. ^1H NMR spectra of quinolone 27 at 1 mM (Bottom) and 0.1 mM (Top) in CDCl_3	26
Figure 25. Proposed modification for a more fluorescent β -sheet mimic.....	27
Figure 26. PAR & QAR shown as solutions with excess metal cations.	45
Figure 27. PAR and other synthesized dyes analyzed for their metal selectivity.....	46
Figure 28. Isolation of PAR & QAR zinc complexes.	47
Figure 29. General schematic for proposed instrument.....	50
Figure 30. Polymerization of 2-HEMA with PEGDMA 575 to form hydrogel to be used as a solid support for azo-dye chelators.....	51
Figure 31. General scheme for glass activation and derivatization.	52

<i>Figure 32. Diagram of our polymer mold capable of producing thin hydrogel films on a glass microscope slide.</i>	<i>52</i>
<i>Figure 33. UV/Vis absorbance spectrum of HEMA hydrogel loaded with QAR₂Zn (20b) before removing metal cation.</i>	<i>53</i>
<i>Figure 34. Optimization of hydrogel optical transparency.....</i>	<i>54</i>
<i>Figure 35. Comparison of cross-linker length on hydrogel transparency in water.</i>	<i>55</i>
<i>Figure 36. Structure of hydrogel obtained from one step polymerization method and its UV/Vis absorbance spectra prior to initial removal of metal template, after removal of metal template and exposed to Zn²⁺ analyte solution.....</i>	<i>56</i>
<i>Figure 37. Synthesis of a polymerizable PAR derivative and UV/Vis Absorbance spectrum of a PAR hydrogel obtained from pre-alkylation of sensor dye.</i>	<i>58</i>
<i>Figure 38. First and last spectra obtained from time-dependent flow experiments (Left) and change in absorbance over time (Right).</i>	<i>59</i>
<i>Figure 39. General scheme for post-polymerization derivatization using hydrogel with primary amines.</i>	<i>60</i>
<i>Figure 40. Scheme to obtain Boc-protected amino terminated monomer 34.</i>	<i>61</i>
<i>Figure 41. Procedure for exposing silanols on glass surfaces.</i>	<i>63</i>
<i>Figure 42. Derivatization of glass with TPM.</i>	<i>64</i>
<i>Figure 43. Aminopropylation of glass with APTMS and corresponding water contact angles.</i>	<i>65</i>
<i>Figure 44. Setup to silanize up to 5 slides at a time.</i>	<i>66</i>
<i>Figure 45. Derivatization of glass with octadecyltrichlorosilane.....</i>	<i>67</i>

<i>Figure 46. Polymers made using aluminum foil (Top) and solvent resistant tape (Bottom) as a spacer.</i>	<i>68</i>
<i>Figure 47. Examples of the final amino terminated hydrogel polymers loaded with PAR. The polymer after exposure to Zn²⁺ (Left), buffered at pH 7.2 MOPS (Middle), and in 1 M HCl solution (Right).....</i>	<i>69</i>
<i>Figure 48. Comparison of co-solvent. Numbers indicated the polymer diameter in mm when soaked in each solvent. Free-standing polymers were cured at a 5 mm diameter</i>	<i>71</i>
<i>Figure 49. Scheme detailing the synthesis of compounds that could be used to perturb the internal properties of the amine terminated hydrogels.....</i>	<i>74</i>
<i>Figure 50. Modification of PAR₂Zn 28b to allow for attachment to the amine terminated hydrogels.....</i>	<i>75</i>
<i>Figure 51. Absorbance values at 508 nm for polymers prepared at the given concentration of metal-dye complex, 2.2 eq. HBTU and >100 eq. triethylamine. Soaked for 24 hours at room temperature without agitation.</i>	<i>76</i>
<i>Figure 52. Scheme for post polymerization derivatization.</i>	<i>77</i>
<i>Figure 53. Results from ninhydrin quantitation of free amines after Boc deprotection. .</i>	<i>78</i>
<i>Figure 54. Time dependent response of PAR amine-based hydrogels derivatized with cationic 31a (red), zwitterionic 31b (green) and anionic 31c (blue).</i>	<i>79</i>
<i>Figure 55. Differential absorbance values of anionic PAR amine-based hydrogel at varying concentrations of Zn²⁺ (Top) and the slope of each graph against its specific [Zn²⁺] (Bottom).....</i>	<i>81</i>

Figure 56. Structures of antibiotics containing enduracididine and β -hydroxyenduracididine (highlighted in red).	96
Figure 57. Proposed pathway from L-arginine to L-enduracididine through MppPQR.....	97
Figure 58. Current proposed mechanism of MppP by the Silvaggi Group.....	98
Figure 59. Mechanism by which β,γ -dehydro-L-arginine may be able to for the Q2 intermediate with MppP in the absence of oxygen.	99
Figure 60. Retrosynthetic analysis for the synthesis of β,γ -dehydroarginine.....	99
Figure 61. Key contributions to the project provided by Robert Hoppe.	100
Figure 62. General scheme for olefin cross metathesis.	101
Figure 63. Hoveyda-Grubbs Generation II Catalyst	102
Figure 64. Scheme for protection of the olefins needed for the cross metathesis.	103
Figure 65. Synthetic scheme for β,γ -dehydro-L-arginine.....	105
Figure 66. UV/Vis absorbance of MppP before and after the addition of our synthetic β,γ -dehydro-L-arginine.	107

LIST OF ABBREVIATIONS

AAS - atomic absorbance spectroscopy	MABA-TEG - methacryloylaminobocamino-TEG
AcOH - acetic acid	MBDA-TEG - monobocdiamine-TEG
AIBN - azoisobutyronitrile	MEA - methoxyethylacrylate
APTMS - (3-aminopropyl)trimethoxysilane	MEEMA - methoxyethoxyethoxymethacrylate
BAA-TEG - bocaminoazido-TEG	MeOH - methanol
BHT - butylated hydroxytoluene	MOPS - 3-(N-morpholino)propanesulfonic acid
Boc - t-butyloxycarbonyl	MS - mass spectrometry
BSA - N,O-bis(trimethylsilyl)acetamide	MsCl - Mesyl chloride
CMS - chloromethylstyrene	MTBE - methyl t-butyl ether
DA-TEG - diazido-TEG	MW - molecular weight
DEOA - diethyl oxaloacetate sodium salt	NBS - N-Bromosuccinimide
DIC - N,N'-Diisopropylcarbodiimide	NMP - N-Methyl-2-pyrrolidone
DIPEA - diisopropylethylamine	NMR - nuclear magnetic spectroscopy
DMAP - 4-Dimethylaminopyridine	PAR - 4-(2-Pyridylazo)resorcinol
DMF - dimethylformamide	PDI - polydispersity index
DMSO - dimethyl sulfoxide	PEGDA - poly(ethylene glycol) diacrylate
DMSS - dimethyl succinylsuccinate	PEGDMA - poly(ethylene glycol) dimethacrylate
DOSY - diffusion-order NMR spectroscopy	PLS - primary least squared
EDTA - ethylenediaminetetraacetic acid	QAR - 4-(8-quinolylazo)resorcinol
EtOH - ethanol	R _f - retention factor
Fmoc - fluorenylmethyloxycarbonyl	RT - room temperature
HBTU - hexafluorophosphate benzotriazole tetramethyl uronium	tBuOH - t-butanol
HEMA - 2-hydroxyethyl methacrylate	TEG - tetra(ethylene glycol)
HGII - second-generation Hoveyda-Grubbs metathesis catalyst	TFA - trifluoroacetic acid
ICP - inductively coupled plasma	THF - tetrahydrofuran
K _a - association constant	TLC - thin layer chromatography
K _d - disassociation constant	TMS - trimethylsilyl
	TPM - 3-(trimethoxysilyl)propyl
	TsOH - tosic acid

ACKNOWLEDGEMENTS

When I first embarked on the path to obtain a PhD, I knew I was in for a challenge unlike any other I have encountered. Looking back on the last 5 years, the experience has been full of highs and lows and I would not have succeeded if it was not for the people closest to me providing support and encouragement along the way.

Mom & Dad -

For your continued financial, emotional, and moral support;

Sarah Oehm, Robert Hoppe, Trevor Hagemann,
Surajadeen Omolabake, and Alex Vincent-

For helping me work through various presentations and milestones;

Mike "Minion" Sportiello, Oseas Medina, Christina Tersine,
Ian Synott, Tye Sideman and Adrienne DiFoggio-

For helping me advance my research and keeping
me entertained during long days in the lab;

Dr. Tom Neal and Dr. Alan Schwabacher-

For your mentorship, guidance, and encouragement;

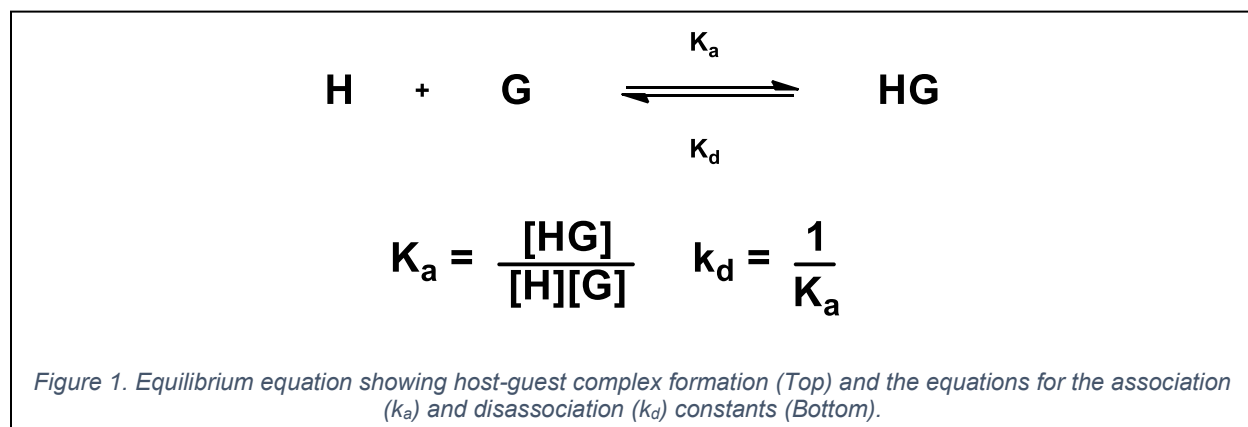
Thank You

Chapter 1: Molecular Recognition

Introduction

Non-covalent and specific molecular interactions are key to the functions of life. While covalent bonds and specific molecular structures give rise to the diversity and complexity of the matter that makes up the world around us, reversible and non-covalent association events allow for the molecular machinery of the world to operate. Over the past half century, chemists have developed a deeper understanding of these specific interactions and have used that knowledge to create new synthetic molecular receptors. This study of molecular recognition has wide ranging academic and practical applications. This chapter will focus on a brief overview of molecular recognition and how it will be applied in this dissertation.

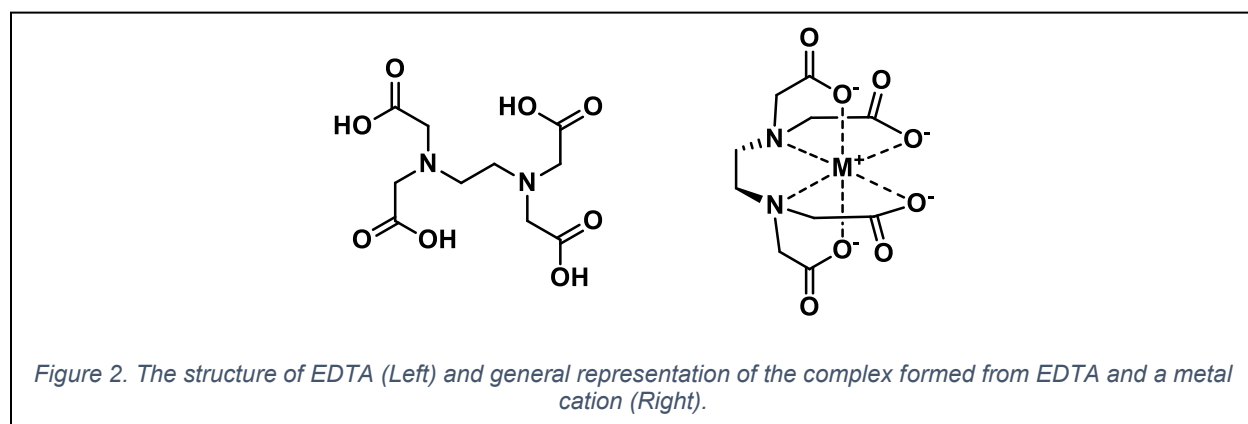
Molecular recognition is the study of association of molecules in solution through favorable non-covalent selective and reversible interactions. Through a lowering of the Gibbs free energy ($-\Delta G$) of a system, “host” and “guest” molecules can form host-guest complexes with the strength of this association defined as the equilibrium constant of the system (K_a). Another common metric used is the inverse of the association constant known as the disassociation constant (K_d) (**Figure 1**). In the Schwabacher lab, we



prefer to use K_d values because it gives the guest concentration where the half of the host is free, and half is complex. Quantitative affinities are difficult to predict. There are many factors (solvent, temperature, geometry, polarity, etc.) that determine the specific enthalpic and entropic contributions to the overall system and the affinity is derived from small differences in these very large numbers. However, they can be understood as trends across a variety of categories that result in higher or lower ΔG .

Metal Ions Chelators

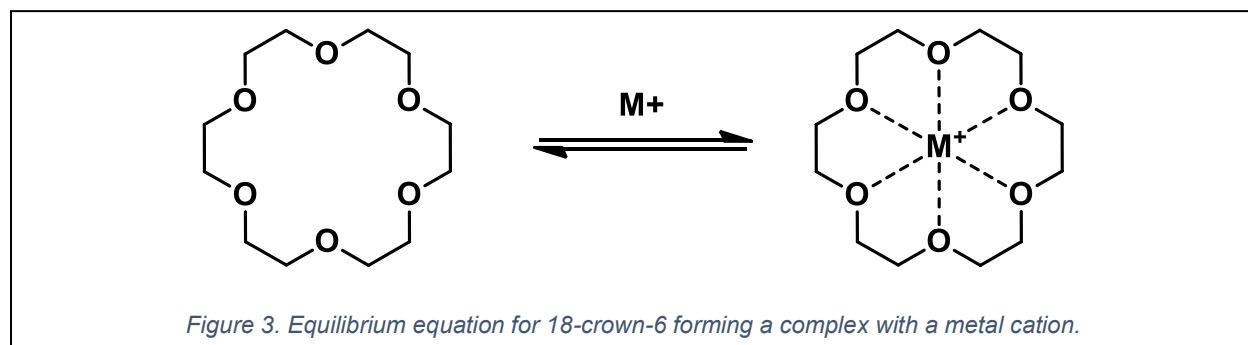
One of the earliest and most well-known synthetic molecular receptors is ethylenediaminetetraacetic acid (EDTA). It was first synthesized in 1935 by Ferdinand Münz and is known to associate with metal cations with a very high affinity.¹ The structure of EDTA and its typical geometry when forming complexes with cation is shown in **Figure 2**. EDTA demonstrates two concepts of molecular recognition that result in greater affinity between host and guest molecules: pre-organization and ionic interactions.



Metal cations can be solvated in aqueous solutions through favorable interactions of the cationic metal atom and the dipole moments of the water molecules that surround it. To be considered soluble, the ΔG of the solvated metal cation and its

counter ion must be lower than the ΔG of its solid crystalline lattice. Carboxylic acids and free amines are well known metal chelators and work to further minimize ΔG of the system by lowering the entropic cost of water organizing into solvation shells and providing electron density in the empty d-orbitals of the metal cation. These non-covalent ionic interactions allow for the formation of a variety of metal complexes in aqueous solutions. In a general sense, the greater the stabilization of a cation by a chelating ligand over the solvation of the cation by the solvent leads to a lower and lower ΔG values. For example, because charged moieties are poorly solubilized by non-polar solvents, polar ligating groups will result in a greater ($-\Delta G$) value compared to the same system with a polar solvent.

Complexes of first and second row transition metals in solution can be found with up to 6 ligating groups and because the complex formation is an equilibrium process, they can be in found in various intermediate states. If the ligating groups are all present on the same compound, the equilibrium can be shifted towards the complex. This lowers the entropic cost of the complex as only two particles need to come together as opposed to seven. Additionally, once one favorable chelating interaction is formed, the molecular receptor is pre-organized in a way that the other chelating groups can quickly

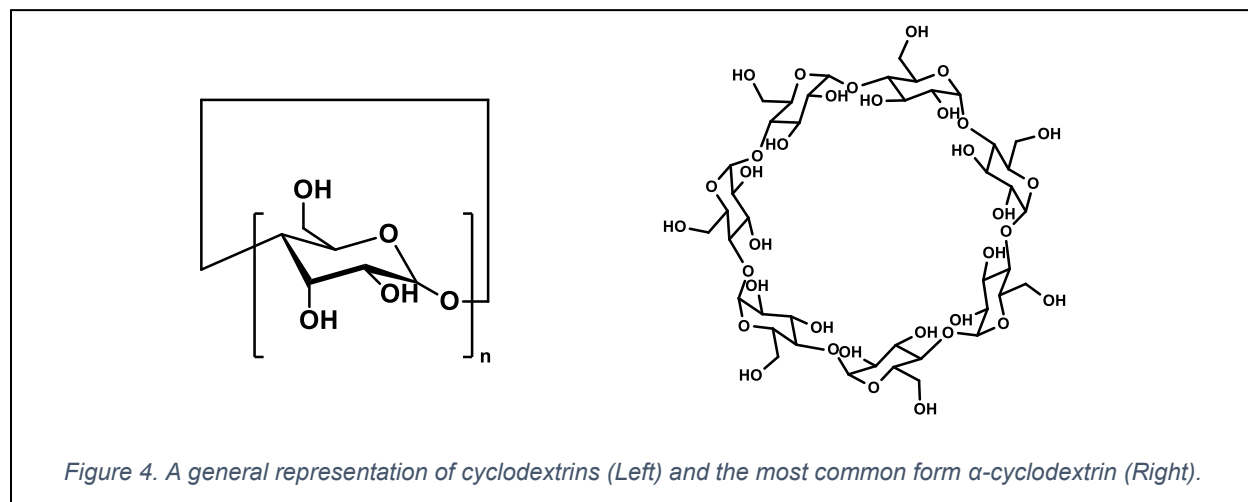


obtain the stable complex formation. This pre-organization leads to a greater degree of association between the receptor and the metal ion.

While studying the how different metal chelators effect the properties of vanadium, Charles Pedersen serendipitously discovered crown ethers in 1960. This discovery led to his Nobel prize in 1987.² Similar to EDTA, crown ethers are preorganized to allow for the lone pairs of oxygen atoms in a cyclic polyether structure to stabilize the positive charge of a metal cation as shown in **Figure 3**. The polar parts of the cyclic polyether are pointed in towards the positive charge and the non-polar alkyl portion is wrapped around the outside of the complex which leads to the astounding property of crown ethers: solubilization of metal cations in non-polar organic solvents.

Organic Host-Guest Systems

Cyclodextrins are among the most common compounds that are used to form inclusions complexes. First observed in the mid-19th century, cyclodextrins are macrocyclic compounds composed of glucose subunits connected via a α -1,4-glycosidic linkage. They are commonly found with 6 (α -cyclodextrin), 7 (β -cyclodextrin), or 8 (γ -



cyclodextrin) glucose subunits.³ β -cyclodextrin is by far the most common form utilized in the literature.

The cyclic structure of cyclodextrins results in a truncated cone-like geometry with a polar exterior and a non-polar pocket in the interior. Cyclodextrins have been studied extensively and are known to form host guest complexes with non-polar molecules. The key property that leads to high affinity inclusion complexes is the hydrophobic effect. Since water is not well solvated by non-polar groups, non-polar molecules have a preference to reside inside the non-polar cavity of the cyclodextrins compared to water molecules. Based on the size of the guest and the specific cyclodextrin used, complex stoichiometry can vary from a simple 1:1 host-guest ratio where the guest lies entirely in the cavity of a single cyclodextrin or a 2:1 ratio where 2 cyclodextrin molecules can form a non-covalent capsule with the guest residing inside.³ Cyclodextrins have been incorporated into various drug delivery systems because of their ability to make non-polar drugs more soluble, shielding biologically unstable drugs from unwanted degradation in the body, and can be paired with “trigger” mechanisms for a higher degree of control for targeted delivery systems.⁴⁻⁷ They have been a key starting point for the design of many other molecular receptors that demonstrate molecular recognition properties using amphipathic molecules.

Inspired by the properties of cyclodextrins and earlier molecular receptors, Dennis Dougherty developed a library of macrocycles capable of binding cations using the π -electrons in aromatic rings. This phenomenon is known as the cation- π effect and plays an important role in the study of molecular recognition.^{8,9} For example the receptor shown in **Figure 5** shows no association for quinoline and isoquinoline. When

these quinolines were methylated with iodomethane they showed appreciable association constants indicating the positive charge is important in the complex formation. These studies by Dougherty and others have greatly contributed to the understanding of catalytic activity in proteins as aromatic side chains of amino acids can add to the stabilization of substrates in the proteins binding pocket.⁸

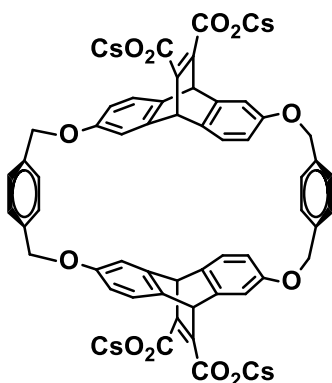


Figure 5. Structure of one of Dougherty's macrocyclic receptors comprised of aromatic moieties.

Overall there are many ways by which chemists can develop molecular receptors and adjust their binding affinity to known guest molecules. Through ionic interactions, varying polarity in structures, cation- π effects, pre-organization, and conformational restriction, a host molecule can be designed to associate with nearly any guest molecule.

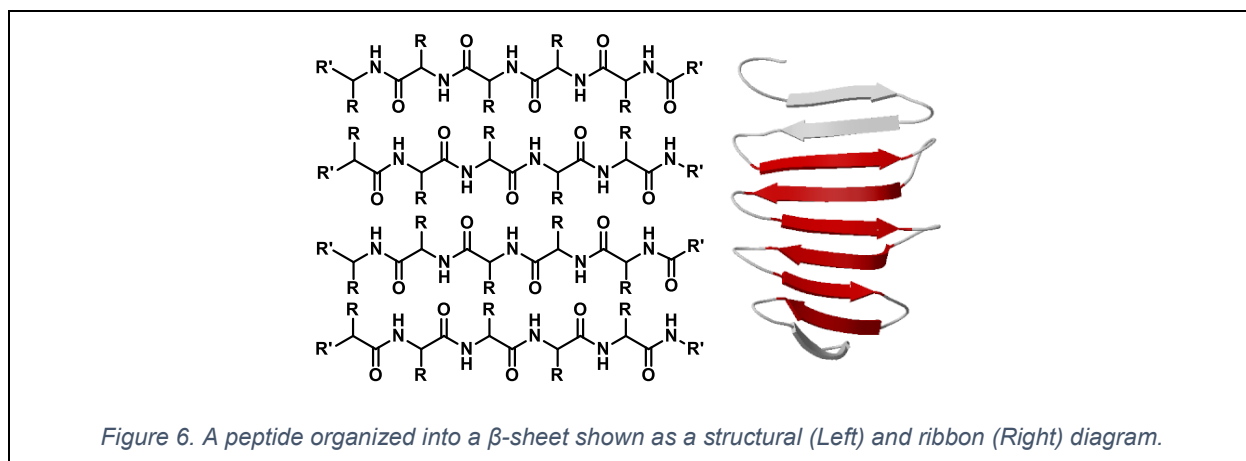
Chapter 2: Synthesis of a β -Sheet Mimic

Background

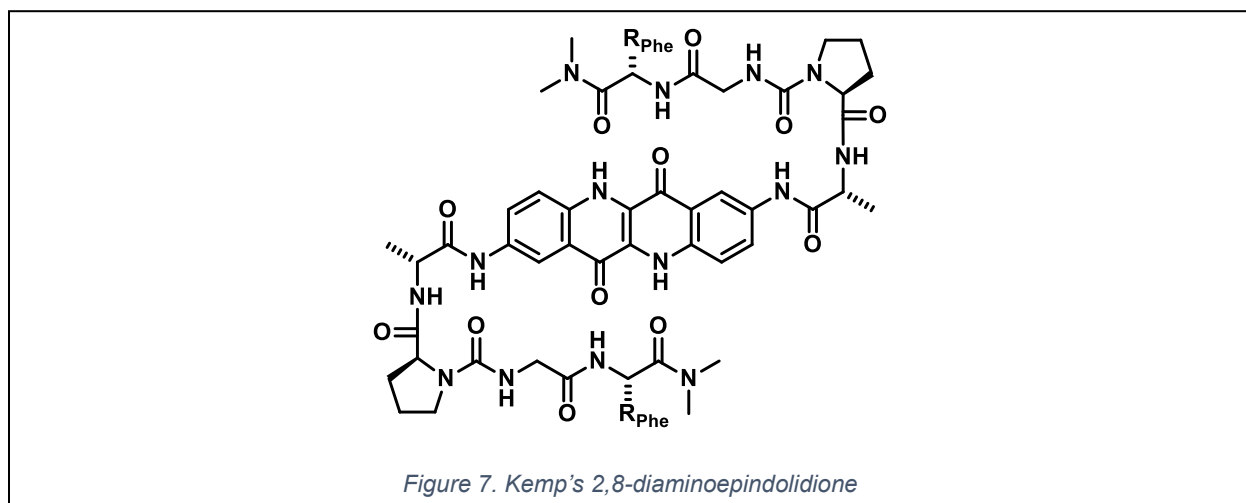
Living organisms rely on complex interactions of intricate molecules that bind to one another, complete a task, and finally disassociate. These processes have been optimized through evolution to allow living beings to accomplish tasks through complex cascading schemes that initially seem impossible. These seemingly impossible tasks are made possible through simple and specific associations between alike molecules.

Molecular association is critical to enzymatic catalysis. Enzymes are long linear polypeptides that are folded into complex conformations. These folding events are driven by intermolecular forces that cause intermolecular associations. Once the enzymes are folded, they are capable of catalyzing transformations of small molecules by transition state stabilization in the enzymes active site. Biological organisms contain many enzymatic systems that accomplish series of systematics transformations. Understanding how these systems work allows scientists to further develop our understanding of chemistry and advance our manipulation of biochemical mechanisms.¹⁰

Specifically, we are interested in the binding interaction that constitutes the formation of β -sheets. Anti-parallel β -sheets are a common secondary structure found in proteins where peptide chains are oriented in alternating directions, held together by hydrogen bonds. The amide groups provide the H-bonding donors (-NH) and acceptors (C=O) to form sheet structures as shown in **Figure 6**.¹⁰

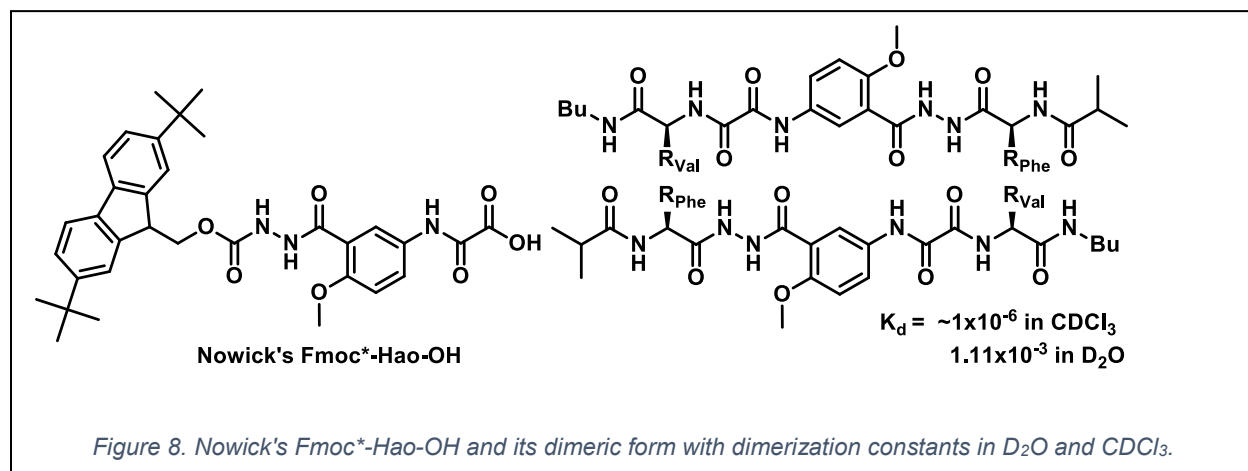


Because β -sheets are such a crucial component involved in numerous aspects of biochemistry it would be useful to have a tool to investigate the interaction of β -sheet like structures in living organisms. Potential medical applications to these interactions are abundant because they are commonly found in proteins.¹¹⁻¹⁴

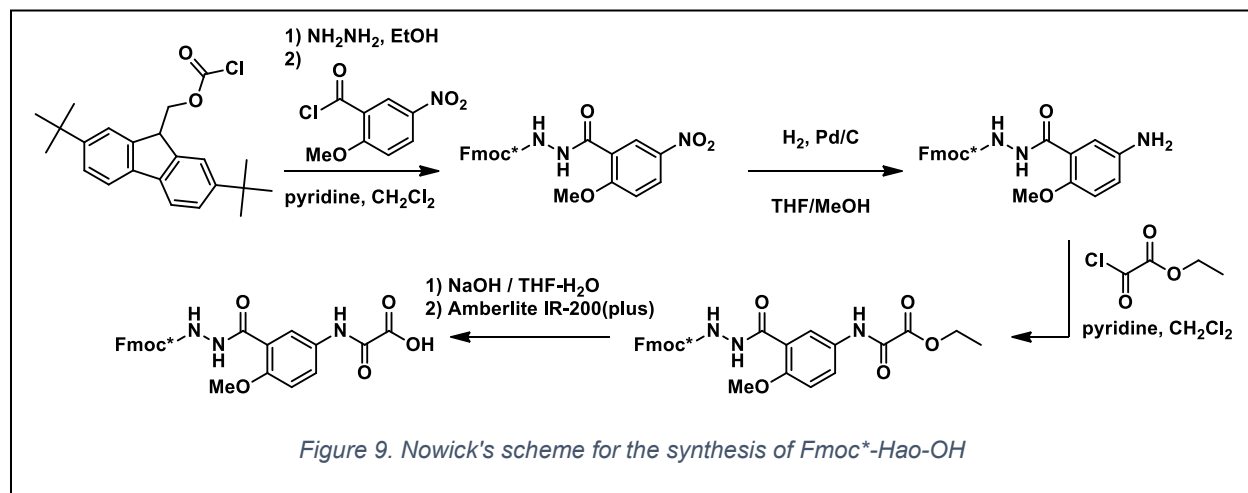


One of the first examples of a synthetic molecule that simulates a β -Sheet binding array came from Kemp.¹⁵ Kemp et al. synthesized the 2,8-diaminoepindolidione derivative shown in **Figure 7**. With the tetrapeptide urea derivative on each side of the epindolidione, Kemp showed that the terminal phenylalanine was in fact in close

proximity to the aromatic core. This was one of the first examples of a synthetic molecule that was capable of intramolecular hydrogen bonding in a similar manner to natural β -sheets.¹⁵

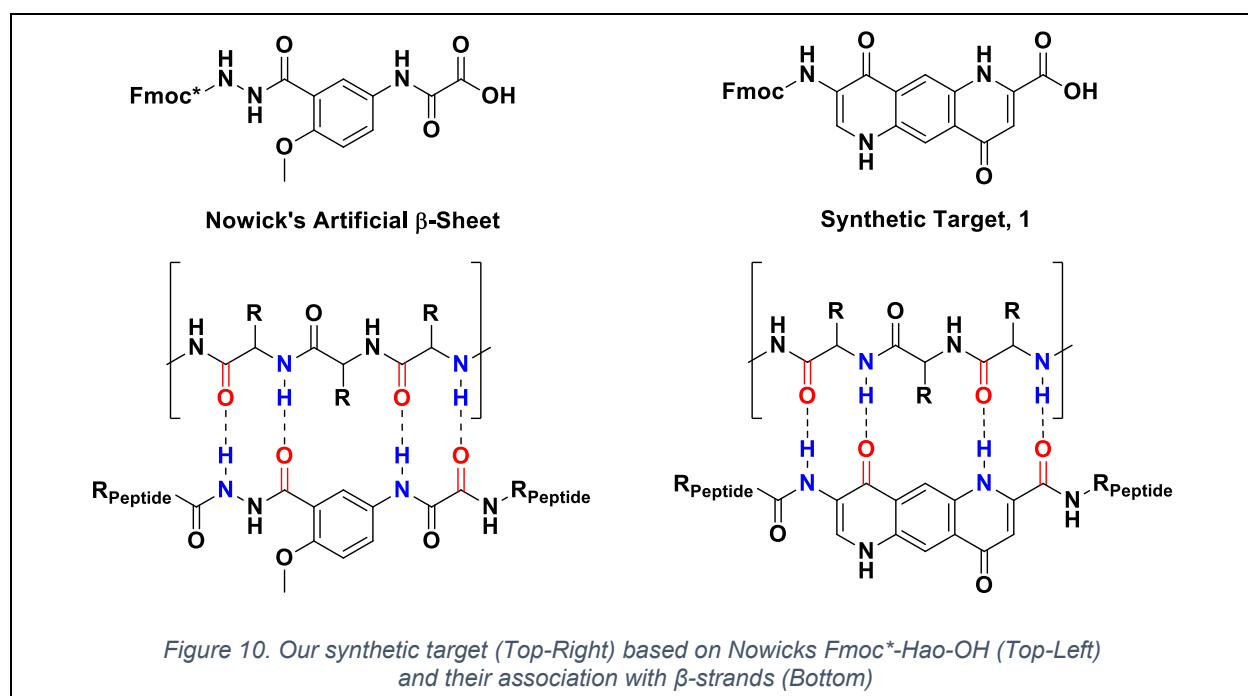


One of the most significant contributions to the area of artificial β -sheet mimicry came from the group of James Nowick. Nowick has published numerous articles on his work.^{12,16–18} His development of an artificial amino acid Fmoc*-Hao-OH allows for future researchers to incorporate an unnatural extended peptide using normal solid-phase methods for peptide synthesis (**Figure 8**).¹⁹ The structure is composed of a Fmoc* hydrazine coupled to a 5-amino-2-methoxybenzoic acid core with the aromatic amine



then coupled to an oxalate group. This gives rise to the acronym Hao (**H**ydrazine-**A**minobenzoic acid-**O**xalate). The synthesis is shown in **Figure 9**.

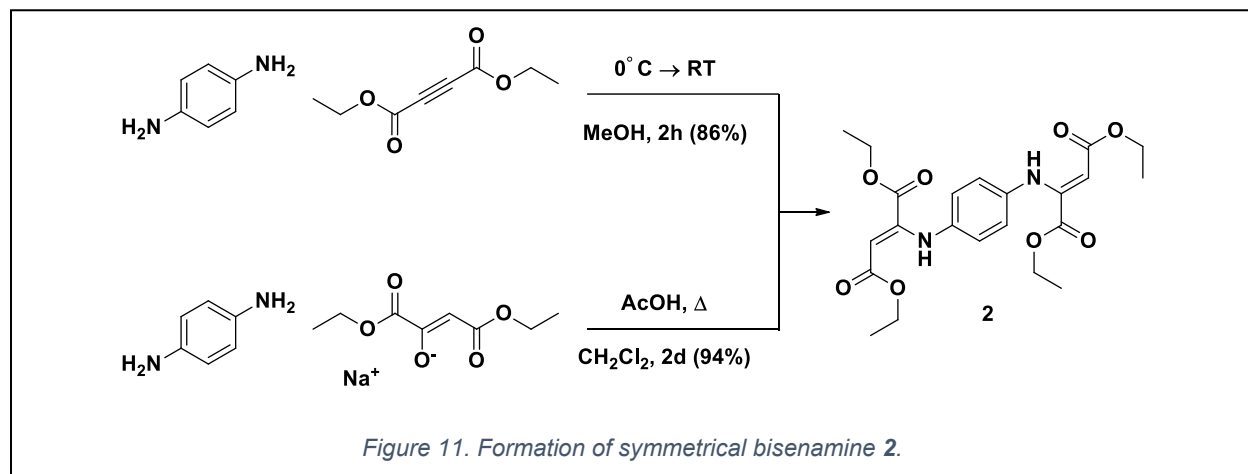
The unnatural extended amino acid Fmoc*-Hao-OH has three key properties that makes it desirable as a tool to study molecular recognition. It has the same length as a tripeptide giving 4 H-bond pairs, its hydrogen-bonding array is found on only one edge of the molecule preventing oligomerization and precipitation from solution, and it can be incorporated into solid-phase methods for peptide synthesis. However, making measurements of its effects requires substantial quantities since it does not have any properties that would make optical spectroscopy useful.



Based on Nowick's design, I set out to synthesize the unnatural extended amino acid **1** capable of mimicking the hydrogen-bonding array found in β -sheets. Like Nowick's Fmoc*-Hao-OH, compound **1** would replace 3 amino acid residues in a peptide chain, contain the binding array on only one edge, and could be incorporated by solid phase methods for peptide synthesis (**Figure 10**). Further improvements would

include the addition of a spectrally informative (between 300 and 800 nm) ring structure and further conformational restriction to improve binding affinity.

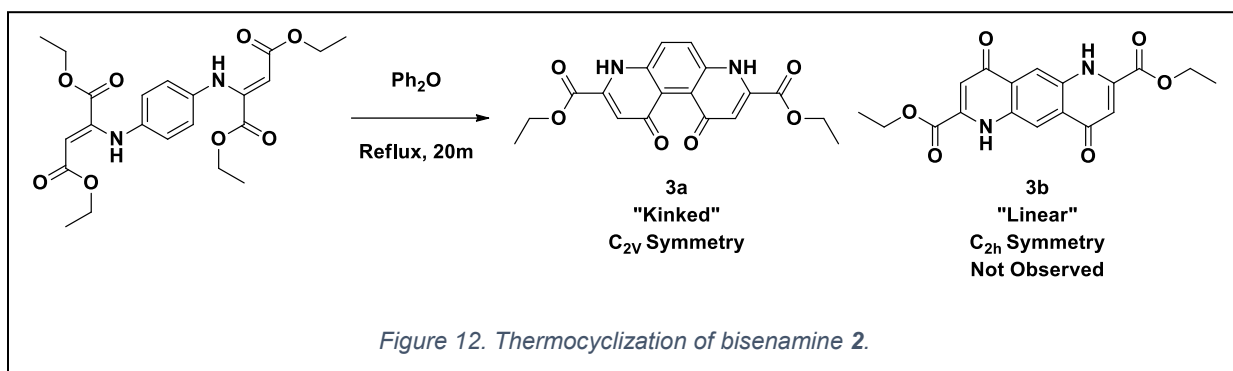
Synthesis towards a pyrido[2,g]quinolone



We first chose a succinct potential route to the core pyrido[2,g]quinol-4-one structure in a symmetrical approach. From the literature available, we believed we could achieve this core structure by applying the standard thermal cyclization conditions used for synthesis of quinolones^{20,21} and applying those conditions to a symmetrical bisenamine. We began with the known reaction to form bisenamine **2**²² from *p*-phenylenediamine and diethyl acetylenedicarboxylate (**Figure 11**). While this reaction provides clean crystalline material, the acetylene reagent is fairly expensive. An alternative procedure allows for the use of diethyl oxaloacetate sodium salt (DEOA), which requires acid, a longer reaction time, and an aqueous organic work-up prior to the final crystallization. It is however significantly less expensive and has provided me with a better average yield.

With bisenamine **2** in hand, we began investigating the cyclization reaction. Quinolone cyclization can be achieved from enamines with esters in the γ -position and

typically proceeds in good yields in refluxing diphenyl ether²³ or heating in highly acidic dehydrating media such as Eaton's reagent (P_4O_{10} in CH_3SO_3H).²⁴ It was believed that this method on a symmetrical bisenamine would give a mixture of products **3a** and **3b** (**Figure 12**). It is known that quinolones can undergo electrophilic substitution at the 5 position,^{25,26} but we have not observed any publications that report attack at the 7 position as we desired. We hoped that the product may form in even trace amounts allowing us to characterize it and make future synthetic routes easier to monitor having the authentic product in hand.

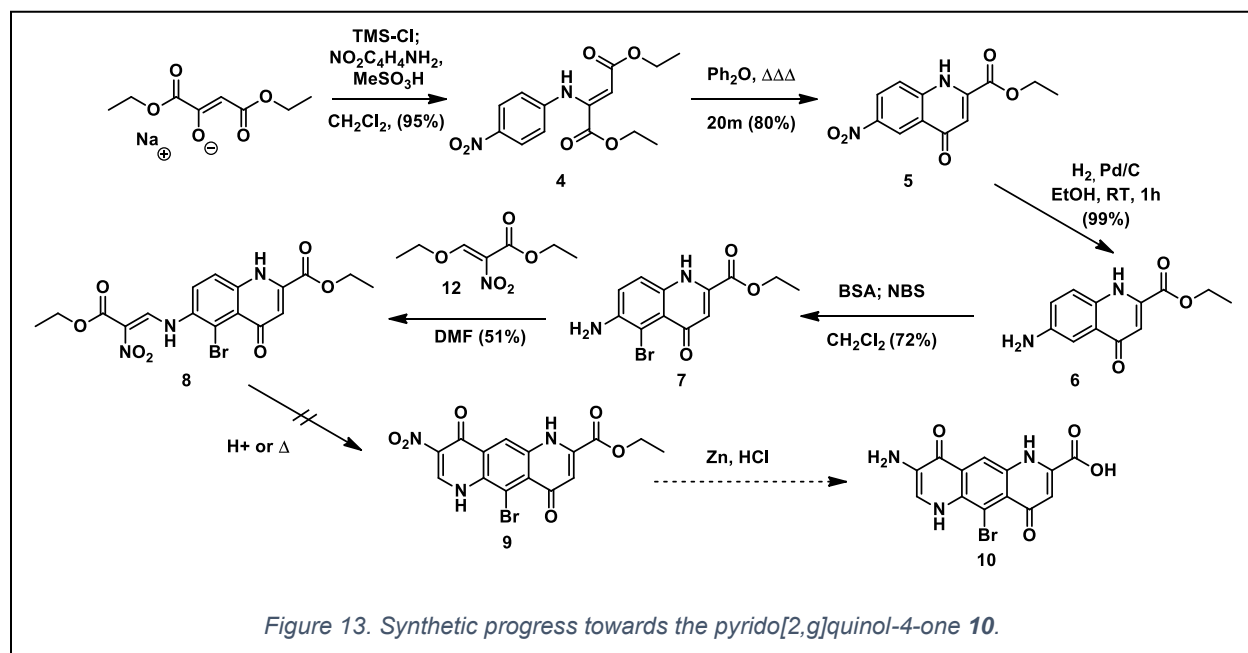


After obtaining the products from both the thermocyclization and acidic cyclization reactions, 1H NMR analysis indicated only single product had formed, however due to the symmetry of both potential products it was not possible to identify the specific regioisomer. It was also reasonable to assume both isomers could have the identical 1H NMR spectra, although unlikely. Additionally, because the mass ions of both isomers were the same, mass spectrometry provided no additional information to identify the product.

Attempts to de-symmetrize the product were then performed to tease out the identity of the isomer, and because the reactions constitute either the continued synthetic route, or an excellent model for such steps. Both nitration and ester hydrolysis

proceeded to give the symmetrical product. Our answer finally came from a more thorough literature review which revealed that this specific cyclization provided only the incorrect phenanthroline derivative **3a** where both new bonds made to the central ring formed ortho to one another.²⁷ Initially overlooked, this was confirmed for our reaction when the aromatic region of the ¹H NMR spectrum was blown up. A small pair of doublets was seen indicating a small amount of our product was de-symmetrized and the aromatic protons were no longer homotopic. These signals in the ¹H NMR spectrum had a coupling constant consistent with what is expected for protons oriented ortho to each other.

After attempts to obtain the desired pyrido[2,g]quinol-4-one core via a short and succinct route that involved de-symmetrization late in the sequence, focus was shifted to a longer route where two separate cyclization steps would be required. After the first cyclization step would be completed, the more active position on the central ring would be blocked by halogenation, followed by a second cyclization (**Figure 13**).

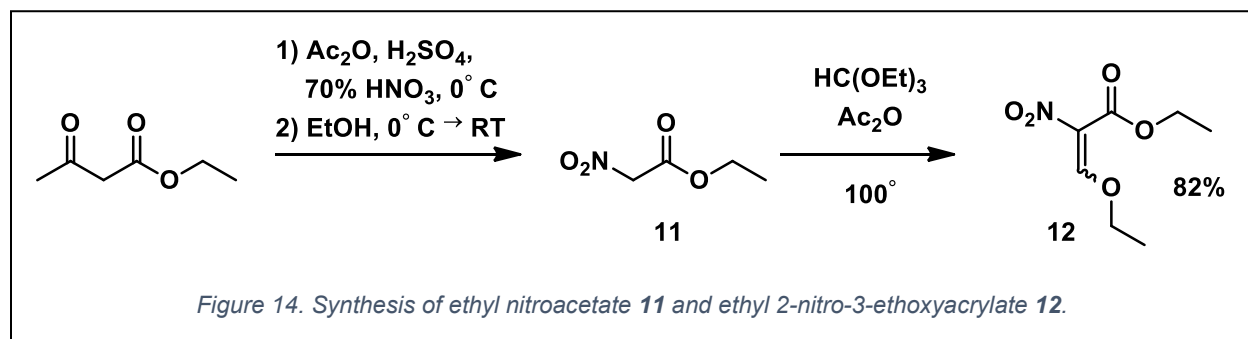


First the 6-nitroquinolone **5** was obtained by enamine formation from *p*-nitroaniline, the sodium salt of diethyl oxaloacetate (DEOA) and an acid. Although this reaction is known to work quite well when using diethyl acetylenedicarboxylate²³, the oxaloacetate form was used due to cost of the more reactive starting material. The reaction has been performed under various conditions. Initially, enamine **4** was formed in refluxing CH₂Cl₂ with one equivalent of TsOH, using a Dean-Stark trap to remove the water formed in the reaction. Although this method initially worked well, the commercially available DEOA came contaminated with ethanol which prevents phase separation of water and toluene in the trap. This could be addressed simply by drying the enolate before performing the reaction. I found that by first forming the TMS ether with TMS-Cl, and then adding *p*-nitroaniline and methanesulfonic acid the product could be obtained in refluxing in CH₂Cl₂ without the Dean-Stark trap. This alteration provided a more robust procedure that could obtain enamine **4** in excellent yields regardless of the quality of the enolate starting material. Subsequent cyclization to 6-nitroquinolone **5** under standard thermal conditions proceeded smoothly providing the product in adequate yields. The aminoquinolone **6** was formed by catalytic hydrogenation over palladium giving near quantitative yields.

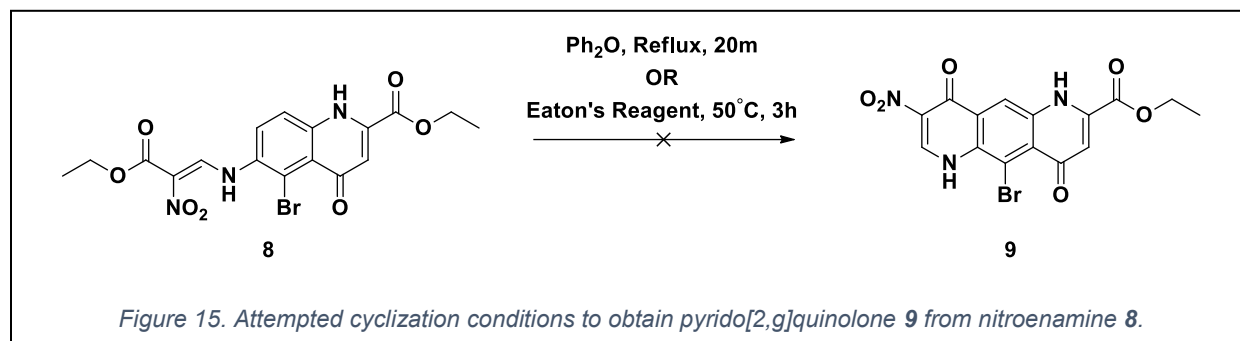
Knowing that simply forming another enamine and cyclizing would result in the incorrect isomer as observed in the first approach we tried, a bromine was introduced by electrophilic bromination using NBS. Initial attempts afforded a mixture of the dibromo, monobromo and unreacted quinolone. We interpreted this to be due to solubility problems with the 6-aminoquinolone. Modification to the procedure to first treat the quinolone with *N,O*-bistrimethylsilylacetamide (BSA) to form the soluble TMS ether

of the hydroxyquinoline tautomer, and then add NBS, allowed the mono-bromo product **7** to be formed exclusively with 1 equivalent of NBS in a matter of minutes. Aqueous workup removed the silyl groups.

We initially attempted a convergent route to install the nitrogen substituent as a nitro group. This required nitroenoether **12**, in analogy to the well preceded ethoxy methylenemalonate derivative, known to lead to carboxy substituted quinolones²⁴. Ethyl nitroacetate **11** was first prepared by nitration of ethyl acetoacetate, followed by solvolysis with ethanol.²⁸ We modified this procedure to use 70% HNO₃, rather than the 90% specified originally, simply by adding more acetic anhydride. Distillation under reduced pressure gave pure ethyl nitroacetate **11**. Trevor Hagemann has shown an aqueous-organic extraction is sufficient to give pure ethyl nitroacetate **11** in 82% yield. Treating ethyl nitroacetate **11** with triethylorthoformate and acetic anhydride, and then removing the volatiles *in vacuo* afforded the pure ethyl 3-ethoxy-2-nitroacrylate **12**.

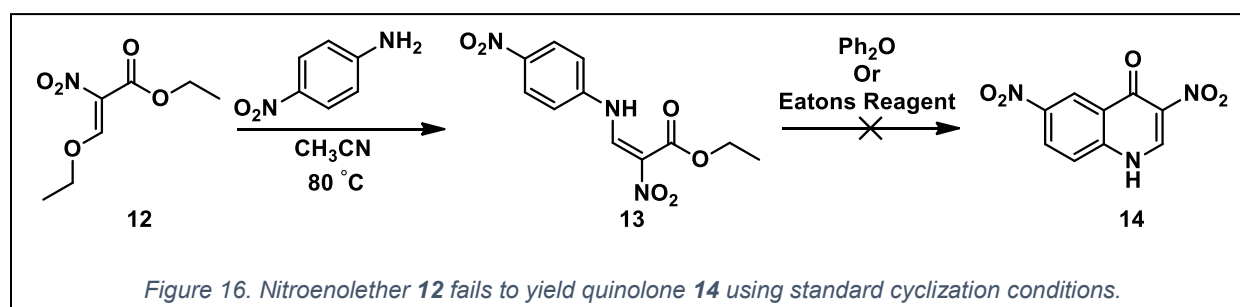


To our surprise, when the aminobromoquinolone **7** was treated with our nitroenoether **12**, the nitroenamine product **8** crystallized out of the reaction solvent in acceptable yields. Various reactions were attempted on nitroenamine **8** to obtain the desired pyrido[2,g]quinol-4-one **9** but preliminary data failed to show formation of the product.



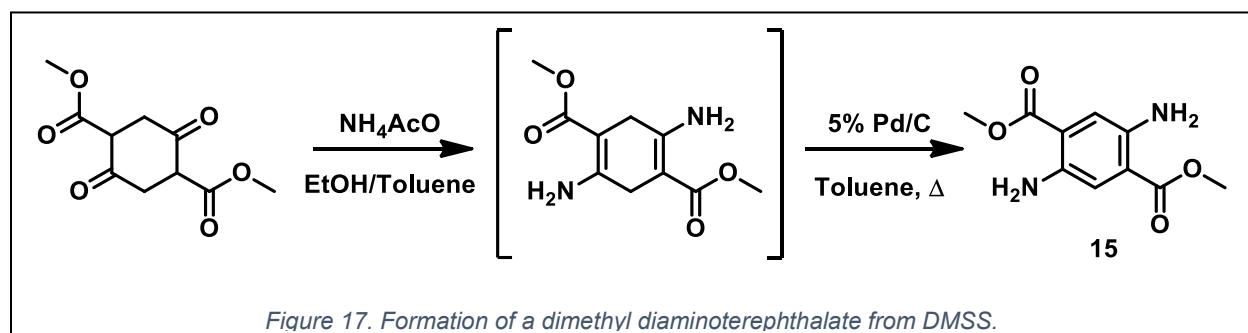
Enamine **8** was submitted to acidic and thermal conditions for cyclization. The crude reaction mixtures were analyzed by mass spectrometry. The crude product obtained from refluxing diphenyl ether did not show mass ions corresponding to the product mass (406.98), but instead ions corresponding to the product with the loss of the nitro group, the product with the loss of the nitro and bromo groups, and starting quinolone **7**. The acidic cyclization showed only quinolone **7** and the starting material **8**.

Concerned by this result, we sought to understand if the inability to form pyrido[2,g]quinol-4-one **9** was due to the non-standard nitroenamine precursor **12**. Nitroenoether **12** was combined with *p*-nitroaniline to form the nitroenamine **13** and submitted to identical cyclization conditions. This reaction failed to produce the known quinolone **14**.²⁹ This was promising to see as it indicates that nitroenoether **12** is not an appropriate precursor for the formation of quinolones, so standard methods may ultimately allow conversion of **7** to target **10**.



Alternative Routes Towards the pyrido[2,g]quinolone

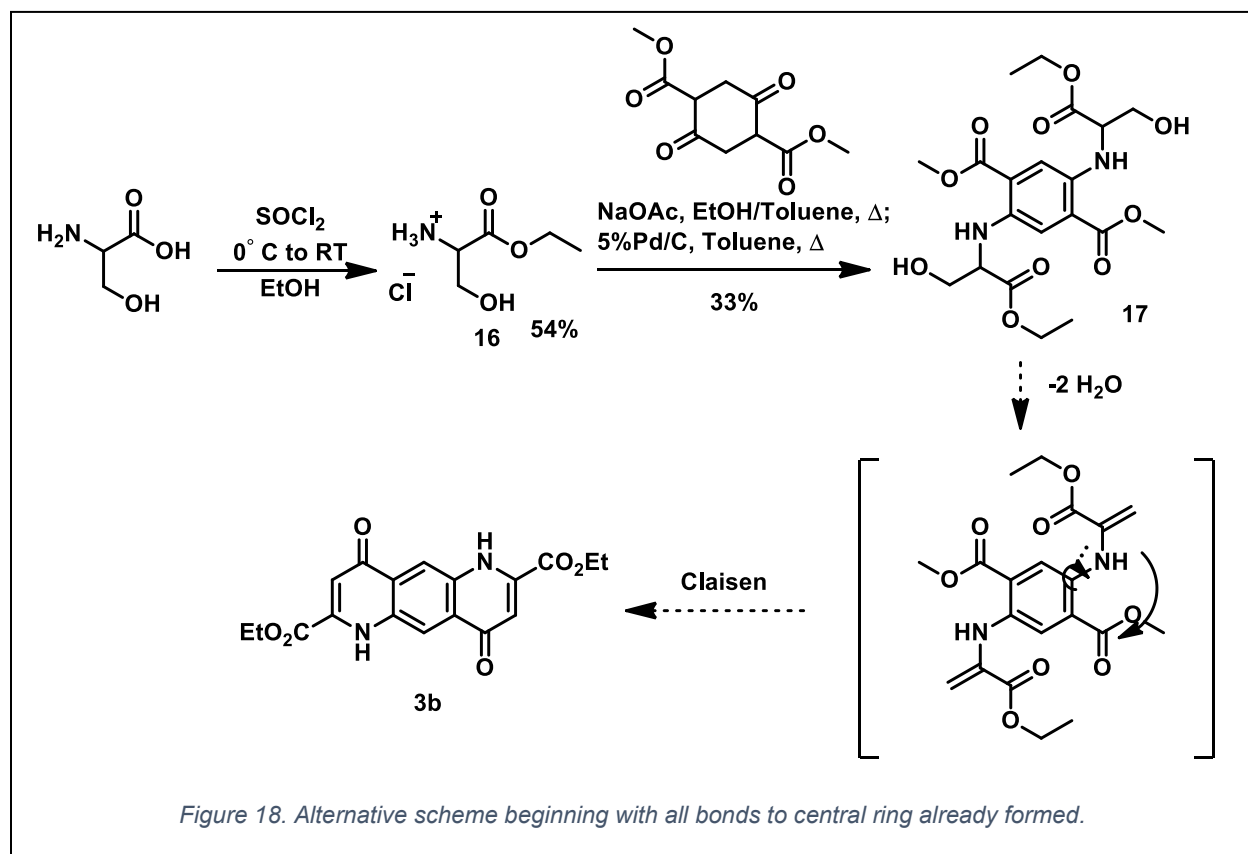
At this point our approach to obtain the pyrido[2,g]quinol-4-one **1** has been to acylate the central ring last. Concurrent work by undergraduates in the Schwabacher group investigated the sequence shown **Figure 18**. By starting with an aromatic ring that already has a 1,2,4,5 substitution pattern and then forming the peripheral rings, we may have better luck.



It has been shown in our lab that dimethyl succinylsuccinate (DMSS) can be transformed to diaminoterephthalate **15** via a bisenamine intermediate as shown in **Figure 17**.³⁰ Under the direction of Sarah Oehm, undergraduate Mike Sportiello showed it's possible to perform the enamine formation using serine ethyl ester **16** in place of the ammonium acetate, and to aromatize the product. Also, under Sarah Oehm's direction, Dan Murphy showed that when Boc-L-Ser-OEt was tosylated, and when exposed to Et₃N, the enamine from an elimination reaction could be obtained. If we had sufficient amounts of the aromatized product **17** derived from serine, we anticipated being able to perform the elimination on both serine residues generating an enamine that could undergo a Claisen condensation with the adjacent ester giving the desired core structure (**Figure 18**).

We foresaw many challenges with this route. Primarily the condensation of DMSS with ammonium acetate uses 6-8 equivalents of ammonium to drive the

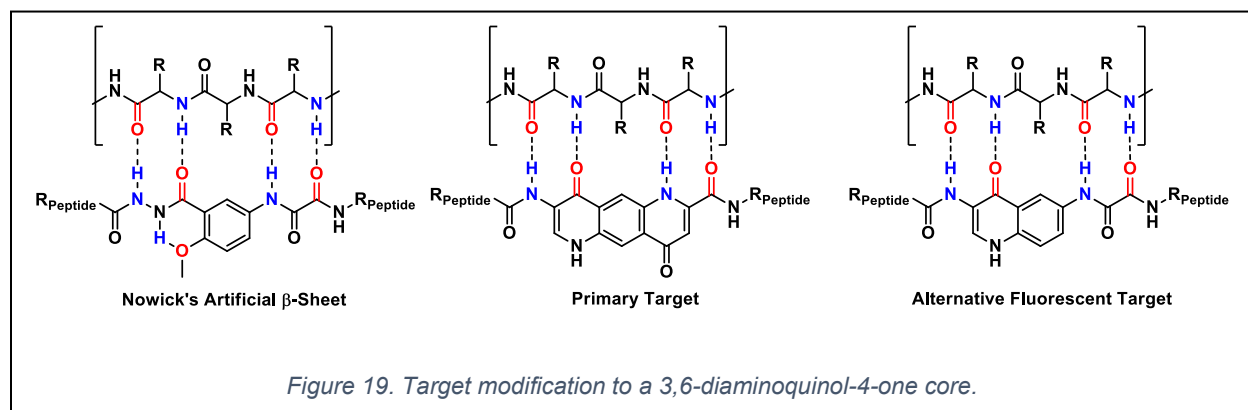
equilibrium, and with serine, that may not be possible. Second, the elimination, demonstrated by Dan Murphy to be nearly quantitative, and Claisen condensation would have to happen twice per molecule to successfully get the target product. The overall yield from these 4 steps could be low. With optimization of these steps after showing viability, we anticipate being able to prepare the pyrido[2,g]quinol-4-one **3b** in preparative amounts.



Undergraduate Mike Sportiello developed conditions to obtain aromatized terephthalate **17**, but had difficulty with isolation. Using his procedure and proper techniques to ensure no water was present in the reaction, I was able to obtain the pure terephthalate **17** in 33% yield after isolation by column chromatography, a more pure and higher yielding result than Mike had been able to obtain up until that point.

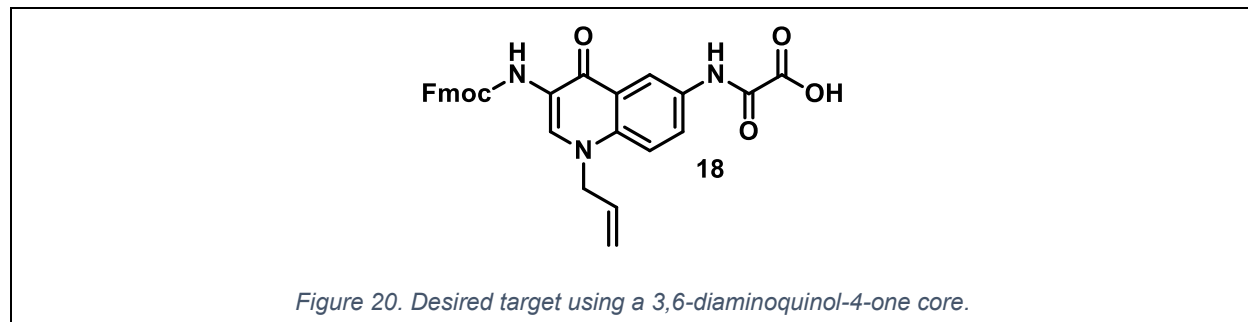
One challenge in driving the equilibrium towards the product most likely had to do with the quality of the serine reagent. The L-serine ethyl ester hydrochloride **16** was previously prepared by other members of the research group and was synthesized using well known procedures for amino acid esterification.³¹ L-serine ethyl ester hydrochloride **16** is extremely hygroscopic; extreme care must be employed to keep it dry, as any water in the next reaction will hinder the equilibrium. Work on this scheme has been carried out by undergraduates with promising but inconclusive results. Recently Trevor Hagemann has undertaken these investigations and conclusive results may soon be obtained.

Synthesis of a 3,6-diaminoquinolone as a β -sheet mimic

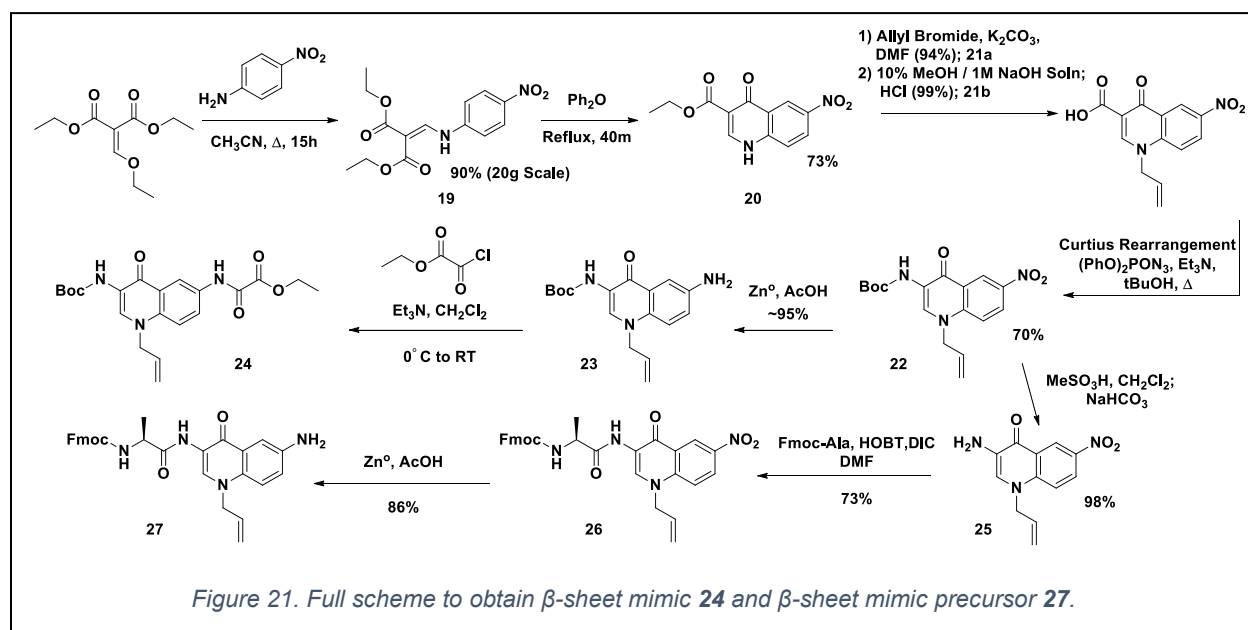


Due to difficulty synthesizing pyrido[2,g]quinol-4-one derivatives we sought to work toward a more precedented core structure, a 3,6-diaminoquinolone.³² This change to the design removes the conformational restriction of the 3rd ring but still allows for the extended H-bonding array that mimics 4 hydrogen bond pairs found in 3 amino acids in a peptide sequence. Aminoquinolone derivatives are also known to be highly fluorescent³³ and we wanted to find out whether the diamino derivative retained this quality when acylated. The oxalate carbonyl adjacent to the quinolone would likely be

rotated out of the plane of the quinolone when not in a β -sheet conformation, potentially resulting in a change in its fluorescence upon binding. This target (**18**), shown in **Figure 20**, could also be incorporated into solid phase peptide synthesis.



Beginning with the condensation of diethyl ethoxymethylenemalonate with *p*-nitroaniline, I was successful in achieving the crystalline product **19** in high yields directly from the reaction mixture. In my initial attempts to form enamine **13**, the reaction was tried with no solvent and worked fairly well but required a 2nd crystallization step to get the product in high purity. Modifying the reaction to include the crystallization solvent allowed for an easier to perform reaction because the reaction could be kept at the reflux temperature and crystallization could be easily performed by cooling down the



reaction mixture. Thermocyclization of enamine **19** proved to be more difficult than previous quinolone cyclizations. ¹H NMR analysis of the initial product showed a mixture of the desired product ethyl 3-carboxy-6-nitroquinol-4-one (**20**) and its decarboxylated analogue.

Literature suggests the *p*-nitroaniline derived enamines are susceptible to loss of ethylene and CO₂ prior to cyclization leading to the decarboxylated quinolone³⁴. Not only was quinolone **20** found as a mixture, but both the obtained compounds are very insoluble, so separation was difficult. Even trifluoroacetic acid and DMSO failed to solubilize either compound to any reasonable extent. The product was finally obtained in reasonable purity after repeated trituration with acetone suggesting the decarboxylated quinolone was more soluble than quinolone **20**.

Once quinolone **20** was clean, I was able to easily hydrolyze the ester and regenerate the acid using methanolic NaOH followed by acidification with HCl. This gave the free acid in high yields, but the product still remained highly insoluble in nearly all organic solvents. Two options were available to convert the acid to an amine: decarboxylation followed by nitration and reduction, or the preferred Curtius rearrangement route where the acid would be converted to an acyl azide, heated to rearrange to the isocyanate and conversion to the Boc-amine by treatment with *t*-butanol. The Curtius rearrangement was attempted first but failed, most likely due to the insolubility of the starting quinolone.

Thermal decarboxylation of the carboxylic acid derived from **20** required refluxing in Ph₂O for nearly 2 hours before the reaction was found to be complete. Since formation of the quinolone is under milder conditions, this proves decarboxylation does

not follow cyclization in the formation of quinolone **20**. Simple nitration consistently provided products that appeared difficult to separate. Even when the 3,6-dinitroquinol-4-one was obtained the reductions were even more frustrating, providing complex products as well, so attention was shifted back to the Curtius rearrangement.

To address the problem with solubility of intermediate and final products, I sought to alkylate the quinolone nitrogen. This would remove a hydrogen bond donor and likely reduce the crystallinity of the solid product, both of which should increase solubility in organics. Additionally, it was thought beneficial to introduce a functional group, an allyl group that could be used for modification to the β -sheet mimic after it was formed.

Alkylation of quinolone **20** with allyl bromide in the presence of carbonate gave the N-allylquinolone **21a** (**Figure 21**). This reaction gave product cleanly in high yields after only an aqueous-organic work up. Alkylated quinolone **21a** was indeed much more soluble in polar organic solvents. The hydrolyzed free acid **21b** was produced using the same conditions as its non-alkylated counterpart. Performing the Curtius rearrangement with diphenylphosphoryl azide and *t*-butanol proceeded smoothly to give the N-Boc-1-allyl-3-amino-6-nitroquinol-4-one **22** after crystallization from ethanol/toluene.

With nitrogens inserted in the proper positions around the quinolone I was able to proceed with 2 different routes, one that would obtain the initial target **18** and another that would give the target without the oxamide and an amino acid already coupled to the other side. The advantage of this derivative is its anticipated faster acylation in solid phase peptide synthesis. Although the latter option would take additional steps to get to the target product, after only a simple deprotection and amide coupling I would have a

product that could be examined via fluorescent titrations to determine whether or not it would be capable of acting as a β -sheet mimic, so it was attempted first.

I first attempted to remove the Boc group of quinolone **22** using standard deprotection conditions of 20% trifluoroacetic acid (TFA) in dichloromethane. Initially the ^1H NMR spectrum of the obtained product showed a new compound that appeared to be the desired product, but the MS spectrum identified the product to be the trifluoroacetamide, an initially puzzling result. I was able to determine that due to the electron withdrawing nature of the adjacent carbonyl of the quinolone the amine was to have significantly reduced basicity so protonation was not complete enough to prevent acylation, and the TFA was capable of catalyzing its own amine acylation. To address this issue, I opted to use a non-acylating acid, methanesulfonic acid in dichloromethane. Using these new conditions, the 1-allyl-3-amino-6-nitroquinolone **25** was obtained with a high yield. Acylation of **25** with Fmoc-Ala-OH was slow and required an overnight reaction for completion. This is consistent with its electron poor nature and acylation in TFA. In order to retain the olefin introduced during quinolone **20** alkylation, reduction of the nitro group was performed using mild conditions that are known to not reduce alkenes, unlike catalytic hydrogenation over palladium. Zinc powder and acetic acid worked well and gave **27** after only a few hours. It was a delight to see that **27** was highly fluorescent and was briefly analyzed for fluorescence variation based on concentration.

A protected version of **24** of the initial target **18** was also synthesized although due to time constraints was not fully purified and analyzed. Aminoquinolone **23** was prepared from nitroquinolone **22** using Zn/AcOH as used to obtain compound **25**.

Aminoquinolone **23** was treated with ethyl oxalyl chloride with triethylamine. Only a few attempts of this reaction were performed due to time constraints and the pure product was never obtained most likely because the reaction temperature was too high. However, starting material was absent by TLC analysis, the product was confirmed to be present by mass ion identification and the ^1H NMR spectrum showed shifted peaks from the starting material indicating an acylated product. The ^1H NMR spectrum also showed a complicated mess of peaks below 4 ppm indicating a large presence of aliphatic byproducts derived from triethylamine. Future attempts to obtain oxamide **24** should use dry pyridine to prevent undesired by products formed when triethylamine is used. Furthermore, the fluorescence observable by the eye had been significantly reduced from aminoquinolone **23**, leading to the hypothesis that acylation may reduce the utility of aminoquinolone's fluorescent properties.

Examination of the Binding Properties of the β -Sheet Mimic

By eye I could already observe that **27** had a bright blue fluorescence under longwave UV (360 nm) at high concentration and a more purple hue after a few serial

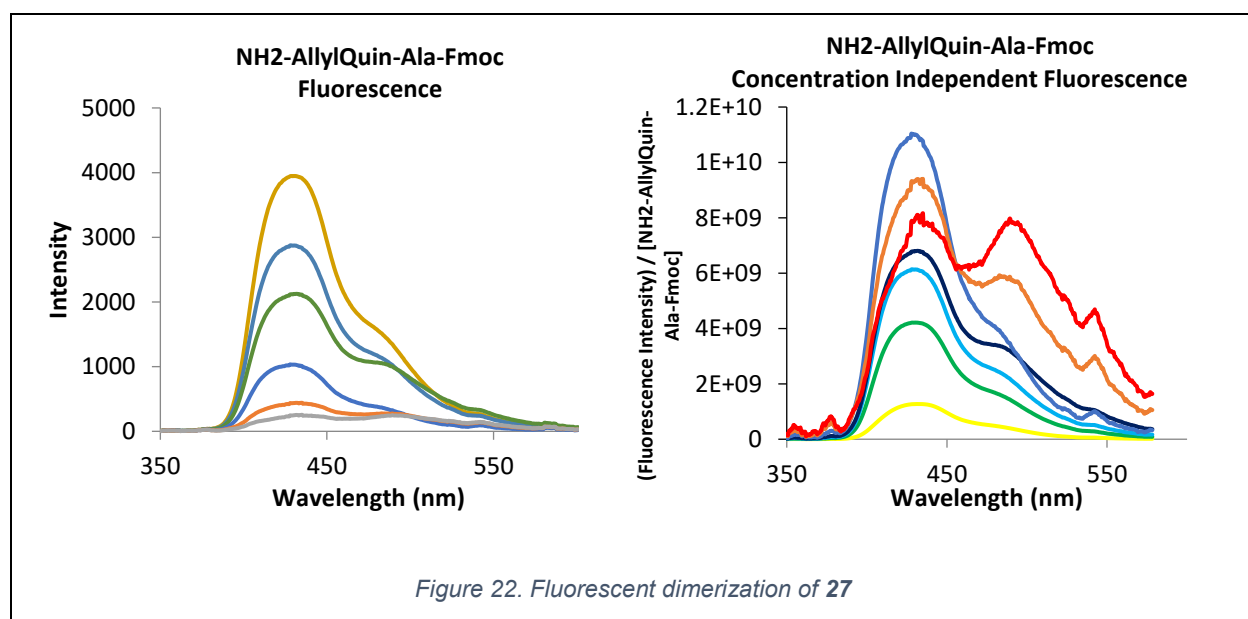
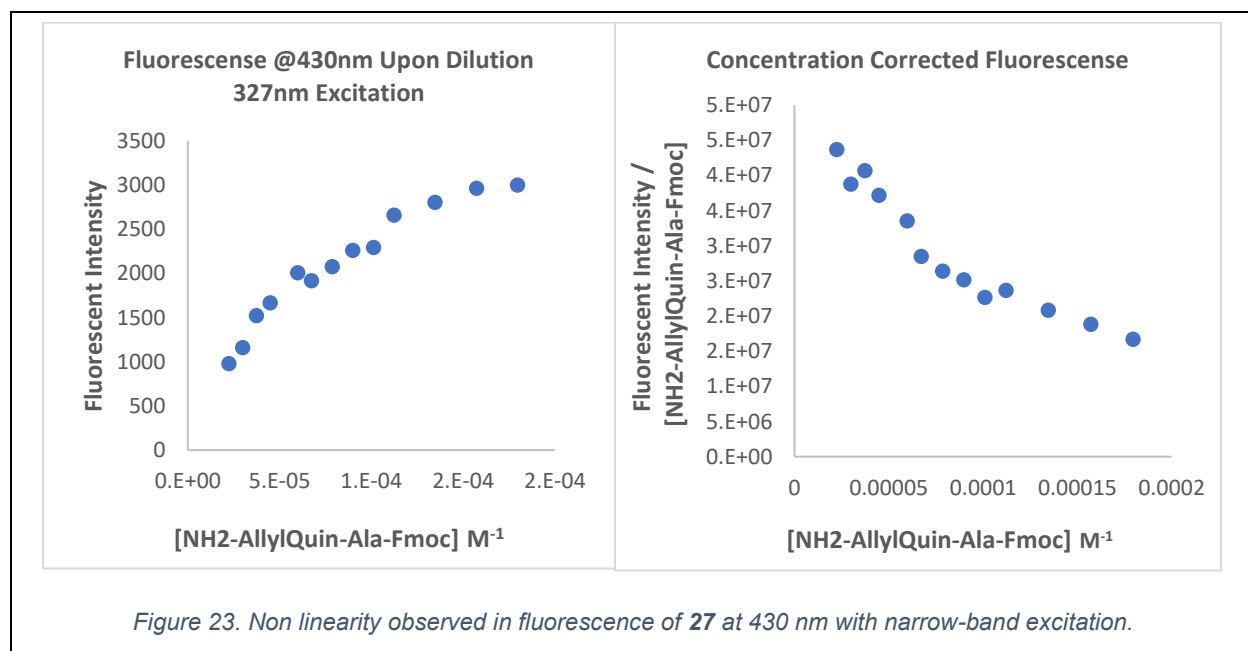


Figure 22. Fluorescent dimerization of **27**

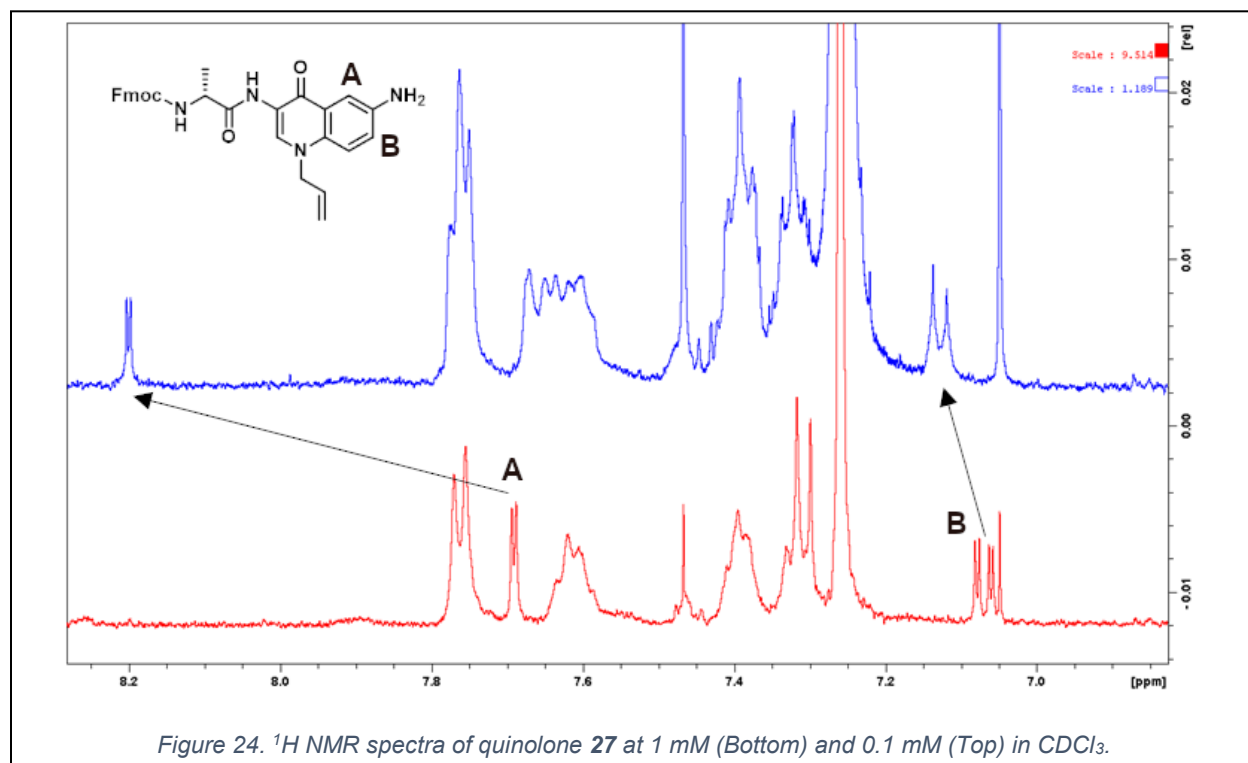
dilutions. Simple analysis by TLC showed the presence of multiple fluorescent spots from a starting material that was only one spot. The ^1H NMR was more complex than expected for a single compound. Although we could not confirm an analytically pure substance from this data we proceeded to do some preliminary fluorescence analysis as a crude mixture.

As expected our synthetic mimic demonstrated non-linear fluorescent intensity as it was diluted indicating a potential association event was occurring (**Figure 23**). The crude data obtained was quite exciting as the spectra revealed that the diamino-derived mimic **27** may act as a ratiometric sensor for β -sheet binding(**Figure 22**). The fluorescence spectrum appears as two distinct emission peaks at 440nm and 475nm. Decreasing the concentration clearly shows a change in the intensity ratio of these two max emission wavelengths. Attempts to fit this data to dimerization equations using non-linear least squared algorithms failed. We propose this inability to fit the curve being due to the lack of data collected: the spectrum is still changing at the lowest

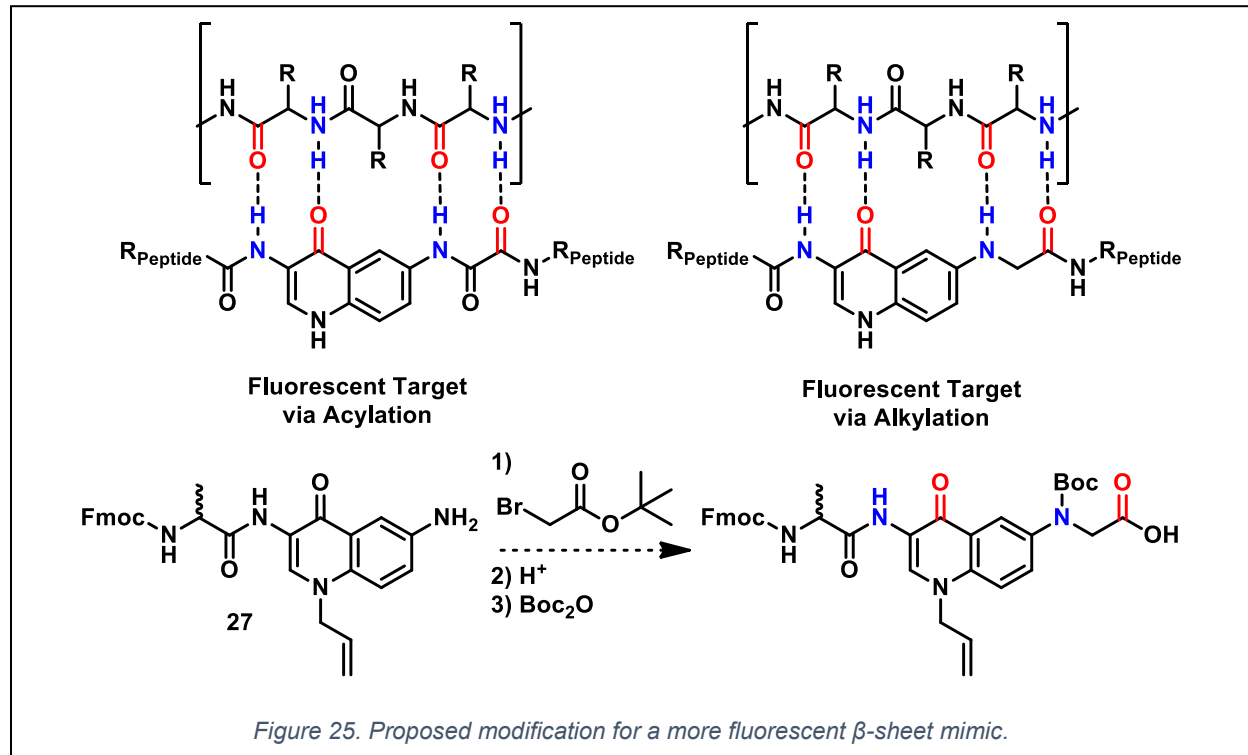


concentration measured. More data will be needed in future experiments at lower concentrations to determine an accurate disassociation constant.

Association of molecules is confirmed, but mode of binding is not. Since our fluorescence data were not conclusive to confirm 1:1 dimerization, we analyzed quinolone **27** using ^1H NMR spectroscopy at different concentrations. When diluted from 1 mM to 0.1 mM the proton assigned to the proton on the binding edge ortho to the amine shifted downfield 0.6 ppm and the proton ortho to the amine on the non-binding edge shift roughly 0.05 ppm (Figure 24). Upon dilution, it would be expected the amine is less likely to participate in a hydrogen bond and would cause up field shifts of adjacent protons. Regardless, a shift in the peaks does indicated a varied state, and that more change is seen at H_A near the expected binding than at the electronically similar H_B . Further investigations will need to be performed to fully understand what is happening.



Proposed Future Direction



Due to the reduced fluorescence of **24** compared to **23**, I propose that the intense fluorescence properties of these quinolone based β -sheet mimics is due to the available lone pair on the amine in the 6 position as is often observed. In order to maintain a similar hydrogen bonding array to the original target quinolone I propose alkylating **27** with *t*-butyl bromoacetate. This small alteration could be easily achieved from quinolone **27** (**Figure 25**). It could present challenges in solid phase methods for creating larger peptides due to the possibility of it forming tertiary amides when submitted to peptide coupling conditions. But this is good problem to have as it's nothing that can't be addressed with the proper protecting groups. A Boc protecting group could keep the amine at bay until the peptide has been completed and cleaved with acid after the fact. This may prove useful in avoiding aggregation of growing peptides during solid phase peptide synthesis.

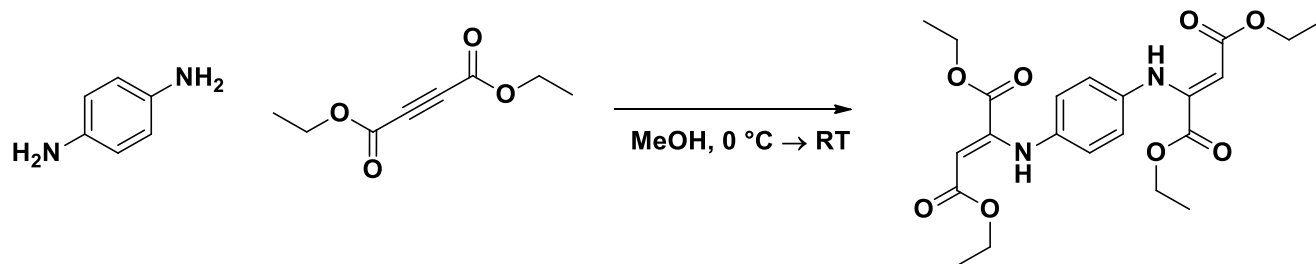
Experimental Details: Compounds 2, 3a, 4-8, 11-14, 17, 19-23, 25-27

All characterization spectra can be found in the appendix to this dissertation.

Bisenamine **2**

(Z)-tetraethyl 2,2'-(1,4-phenylenebis(azanediyl))difumarate

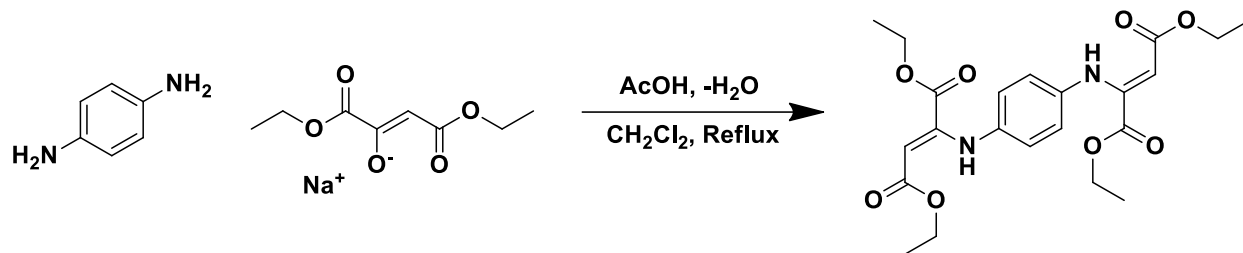
From acetylene:



To a chilled (0° C) solution of *p*-phenylenediamine (0.5058g, 4.7 mmol) in methanol (4 mL), diethylacetylenedicarboxylate (1.75 mL, 1.77g, 10.4 mmol) was added via syringe. Methanol (1 mL) was used to ensure complete transfer from the syringe. After stirring for 5 minutes, the reaction mixture was removed from the ice-water bath and allowed to warm to room temperature. After 2 hours, the product had precipitated out of the reaction mixture. Solid was collected by vacuum filtration, washed with MTBE (5 mL) and then hexanes (10 mL) to yield 0.9045g of yellow solid. The supernatant was then crystallized overnight to yield an additional 0.9179g of product. Solids were combined to give 1.8224g of yellow solid (**86%**). M.P. 90-92° C

¹H NMR (500 MHz, CDCl₃) δ 9.62 (s, 2H), 6.84 (s, 4H), 5.37 (s, 2H), 4.19 (q, J = 7.1 Hz, 4H), 4.15 (q, J = 7.1 Hz, 4H), 1.30 (t, J = 7.1 Hz, 6H), 1.13 (t, J = 7.1 Hz, 6H). ¹³C NMR (500 MHz, CDCl₃) δ 169.62, 164.23, 148.37, 136.97, 121.89, 93.70, 62.10, 59.98, 14.35, 13.75. ESI-MS Calculated for C₂₂H₂₈N₂O₈ [M+H⁺] 449.19, Found 449.20

From enolate:

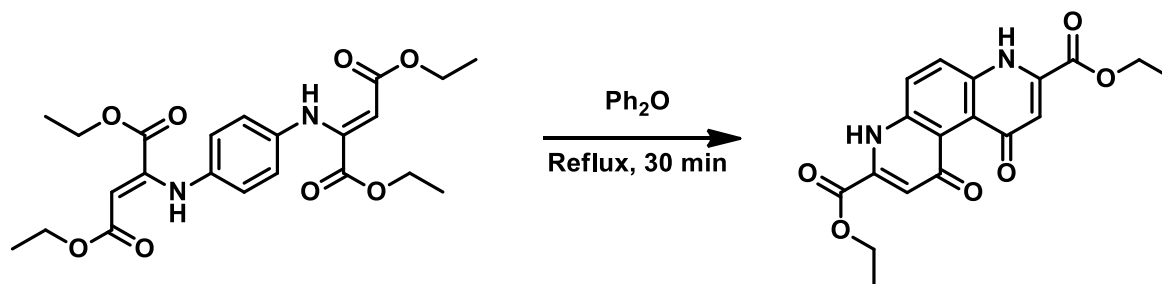


A suspension of diethyl oxalacetate sodium salt (8.0104g, 36.2 mmol) and *p*-phenylenediamine (1.0268g, 9.50 mmol) in CH₂Cl₂ (100 mL) and glacial acetic acid (4.2 mL, 4.4058g, 73.4 mmol) was heated at reflux for 2 days fitted with a heavier than water Dean-Stark trap, prefilled with CH₂Cl₂. Reaction progress assessed by ¹H-NMR integrations and found to be complete. Reaction mixture was washed with H₂O (20 mL), saturated Na₂CO₃ solution (4x30 mL). Organic layer was separated, dried with Na₂SO₄ and concentrated to dryness by rotary evaporation to yield 9.3246g of crude material. Crude mass was recrystallized from methanol (60 mL) to give 3.9893g (**94%**) of yellow solid. M.P. 90-92° C

Characterization data identical to procedure listed above.

4,7-Phenanthroline-1,10-dione **3a**

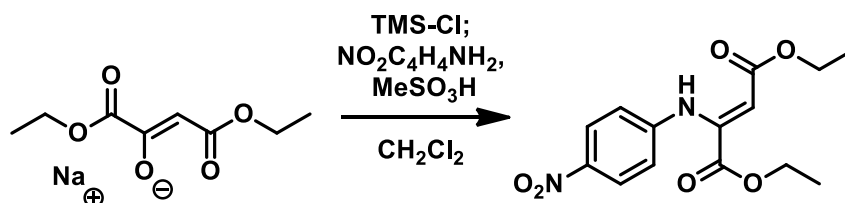
diethyl 1,10-dioxo-1,4,7,10-tetrahydro-4,7-phenanthroline-3,8-dicarboxylate



A solution of bisenamine **2** (416.8 mg, 0.929 mmol) in diphenyl ether (10 mL) was refluxed for 30 minutes, cooled, and poured into hexanes (100 mL). Solid was collected by vacuum filtration and dried under reduced pressure to give 320.6 mg (97%) of a tan solid. M.P. > 300 °C

^1H NMR (500 MHz, DMSO) δ 7.85 (s, 2H), 7.17 (s, 2H), 4.35 (q, J = 6.7 Hz, 4H), 1.36 (t, J = 7.1 Hz, 6H). ^{13}C NMR (126 MHz, DMSO) δ 188.40, 177.82, 134.46, 133.10, 121.65, 111.66, 61.19, 14.73. . ESI-MS Calculated for $\text{C}_{18}\text{H}_{16}\text{N}_2\text{O}_6$ $[\text{M}+\text{H}^+]$ 357.11, Found 357.10

p-nitrophenyl enamine **4**
diethyl 2-((4-nitrophenyl)amino)fumarate



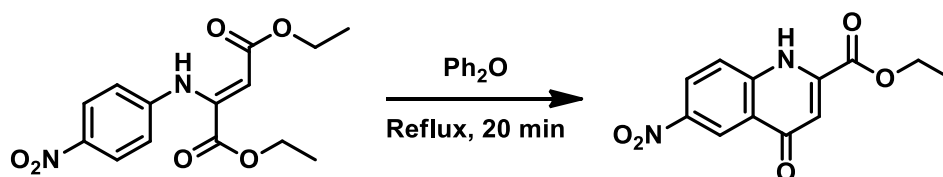
To a suspension of diethyl oxalylacetate sodium salt (6.063g, 28.8 mmol) in CH_2Cl_2 (100 mL) in a 2-necked RBF equipped with a condenser and a rubber septum, under N_2 was added trimethylsilylchloride (6.8 mL, 53.6 mmol) by syringe. The reaction was stirred until diethyl oxalylacetate sodium salt became soluble (~30 mins): sodium chloride will precipitate so careful observation is needed to know when this occurs. Once soluble, *p*-nitroaniline (2.0910g, 15.1 mmol) and methanesulfonic acid (0.10 mL, 1.54 mmol) were added via second neck. Apparatus was resealed and heated to reflux. After 20 hours reflux, pyridine (3.1 mL, 38.5 mmol) was added. Reaction was refluxed an additional 2 days and an additional 1 mL of methane sulfonic acid was added. Reaction refluxed for 2 days before workup was performed. Reaction mixture was filtered and washed with

Na₃PO₄ (0.5 M, 3x75 mL) and brine (1x75 mL). The organic layer was dried over Na₂SO₄ and concentrated by rotary evaporation. Placed under reduced pressure overnight to remove trace solvents to give 5.0085g of an amber oil. **95%** yield by NMR integration.

¹H NMR (300 MHz, CDCl₃) δ 9.82 (s, 1H), 8.16 (d, *J* = 9.1 Hz, 3H), 6.90 (d, *J* = 9.1 Hz, 3H), 5.69 (s, 1H), 4.26 (q, *J* = 7.1 Hz, 6H), 4.23 (q, *J* = 7.1 Hz, 6H), 1.32 (t, *J* = 7.1 Hz, 5H), 1.22 (t, *J* = 7.1 Hz, 5H). ESI-MS Calculated for C₁₄H₁₆N₂O₆ [M-] 307.09, Found 30d7.10.

Nitroquinolone **5**

ethyl 6-nitroquinol-4-one-2-carboxylate



Enamine **4** (4.41g, 14.3 mmol) in diphenyl ether (80 mL) was heated to reflux for 20 minutes. After cooling to room temp slowly, the reaction mixture was poured into 150 mL hexanes. Solid was filtered and dried under reduced pressure to give 2.7247g (**73%**) of crude product as a brown powder. MP 284-286° C (Melts w/ Decomposition)

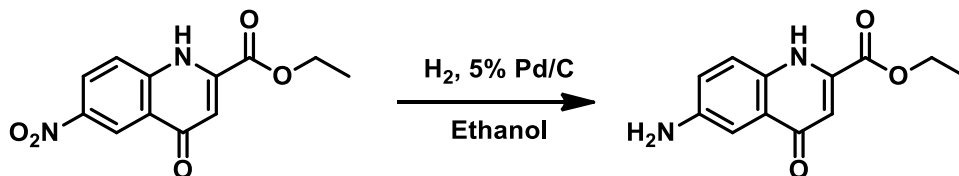
Crude product (1.422g) was recrystallized from toluene:ethanol (2:1 by vol, 225 mL) to give 0.8644 g of light brown crystals. M.P. 285-286° C (Melts w/ Decomposition)

¹H NMR (500 MHz, DMSO) δ 12.55 (s, 1H), 8.82 (d, *J* = 2.7 Hz, 1H), 8.50 (dd, *J* = 2.7, 9.3 Hz, 1H), 8.13 (d, *J* = 9.3 Hz, 1H), 6.77 (s, 1H), 4.45 (q, *J* = 7.1 Hz, 1H), 1.39 (t, *J* = 7.1 Hz, 1H). ¹³C NMR (126 MHz, DMSO) δ 177.1, 161.7, 143.8, 143.1, 139.2, 126.5,

124.7, 121.4, 121.2, 111.3, 62.9, 13.8. ESI-MS Calculated for C₁₂H₁₀N₂O₅ [M-] 261.05, Found 261.00

Aminoquinol-4-one **6**

ethyl 6-aminoquinol-4-one-2-carboxylate

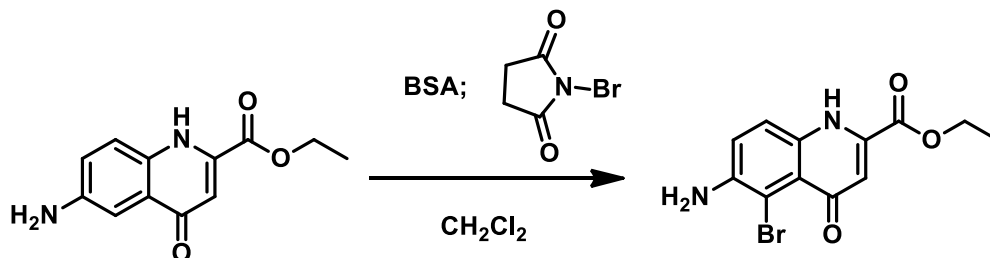


A suspension of nitroquinolone **5** (0.8553g, 3.26 mmol) and 5% Pd/C (208.1 mg) in 100 mL ethanol was flushed with hydrogen gas and stirred rapidly for 1 hour. The reaction mixture was filtered through celite and celite pad rinsed with hot ethanol until the filtrate appeared colorless. Supernatant was then concentrated by rotary evaporation and dried under reduced pressure to give 0.7293g (**96%**) of yellow solid. M.P. 251-253 °C

¹H NMR (300 MHz, DMSO) δ 7.70 (d, J = 8.9 Hz, 1H), 7.13 (d, J = 2.3 Hz, 1H), 7.08 (dd, J = 2.4, 8.9 Hz, 1H), 6.66 (br-s, 1H), 4.38 (q, J = 7.1 Hz, 2H), 1.35 (t, J = 7.1 Hz, 3H). ESI-MS Calculated for C₁₂H₁₂N₂O₃ [M+H⁺] 233.09, Found 233.15.

Bromoaminoquinolone **7**

ethyl 6-amino-5-bromoquinol-4-one-2-carboxylate



To a suspension of aminoquinolone **6** (0.4423 g, 1.90 mmol) in 100 mL of CH₂Cl₂, 0.5 mL of N,O-bistrimethylsilylacetamide (2.05 mmol) was added. After the reaction mixture

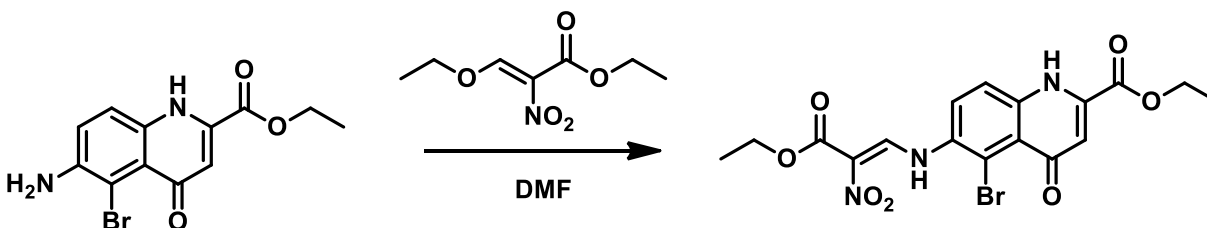
appeared homogenous (~ 5 minutes) N-bromosuccinimide (0.3556g, 2.00 mmol) was added. Reaction was stirred for 5 minutes before the addition of 15 mL DI H₂O and was gently swirled by hand once. Reaction mixture was placed at 4° C overnight and then filtered. The solid mass was dried under reduced pressure to give 0.4300g (**73%**) as dark yellow brown solid. M.P. 210-212 °C

¹H NMR (500 MHz, DMSO) δ 7.88 (d, *J* = 9.1 Hz, 1H), 7.37 (d, *J* = 9.1 Hz, 1H), 6.91 (s, 1H), 4.42 (q, *J* = 7.1 Hz, 1H), 1.37 (t, *J* = 7.1 Hz, 1H). ¹³C NMR (126 MHz, DMSO) δ 162.51, 160.29, 145.40, 145.36, 144.48, 137.11, 129.74, 123.12, 109.20, 62.89, 14.46.

ESI-MS Calculated for C₁₂H₁₁BrN₂O₃ [M+H⁺] 311.00, Found 310.95

Quinolone Enamine **8**

ethyl 5-bromo-6-((3-ethoxy-2-nitro-3-oxoprop-1-en-1-yl)amino)-quinol-4-one-2-carboxylate

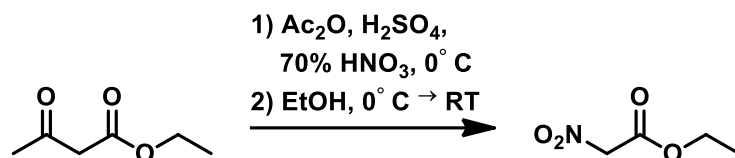


To a solution of aminobromoquinol-4-one **7** (120.0 mg, 0.386 mmol) in 1.5 mL DMF, nitroenoether **12** (~160 mg, 0.9 mmol) was added. After 30 minutes a yellow precipitate had formed and was collected via vacuum filtration and rinsed with hexanes. Solid dried under reduced pressure to give 85.4 mg (51%) of yellow solid.

¹H NMR (300 MHz, TFA) δ 12.22 (d, *J* = 14.1 Hz, 1H), 9.37 (d, *J* = 13.9 Hz, 1/3 H), 8.88 (d, *J* = 13.7 Hz, 2/3 H), 8.43 (d, *J* = 9.7 Hz, 1H), 8.41 (d, *J* = 9.0 Hz, 1H), 8.27 (d, *J* = 9.7 Hz, 1/3 H), 8.21 (d, *J* = 9.4 Hz, 2/3 H), 7.97 (s, 1H), 4.63 (q, *J* = 7.1 Hz, 2H), 4.53 (q, *J* =

7.1 Hz, 2/3 H), 4.40 (q, $J = 7.1$ Hz, 4/3 H), 1.44 (t, $J = 6.9$ Hz, 4H), 1.34 (t, $J = 7.3$ Hz, 2H).

Ethyl nitroacetate **11**

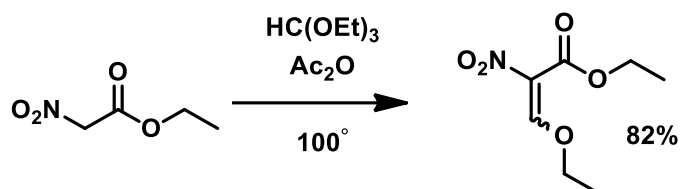


Acetic Anhydride (120 mL, 1.27 mol) and sulfuric acid (0.15 mL, 18M, 2.8 mmol) were combined in a 2-necked round bottom flask equipped with a stir bar, addition funnel, thermometer, and an ice bath. The addition funnel was charged with ethyl acetoacetate (25.0 mL, 0.196 mol). The reaction flask was cooled to 0°C before slow addition (weak exotherm) of the ethyl acetoacetate. The addition funnel was then swapped for a clean addition funnel charged with HNO_3 (70% wt/wt, 13.5 mL). With the reaction flask still at 0°C or less, the nitric acid was added very slowly. A strong exotherm is observed: use a dry ice/salt water bath with the rapidly stirred flask fully submerged. After complete addition of the nitric acid, the reaction was stirred for an additional 60 minutes (TLC: 30% EtOAc/Hex, watch for disappearance of ethyl acetoacetate; Rf: 0.61). The reaction mixture was diluted into ice-cold ethanol (250 mL) and stirred for 10 minutes on an ice bath, then 30 minutes room temperature. Sodium carbonate (2.421g, powdered) was added to the reaction mixture, resulting in a yellowing of the suspension. Suspension was then filtered through celite and volatiles were removed under reduced pressure. Crude product was distilled under reduced pressure ($70\text{-}73^\circ\text{C}$ @ $\sim 0.5\text{-}2$ mm Hg) to yield 16.6227g (64%) of a yellow oil.

^1H NMR (300 MHz, CDCl_3) δ 5.16 (s, 1H), 4.34 (q, $J = 7.1$ Hz, 1H), 1.34 (t, $J = 7.1$ Hz, 1H).

Nitroenoether **12**

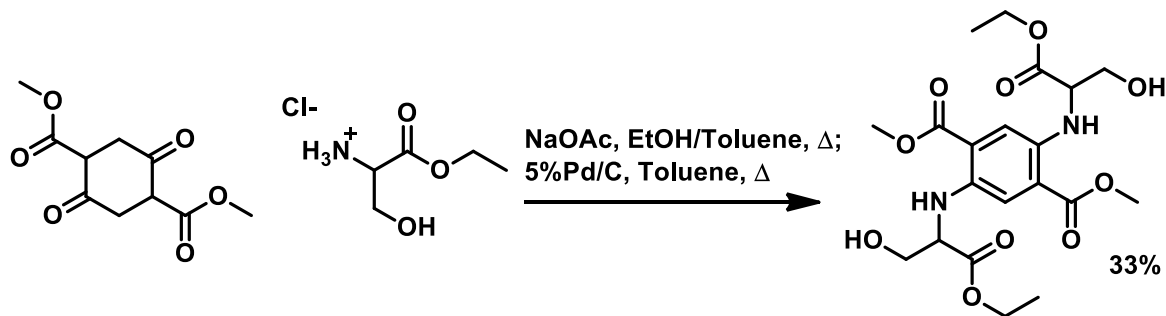
ethyl 3-ethoxy-2-nitroacrylate



A solution of ethyl nitroacetate (0.3 mL, 0.3657g, 2.74 mmol), triethyl orthoformate (0.90 mL, 0.8175g, 5.52 mmol) and acetic anhydride (2.0 mL, 2.2725, 22.3 mmol) was heated to 100° C for 28 hours. An aliquot of the reaction was analyzed by NMR and there was no more ethyl nitroacetate remaining. Volatiles were then removed under reduced pressure to yield 0.4296g (82%) of a yellow liquid.

^1H NMR (300 MHz, CDCl_3) δ 8.22 (s, 1H), 7.52 (s, 1H), 4.31 (q, $J = 3.7$ Hz, 1H), 4.28 (q, $J = 3.4$ Hz, 1H), 4.27 (s, 1H), 1.43 (t, $J = 7.1$ Hz, 1H), 1.31 (t, $J = 7.1$ Hz, 1H).

Dimethyl N,N'-bis(1-carboxyethyl-2-hydroxyethyl)-2,5-diaminoterephthalate **17**

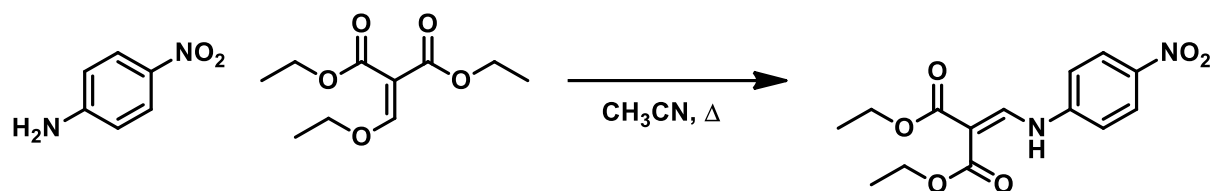


A solution of L-serine ethyl ester HCl **16** (417.9 mg, 2.46 mmol), dimethyl succinylsuccinide (199.3 mg, 0.873 mmol), and sodium acetate (217.3 mg, 2.64 mmol) in a mixture of toluene and ethanol (1:1 by vol., 20 mL) and brought to reflux. After

refluxing for 47 hours, the solvent was distilled until ~1 mL remained and replaced with fresh toluene (20 mL) and refluxed for an additional 15 hours with a Dean Stark trap loaded with 3Å MS before the addition of 5% Pd/C (17 mg) and refluxed for 3 hours. Reaction mixture was then allowed to cool and filtered through celite, using hot toluene to rinse the filter pad concentrated via rotary evaporation and dried under reduced pressure to give 595.2 mg of crude residue. The product was purified via column chromatography using increasing concentrations of CH₃CN in CH₂Cl₂ (10% -> 25%) to give 133.0 mg (**33%**) of red solid. M.P 145-148° C

¹H NMR (500 MHz, CDCl₃) δ 7.35 (s, 2H), 4.27 (m, 4H), 4.24 (m, 2H), 4.00 (s, 4H), 3.90 (s, 6H), 1.27 (s, 6H). ¹³C NMR (126 MHz, DMSO) δ 171.77, 167.80, 140.42, 118.06, 115.35, 63.01, 61.63, 58.63, 52.21, 14.19. ESI-MS Calculated for C₂₀H₂₈N₂O₁₀ [M+H⁺] 457.18, Found 457.10

Diethyl (*p*-nitrophenylamino)methylenemalonate **19**



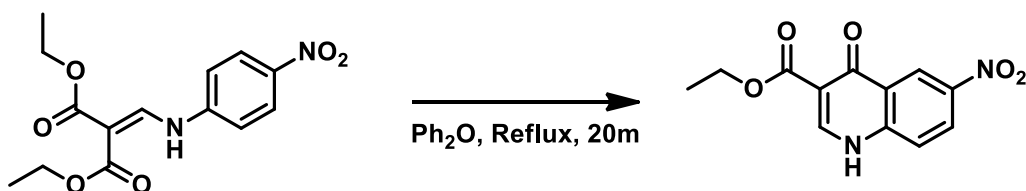
A solution of *p*-nitroaniline (2.8072g, 20.3 mmol) and diethyl ethoxymethylenemalonate (4.900g, 22.7 mmol) in 5 mL acetonitrile was heated at 80 °C on an oil bath for 16 hours. The reaction mixture was allowed to cool to room temperature and solid was collected via filtration and rinsed with minimal acetonitrile. Solid was dried under reduced pressure. The supernatant was concentrated to dryness in order to collect a 2nd crop. Acetonitrile (10 mL) was added to concentrated supernatant and heated until soluble. Solution was then slowly cooled back to room temperature and then placed in

freezer overnight. Second crop collected via vacuum filtration, rinsed with minimal cold acetonitrile, dried under reduced pressure and combined with first crop to give a combined mass of 5.605g (90%). M.P. 143-144° C

^1H NMR (500 MHz, CDCl_3) δ 11.20 (d, $J = 13.05$ Hz, 1H), 8.50 (d, $J = 13.15$ Hz, 1H), 8.27 (d, $J = 9.03$ Hz, 2H), 7.22 (d, $J = 9.03$ Hz, 2H), 4.31 (overlapping q, $J = 7.12$ Hz, 4H), 1.37 (overlapping t, $J = 7.13$ Hz, 6H). ^{13}C NMR (500 MHz, CDCl_3) δ 168.58, 165.09, 149.70, 144.56, 143.90, 126.02, 116.36, 97.41, 60.99, 60.67, 14.37, 14.21.

ESI-MS Calculated for $\text{C}_{14}\text{H}_{16}\text{N}_2\text{O}_6$ $[\text{M}+\text{H}^+]$ 309.11, Found 309.20

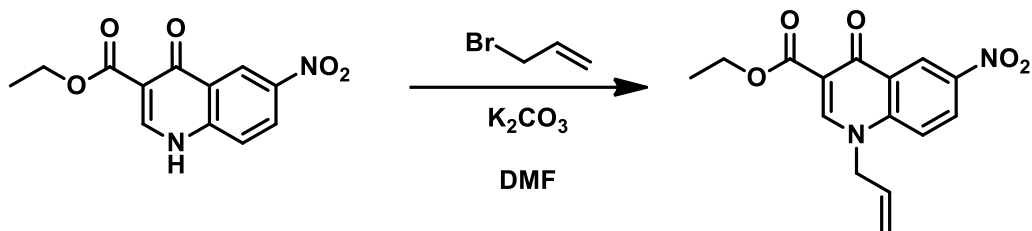
Ethyl 6-nitroquinol-4-one-2-carboxylate **20**



A solution of diethyl (*p*-nitrophenylamino)methylenemalonate **19** (2.0939g, 6.79 mmol) was in 125 mL diphenyl ether was slowly brought to reflux using a sand bath and refluxed for 20 minutes. Solution allowed to cool to room temperature and poured into 650 mL hexanes. Solid was collected by vacuum filtration, rinsed with hexanes and dried under reduced pressure to yield 1.5261g (73%) of a light brown solid. Compound was used without further purification.

^1H NMR (500 MHz, $d\text{-DMSO-}d_6$) δ 8.89 (d, $J = 2.7$ Hz, 1H), 8.68 (s, 1H), 8.40 (dd, $J = 2.4, 8.9$ Hz, 1H), 7.76 (d, $J = 9.1$ Hz, 1H), 4.22 (q, $J = 7.1$ Hz, 2H), 1.28 (t, $J = 7.1$ Hz, 3H). ESI-MS Calculated for $\text{C}_{12}\text{H}_{10}\text{N}_2\text{O}_5$ $[\text{M}^-]$ 261.05, Found 261.05

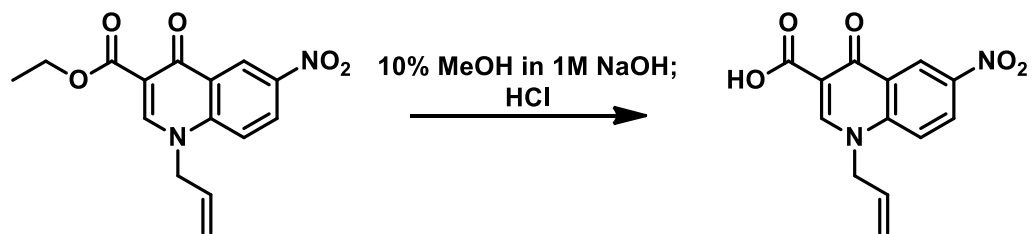
Ethyl 1-allyl-6-nitroquinol-4-one-2-carboxylate **21a**



To a suspension of ethyl 3-carboxy-6-nitroquinol-4-one **20** (1.5082g, 5.75 mmol) and K_2CO_3 (3.5760g, 25.8 mmol) in 25 mL DMF, allyl bromide (2.44 mL, 28.2 mmol) was added. The mixture was stirred at 83°C under a nitrogen atmosphere until reaction was complete by TLC (~2.25 hours). Reaction mixture cooled and poured over ice (~150g) and stirred until the ice had completely melted. Solid collected by vacuum filtration and dried under reduced pressure to yield 1.6392g (94%) of a tan solid. No further purification required. M.P. $223\text{-}227^\circ\text{C}$

^1H NMR (500 MHz, d-DMSO- d_6) δ 8.93 (d, $J = 2.8$ Hz, 1H), 8.80 (s, 1H), 8.50 (dd, $J = 2.8, 9.3$ Hz, 1H), 7.93 (d, $J = 9.4$ Hz, 1H), 6.07 (m, 1H), 5.27 (dd, $J = 1.0, 10.5$ Hz, 1H), 5.15 (dd, $J = 1.0, 17.3$ Hz, 1H), 5.12 (d, $J = 5.0$ Hz, 2H), 4.26 (q, $J = 7.1$ Hz, 2H), 1.30 (t, $J = 7.1$ Hz, 3H). ^{13}C NMR (500 MHz, d-DMSO- d_6) δ 172.65, 164.42, 151.39, 144.25, 143.47, 132.69, 128.33, 127.05, 122.70, 120.31, 118.61, 112.28, 60.67, 55.50, 14.75.

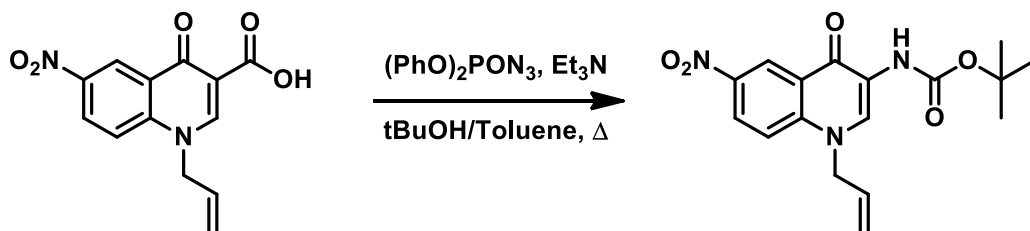
1-allyl-6-nitroquinol-4-one-2-carboxylic acid **21b**



Ethyl 1-allyl-6-nitroquinol-4-one-3-carboxylate **21a** (1.2081g, 4.00 mmol) was stirred in a 10% methanol in 1M NaOH solution and heated to a boil. Once solution appeared soluble, the methanol was quickly evaporated by placing the solution under a stream of nitrogen resulting in some precipitation of product. Heat was removed, and the solution was acidified with 12M HCl to pH 2 while stirring rapidly. Solution was cooled on an ice bath, initiating rapid solid formation. Solid was collected by vacuum filtration and dried under reduced pressure to yield 1.0809g (99%) of a pale-yellow solid. M.P. 237-238 °C

¹H NMR (500 MHz, d-DMSO-d₆) δ 14.43 (br-s, 1H), 9.18 (s, 1H), 9.04 (d, J = 2.7 Hz, 1H), 8.65 (dd, J = 2.8,9.4 Hz, 1H), 8.14 (d, J = 9.4 Hz, 1H), 6.10 (m, 1H), 5.30 (overlapping signals, 3H), 5.22 (d, J = 17.3 Hz, 1H). ¹³C NMR (500 MHz, d-DMSO-d₆) δ 178.00, 165.61, 152.19, 144.98, 143.42, 132.45, 128.12, 126.10, 122.19, 121.27, 119.19, 109.86, 56.35. ESI-MS Calculated for C₁₃H₁₀N₂O₅ [M+H⁺] 275.07, Found 275.05.

Boc-N-1-allyl-3-amino-6-nitroquinol-4-one **22**

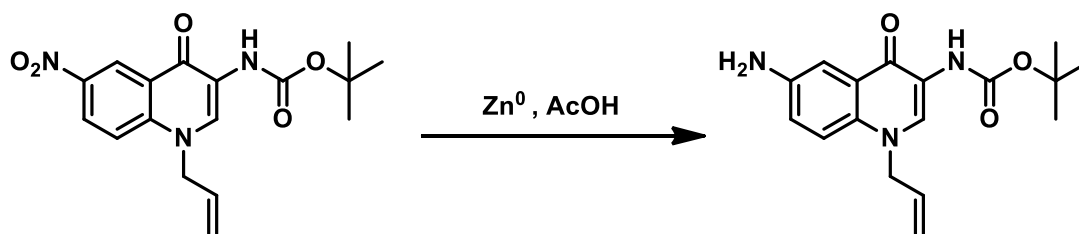


To a solution of 1-allyl-6-nitroquinol-4-one-3-carboxylic acid **21b** (0.8949g, 3.26 mmol) and triethylamine (2.10 mL, 15.8 mmol) in a solution of tBuOH and toluene (1:1 by vol., 40 mL tot.), diphenylphosphoryl azide (0.81 mL, 3.75 mmol) was added, and the solution was refluxed under N₂ for 24 hours. Solvent was removed by rotary evaporation and the crude residue in CH₂Cl₂ (75 mL) was washed with sat. Na₂CO₃ (3x50 mL). Each

aqueous wash was back extracted with CH₂Cl₂ (2x25 mL). All organic layers were combined, dried over Na₂SO₄, filtered and concentrated via rotary evaporation. Crude residue was crystallized from a solution of CH₂Cl₂ in hexanes (2:3, 100 mL) to yield 0.7837g (**70%**) of yellow crystals. M.P. 171-172° C.

¹H NMR (500 MHz, CDCl₃) δ 9.37 (d, J = 2.68 Hz, 1H), 8.78 (s, 1H), 8.39 (dd, J = 2.72, 9.48 Hz, 1H), 7.61 (s, 1H), 7.49 (d, J = 9.51 Hz, 1H), 6.00 (m, 1H), 5.36 (dd, J = 1.95, 10.55 Hz, 1H), 5.14 (dd, J = 1.68, 17.17 Hz, 1H), 4.84 (dt, J = 4.81, 1.96 Hz, 1H), 1.53 (s, 9H). ¹³C NMR (500 MHz, CDCl₃) δ 169.94, 153.24, 142.77, 140.90, 130.39, 129.99, 125.72, 124.90, 124.34, 122.84, 119.38, 117.21, 81.31, 55.31, 28.45. ESI-MS Calculated for C₁₇H₁₉N₃O₅ [M+H⁺] 346.14, Found 346.20.

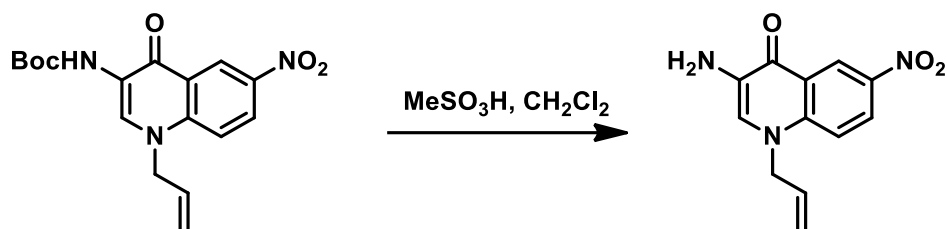
Boc-3-N-1-allyl-3,6-diaminoquinol-4-one **23**



Boc-N-1-allyl-3-amino-6-nitroquinol-4-one **22** (0.7265g, 2.10 mmol) and zinc dust (2.7566 g) was stirred in 40% glacial acetic acid in dichloromethane for 2 hours at room temperature. Reaction mixture was filtered through celite and supernatant was diluted with 50 mL CH₂Cl₂ and then poured into 100 mL saturated Na₂CO₃ solution and stirred until gas evolution had ceased. Organic layer washed with saturated Na₂CO₃ (2x50 mL) and then brine(1x25 mL). The organic layer was dried over Na₂SO₄, concentrated by rotary evaporation and dried under reduced pressure to give 628.9 mg (95%) of product as a red solid.

^1H NMR (500 MHz, CDCl_3) δ 8.67(s, 1H), 7.68 (d, J = 2.79 Hz, 1H), 7.63 (s, 1H), 7.27 (d, J = 9.15 Hz, 1H), 7.04 (dd, J = 2.08, 9.08 Hz, 1H), 5.97 (m, 1H), 5.27 (d, J = 10.47 Hz, 1H), 5.10 (d, J = 17.22 Hz, 1H), 4.76 (m, 2H), 3.85 (br-s, 2H), 1.52 (s, 9H). ^{13}C NMR (500 MHz, CDCl_3) δ 168.81, 153.44, 142.20, 131.82, 131.32, 129.33, 125.22, 121.79, 121.76, 118.35, 117.15, 108.63, 80.26, 55.68, 28.40.

1-allyl-3-amino-6-nitroquinol-4-one **25**



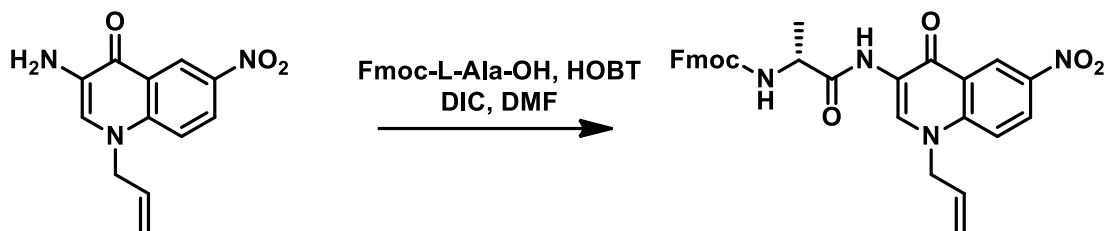
A solution of Boc-N-1-allyl-3-amino-6-nitroquinol-4-one **23** (444.6 mg, 1.29 mmol) in 50 mL CH_2Cl_2 and 5 mL of MeSO_3H was stirred 30 minutes at room temperature and then boiled uncovered for 15 minutes. While boiling, solid Na_2CO_3 (powderized, ~2 g) was added and heating was continued for an additional 20 minutes. The mixture was cooled to room temperature, dried with MgSO_4 , and filtered through celite. Supernatant was concentrated via rotary evaporation and dried under reduced pressure to give 0.3363g (~106%) of crude product as a red solid. A portion of the crude mass (144.1 mg) was recrystallized from ethanol and toluene (bp 91°C , 25 mL) to give 73.6 mg (~50% recovery) of crystallized material as a red solid. MP: $>213^\circ\text{C}$ decomp.

^1H NMR (500 MHz, MeOD) δ 9.24 (d, J = 2.7 Hz, 1H), 8.37 (dd, J = 2.7, 9.6 Hz, 1H), 7.82 (d, J = 9.6 Hz, 1H), 7.78 (s, 1H), 6.10 (tdd, J = 5.1, 10.2, 17.2 Hz, 1H), 5.31 (dd, J = 0.9, 10.5 ^{13}C NMR (126 MHz, DMSO) δ 169.95, 141.40, 134.07, 132.98, 124.35,

123.73, 123.14, 118.83, 117.86, 54.92, 49.07. . ESI-MS Calculated for C₁₂H₁₁N₃O₃

[M+H⁺] 246.09, Found 246.15

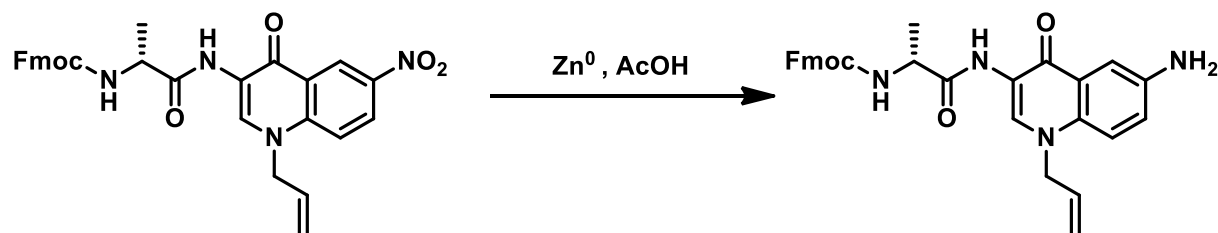
1-allyl-3-(Fmoc-N-alanyl)amino)-6-nitroquinol-4-one **26**



A 1M solution of each HOBT and DIC were prepared separately in DMF. To Fmoc-Ala-OH (0.5156g, 1.66 mmol), 1.70 mL of each solution was added. Solution was allowed to stir for 30 mins prior to the addition of 1-allyl-3-amino-6-nitroquinol-4-one **25** (0.1922g, 0.784 mmol). Solution was stirred overnight. Reaction mixture was poured into water and solid isolated by filtration and was azeotropically dried with toluene twice before drying under reduced pressure to give 427.1 mg (101%). M.P. 105-108 °C

¹H NMR (500 MHz, DMSO) δ 11.62 (s, 1H), 9.44 (s, 1H), 9.18 (s, 1H), 9.02 (d, *J* = 2.8 Hz, 1H), 9.02 (d, *J* = 2.8 Hz, 1H), 8.45 (dd, *J* = 2.8, 9.6 Hz, 1H), 8.45 (dd, *J* = 2.8, 9.6 Hz, 1H), 7.94 (d, *J* = 9.6 Hz, 1H), 7.94 (d, *J* = 9.6 Hz, 1H), 7.90 (d, *J* = 7.4 Hz, 1H), 7.90 (d, *J* = 7.4 Hz, 1H), 7.75 (d, *J* = 6.9 Hz, 1H), 7.75 (d, *J* = 6.9 Hz, 1H), 7.43 (t, *J* = 7.6 Hz, 1H), 7.35 (q, *J* = 6.8 Hz, 1H), 6.07 (tdd, *J* = 5.2, 10.4, 16.6 Hz, 1H), 5.48 (d, *J* = 7.4 Hz, 1H), 5.25 (d, *J* = 11.4 Hz, 1H), 5.10 (s, 1H), 5.08 (d, *J* = 17.8 Hz, 1H), 4.41 (t, *J* = 7.2 Hz, 1H). ¹³C NMR (126 MHz, DMSO) δ 169.84, 157.25, 144.26, 142.66, 141.67, 141.19, 134.11, 132.75, 128.10, 127.57, 125.92, 125.73, 124.80, 123.44, 123.22, 122.77, 120.59, 119.65, 118.20, 66.21, 55.56, 51.21, 47.12, 18.25.

1-allyl-3-(Fmoc-N-alanyl)amino)-6-aminoquinol-4-one **27**



To a solution of 1-allyl-3-(Fmoc-N-alanyl)amino)-6-nitroquinol-4-one **19** (0.2351g, 0.435 mmol) in 5 mL glacial acetic acid, 0.4701g of zinc dust was added. The suspension was stirred rapidly for 4 hours before being neutralized into saturated Na₂CO₃ solution (150 mL) and ethyl acetate (100 mL). The organic layer was washed with additional saturated Na₂CO₃ solution (2x50 mL) and brine (1x50 mL), dried over Na₂SO₄, concentrated by rotary evaporation and dried under reduced pressure to give 0.1910g (**86%**) of yellow solid. M.P. 129-135 °C (Turns to semi-solid) 145 °C (decomp)

¹H NMR (500 MHz, DMSO) δ 9.17 (s, 1H), 8.95 (s, 1H), 7.94 (d, *J* = 6.9 Hz, 1H), 7.90 (d, *J* = 7.0 Hz, 1H), 7.76 (t, *J* = 5.3 Hz, 1H), 7.47 (d, *J* = 9.1 Hz, 1H), 7.42 (q, *J* = 6.3 Hz, 1H), 7.36 (d, *J* = 2.7 Hz, 1H), 7.35 (q, *J* = 7.0 Hz, 1H), 7.06 (dd, *J* = 2.8, 9.1 Hz, 1H), 6.02 (tdd, *J* = 5.4, 11.2, 16.3 Hz, 1H), 5.48 (d, *J* = 7.7 Hz, 1H), 5.41 (s, 1H), 5.21 (dd, *J* = 1.3, 10.4 Hz, 1H), 5.04 (dd, *J* = 1.3, 17.2 Hz, 1H), 4.91 (d, *J* = 4.5 Hz, 1H), 4.32 (t, *J* = 5.2 Hz, 1H), 4.29 (d, *J* = 10.0 Hz, 1H), 4.26 (d, *J* = 7.1 Hz, 1H), 3.32 (s, 1H), 1.33 (d, *J* = 7.2 Hz, 1H).

Chapter 3: Development of a Metal Ion Chemosensor

Introduction

Rapid quantitation of metals ions in aqueous solution is an important area of interest to many disciplines. Currently the gold standard for quantitating metals in non-biological systems is atomic absorption spectroscopy (AAS) and while AAS is accurate and can quantify metals in the part-per-billion range³⁵, it suffers from expensive instrumentation and is typically done by a third party significantly increasing the time between sampling and analysis. Modern instrumentation such as ICP-MS have a much greater sensitivity but also requires expensive instrumentation and trained operators to maintain them.³⁵

Use of optically responsive chelating molecules allows for titrimetric methods of metal ion analysis. Fluorescent molecules are preferred in the literature for biological purposes because of their high affinity for analytes and the fluorescent signal is adequately observable at the low concentrations needed for intracellular analysis. For this reason, UV/Vis absorbing chemosensors have been largely ignored due to being needed in larger amounts for accurate quantitation. Specifically, azo dye chemosensors have additional challenges due to their potential for bio-reduction.³⁶ However, for use in long term non-biological applications, absorbing indicators are desirable because of fluorescent probes tendency to undergo photobleaching reduces their lifetime.^{37,38}

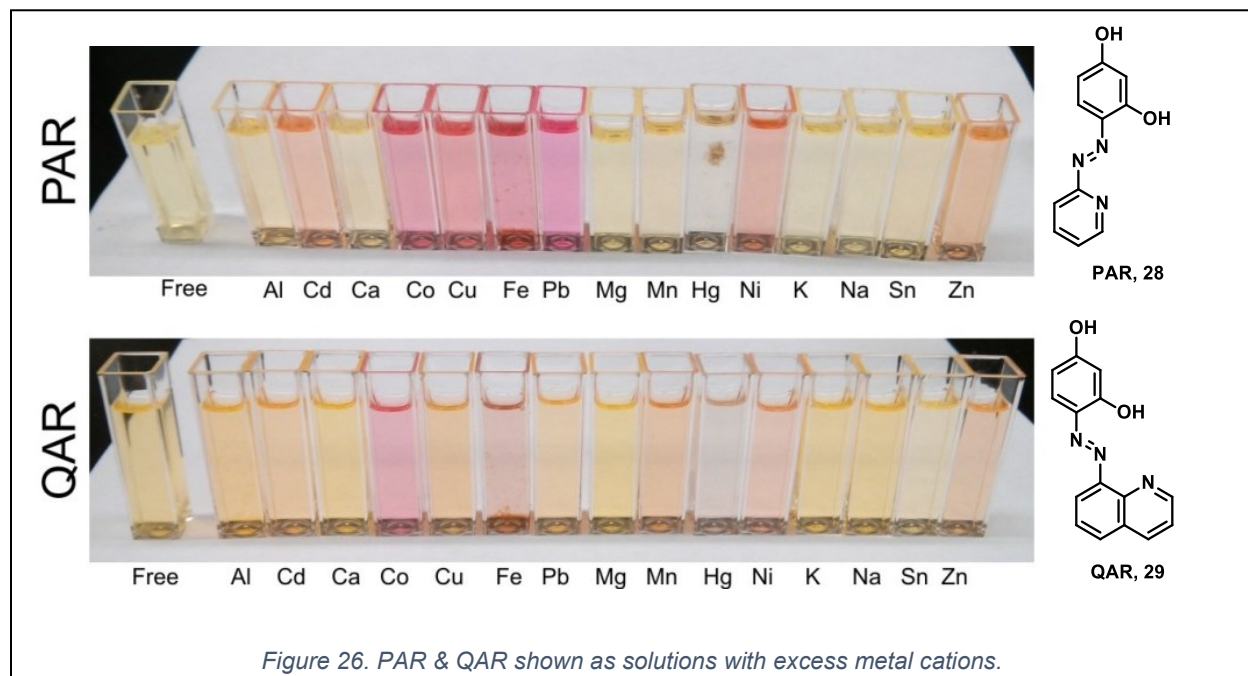
Complexation colorimetric indicators has largely been used as a single use analysis due to the complexity in separation from the analyte after the measurement has been made. However, immobilization in solid supports has been shown as an

effective solution to overcome this problem.³⁹⁻⁴² This methodology allows for simple processes that can remove the soluble analyte while leaving the chemosensing moiety attached to a scaffold.

Instrument Design and Function

Azo dyes are a class of highly colored organic compounds and are used widely in commercial products(textiles, plastics, cosmetics, etc.).⁴³ 4-(2-Pyridylazo)resorcinol (PAR, **28**) is one of a class of azo-dye chemosensors useful for identifying and quantifying metal ions.^{44,45}

Although azo-dyes have useful metal sensing properties, they typically have poor selectivity. As shown in **Figure 26**, PAR has a visible response to about half of the metals shown and 4-(8-quinolylazo)resorcinol (QAR, **29**) has a visible response to a different set of the same metals.⁴⁶ Various chemists have focused on developing chemosensors with high selectivity to single metals.⁴⁷⁻⁵⁰ However, due to the advances in computational modeling we believe



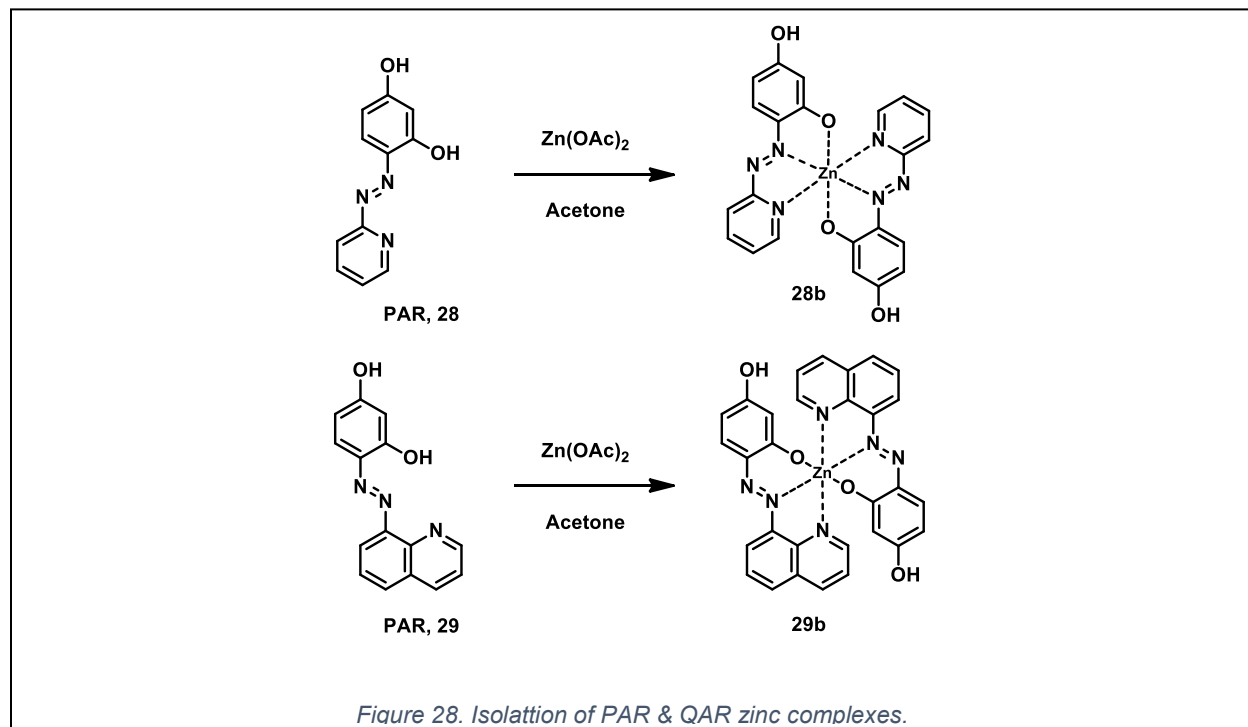
	Al	Cd	Ca	Cr	Co	Cu	Fe	Pb
PAN-7OH	NR	519nm/565nm	NR	454nm(S)	530nm	536nm	464nm(S)	515nm
PAN-4OH	NR	NR	NR	NR	481nm	476nm	419nm(S)	NR
PAN-1,5OH	365nm	567.5nm	NR	NR	635.5nm	601.5nm	599.5nm	585nm
DAR	335nm	305nm/410nm	310nm/416.5nm	332nm/415.5nm	352.5nm(S)	344nm(S)	S	300.5nm/411nm
QAN-1,5OH	NR	NR	NR	545nm	NR	546.5nm	S	534nm(S)
QAN-1A	NR	NR	NR	498nm(S)	581.5nm	532.5nm	471nm(S)	NR
QAN-4OH	NR	NR	NR	456nm(S)	568nm	526nm	S	450nm
QAN-7OH	NR	NR	NR	472.5nm(S)	NR	485nm	S	NR
PAR	NR	497nm	NR	X	509nm	509nm	491nm/530nm	521nm
QAR	468nm	453nm	NR	NR	525nm	492nm	S	453nm
DAR*	NR	NR	NR	X	451nm	NR	NR	NR
	Mg	Mn	Hg	Ni	K	Na	Sn	Zn
PAN-7OH	NR	NR	447nm	525nm/564nm	NR	NR	443nm	513nm/550nm
PAN-4OH	NR	NR	392.5nm	492nm	NR	NR	403.5nm	491.5nm
PAN-1,5OH	NR	566.5nm	572.5nm	602nm	NR	NR	482nm	567.5nm
DAR	332.5nm/423.5nm	330nm	302.5nm	343.5nm	328.5	330nm	410.5nm	338nm
QAN-1,5OH	NR	NR	543.5nm	NR	NR	NR	NR	NR
QAN-1A	493.5(S)	NR	511.5nm	539.5nm	NR	NR	NR	528nm
QAN-4OH	NR	470.5nm	480nm	550nm	NR	NR	460nm	528.5nm
QAN-7OH	NR	NR	NR	NR	NR	NR	NR	NR
PAR	NR	NR	414nm	495nm	NR	NR	393nm	491nm
QAR	NR	463nm	NR	386nm/492nm	NR	NR	413nm	388nm/490nm
DAR*	NR	NR	NR	NR	NR	NR	NR	NR

Figure 27. PAR and other synthesized dyes analyzed for their metal selectivity and λ_{max} for each specific metal shown. Dye-Metal pairs that showed no response are shown in red, small shifts in yellow, and large responses in green.

we can use this semi-selectivity to our advantage.⁵¹⁻⁵³ Efforts initiated by Sarah Oehm and continued by Trevor Hagemann have focused on developing a large array of azo dye chemosensors in the hopes of finding a specific group that would be capable of accurately discriminating between a large number of metals with only a few chemosensors.⁴⁶ In collaboration with the Geissinger group, we have assessed these synthetic dyes and their response to a variety of soluble metals.⁵⁴

In order to turn the azo dyes in to reusable chemosensors we needed a method to easily separate the metal and dyes after their initial use. By forming covalent attachments between the azo dyes and an optically transparent solid support, we could utilize their optical properties and rinse away the metals after the analysis regenerating the original chemosensor.

The first method by which we chose to attach the dye was alkylation. In order for the chemosensors to retain their metal sensing properties we have to use only the non-



ligating atoms present in the azo dye for these alkylations. PAR ligates metal ions through the pyridyl nitrogen, one of the azo group nitrogens, and the phenol adjacent to the azo group (**Figure 28**). The phenol in the para position to the azo group does not participate in the metal chelation and can be used as a point for attachment to the solid support. Many azo dyes contain an additional group like PAR. By first isolating the metal-dye complex and then performing the alkylation reactions, the binding pocket is protected from undesired alkylation.

The chosen solid support would need to be robust, optically transparent, water compatible and allow for diffusion of aqueous bound analytes. Various solid supports were considered but we focused solely on cellulose and hydrogel polymers. Initially cellulose-based dialysis membranes were investigated by Sarah Oehm. While she found that the dye could be successfully attached via modification of the hydroxyls found in the cellulose, the membrane films displayed a high degree of light scattering making spectral interpretation difficult.⁴⁶

Hydrogels are well known to possess all of our desired characteristics, without the issue of light scattering.⁵⁵ However, when made in ways to optimize their water content, they become increasingly softer and more fragile, a problem familiar to anyone who wears corrective contact lenses. In order to compensate for this, we proposed to perform the hydrogel polymerization in the presence of a glass surface that has been derivatized with terminal polymerizable functional groups.⁵⁶⁻⁵⁸ The result of this method would provide an optically transparent hydrogel solid support with a rigid backing. Two general methods for how we went about generating our derivatized glass were solution phase methods using 3-(trimethoxysilyl)propyl methacrylate (TPM) and gas phase

methods using (3-aminopropyl)trimethoxysilane (APTMS) These methods will be discussed in further detail later in this chapter.

Once the hydrogel with covalently attached azo dyes has been made it could be placed in an analyte solution and optical measurements could be made. A general schematic of an instrument capable of both identification and quantification of an unknown mixture of metals in a flowing stream is shown in **Figure 29**. The instrument would use multiple hydrogel polymers each with a different azo dye. These polymers would all be placed in the same analyte stream and individual UV/Vis absorbance spectra would be collected and processed using a primary least squared (PLS) model to determine the identity and concentration of the metals present. The focus of the rest of this chapter will detail the work I have done to develop the hydrogel polymers, the attachment of the dyes, and alteration of the diffusion characteristics.

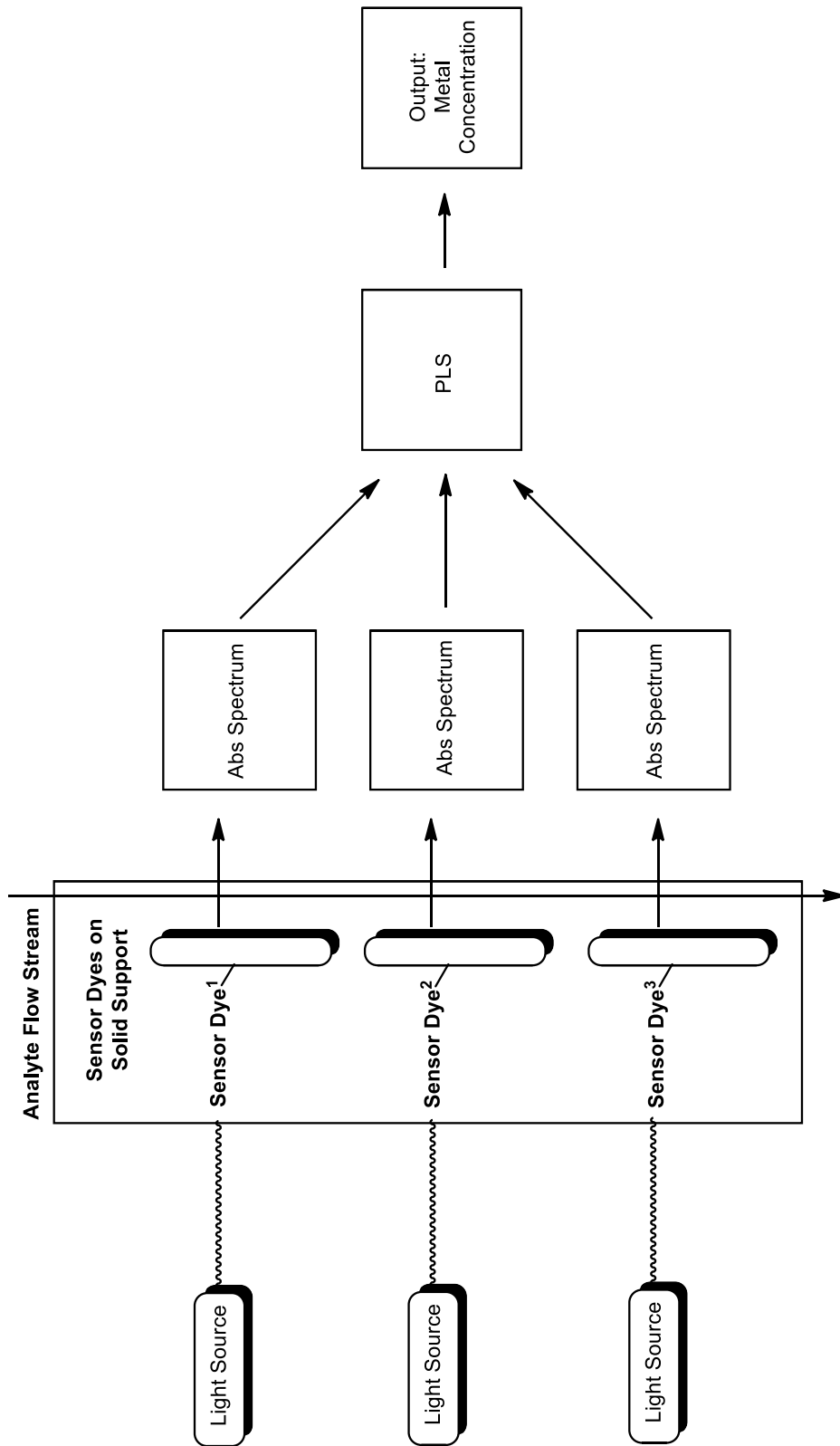
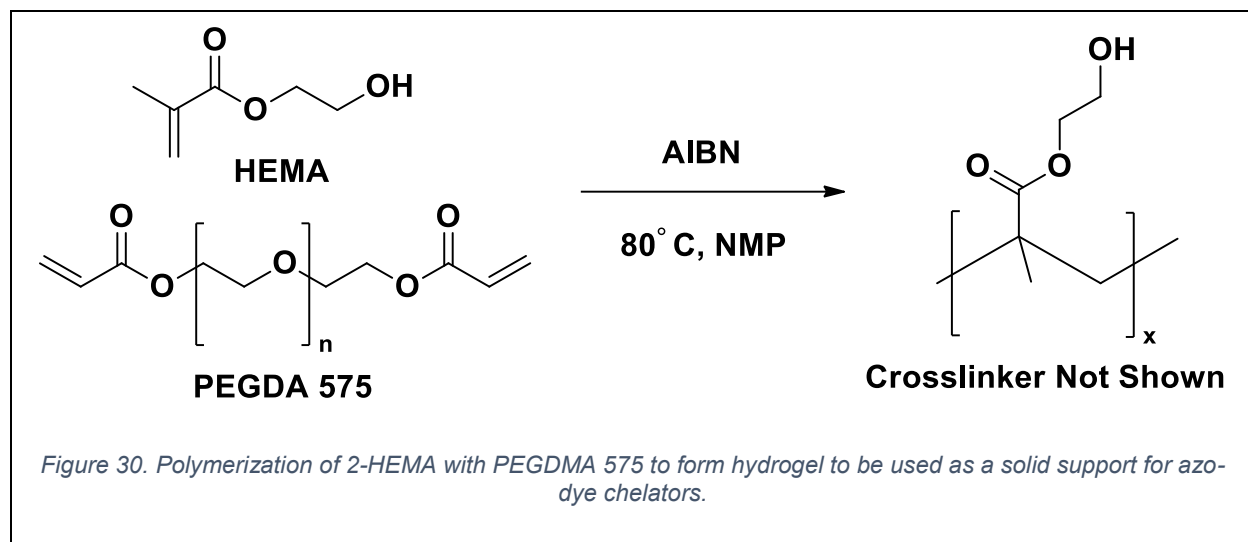


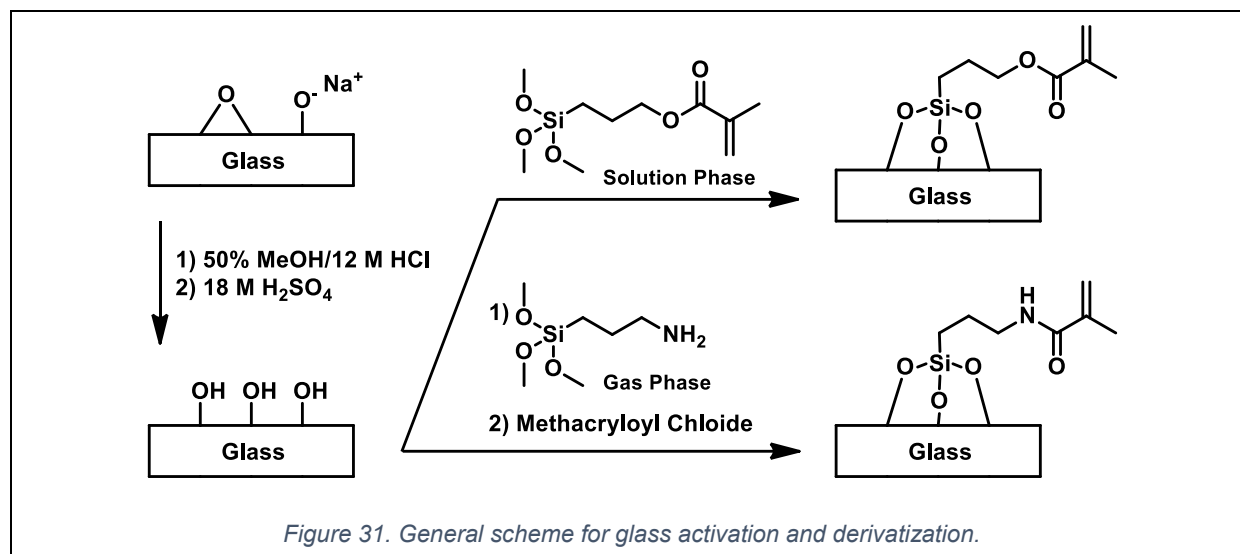
Figure 29. General schematic for proposed instrument.

Preliminary Work on Hydrogel Solid Support

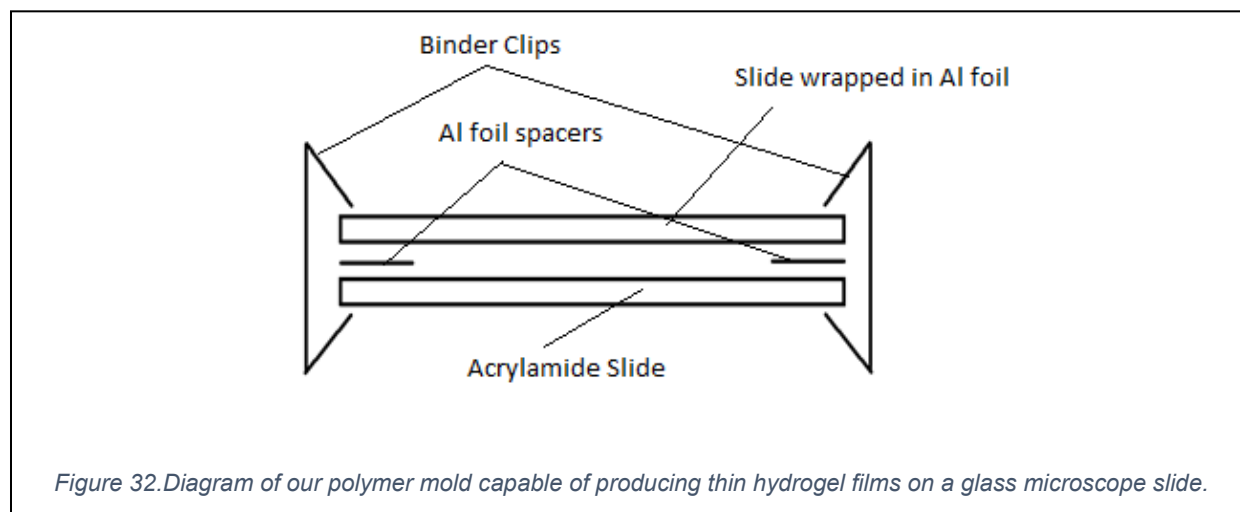


Initially the hydrogel polymer was synthesized using hydrophilic monomers that are commonly used in contact lenses.⁵⁹ Using 2-hydroxyethyl methacrylate (2-HEMA), polyethylene glycol diacrylate (Avg MW 575, PEGDA575) as a crosslinker, and azoisobutyronitrile (AIBN) as a thermally induced free radical initiator we were able to generate a hydrogel with a high concentration of hydroxyls that could be modified to allow for alkylation to our sensor dye complexes (**Figure 30**).

Glass slides were activated using concentrated acid baths and silanized with AMPTS followed by acylation with methacryloyl chloride first. The results were inconsistent using solution phase methods. We theorized this poor silanization was due to the basic properties of the amine group however the addition of mild acids did not improve the results. Polymers formed on the glass surface tended to delaminate from the surface. While optimizations to this method were ongoing, attention was shifted to silanization with TPM (**Figure 31**). While this method produced more consistent results, its long-term hydrolytic stability was still a concern. Optimization of the glass derivatization will be discussed later.

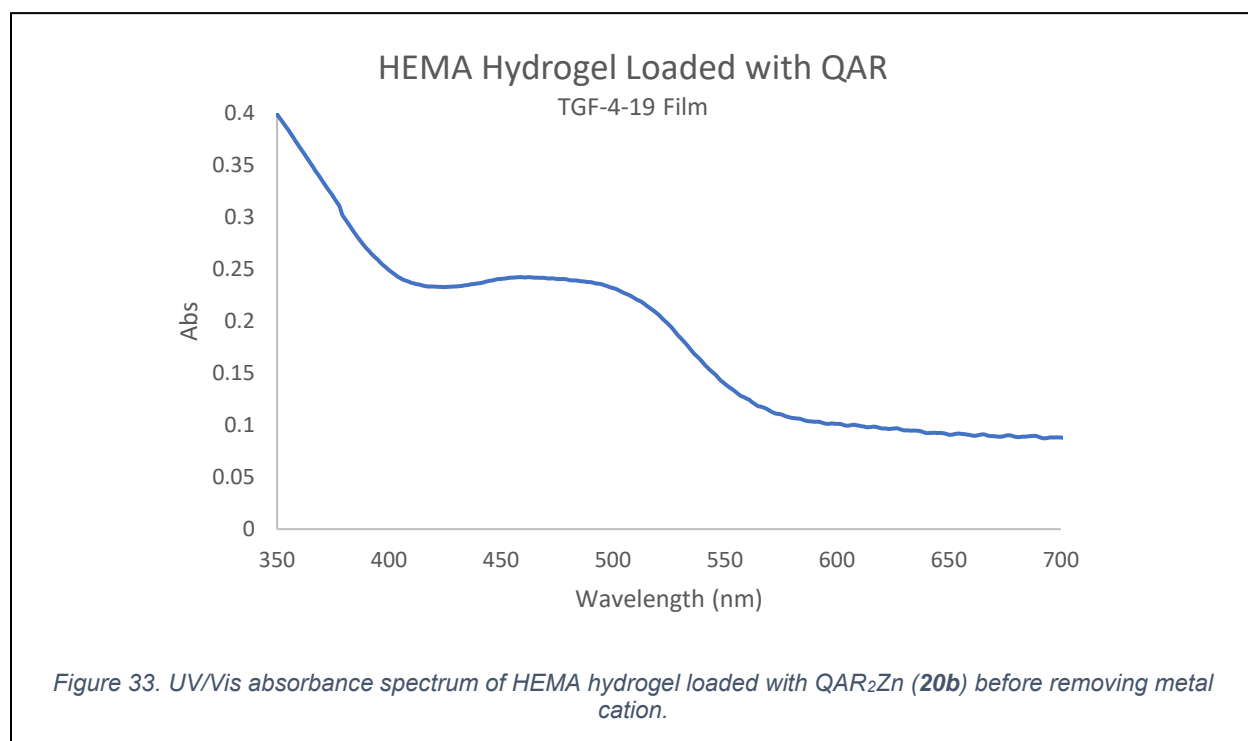


At first polymers were formed using in a mold consisting of two glass slides, where only one was submitted to silanization conditions, separated by a thin spacer made out of aluminum foil (**Figure 32**). The slides were clamped together with ordinary binder clips after loading of the monomers in the void between the slides and placed in a heated chamber to initiate polymerization. While this method was somewhat successful, it was challenging to remove the underivatized slide after polymerization



without destroying the formed polymer. Easier removal of the cover slide was accomplished by wrapping it with aluminum foil.

Soaking the glass-backed hydrogel in THF, methanesulfonyl chloride, and triethylamine followed by alkylation with QAR₂Zn (**29b**) produced a highly colored hydrogel. Repeated rinses of this gel did not produce colored washes, indicating covalent attachment of the dye. To our delight, the polymers did appear to change color upon exposure to zinc ions and returned to the zinc free color in solutions of buffered (pH 7) EDTA. Spectral analysis of this film had less light scattering than the cellulose based films that Sarah had obtained but suffered from low dye loading (**Figure 33**).⁴⁶



Optimization of Hydrogels

After seeing that the hydrogels were a feasible option as a solid support, I sought to improve the polymers. Although the scattering was lower than we had seen in cellulose, a small degree of scattering was still observed. This was believed to be

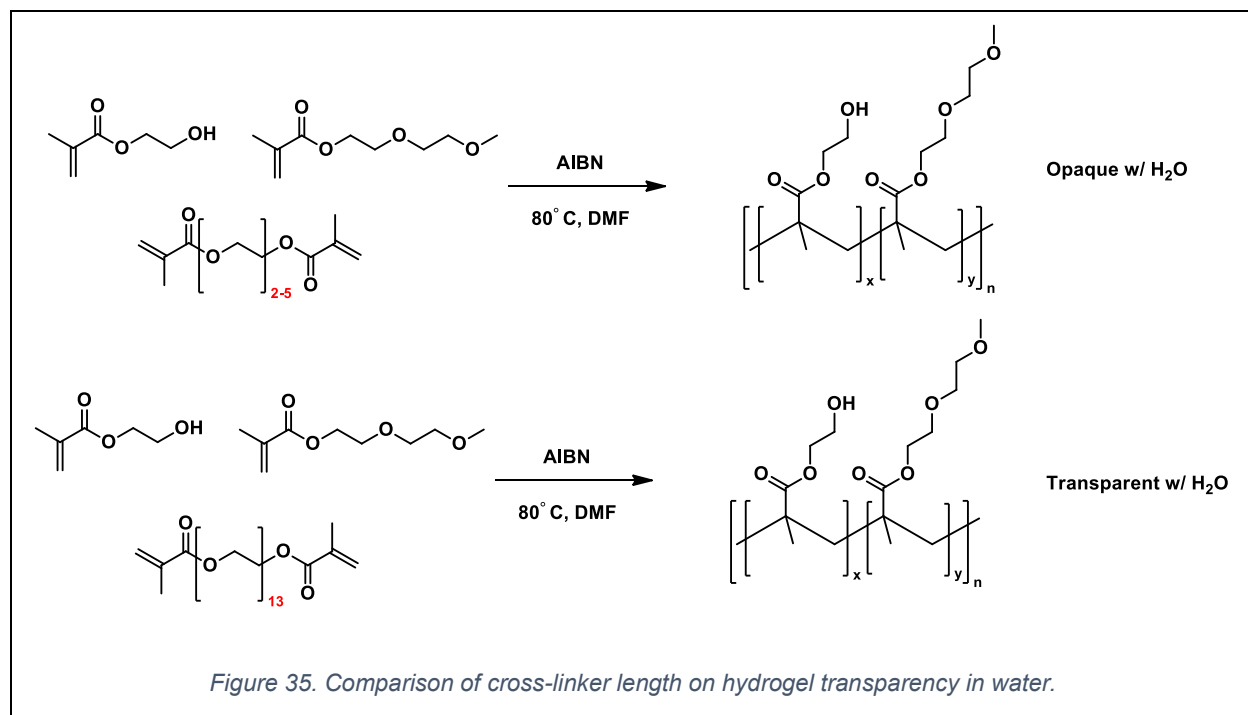
derived from the rough surface due to the aluminum wrapped cover slide. This was easily addressed by using glass slides derivatized with octadecyltrichlorosilane⁶⁰ which, when used as the cover slide gave a much smoother optically transparent polymer.

Determination of the optimal co-solvent and co-solvent concentration was first done while exploring alternative polymer compositions. A quick assessment was performed to compare the use of an equimolar amount of methoxyethyl acrylate (MEA) with the HEMA with varying amounts of water and acetonitrile as co-solvents. Using a co-monomer decreases polymer crystallinity and allows for a more solution like environment inside the polymer bulk.⁶¹ Both monomer compositions examined with water as a co-solvent with, the resulting polymers were opaque and white in color indicating a very high degree of light scattering by the polymer. In contrast, a 1:1 ratio of HEMA and MEA with acetonitrile as a co-solvent worked much better generating transparent polymers when solvent was below a 60% (v/v) concentration. Without the addition of the co-monomer MEA, the polymers did not form at high concentrations of acetonitrile and phase separated at the lower range examined. This experiment

Monomer Solution	Solvent					
	% (v/v) Solvent	50	60	70	80	90
HEMA (50% PEGDMA 575)	Water	White/Bubbles/Rubber Like	Opaque/White	Opaque/White	Opaque/White	Opaque/White/Soft
HEMA-co-MEA (1:1)(50% PEGMA 575)	Water	White/Bubbles/Rubber Like	Opaque/White	Opaque/White	Opaque/White	Opaque/White/Soft
HEMA (50% PEGDMA 575)	Acetonitrile	Biphasic	Biphasic/did not retain all solvent	did not retain all solvent	did not retain all solvent	Did not polymerize
HEMA-co-MEA (1:1)(50% PEGMA 575)	Acetonitrile	Clear	Clear	Clear/Phase Separated	Did not polymerize	Did not polymerize

Figure 34. Optimization of hydrogel optical transparency.

showed that the mixed monomer composition gave optically transparent hydrogels even after polymerization was complete (**Figure 34**).

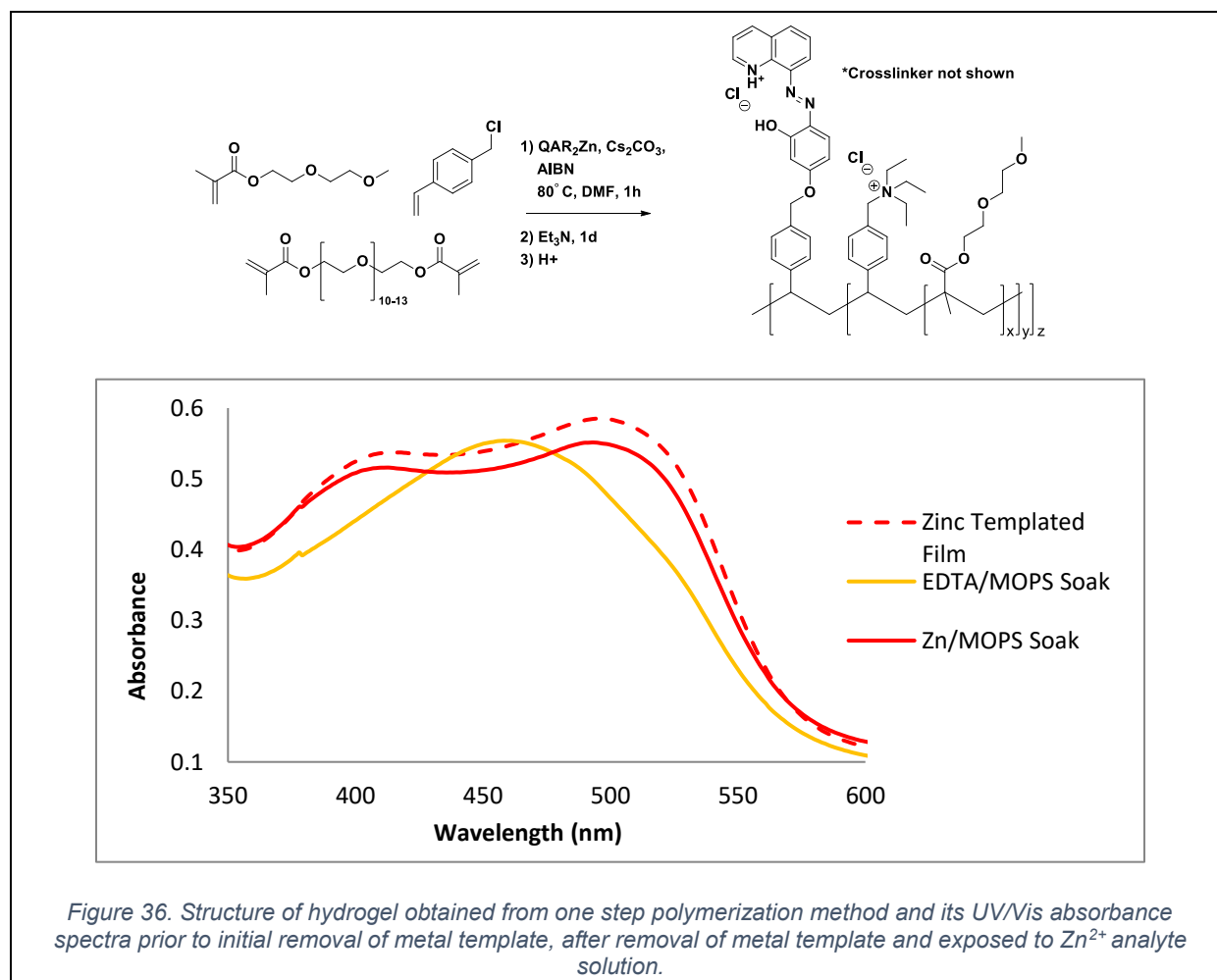


After preliminary optimization, the hydrogels polymerized using acetonitrile as a co-solvent became opaque after being exposed to water. The literature suggested this may be due to the size of the cross-linker.⁶² The crosslinker poly(ethylene glycol) dimethacrylate (Avg MW: 750) (PEGDMA 750) was compared to the optimized results. The polymers with the longer cross linker remained transparent when the soaked in water (**Figure 35**).

Having in hand a method to produce an optically transparent solid support, we set out to covalently attach a controlled amount of sensor dye to the polymers at a high enough concentration to facilitate optical measurements. Sarah Oehm developed methods to attach sensor dyes to the hydroxyls present in cellulose and replicated these methods with some of the hydroxy based polymers that I had been developing.

Her method involved activating the hydroxyls with carbonyldiimidazole, acylating to 1,9-diamino-3,6-oxanonane, amide coupling to t-butyl bromoacetate, and finally alkylation with the sensor dye. This method gave colored films but with loading levels too low to make accurate optical measurements.⁴⁶

A more direct alkylation was thought to be more robust. Chloromethylstyrene (CMS) is a polymerizable alkylating agent and was introduced to the polymer in the monomer solution. Acetonitrile was replaced with DMF, a solvent more preferential for alkylation reactions. The HEMA was replaced with 2-(2-(methoxy)-ethoxy)ethoxy methacrylate (MEEMA) as HEMA could not be used because it would slow the S_N2



alkylation of the azo dye. A MEEMA-co-CMS (8:1) (1% PEGMA 575) was prepared using a DMF co-solvent containing the QAR₂Zn (**29b**) complex with 2 equivalents of cesium carbonate (**Figure 36**). Performing the alkylation during the polymerization would produce hydrogels with higher dye loading with a homogenous distribution. Additionally, the heat needed for the polymerization would increase the rate of dye alkylation.

The hydrogels obtained by this method were more intensely colored than previous dye bound polymers. When exposed to pH 7 buffered EDTA solutions, the color change showed the zinc was being removed. And after being exposed to solutions containing dissolved zinc the characteristic zinc bound red color returned. After a few iterations of this cycling, the change in color became less pronounced. We thought this was due to excess alkylating agent remaining after the polymerization was complete and after removing the Zn²⁺ template the interior hydroxyl of the dye could latch down removing its metal sensing properties. To address this, the hydrogels were soaked in a 5% trimethylamine in DMF solution prior to removal of the metal template. The benefit to this would be two-fold, first any excess alkylating agent would be consumed and second, a cationic tertiary alkylammonium moiety would be present that would perturb the internal properties of the polymer bulk. The resulting polymer gel demonstrated a color change upon treatment with metal ions that could be reversed using MOPS buffered EDTA. This process could be cycled multiple times without any loss in signal. There was a small decrease in signal after the initial removal of the metal template. This is observed in all cases of the dye metal complex being used and is due to the

occurrence where only one of the dyes in the complex becomes alkylated and the other washes out after removal of the template.

In addition to this method that combine polymerization and alkylation, an alternative method was explored. Pre-polymerization alkylation was achieved by treating PAR₂Zn (**28b**) with 4-(chloromethyl)styrene in the presence of cesium carbonate (**Figure 37**). The alkylation product **30** was slow to form and needed to be isolated via column chromatography. Polymerizable PAR derivative **30** was combined with MEEMA, PEGMA 575, AIBN and then polymerized into a hydrogel film. This film behaved in a similar fashion to the one-step method but did not show any obvious advantage and was not studied any further.

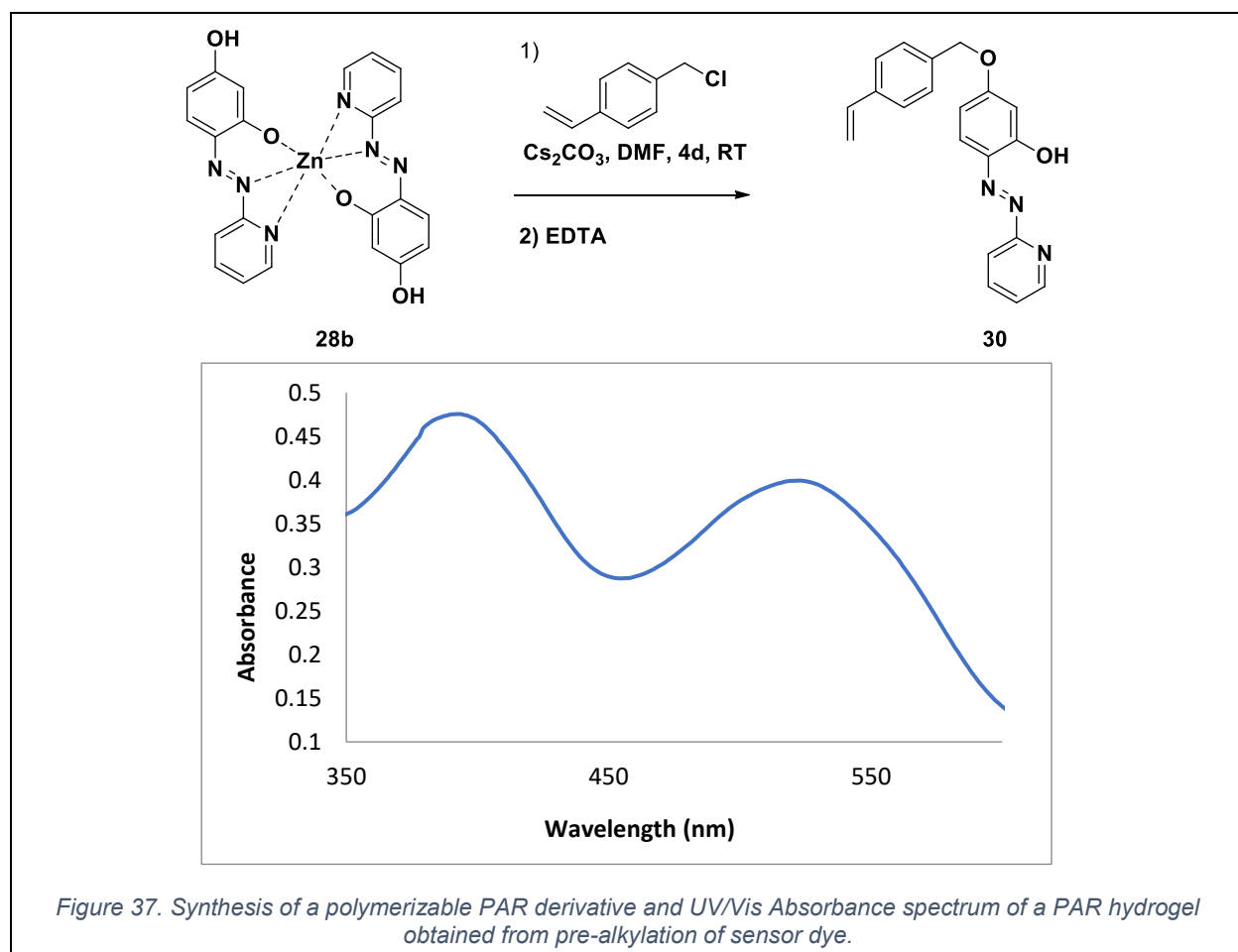
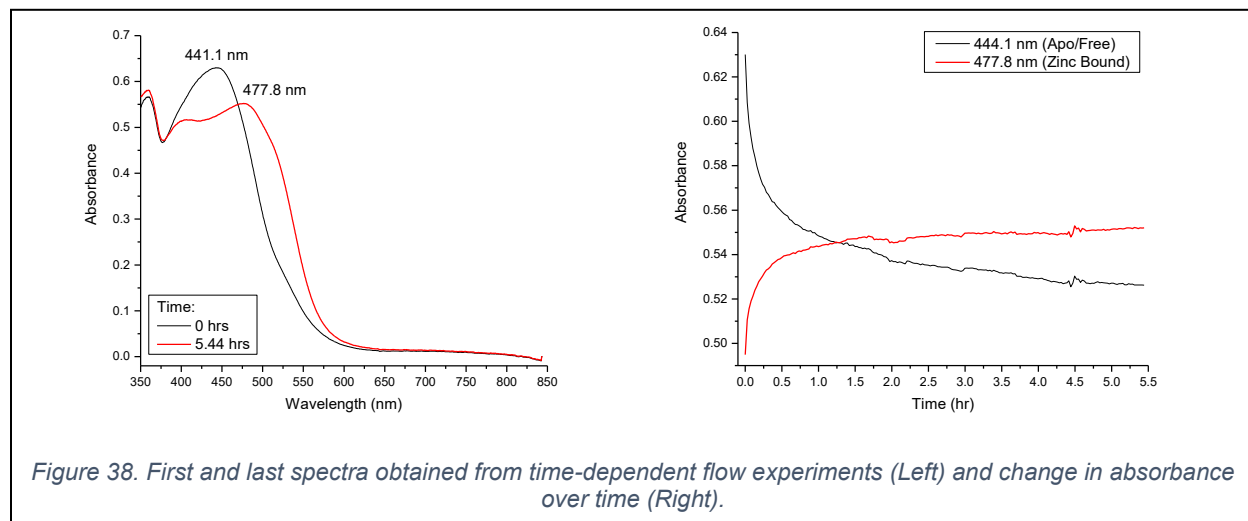


Figure 37. Synthesis of a polymerizable PAR derivative and UV/Vis Absorbance spectrum of a PAR hydrogel obtained from pre-alkylation of sensor dye.

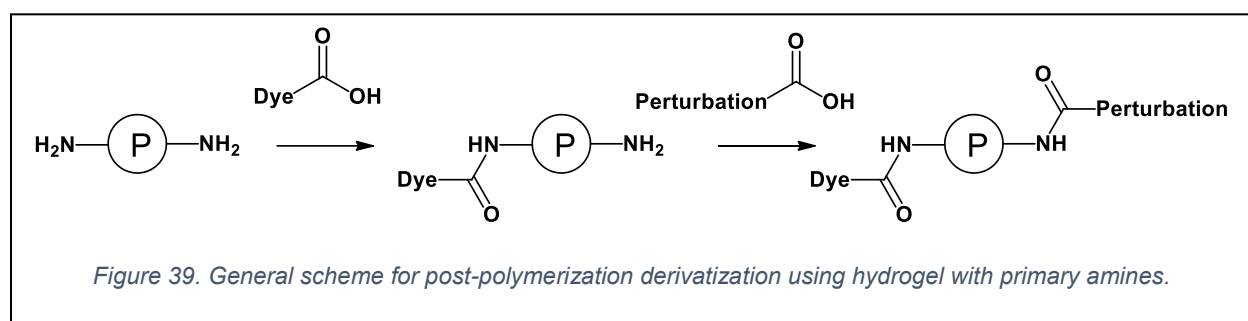
The time-dependent response to solubilized metal ions using the polymers derived from the one-step hydrogel chemosensor method were then performed. Paul Henning in the Geissinger group analyzed the cationic hydrogel chemosensor with a flow cell designed and provided by our industrial collaborator, AquaMetals LLC. The cationic hydrogel displayed the response to 250 μM Zn^{2+} (**Figure 38**).



While the one-step method of alkylating polymers was successful in demonstrating the utility of these covalently tethered azo-dye chemosensors it was thought to be challenging to alter the various functionalities. Some dyes tested by this method showed very low loading and introducing other moieties other than tetraalkylammonium were proposed but not attempted due to their complexity. Attention was shifted to focus on developing a more versatile approach that would allow for more facile changes to the parts we saw as important to the hydrogel structure, the specific azo dye to attach and the charge of the perturbation moiety.

Sarah had demonstrated the viability of using amine acylation to attach the dyes with moderate success.⁴⁶ Her scheme was hindered only by the number of modifications needed. Low loading was an issue but could be improved with a more

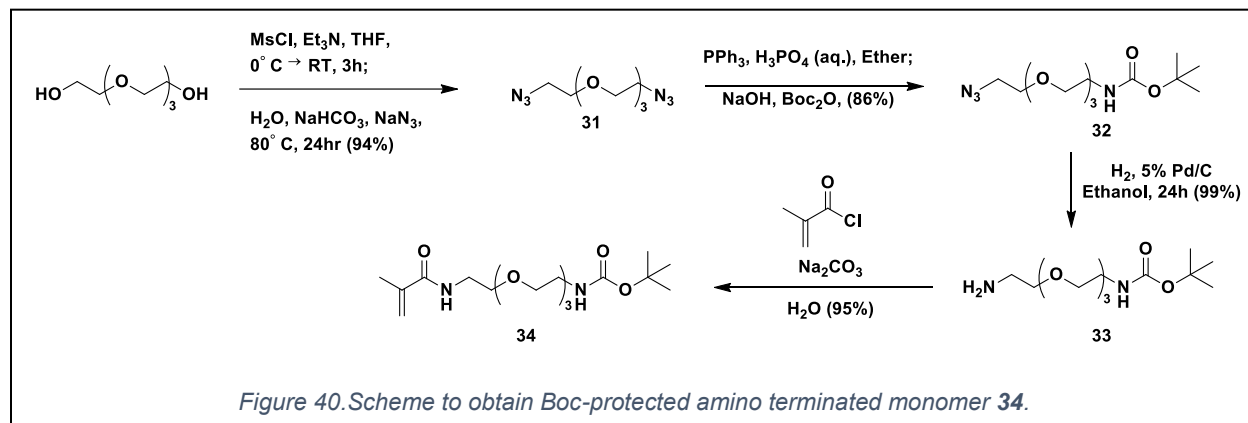
robust scheme. Alkylating the dye with *t*-butyl bromoacetate using a solution phase reaction and removing the ester to obtain the free acid would give a derivative capable of amine acylation. If a polymer could be made with a high concentration of amines, the amide forming reaction would be the only reaction needed to obtain an azo dye bound hydrogel. In an analogous fashion to how excess alkylating agent was consumed in the one step method, the remaining amines could be used to introduce a variety of perturbation moieties through acylation (**Figure 39**).



Development Towards a more Amino Terminated Monomer

Robust methods for post-polymerization dye attachment were desirable to produce hydrogel polymers with a large variety of azo dye chemosensors that would be needed for viable PLS modeling. Due to the availability of efficient amide coupling reagents, a hydrogel with a high concentration of primary amines was developed. Covalent attachment of azo dyes derivatized to contain carboxylic acids could be achieved by polymer acylation. Various charged perturbation moieties could be introduced via acylation of the amines not consumed during the dye attachment step. Methacrylate monomers with terminal amines are available commercially but are undesirable due to their propensity for hydrolysis over time. A methacrylamide monomer had to be synthesized.

Synthesis of methacrylamide monomer **34** was started by activating the hydroxyls of terta(ethylene glycol) using methanesulfonyl chloride and triethylamine in THF followed by substitution with sodium azide giving **31** as describe in the literature.⁶³



The diazidotetra(tetraethylene glycol) (DA-TEG) **31** was selectively reduced using a procedure developed by the Schwabacher group⁶³ affording good selectivity for the mono-reduction over the di-reduction. This reaction employs a biphasic mixture of aqueous phosphoric acid and ether solution containing triphenylphosphine to achieve its selectivity. Once one of the terminal azides is reduced to the amine it is protonated at the water-ether interface and pulled into the aqueous layer preventing any further reduction of the other azide.

The selective reduction of **31** was modified to include the protection in the final step of the workup while the product is in aqueous hydroxide. This not only removed the need for an additional step in the synthesis, but also made the final extraction much simpler by increasing the extraction efficiency of **32**. Roughly 16 extractions were needed to extract the unprotected product, but when Boc protected as little as 5 extractions were needed to obtain comparable yields of the Boc-N-aminoazidotetra(ethylene glycol) (BAA-TEG, **32**).

This step Boc protects any small amounts of diamine. This is important because it makes the impurity essentially inert until the polymerization will be performed at which point it can be washed out. Contamination from diazide **31** is easily avoided as it is efficiently washed out of the acidic aqueous reaction mixture with ether.

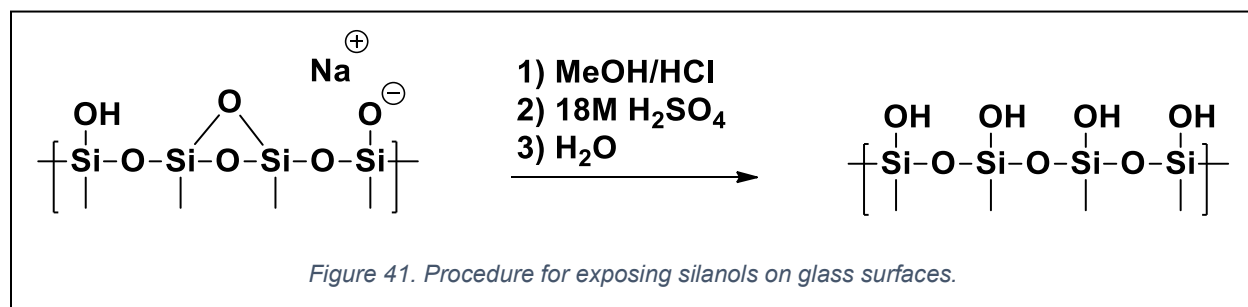
The BAA-TEG **32** was then reduced via catalytic hydrogenation over palladium mono-Boc-diaminetetra(ethylene glycol) (MBDA-TEG, **33**). Monitoring this reaction by TLC proved challenging. It was discovered the protected diamine impurity eluted at the same R_f as **33**. Because the spots are both positive to the acidic ninhydrin stain it difficult to identify the disappearance of the starting material. As a workaround, the plate can be stained with the basic ninhydrin stain which has to be made fresh daily or a small aliquot of the reaction mixture can be worked up and analyzed by NMR. Observing the lack of the peak associated with the hydrogens adjacent to the azide indicates a complete reaction.

Finally, the MBDA-TEG **33** can be methacryloylated to methacryloyl-N-Boc-N'-diaminotetra(ethylene glycol) (MABA-TEG, **34**) using methacryloyl chloride in the presence of sodium carbonate in water. Water was chosen as a solvent to make the isolation of the product an easier process. The free amine is much more reactive than the water and after the consumption of starting material the excess methacryloyl chloride is consumed leaving only the desired monomer soluble in organic solvents giving a clean product after only an aqueous-organic extraction. It is important to add a small fraction of butylated hydroxytoluene (BHT) to inhibit any unwanted polymerization. The entire synthetic procedure goes in an overall 76% yield and has been incorporated in a hydrogel polymer (**Figure 40**).

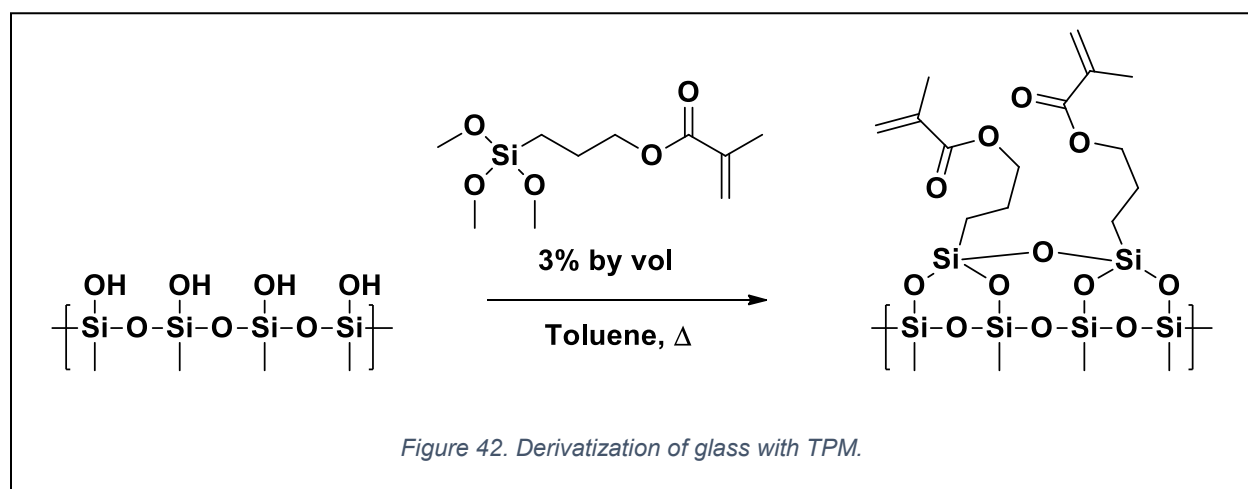
Derivatization of Glass

Glass silanization has been thoroughly researched to give very specific coverages of desired silanes but most require complex and difficult to perform procedures.⁶⁴⁻⁶⁷ Luckily, our interest was less demanding. Primarily, the challenges to overcome were to develop a method to assess the coverage of silylating agent without the use of expensive instrumentation⁶⁶ and to produce enough coverage to give a robust attachment but also not so much as it would reduce the optical transparency of the glass.

Before silanization can be performed, the glass surface must be activated for derivatization. When glass is obtained from the manufacture it is typically found in a state where the surface contains a mix of sodium salts, silyl ethers, and silanols.⁶⁸ The glass slides can also be contaminated with organics left over from the manufacturing process. To prepare the slides for subsequent modification, they must first be cleaned and the functional groups on the surface must be converted to silanols. To accomplish this, the slides were first soaked in a solution of methanol (50% v/v) in 12 M HCl followed by a concentrated sulfuric acid bath according to optimized procedures in the literature (**Figure 41**).⁶⁸

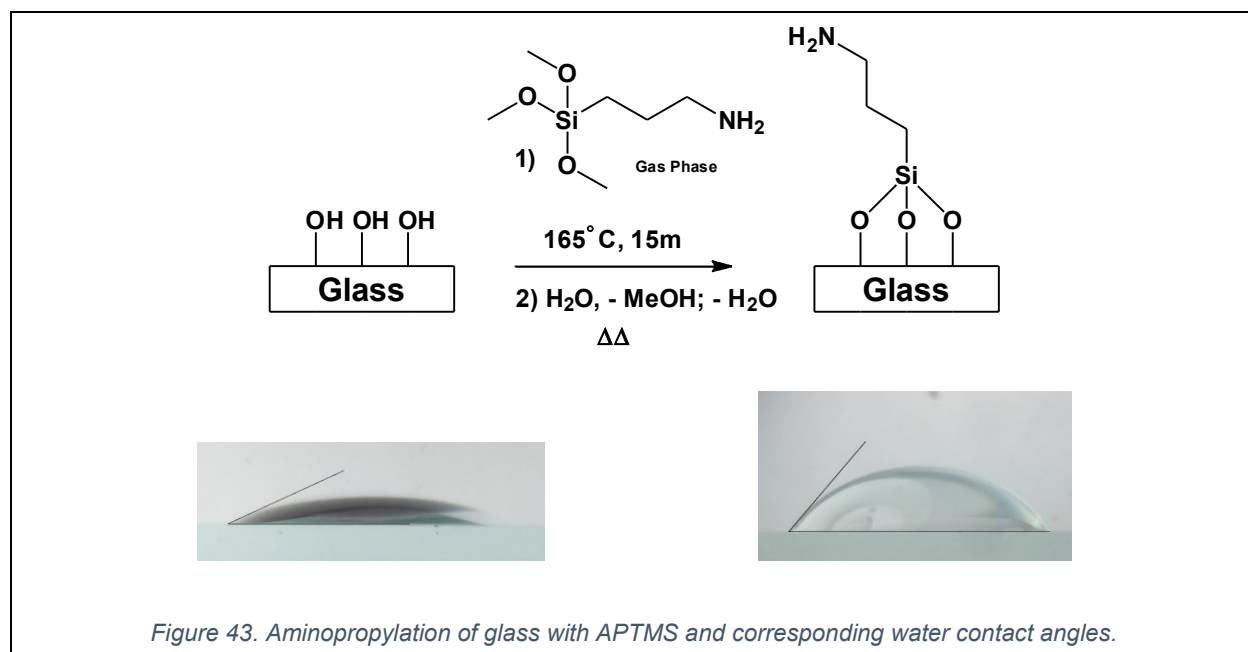


Once the glass surface has been activated, surface silanization is achieved by treating it with an appropriate silylating agent. (3-aminopropyl)trimethoxysilane (APTMS) was used first but results were inconsistent for initial hydrogels. This inefficiency was hypothesized to be due to the basic amine terminus was slowing the silanization process. 3-(Trimethoxysilyl)propyl methacrylate (TPM) was found to give consistent results in the solution phase (**Figure 42**). By treating activated glass slides in a 3% solution of TPM in refluxing toluene and then heating them in contact with a monomer solution appropriate robust polymer attachment was achieved. Polymers formed on these slides showed good attachment to glass with minimal delamination of the polymer due to its swelling properties.



Use of TPM however does have drawbacks. The methacrylate is not as hydrolytically stable as the desired methacrylamide. Silanization has to be done in the solution phase to obtain the coverage we needed for a robust attachment. This requires substantial amounts of reagent to work. There are various examples of gas phase depositions of APTMS under reduced pressure to obtain very specific coverages on the atomic scale.^{67,69} Because we not interested this atomic consistency, modifications of

conditions to perform a gas phase deposition at atmospheric pressure and elevated temperature were examined. Absolute measurements of surface coverage were unobtainable with the equipment available, so an alternative method had to be used. Using known values for water contact angles on the surface of a silanized glass surface, evaluation of consistency of silanization was possible (**Figure 43**).⁵⁸



Viability of a gas phase deposition was assessed by placing an activated slide on small capillary tubes in a petri dish preheated on top of an aluminum block set at various temperatures. Roughly 20 μL of APTMS was dispensed on the hot glass base and the dish was covered with a watch glass. The slide was incubated in the vaporized APTMS removed and rinsed with hexanes, placed back in the dish and incubated with water vapor. This method was optimized by varying the aluminum block temperature and the incubation time with APTMS. Water contact angles were observed by eye. Incubation at 165° C for 15 minutes gave the largest observable contact angles. The incubation with water vapor is necessary to ensure all three methoxy groups are

converted in to silyl ethers to the glass surface.⁶⁵ After rinsing the slides with methanol and then dichloromethane they were then soaked overnight in a solution of methacryloyl chloride (3% v/v) and triethylamine (5% v/v) in dichloromethane. Hydrogel films formed on slides prepared with this method showed significant improvements in occurrences of delamination.

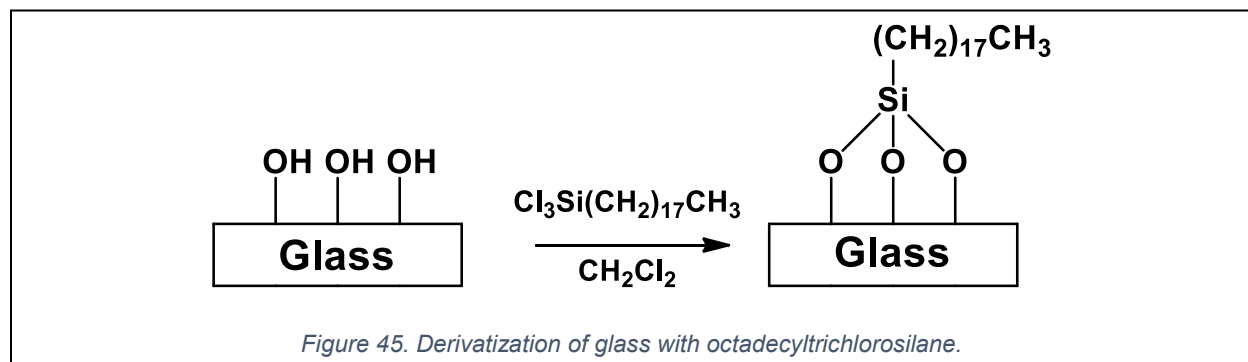
The method was then modified to silanize up to 5 glass slides at a single time. A crystallization dish was used in place of the petri dish and a custom-made slide holder was made to stand 5 slides upright (**Figure 44**). The whole procedure was performed in a vacuum oven, but a large watch glass was still used over top of the crystallization dish to minimize loss of the vapor. It was found that to achieve adequate coverage of all the slides, they had to held vertically and separated by at least 2 cm. Using the vacuum oven, a mild vacuum can be pulled after the water treatment to further facilitate the final step of the attachment process.



Figure 44. Setup to silanize up to 5 slides at a time.

This method was successful in producing glass slides derivatized with hydrolytically stable methacrylamides and greatly reduced the amount of silylating agent needed by a factor of ~200,000.

For a non-stick hydrophobic cover slide for the mold, activated glass slides were derivatized with octadecyltrichlorosilane (**Figure 45**). Water contact angles on this derivatized surface were nearly 90° indicating very good coverage. The procedure used was a solution phase method to derivatize silica gel to C18 silica.⁷⁰ Once derivatized the hydrophobic slides could be used multiple times, checking the water contact angle before each use. If the droplets did not appear to have a contact angle of about 90° or the water would not move freely when the slide was tilted the slide was discarded. On average each cover slide could be used 4 to 5 times before the surface had degraded.



While this procedure does work, it was not modified to minimize the reagent used. Silica gel has a significantly larger surface area than glass microscope slides. The concentration of silylating reagent used was much greater than required and can be significantly reduced and soaking the slides for a longer duration.

Modifications to Polymer Mold

The initial mold discussed earlier in this chapter had a very crude design. Incremental improvements were made in parallel to the polymer development. While the

mold was more of an engineering challenge, it's important to consider the resulting polymer and how it can affect the signal generated.

There are three main parts to the mold design: the rigid backing that the polymers will stay attached to, the hydrophobic cover slide that needs to easily removable after polymerization is complete, and the spacer that is placed in between the two glass slides. The first two parts have already been discussed earlier so the focus of this section will be on the spacer.

The spacer is a key component that gives the polymer its shape and size. To begin the spacer used was household aluminum foil with the center cut out leaving a ~5mm edge going around the edge of the glass slides. The monomer solution was loaded in and clapped snugly with binder clips. This was functional but did not give consistent results. The solution would leak slowly leaving behind large gaps in the film (**Figure 46**). A typical polymer thickness with the aluminum foil was about 5 mil (~125 μm). The thickness was a concern for two reasons: thicker polymers were more prone

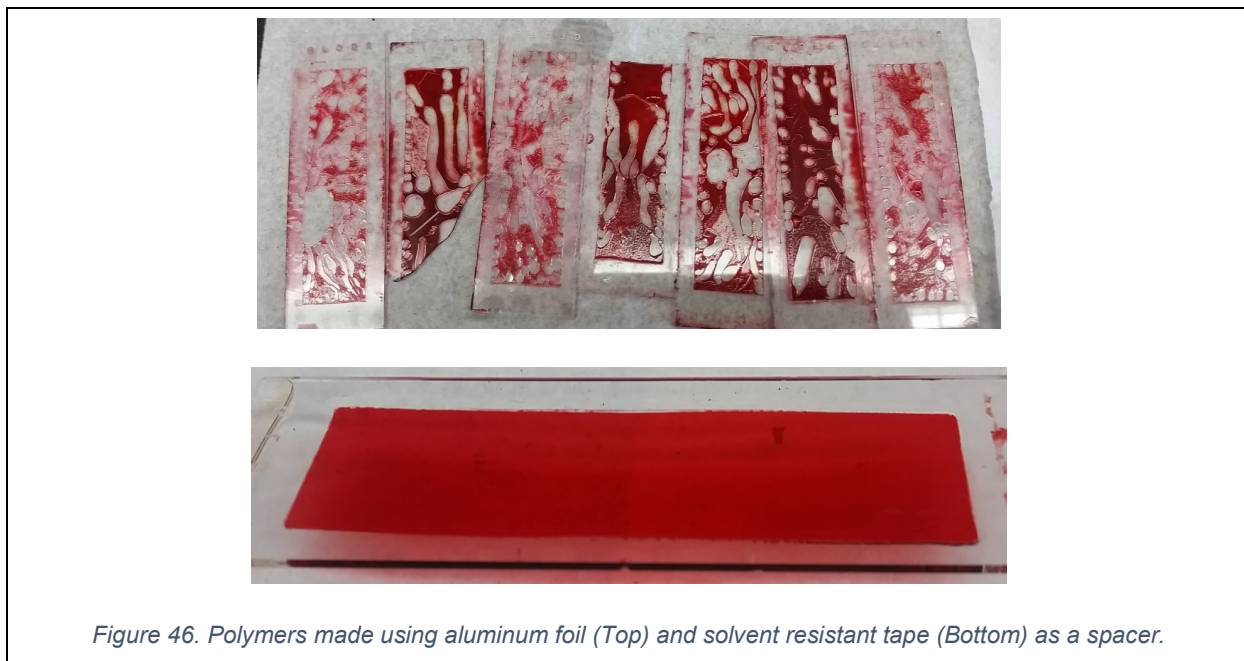


Figure 46. Polymers made using aluminum foil (Top) and solvent resistant tape (Bottom) as a spacer.

to delamination from the glass backing and metals ions would take longer to diffuse to the entire bulk.

Polyethylene tape (thickness: 3 mil; $\sim 75 \mu\text{m}$) with a solvent resistant silicone adhesive was the next iteration. The tape could be applied to the hydrophobic cover slide and voids cut in any shape desired. The reduced thickness of the polymers gave polymers more resistant to swelling. Hand cutting the voids introduced unwanted surface imperfections that occasionally resulted in polymers being pulled off the rigid glass backing when the cover slide was removed. Consistency with polymer shape was again an issue but multiple polymers dots could be polymerized on a single slide. After polymerization was complete, the glass slide was etched between the dots and the dots could be snapped apart and used separately. A stencil was machined to assist with this problem but was labor intensive and not appropriate for producing large amounts of polymers needed for the project goals.

The current mold uses Kapton tape (thickness: 1 mil, $\sim 25 \mu\text{m}$) with a solvent resistant silicone adhesive and pre-cut with 12 circular voids. Examples of the polymers obtained from the Kapton tape spacer are shown in **Figure 47**. This greatly reduced the labor needed to prepare a mold for loading and polymerization, eliminated the cutting process entirely, and minimized the polymer thickness. Again, a significant improvement



Figure 47. Examples of the final amino terminated hydrogel polymers loaded with PAR. The polymer after exposure to Zn^{2+} (Left), buffered at pH 7.2 MOPS (Middle), and in 1 M HCl solution (Right).

in polymers resistance to delamination was observed. In some of the first attempts to make 5 slides each with 12 polymer dots would produce around 30 usable polymers (~50% failure rate) and with the optimized process it was not uncommon to get 60 usable polymer dots. Typically, the only dots that would become unusable did so because of mishandling during the cutting and snapping process. Furthermore, the pre-cut voids could be positioned in essentially the same position on the glass slide every time which allowed for the use of a miter box to guide glass etches.

The mold has been optimized for laboratory purposes. The reduction in polymer thickness improved the resiliency of the polymer attachment and templated Kapton tape allowed for faster production needed for the amino terminated polymer.

Formation of a Versatile Amino Terminated Hydrogel

Amino terminated polymers were formed using the optimized mold and the optimized silanization conditions using MABA-TEG (**34**) in equimolar amounts with 2-hydroxyethylmethacrylate and polyethylene glycol dimethacrylate (Avg. MW 750) as a crosslinker. Delamination from the glass backing continued to be an issue. Polymer inhomogeneity was suspected to be a contributing factor. Large variations in the length of the polymer back bone between crosslinks would result in a more inhomogenous polymer bulk. An uncontrolled polymerization is typically the causing factor.⁶¹ Eliminating factors that could lead to unwanted early termination of the free radical process was an important consideration in achieving viable chemosensing gels. Formyl hydrogens are known to be reactive towards free radicals⁷¹, so it was hypothesized that DMF may be contributing to undesired early termination of the polymerization process. Polymer swelling, using polymers made with either DMF or NMP, was analyzed to find

test this theory. Free-standing polymers, with a 5 mm diameter, were made using the two solvents with a mold consisting of two hydrophobic cover slides. The resulting gels could be evaluated without the rigid glass backing. The free-standing polymers were soaked in various solvents and the swelled diameter was compared to the initial diameter (**Figure 48**).

MABATEG-co-HEMA Hydrogel; PEGDMA 750 (11.5% by mol); 60% (v/v) DMF									
Solvent	DMF	NMP	MeOH	CH ₃ CN	EtOH:H ₂ O (1:1)	H ₂ O	2M HCl	pH 9 Borate	pH 7 MOPS
Boc-Protected	5.5-6	6	5.5-5.7	5.0-5.2	5.0-5.1	4.0-4.2			
-NH ₃ Cl	5.9-6.1	5.8	6.0-6.2	4.2			5.8-6	5.7-5.9	6.2-6.5

MABATEG-co-HEMA (1:1) Hydrogel; PEGDMA 750 (13.2% by mol); 60% (v/v) NMP									
Solvent	DMF	NMP	MeOH	CH ₃ CN	EtOH:H ₂ O (1:1)	H ₂ O	2M HCl/EtOH	pH 9 Borate	pH 7 MOPS
Boc-Protected	5.5-6	6	5.5-5.7	5.0-5.2	5.0-5.1	4.0-4.2	5.0		
-NH ₃ Cl		5.0			5.0	5.0	5.0	~5	~5

Figure 48. Comparison of co-solvent. Numbers indicated the polymer diameter in mm when soaked in each solvent. Free-standing polymers were cured at a 5 mm diameter

Prior to Boc deprotection, polymerization co-solvent did not appear to play a role. Polar organic solvents (methanol, DMF, and NMP) swelled the gel to a larger diameter. Interestingly, acetonitrile was excluded from this trend. Although acetonitrile is polar does not have similar hydrogen bonding characteristics as the other polar organic solvents.^{72,73} After the Boc deprotection, swelling was analyzed again. Consistent with our hypothesis, gels polymerized in DMF were ~20% more susceptible to swelling compared to the gels prepared in NMP. The DMF derived polymers swelled to about a 20% greater diameter from their initial size in nearly all solvent tested. The only

exception was acetonitrile which reduced the diameter by 16%. This is most likely due to acetonitrile interfering with the hydrogen network inside the polymer scaffold. In comparison, after deprotection, the gels polymerized in NMP did not show any observable swelling in all solvents tested. All polymerizations performed were done in NMP moving forward.

Although conditions had been identified to give robust polymers, we were still interested in getting a better understanding of the homogeneity of the polymer. One way about determining this information involves the formation of soluble polymers chains (not crosslinked) and analyzing the average molecular weight and the distribution of molecular weights commonly referred to as the polydispersity index (PDI). These values are typically determined using size exclusion chromatography or gel permeation chromatography. Unfortunately, this instrumentation was not available. Classical methods to determine molecular weight values such as viscometry⁷⁴ gave inconsistent results on a small scale and required too much material to perform on a scale that would be more appropriate. Diffusion-order NMR spectroscopy (DOSY) has emerged as an alternative method for determining molecular weights of polymers.⁷⁵⁻⁷⁸ DOSY is a NMR technique that uses two gradient pulses to determine a diffusion coefficient (D) which can be correlated to the polymer hydrodynamic radius by the Stokes-Einstein equation

$$D = \frac{kT}{6\pi\eta R_H} \quad (1)$$

where R_H is the hydrodynamic radius, k is the Boltzmann constant, η is the solvent viscosity and T is the absolute temperature of the solution.⁷⁹ For polymers of similar structure this relationship can be simplified to

$$D = AM^\alpha \quad (2)$$

where A and α are polymer specific coefficients and M is the molecular weight.⁸⁰ Values for D can be obtained through DOSY by the decay of NMR signals as gradient strength increases. This can be modeled as

$$I = I_0 \exp(-DZ) \quad (3)$$

where Z is a variable that describes the gradient amplitude, the gyromagnetic ratio, the duration of each pulse, and the interval between pulse.⁸¹

For DOSY to give absolute values for molecular weight a known standard needs to be used to build a calibration curve. The polymers used in the amino terminated hydrogels are unique and standards were not available. Instead DOSY was used to as further evidence to confirm NMP was in fact giving a more homogenous polymer bulk compared to DMF. Since the polymers were only varied in their MW and PDI, the values can be compared to determine the larger are more consistent polymer.

Monomer solutions were prepared analogously to those used to form the gels but crosslinkers were excluded. The solution was treated under similar conditions and the crude soluble polymers were used to perform simple DOSY experiments. Values for D were obtained for the polymers from NMP ($2.7858 \times 10^{-10} \text{ m}^2/\text{s}$) and for polymers from DMF ($4.090 \times 10^{-10} \text{ m}^2/\text{s}$). The smaller value for the soluble polymer made in NMP is consistent with the swelling analysis and added further evidence that NMP yields a polymer with a larger molecular weight. There is precedent to determine PDI with DOSY but values were too similar to make any statement with confidence.

Perturbation Moieties & Dye Preparation

To study the effects of ionized functional groups on the sensor response, a library of compounds was synthesized (**Figure 49**). The compounds were synthesized with activated esters to increase the reactivity towards amine acylation. Starting with a known synthesis, *p*-nitrophenyl bromoacetate **36** was prepared.⁸² Refluxing **36** in the presence of triethylamine gave *p*-nitrophenyl N,N,N-(triethyl)ammoniumacetate (**37a**) as a bromide salt in 51% yield. When in the presence of the free amines inside the hydrogel, tetraalkylammonium **37a** would generate an internal cation analogous to the one made after quenching excess 4-(chloromethyl)styrene in earlier versions of the hydrogel.

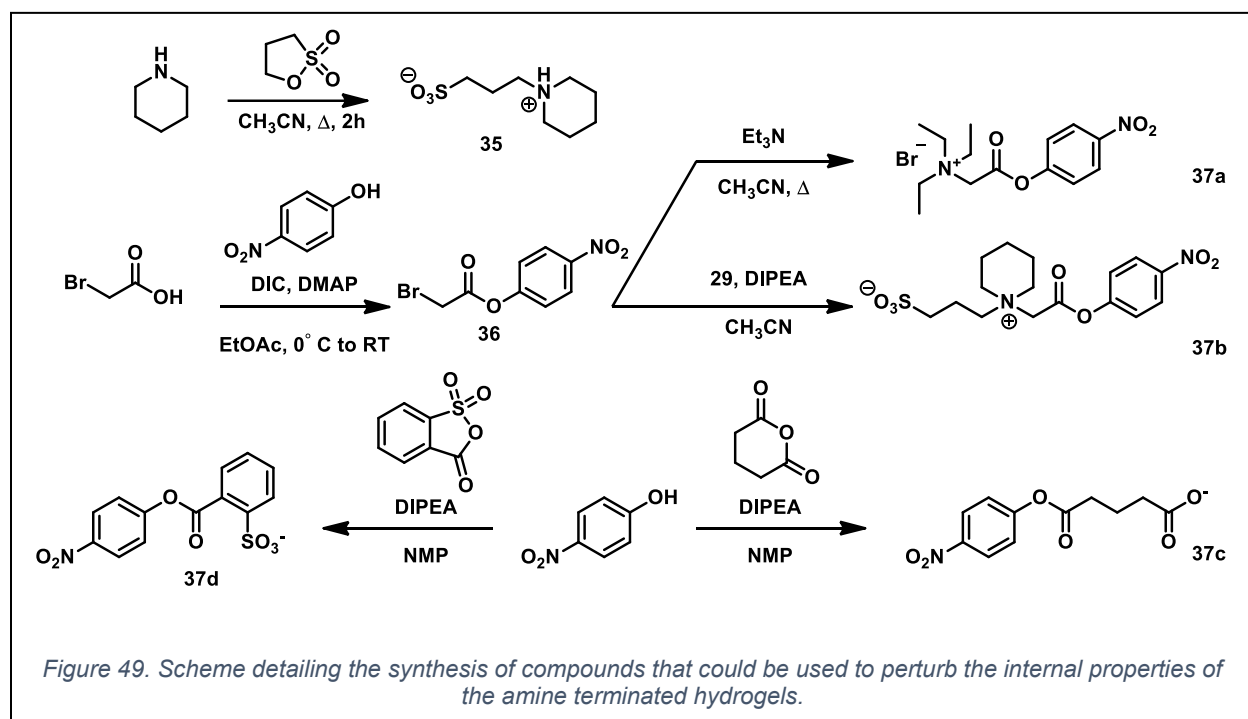


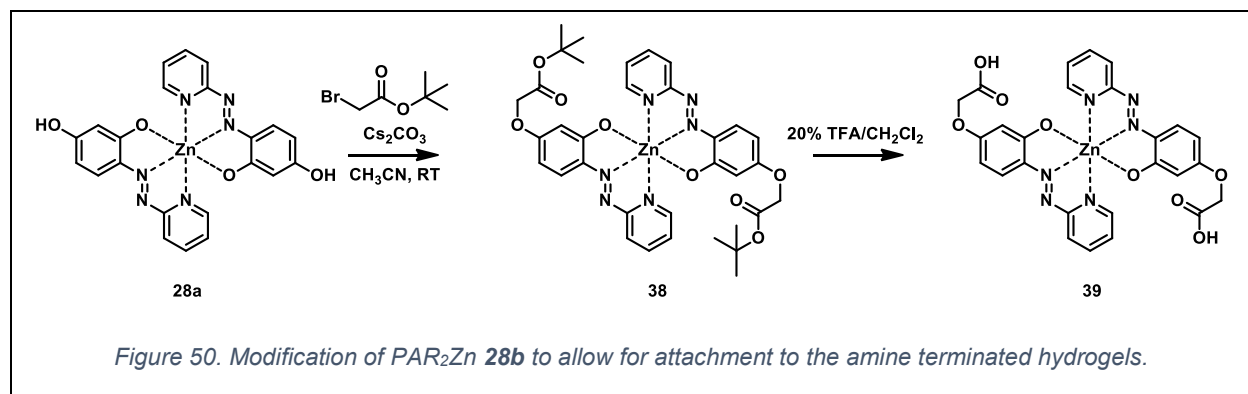
Figure 49. Scheme detailing the synthesis of compounds that could be used to perturb the internal properties of the amine terminated hydrogels.

A zwitterionic compound was synthesized by heating 1,3-propanesultone in the presence of piperidine to give 3-(piperidyl)propylsulfonic acid (**35**). As alkyl sulfonic acids have a pK_a significantly lower than protonated alkylamines compound **35** was already in a zwitterionic state. Also, since **37a** forms fairly readily, triethylamine was an

inappropriate choice since it could undergo a substitution reaction. The reactivity of diisopropylethylamine (DIPEA) was examined and no reaction was observed with **36**. Using excess DIPEA, **35** was heated in the presence of **36** to give zwitterionic **37b** which is structurally similar to (3-(N-morpholino)propanesulfonic acid) (MOPS), a Good buffer that maintains a roughly neutral pH.⁸³ Compound **37b** can be isolated using vapor diffusion crystallization methods by diffusing ether vapor into a solution of **37b** in acetonitrile. This was done only for characterization purposes as the byproducts of the reaction will not interfere with the hydrogel amine acylation and the crude residue is sufficient.

Two anionic moieties were prepared to compare the difference between ligating (carboxylate) and non-ligating (sulfonate) anionic moieties. Treating glutaric anhydride and *o*-sulfobenzoic anhydride with *p*-nitrophenol gave **37c** and **37d** respectively. These proved difficult to isolate without cleaving the active ester and were prepared as solutions to use for polymer derivatization.

The dye-metal complex was again used to protect the metal binding pocket of the azo dye from undesired alkylation (**Figure 50**). In an analogous fashion to earlier dye alkylation procedures, the dye-metal complex was stirred with *t*-butyl bromoacetate to



give ester **38** followed by deprotection in TFA, giving **39** as a dye complex with distal carboxylic acids. To activate **39** towards acylation, amide coupling reagents were used to activate the acid instead of using the *p*-nitrophenyl esters that were used for the perturbation moieties.

Amino Terminated Polymer as a Versatile Assembly

Before large scale efforts could be applied to producing a large number of polymers with various different dye and charged moieties, robust procedures had to be developed in order to ensure the reactions were working as intended.

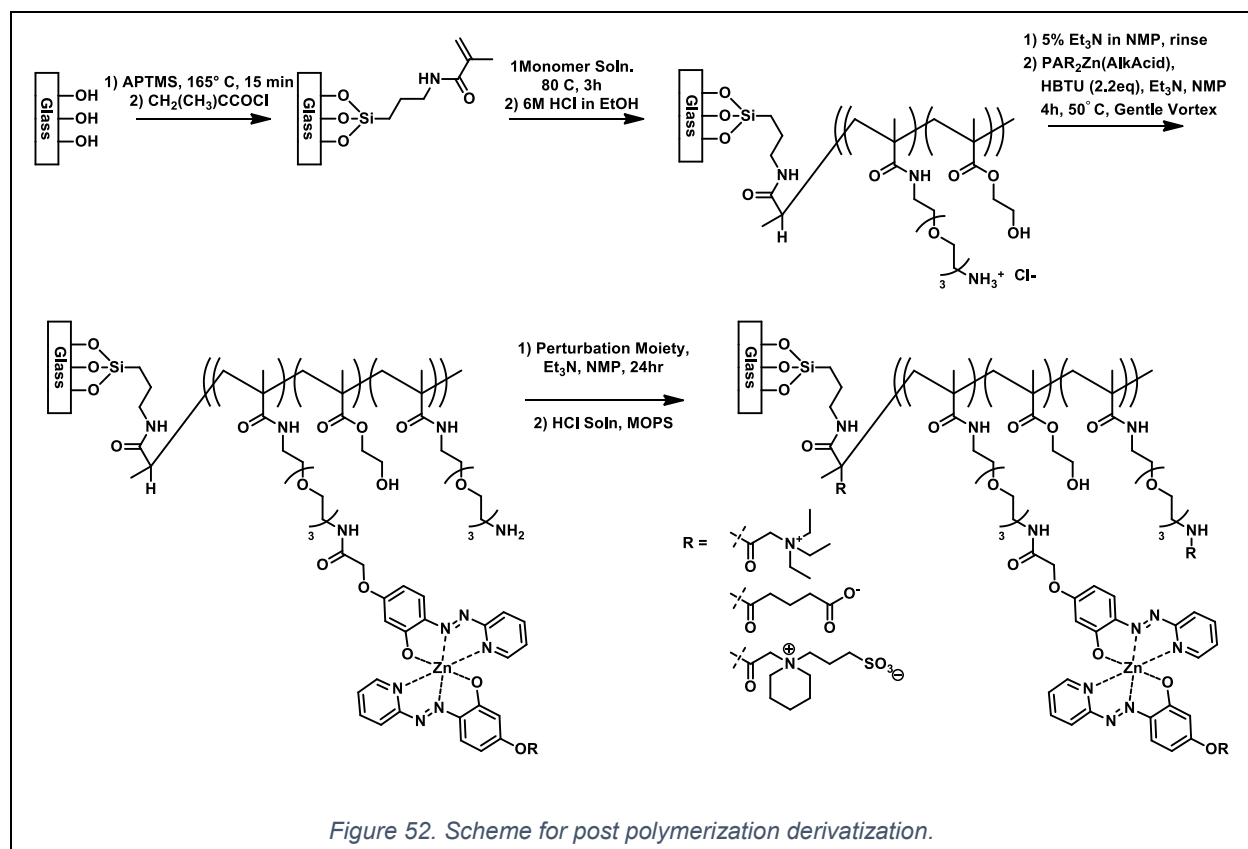
The first step involves loading the dye on to the hydrogel. Polymer dots (MABA-TEG(**34**)-co-HEMA) were soaked in solutions of derivatized PAR₂Zn **39**, hexafluorophosphate benzotriazole tetramethyl uranium (HBTU), and triethylamine in NMP. Initially the acylation was performed without agitation at room temperature. While amide couplings typically achieve completion within 24 hours using stoichiometric amounts of acid and amine, the polymers were only partially acylated after a 24-hour period using a large excess of the dye over the calculated number of amines in the

[Dye Complex] (mM)	1 M HCl	10 mM MOPS	100 uM Zn ²⁺ , 10 mm	Abs(Zn)-Abs(Buffer)
1	0.15	0.27	0.43	0.16
2	0.26	0.42	0.72	0.30
3	0.44	0.37	0.92	0.55
4	0.57	0.42	1.13	0.71
5	0.85	0.64	1.82	1.19
6	1.15	0.73	2.42	1.70

Figure 51. Absorbance values at 508 nm for polymers prepared at the given concentration of metal-dye complex, 2.2 eq. HBTU and >100 eq. triethylamine. Soaked for 24 hours at room temperature without agitation.

polymer dot. This was a surprising result and indicates the diffusion of the dye complex is much slower through the polymer than expected. Serendipitously, the 24-hour soaking period gave polymers with absorbance values appropriate for UV/Vis absorbance spectroscopy using low millimolar concentrations of metal-dye complex **33** in the soaking solution. The absorbance value was correlated with the concentration of the dye acylation solution (**Figure 51**) but not enough data was collected to determine the precise relationship.

The procedure was modified to speed up the dye acylation by agitating gently on a vortexer and heating the solution. At 50 °C with gentle agitation, the polymers could obtain similar absorbance values after only 4 hours using the same low millimolar concentration range (1-6 mM). The complete scheme for the post polymerization modifications is shown in **Figure 52**. Control of the polymer bound dye loading can be



controlled by reaction time, reaction temperature or concentration of the dye in the acylating solution.

Following dye loading, the polymer dot can be swamped with the perturbation moiety compounds developed to acylate the remaining free amines present. There is currently a concern that these may be also acylating the terminal hydroxyls from the 2-hydroxymethacrylate if the conditions are too harsh and is currently being investigated by the Schwabacher group. Using 0.5 to 1 M solutions of the perturbation moieties with excess base and gentle agitation of the solution should be adequate to achieve complete acylation. Methods to quantify the free amines present have been attempted but with inconsistent results. Even for the simple Boc deprotection step, ninhydrin quantitation gave values much lower and much higher than the calculated concentration (**Figure 53**).

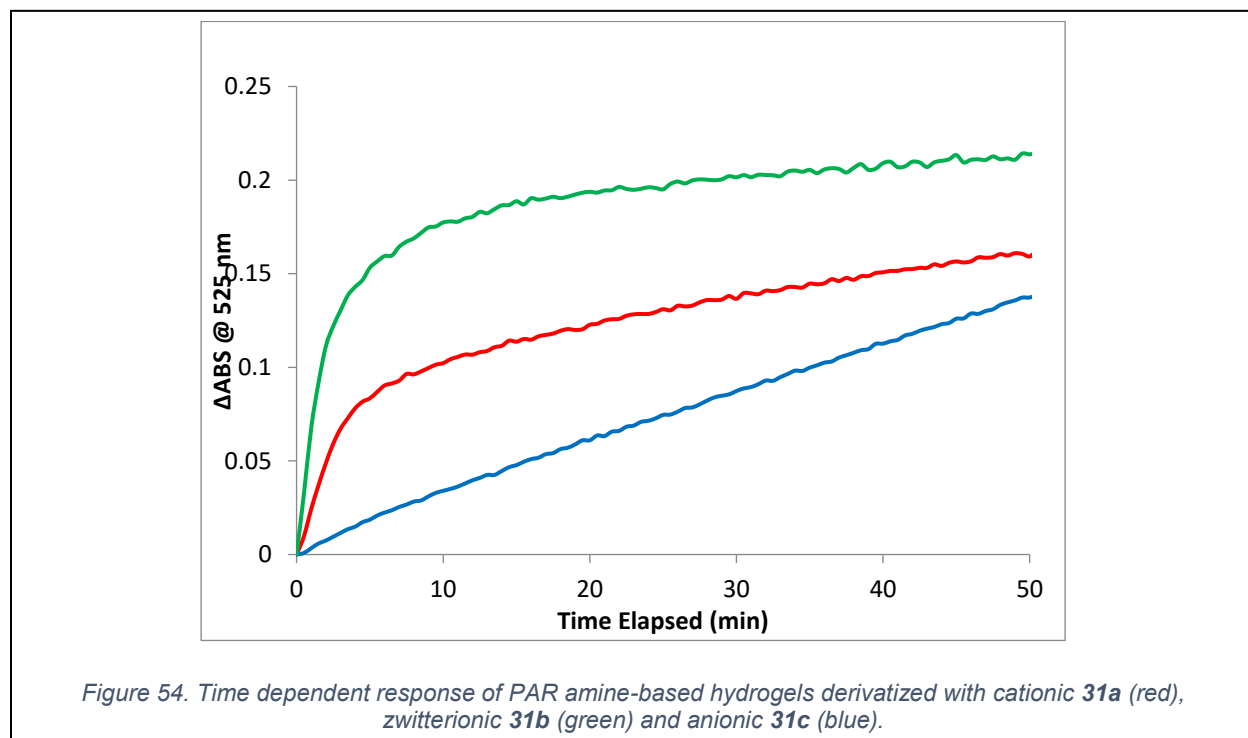
Acid/Solvent	Time (Hr)	Temperature (At Block Temp)	Vortexed	# of Amines by Ninhydrin (nmol/dot)	# of Amines Calc'd (nmol/dot)
No Treatment	N/A	N/A	N/A	23 (Below Curve)	280
(1:1 by vol) 4 M HCl/ EtOH	18	RT	No	237	280
(1:1 by vol) 4 M HCl/ EtOH	3	RT	No	35	280
(1:1 by vol) 12 M HCl/ EtOH	3	RT	No	183	280
(1:1 by vol) 12 M HCl/ EtOH	1	RT	No	144	280
(1:1 by vol) 12 M HCl/ EtOH	1	70 C	No	449 (Above Curve)	280
(1:1 by vol) 12 M HCl/ EtOH	1	RT	Yes	430 (Above Curve)	280
20% TFA in CH ₂ Cl ₂	0.083	100 C	No	294	280
1 M H ₂ SO ₄ in Dioxane	1	RT	No	Below Curve	280
1 M H ₂ SO ₄ in Dioxane	1	70 C	No	Destroyed Polymer	280

Figure 53. Results from ninhydrin quantitation of free amines after Boc deprotection.

Spectral Interpretation of Chemosensing Hydrogels (MABA(TEG)-co-HEMA)

Comparisons across the variety of polymers made are currently underway. Initial results are promising and indicate that PAR bound hydrogels can be used to quantitate single digit ppb concentrations of Zn^{2+} in buffered aqueous solutions.

First the difference between perturbation moieties was compared using a flow system. Running at 4.5 mL/min with 100 ppb Zn^{2+} in MOPS buffer water, three PAR hydrogel films, each with a different charged moiety, were analyzed. The hydrogels were rinsed thoroughly with 0.1 M HCl to remove any trace metal that may be present in the polymer. Once the polymer is adequately rinsed, the flow stream was switched to the analyte solution and after an initial buffering period the data collection was started. The absorbance values at 525 nm were monitored and the results are shown in **Figure 54**. The cationic and zwitterionic hydrogels behaved as expected with an initial fast response that diminished as the binding sites became populated. To our surprise, the



anionic polymer had a linear response for nearly the entire duration of the flow experiment (slightly reduced on-rate towards saturation, not shown). With this encouraging result, it was tested again with various concentrations of Zn^{2+} (**Figure 55**).

The linear response was seen again for each concentration of Zn^{2+} tested and showed good repeatability across multiple trials. When the slope of the time-dependent response was plotted against the concentration a linear regression was obtained with an R^2 of 0.999 (**Figure 55**). The lowest concentration tested (75 nM) gave very consistent slopes indicating a limit of quantitation possibly in the single digit nanomolar range, a value not seen for a real-time method for metal ion quantification.

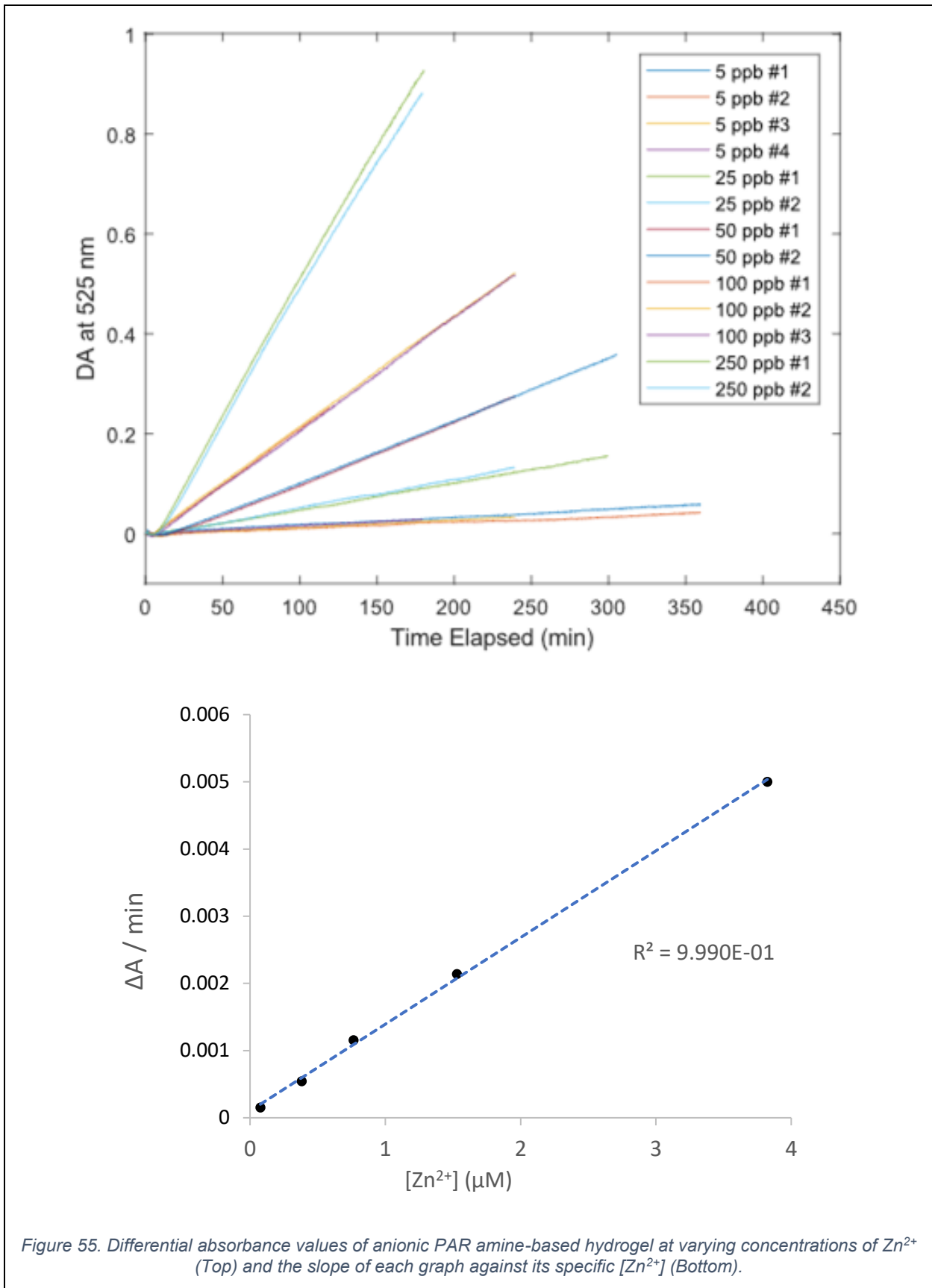


Figure 55. Differential absorbance values of anionic PAR amine-based hydrogel at varying concentrations of Zn²⁺ (Top) and the slope of each graph against its specific [Zn²⁺] (Bottom).

Future Directions

We have demonstrated the utility of covalently bound azo dye chemosensors as a viable approach for the quantitation of aqueous bound metal ions. Further development on the hydrogel solid support include a simpler approach to polymer preparation. Plans include dye and possibly perturbation moiety attachment to soluble polymers that would be transformed into gels using the crosslinking as a final step. This would allow for more in-depth characterization of the polymer structure using described NMR methods as well as other techniques.

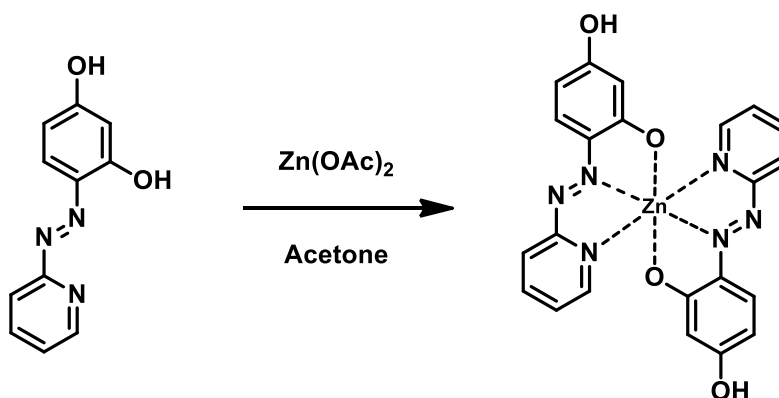
The library of azo dyes developed by Trevor Hagemann will be fully characterized using flow injection analysis and transformed into derivatives that can be attached via acylation reactions. Paul Henning has developed preliminary PLS models capable of quantifying multiple metals with only a few dyes. Once there is a enough hydrogel bound dyes, these models will be applied to the flow system to attempt to develop an instrument capable of monitoring the metal ion concentration of complex analyte mixtures.

Further development of the methodology could lead to real time monitoring of analytes other than metal ion by using optically active compounds that form association complexes with dissolved species. The possibilities are endless.

Experimental Details: Compounds 28b, 29b, 30-36, 37a, 37b, 38, 39; Polymer Preparation

All characterization spectra can be found in the appendix to this dissertation.

[4-(2-Pyridylazo)resorcinol]₂Zn **28b**

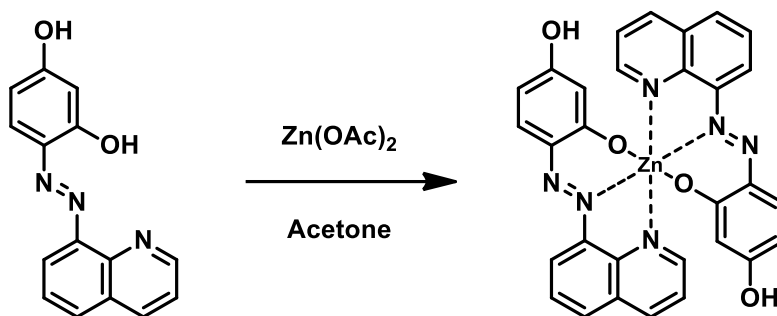


A suspension of PAR (95.3 mg, 0.443 mmol) in acetone (150 mL) was brought to a boil. Once soluble, Zn(OAc)₂ (51.3 mg, 0.234 mmol, 0.53 eq) was added and resulted in an instant color change from red-orange to a dark red-purple color. Solution was then concentrated to ~100 mL total volume and placed on an ice bath to cool for 1 hour. Solid was collected via vacuum filtration to give 77.8 mg (**71%**) of a dark red-black solid.

M.P. > 360 °C

¹H NMR (500 MHz, DMSO) δ 7.97 (td, J = 7.7, 1.5 Hz, 2H), 7.68 (dd, J = 10.8, 9.0 Hz, 4H), 7.56 (d, J = 4.4 Hz, 2H), 7.17 (dd, J = 6.8, 5.6 Hz, 2H), 6.17 (dd, J = 2.3, 9.4 Hz, 2H), 5.82 (d, J = 1.9 Hz, 2H). ESI-MS Calculated for C₂₂H₁₆N₆O₄Zn [M+H⁺] 493.06, Found 493.20

[4-(8-Quinolylazo)resorcinol]₂Zn **29b**

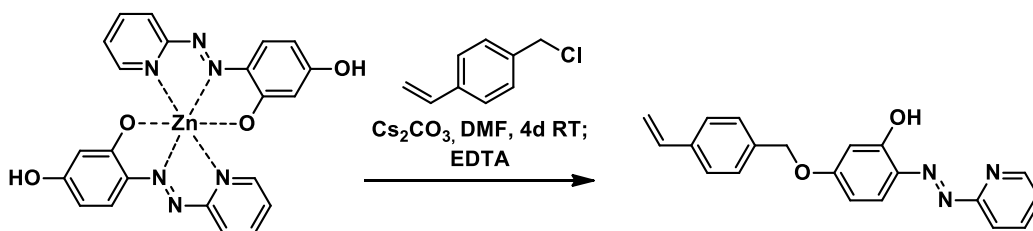


Followed procedure for PAR₂Zn **28b** to get 65% yield. M.P. > 360 °C

¹H NMR (300 MHz, MeOD) δ 8.88 (dd, *J* = 1.6, 4.3 Hz, 2H), 8.26 (dd, *J* = 1.6, 8.5 Hz, 2H), 8.01 (dd, *J* = 5.2, 3.8 Hz, 2H), 7.60 (d, *J* = 1.3 Hz, 2H), 7.58 (s, 2H), 7.52 (dd, *J* = 8.2, 4.2 Hz, 2H), 7.03 (d, *J* = 9.6 Hz, 2H), 6.24 (dd, *J* = 1.9, 9.7 Hz, 2H), 5.73 (d, *J* = 2.3 Hz, 2H).

CMS-PAR **30**

3-hydroxy-4-(2-pyridylazo)-1-(4-vinylphenyl)methoxy-benzene

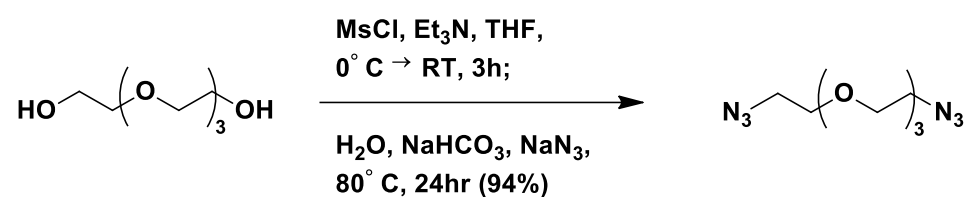


To a solution of PAR₂Zn **28b** (49.8 mg, 0.101 mmol) and Cs₂CO₃ (82.1 mg, 0.252 mmol) in DMF (25 mL) was added chloromethyl styrene (0.04 mL, 0.282 mmol) and stirred for 4 days. Reaction mixture washed with hexanes (25 mL), diluted into a phosphate buffered (10 mM, pH 5) EDTA solution (10 mM, 300 mL), extracted with ethyl acetate (3x100 mL) dried over Na₂SO₄, concentrated by rotary evaporation and dried under reduced pressure to give 80.9 mg (>100%).

^1H NMR (500 MHz, CDCl_3) δ 8.60 (d, $J = 4.0$ Hz, 1H), 7.85 (t, $J = 7.2$ Hz, 1H), 7.77 (d, $J = 8.3$ Hz, 1H), 7.63 (d, $J = 9.2$ Hz, 1H), 7.45 (d, $J = 7.9$ Hz, 2H), 7.39 (d, $J = 8.0$ Hz, 2H), 7.30 (d, $J = 11.8$ Hz, 1H), 6.73 (dd, $J = 17.6, 10.9$ Hz, 1H), 6.62 (dd, $J = 9.2, 2.4$ Hz, 1H), 6.42 (d, $J = 2.0$ Hz, 1H), 5.78 (d, $J = 17.7$ Hz, 1H), 5.28 (d, $J = 11.0$ Hz, 1H), 5.10 (s, 2H).

Diazido tetra(ethylene glycol) **31**

1-Amino-11-azido-3,6,9-trioxaundecane

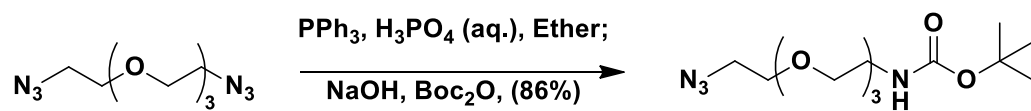


Procedure followed from Schwabacher et al. J. Org. Chem. 1998, 63, 1727-1729

^1H NMR (300 MHz, CDCl_3) δ 3.68 (s, 12H), 3.40 (t, $J = 4.9$ Hz, 4H).

Boc-N-1-amino-11-azido(tetra(ethylene glycol)) (BAA TEG) **32**

tert-butyl (2-(2-(2-(2-azidoethoxy)ethoxy)ethoxy)ethyl)carbamate

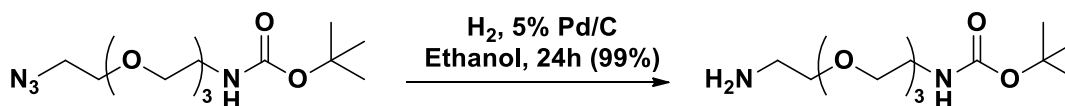


Diazido tetra(ethylene glycol) **31** (4.2233g, 17.3 mmol) was combined with aq. H_3PO_4 (40 mL, 0.65M). A solution of PPh_3 (3.9946g, 15.2 mmol) in ether (30 mL) was added slowly over a 15-minute period. This bi-phasic solution was then stirred for 45 hours before separating the layers. The aqueous layer was then washed with ethyl ether (3x50 mL). Aqueous layer was then basified with NaOH (3.24g). Resulting solution became warm, driving off any trace ether remaining. This solution was chilled overnight to crystallize out PPh_3O . Solution was filtered and NaOH (8.23g) added, which resulted

in more PPh₃O precipitating. The solution was filtered again followed by addition of Boc₂O (4.33g, 19.8 mmol). Solution was then boiled for 1 hour and allowed to cool to room temperature. Aqueous solution was then extracted with ethyl acetate (3 x 30 mL), organic layers combined, dried over Na₂SO₄, volatiles removed and dried under reduced pressure to yield 4.1475g (86%) of a pale-yellow oil.

¹H NMR (500 MHz, CDCl₃) δ 5.00 (br-S, 1H), 3.68 (m, 10H), 3.54 (t, J = 5 Hz, 2H), 3.39 (t, J = 5 Hz, 2H), 3.31 (br-S, 1H), 1.45 (s, 9H). ¹³C NMR (126 MHz, CDCl₃) δ 155.99, 79.17, 70.73, 70.67, 70.64, 70.26, 70.23, 70.08, 50.69, 40.37, 28.43. ESI-MS Calcd for C₁₃H₂₆N₄O₅ (M+H⁺) 319.37, found 319.15.

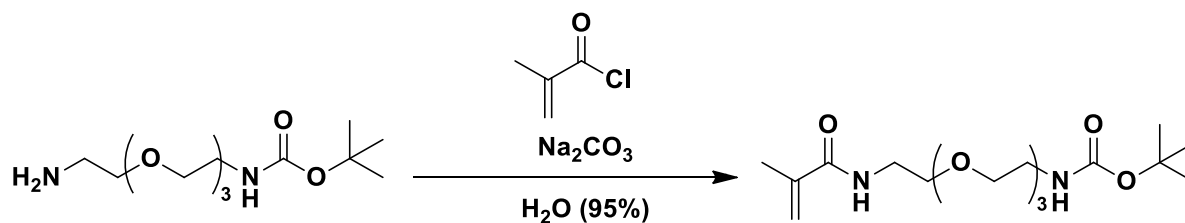
Mono-Boc-Diamine tetra(ethylene glycol) (MBDA-TEG) **33**
tert-butyl (2-(2-(2-(2-aminoethoxy)ethoxy)ethoxy)ethyl)carbamate



To a solution of BAA-TEG **32** (4.1189g, 12.9 mmol) in ethanol (20 mL) was added 5% Pd/C (74.9 mg). Reaction flask sealed and flushed with H₂ and balloon used to provide reservoir of additional H₂. Reaction was stirred rapidly for 48 hours, replacing H₂ balloon when it was deflated. Reaction mixture was filtered through celite, concentrated under reduced pressure to give 3.7503g (99%) of a pale-yellow oil.

¹H NMR (500 MHz, CDCl₃) δ 5.42 (br-S, 1H), 3.65 (m, 10H), 3.54 (t, J = 5 Hz, 2H), 3.31 (br-S, 2H), 2.81 (t, J = 5 Hz, 2H), 1.44 (s, 9H). ¹³C NMR (126 MHz, CDCl₃) δ 156.41, 70.56, 70.38, 70.32, 70.28, 70.12, 70.06, 40.93, 28.46. ESI-MS Calcd for C₁₃H₂₈N₃O₅ (M+H⁺) 293.97, found 293.25.

Boc-N-amino-11-(Methacryloylamino)tetra(ethylene glycol) (MABA TEG) **34**

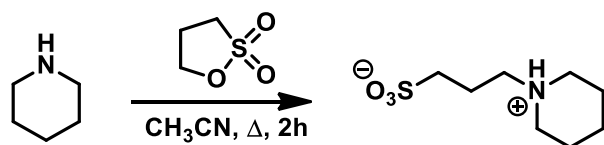


To a solution of **33** (1.0536g, 3.60 mmol) and powderized Na_2CO_3 (0.8771g, 8.28 mmol) in DI water (5 mL) chilled to 0° was added methacryloyl chloride (0.40 mL, 4.09 mmol). After 2 hours, the reaction mixture was diluted with an additional 20 mL DI water and extracted with dichloromethane (3x10 mL), combined organic layers back washed with brine solution (10 mL), dried over Na_2SO_4 , volatiles removed and dried under reduced pressure to give 1.2324g (95%) of a pale-yellow oil.

^1H NMR (500 MHz, CDCl_3) δ 6.38 (br-s, 1H), 5.70 (s, 1H), 5.33 (s, 1H), 5.00 (br-s, 1H), 3.63 (m, 10H), 3.54 (t, $J = 5$ Hz, 4H), 3.30 (t, $J = 5$ Hz, 2H), 1.97 (s, 3H), 1.45 (s, 9H).

^{13}C NMR (500 MHz, CDCl_3) δ 168.46, 155.97, 140.11, 119.41, 70.51, 70.24, 69.80, 39.38, 28.42, 18.65.

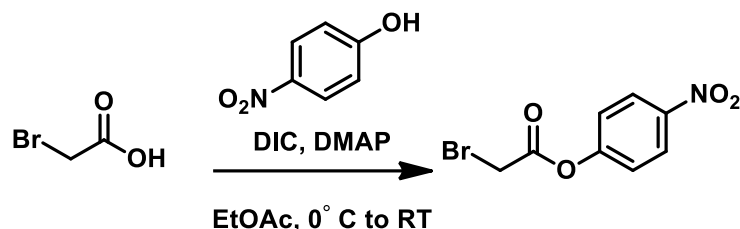
N-(propylsulfonate)piperidinium **35**



A solution of 1,3-propanesultone (0.3072g, 2.52 mmol) and piperidine (0.26 mL, 2.63 mmol) in acetonitrile (5 mL) was refluxed for 1 hour and cooled giving product as a precipitate. Solution was filtered, rinsed with acetonitrile and dried under reduced pressure to give 237.5 mg (45%) as a white solid.

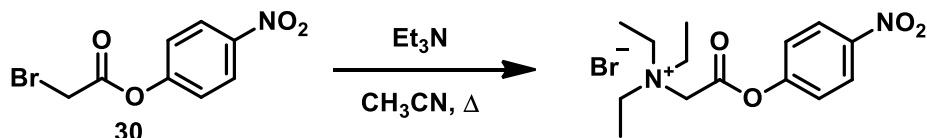
^1H NMR (500 MHz, D_2O) δ 3.56 (d, J = 12.2 Hz, 2H), 3.24 (t, J = 8.2 Hz, 2H), 2.99 (t, J = 7.3 Hz, 2H), 2.95 (td, J = 12.5, 2.3 Hz, 2H), 2.18 (tdt, J = 2.8, 0.6, 7.3 Hz, 2H), 1.95 (td, J = 3.2, 15.1 Hz, 2H), 1.82 (td, J = 3.5, 13.3 Hz, 1H), 1.71 (q, J = 13.7 Hz, 2H), 1.50 (tq, J = 3.9, 21.3 Hz, 2H). ^{13}C NMR (126 MHz, D_2O) δ 55.36, 53.26, 47.82, 22.81, 21.07, 19.35. . ESI-MS Calculated for $\text{C}_8\text{H}_{17}\text{NO}_3\text{S}$ $[\text{M}+\text{H}^+]$ 208.10, Found 208.15.

p-nitrophenyl bromoacetate **36**



Followed procedure from Org. Lett. 2017, 19, 5182-5185; Supporting Information. ^1H NMR (500 MHz, CDCl_3) δ 8.30 (d, J = 9 Hz, 2H), 7.34 (d, J = 9 Hz, 2H), 4.08 (s, 2H). ^{13}C NMR (126 MHz, CDCl_3) δ 164.92, 154.87, 145.77, 125.39, 122.11, 24.94.

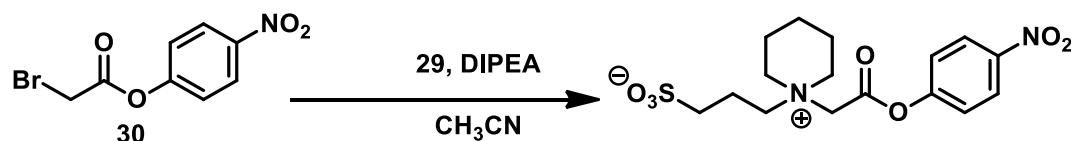
p-nitrophenyl N,N,N-triethylammoniumacetate bromide **37a**



A solution of *p*-nitrophenyl bromoacetate **36** (285.7 mg, 1.10 mmol) and trimethylamine (0.16 mL, 1.15 mmol) in 40 mL CH_3CN was refluxed for 2 hours. Volatiles then removed under reduced pressure and crude residue was recrystallized from 100 mL of a solution of 5% of CH_3CN in ether to yield 204.3 mg (51%) of an off-white solid. M.P. (decomp) 170°C .

^1H NMR (500 MHz, D_2O) δ 8.38 (d, $J = 9.1$ Hz, 2H), 7.48 (d, $J = 9.1$ Hz, 2H), 4.62 (s, 2H), 3.66 (q, $J = 7.3$ Hz, 6H), 1.39 (t, $J = 7.3$ Hz, 9H). ^{13}C NMR (^{13}C NMR (126 MHz, D_2O) δ 169.38, 163.51, 153.70, 125.69, 122.38, 54.72, 53.39, 8.20.

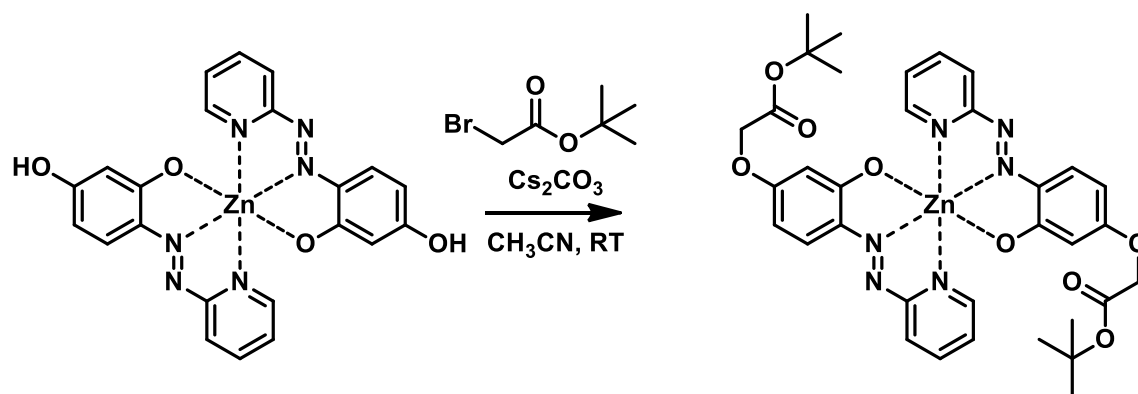
p-nitrophenyl N-(N-(propylsulfonate)pyridine)acetate **37b**



A suspension of **35** (0.2827g, 1.36 mmol), *p*-nitrophenyl bromoacetate **36** (0.3604 g, 1.39 mmol) and diisopropylethylamine (0.23 mL, 2.47 mmol) in acetonitrile (25 mL) as refluxed was 24 hours. Reaction mixture was diluted into boiling ether/acetonitrile (8:1 by vol, 90 mL tot. vol.) and chilled overnight at -20 °C. Solid collected by vacuum filtration and dried under reduced pressure to give 132.5 mg (26%) of white crystals.

$\text{PAR}_2\text{Zn}(\text{AlkEster})$ **38**

t-butyl 2-(3-hydroxy-4-(pyridin-2-ylidiazenyl)phenoxy)acetate zinc complex



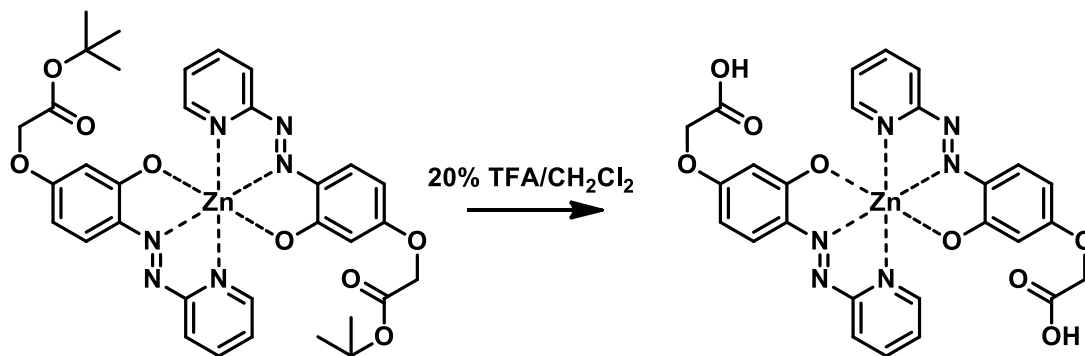
To a suspension of **28b** (2.15g, 4.4 mmol) and cesium carbonate (3.128g, 9.6 mmol) in acetonitrile (50 mL) was added *t*-butyl bromoacetate (1.31 ml, 8.6 mmol) and stirred

rapidly for 24 hours. Suspension was filtered through cotton and concentrated by rotary evaporation. The crude residue was boiled in ether (75 mL), cooled to room temperature, filtered and dried under reduced pressure to give 3.0245g (96%) of a deep purple crystalline solid. M.P. $\sim 50^{\circ}\text{C}$ (decomp).

^1H NMR (500 MHz, DMSO) δ 8.03 (td, $J = 7.7, 1.7$ Hz, 2H), 7.78 (d, $J = 8.0$ Hz, 2H), 7.73 (d, $J = 9.5$ Hz, 2H), 7.63 (dd, $J = 1.1, 5.1$ Hz, 2H), 7.24 (ddd, $J = 5.1, 0.8, 7.3$ Hz, 2H), 6.27 (dd, $J = 2.7, 9.5$ Hz, 2H), 5.91 (d, $J = 2.7$ Hz, 2H), 4.66 (s, 4H), 1.41 (s, 18H).
 ^{13}C NMR (126 MHz, DMSO) δ 176.28, 168.45, 167.47, 159.04, 146.24, 142.22, 132.45, 124.54, 122.94, 119.49, 110.93, 103.71, 82.19, 79.67, 65.45, 28.16. ESI-MS Calculated for $\text{C}_{34}\text{H}_{36}\text{N}_6\text{O}_8\text{Zn}$ $[\text{M}+\text{H}^+]$ 721.20, Found 721.55

PAR₂Zn(AlkAcid) **39**

2-(3-hydroxy-4-(pyridin-2-yl)diazenyl)phenoxy)acetic acid zinc complex



A solution of ester **38** (2.9245g, 4.1 mmol) in TFA (4 mL) was stirred for 1 hour before solvent was removed by rotary evaporation. The solid was suspended in methanol and concentrated multiple times followed by azeotropic drying with toluene. The solid was left under vacuum to achieve constant mass and afforded 2.321g (94%) of a bright red solid M.P. 133 – 135 $^{\circ}\text{C}$

^1H NMR (500 MHz, DMSO) δ 8.55 (s, 2H), 8.07 (td, $J = 7.8, 1.8$ Hz, 2H), 7.87 (d, $J = 8.1$ Hz, 2H), 7.69 (d, $J = 9.3$ Hz, 2H), 7.50 (ddd, $J = 5.0, 0.8, 7.3$ Hz, 2H), 6.57 (d, $J = 8.3$ Hz, 2H), 6.38 (s, 2H), 4.81 (s, 4H). ^{13}C NMR (126 MHz, DMSO) δ 169.86, 160.03, 158.98, 158.70, 158.41, 148.87, 140.47, 133.36, 129.36, 128.67, 125.78, 124.87, 117.41, 115.09, 110.82, 103.13, 65.32. ESI-MS Calculated for $\text{C}_{13}\text{H}_{11}\text{N}_3\text{O}_4$ $[(1/2)\text{M}+\text{H}^+]$ 274.08, Found 274.05.

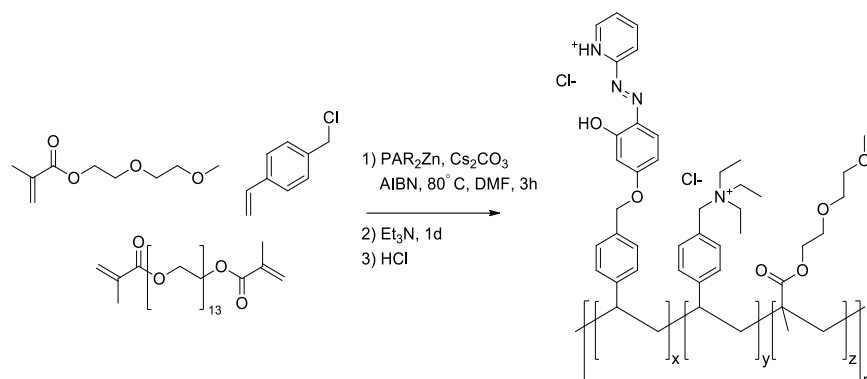
Activation of Glass Surface

Glass Slides can be activated for derivatization by first soaking them in a solution of methanol in 12 M HCl (50% v/v) for at least 30 minutes. Slides are then rinsed with DI H_2O by submerging them in a large desiccator of water. Following the rinse, the slides can be soaked in 18 M H_2SO_4 for at least 30 minutes. Slides are once again then rinsed with DI and stored in water until further use.

Silanization with 3-(trimethoxysilyl)propyl methacrylate:

A glass slide was cleaned and prepped by soaking in a methanol/HCl(12M) (1:1 v/v) bath for 30 minutes, rinsed with DI water and then soaked in a sulfuric acid bath for 30 minutes, rinsed with DI water and then rinsed with ethanol. The slide was then submerged in a 3% (v/v) solution of 3-(trimethoxysilyl)propyl methacrylate in 5% HCl (12M)/Ethanol for 1 hour. Slide was rinsed with ethanol and then dried under a stream of nitrogen.

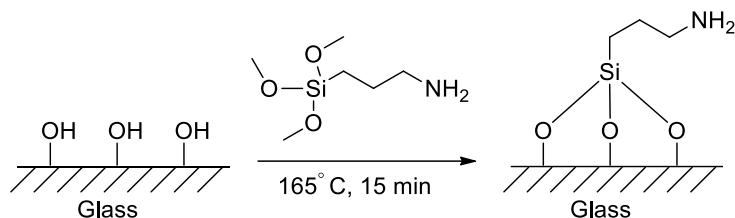
One Step Hydrogel Sensor:



A solution was prepared by combining di(ethylene glycol) methyl ether methacrylate 95% (1.84 mL, 1.9254 g, 9.72 mmol), 4-vinylbenzyl chloride 90% (0.16 mL, 163.4 mg, 0.964 mmol), poly(ethylene glycol) methacrylate (Avg. MW 750, 1.20 mL, 1.3373 g, 1.78 mmol) and toluene (~20 mL). This solution was then passed through a column to remove the inhibitors present. The solution was then concentrated under reduced pressure to remove any toluene. AIBN (100.8 mg) and DMF (1.2 mL) was added. Using 0.73 mL of this solution (1/6) and 0.2 mL of a dye alkylation solution (0.02 M Dye complex, 0.04 M Cs₂CO₃ in DMF) was added to each. This monomer solution is then loaded on to a glass slide silanized with octadecyltrichlorosilane and an appropriate mold. With the mold loaded with the monomer solution, a glass slide silanized with (trimethoxysilyl)propylmethacrylate is placed carefully over the top of the mold and air bubbles removed by sliding the glass slide back and forth. The two glass slides and the mold are then tightly clamped together with small binder clips and placed in an oven set at 80° C. The oven is then flushed with nitrogen gas. The polymer is the allowed to polymerize in the oven for 1 hour before being removed and allowed to cool to room temperature before removing the polymers from the mold. Once the glass slide with the

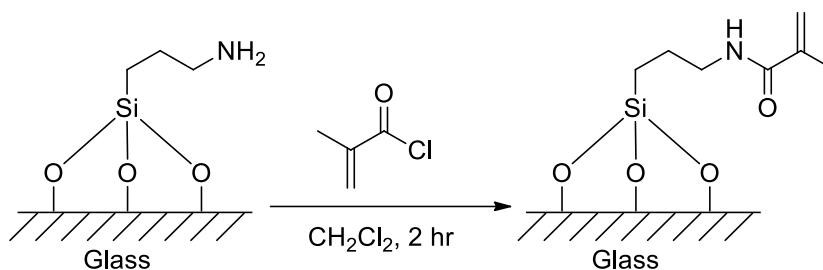
polymers attached is separated from the mold it is quickly rinsed thoroughly with DMF. The rinsed slide is then submerged in a 20% Et₃N in NMP solution overnight. The slide was then removed and rinsed thoroughly with DMF before storing in 18Ω H₂O.

Silanization with (3-aminopropyl)trimethoxysilane:



5 activated slides were rinsed with methanol and dried with a stream of nitrogen. A vacuum oven is heated to 165 °C and a large crystallization dish is placed inside to equilibrate with the oven temperature. The dried slides are placed on a custom-made holder that holds the slides upright and each slides is separated by 2 cm. Two small pieces of glass wool are soaked with 40 μL of (3-aminopropyl)trimethoxysilane. As fast as possible, the rack with the slides is placed in the heated crystallization dish and the pieces of glass wool are placed on each side of the rack (end to end of each slide). A larger crystallization dish is then place upside down over the top of the other and the oven is closed and flushed with nitrogen. After 15 minutes the slides are removed allowed to cool, rinsed with hexanes and then placed back in the oven with ~100 μL water placed on the base of the crystallization dish and loosely covered, heated at 1 atm for 30 minutes and then a slight vacuum (~1/5 atm) for 1 hour. The slides are removed and rinsed with toluene and stored in toluene until further use.

Methacryloylation



Aminopropylated glass slides were submerged in a solution of methacryloyl chloride (2% v/v in CH₂Cl₂) and triethylamine (3% v/v in CH₂Cl₂) for 24 hours. Slides then removed and rinse with CH₂Cl₂ and dried under a stream of nitrogen.

C18 Slides

Acid treated glass slides were submerged in an octadecyltrichlorosilane solution (2% v/v CH₂Cl₂) for 3 hours. Slides removed and rinsed with hexanes.

Polymer Formation

Tape mold first applied to a C18 slide. Monomer solution (Made from 1 eq. MABA-TEG, 1 eq. HEMA, 15% by mol PEGDMA 750, AIBN, 60% by vol NMP) loaded into voids. Methacryloylated slide then placed over top and manipulated to remove any air bubbles. Mold is then clamped with 3 other glass slides on each slide to even the pressure. Mold placed in an oven set at 80 °C for 3 hours. Mold removed after polymerization is complete and mold submerged in NMP before prying apart to give a plate with polymer dots attached. Plate can be etched with a diamond scribe and snapped apart to give individual polymer dots.

Polymer Deprotection:

Glass back polymers were submerged in a 50% ethanol in 6 M HCl solution overnight with mild agitation from a vortexer.

General Procedure for Dye Attachment:

Stock solution prepared (0.1 M **39**, 0.24 M HBTU in NMP). Deprotected polymers rinsed 3x with 5% triethylamine (v/v in NMP) solution and submerged in 1 mL of diluted stock solutions (final concentration of dye complex between 1 and 6 mM in NMP). To this 0.1 mL of Et₃N is added, swirled and let sit for 24 hours. Solution then removed via pipet and rinsed with 5% triethylamine (v/v in NMP) solution until the rinse solution did not contain any color.

General Procedure for Perturbation Moiety Loading

Polymer with dyes attached were submerged in 1 mL NMP containing 1 M activated ester (glutaric anhydride, **37c**). To this 0.1 mL of Et₃N is added, swirled and let sit for 24 hours. Solution then removed via pipet and rinsed with 5% triethylamine (v/v in NMP) solution. Solvent was then exchanged (3x) with 50% aq. ethanol and finally (3x) with 18Ω H₂O.

Chapter 4: Synthesis of β,γ -dehydroarginine for Enzymatic Studies of MppP

Introduction

Enduracidine is a non-proteogenic amino acid found in teixobactin⁸⁴ and enduracidin (also known as enramycin)^{85–87}. β -hydroxyenduracidine, itself derived from enduracidine⁸⁸, is found in mannopeptimycin (**Figure 56**).⁸⁹ These three natural products are potent macrocyclic peptidic antibiotics active against multi-drug resistant gram-positive bacteria. They function by inhibiting cell wall synthesis through lipid II binding in a manner that differs from the known lipid II inhibitors such as vancomycin.^{85,86,90,91}

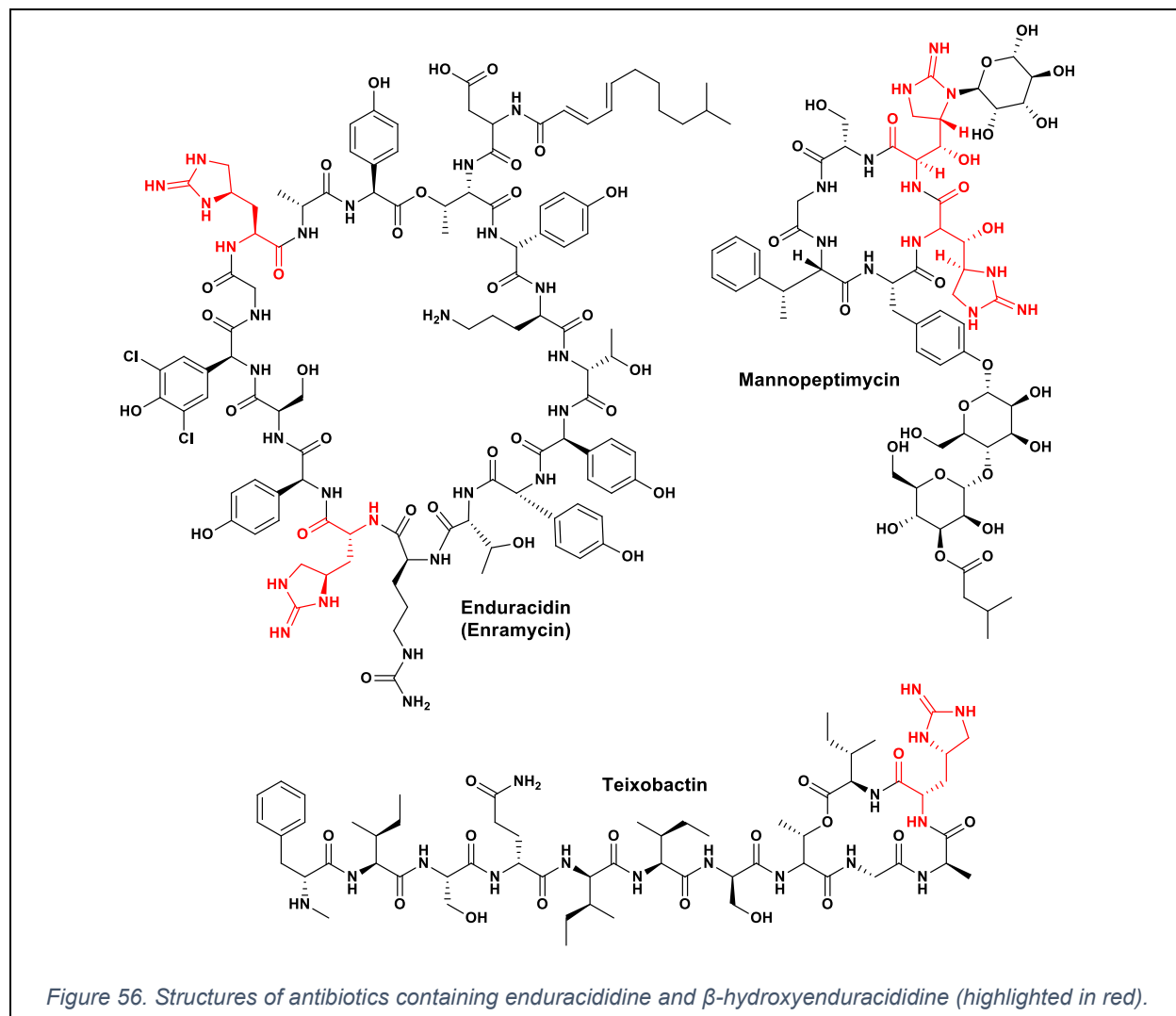
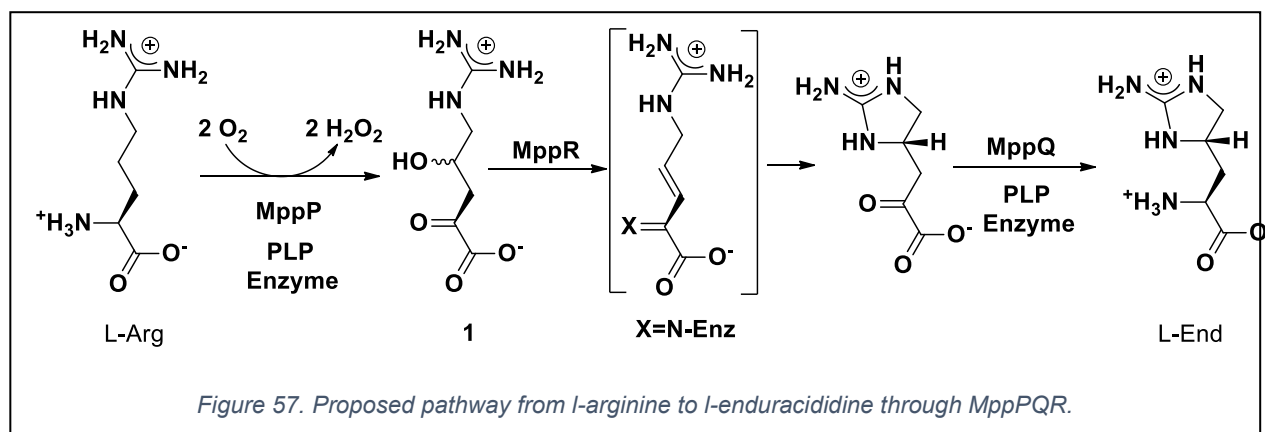


Figure 56. Structures of antibiotics containing enduracidine and β -hydroxyenduracidine (highlighted in red).

It has been shown that in replacing the enduracididine in teixobactin with L-Arg reduces the antibiotic activity by almost a full order of magnitude.⁹² This observation provides evidence towards the theory that the conformational restriction of the enduracididine plays a crucial role in its function. Understanding the role of this conformationally restricted arginine in these antibiotics is important to developing new antibiotics as bacteria continues to grow increasingly more drug-resistant.

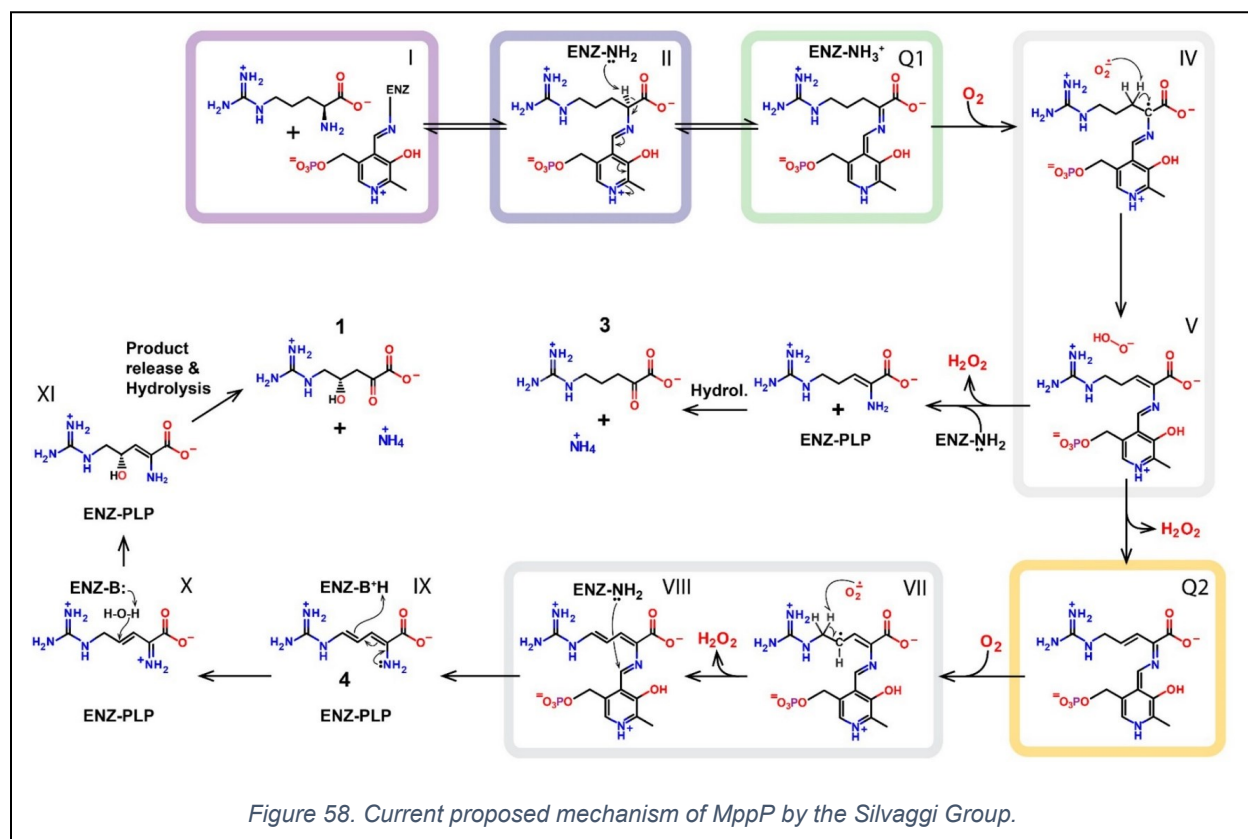
Biosynthesis of Enduracididine

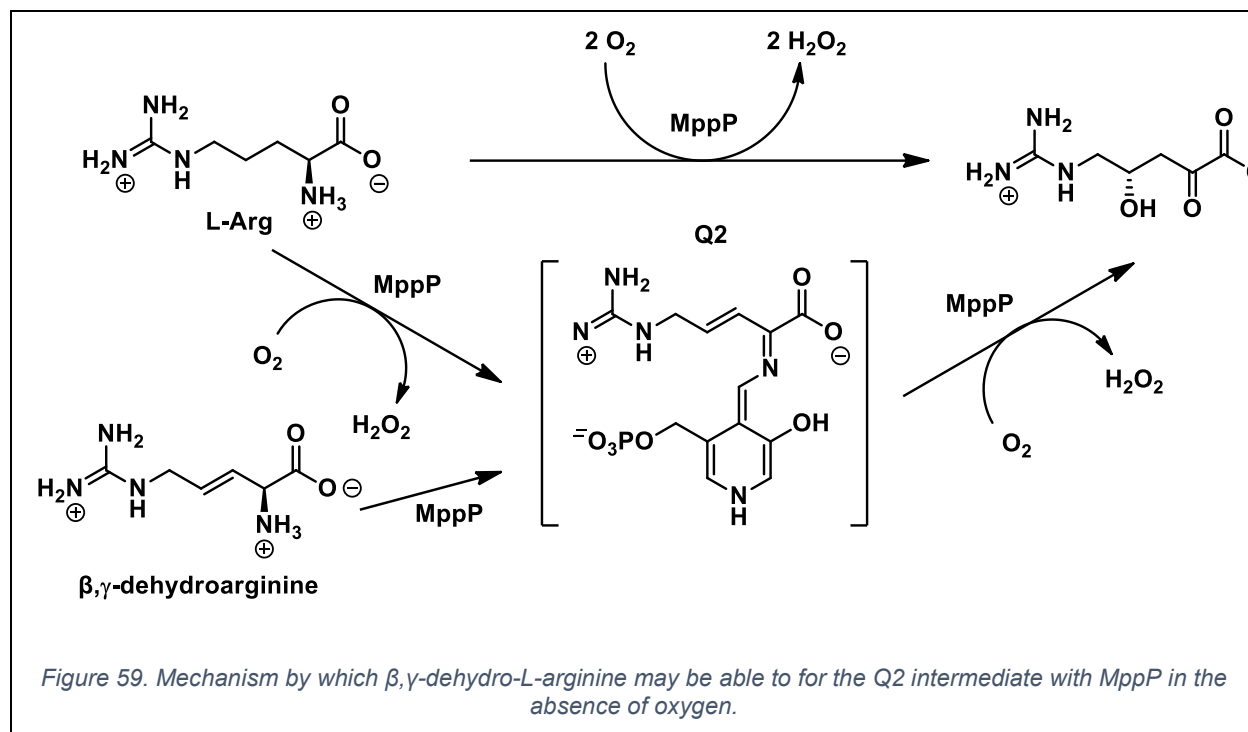
We are interested in understanding the biosynthetic pathways that produce enduracididine in the MppPQR enzyme family, referred to as the Mpp pathway, obtaining its name from mannopeptimycin where it was first discovered in its biosynthetic pathway.⁹³



Enduracididine is biosynthetically produced through a post-translational modification of arginine through γ -hydroxylation of arginine with MppP using 2 equivalents of molecular oxygen outputting a mixture of the ketoacid of arginine and γ -hydroxyarginine.^{85,94} The cyclization to form the ketoacid of enduracididine is done by MppR⁹³ and presumably converted back to the amino acid with MppQ (**Figure 57**).⁹⁴

MppP is the first reported instance of a PLP oxygenase and recently the Silvaggi group has shown the presence of 2 quinonoid intermediates are involved in the MppP mechanism indicating the transient presence of a β,γ -dehydro-L-arginine analogue bound to the PLP during the transformation. MppP reaches the first quinonoid intermediate **Q1** in the absence of O_2 and is extremely stable indicating the active site stabilizes the electron rich nature of **Q1** until oxygen is present and is characterized by a strong absorbance at 510 nm. Upon exposure to O_2 a weak absorbance is observed at 560 nm indicating a slightly more conjugated intermediate quinonoid intermediate **Q2** followed by cleavage from the enzyme generating the keto acid of γ -hydroxy-L-arginine (**Figure 58**). Since **Q2** is formed in the presence of O_2 and then hydroxylated also with O_2 it makes it difficult to understand the enzyme kinetics because the two paths cannot be studied independently.⁹⁴

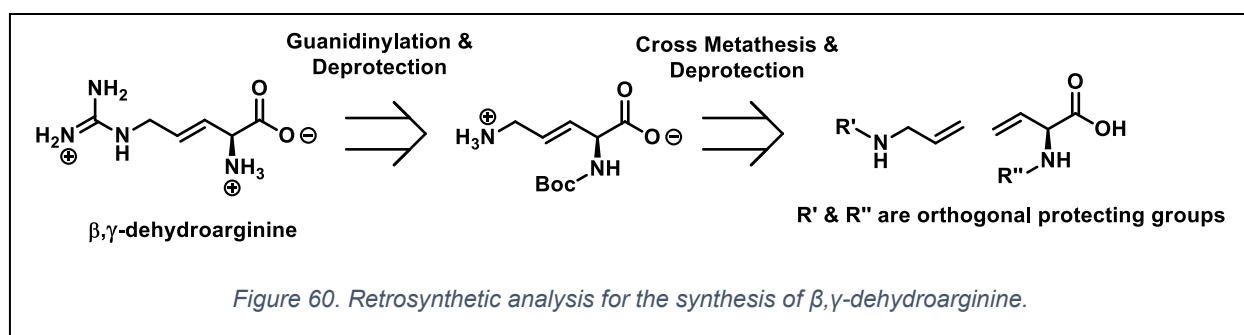




We propose that by feeding MppP synthetically produced β,γ-dehydro-L-arginine, **Q2** can be obtained in the absence of oxygen and the 2nd half of the enzymatic pathway can be studied independently after oxygenating the solution (**Figure 59**).

Retrosynthetic Analysis and Work Done by Robert Hoppe

We propose that β,γ-dehydro-L-arginine **40** can be achieved through an olefin cross metathesis reaction of protected allyl amine and protected L-(vinyl glycine), selective deprotection, guanidinylation and complete deprotection (**Figure 60**). Synthetic work towards **40** was started by Robert Hoppe. Robert developed the



synthetic scheme to obtain L-(vinyl glycine) in consistent yields and high purity and identified conditions in which L-(vinyl glycine) could undergo undesired isomerization.⁹⁵

Aside from providing a large stock of L-vinyl glycine and procedures, Robert showed that certain protected forms of L-(vinyl glycine) are prone to isomerization to the α,β -unsaturated derivative in the presence of base. The TMS ester of N-Boc-L-vinyl glycine and the HCl salt of L-vinyl glycine methyl ester both showed nearly complete isomerization within only a couple hours in the presence of trimethylamine. Because of this observation, Robert used the free acid of L-(vinyl glycine) in his attempts to perform the olefin cross metathesis. All attempts failed to produce any observable quantity of the desired metathesis product (**Figure 61**).⁹⁵

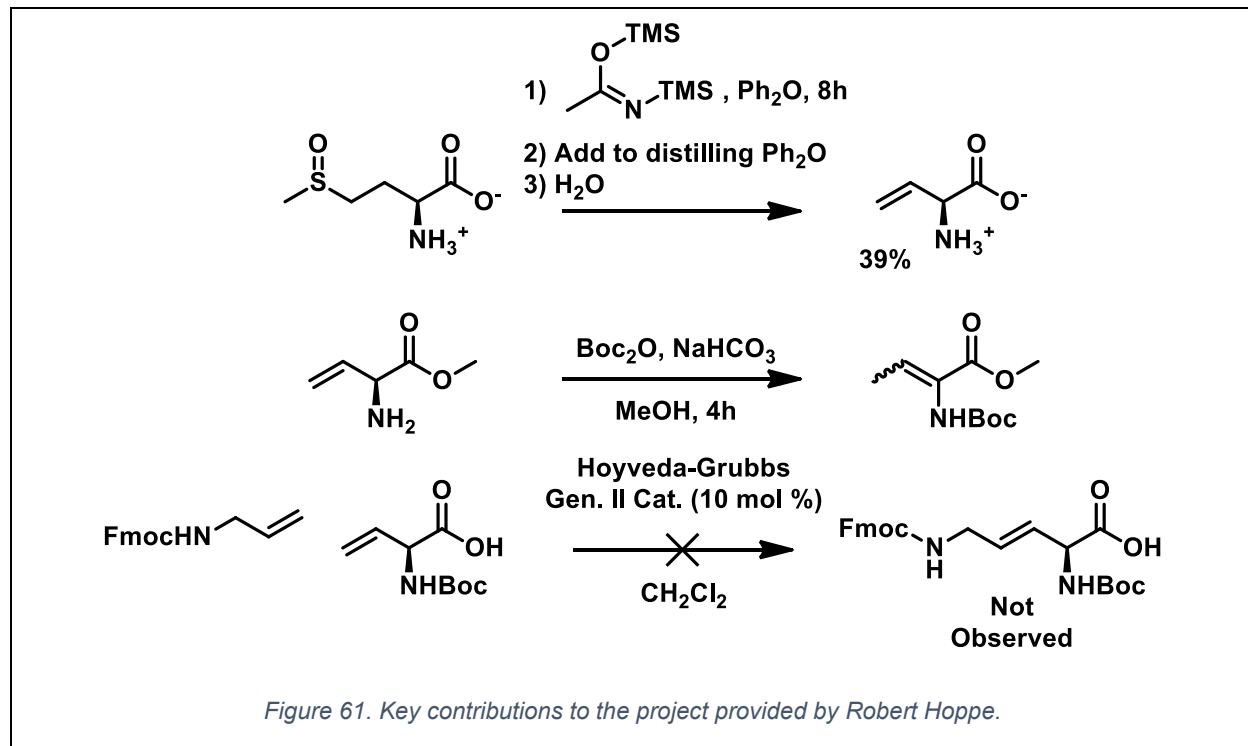
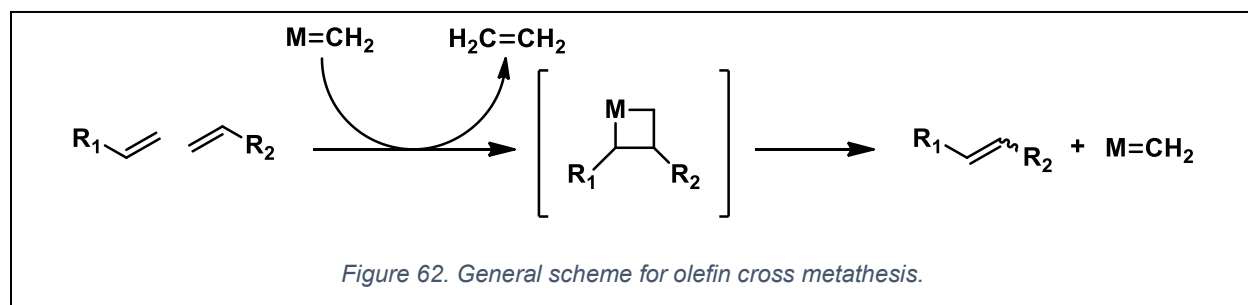


Figure 61. Key contributions to the project provided by Robert Hoppe.

Synthesis of β,γ -dehydro-L-arginine

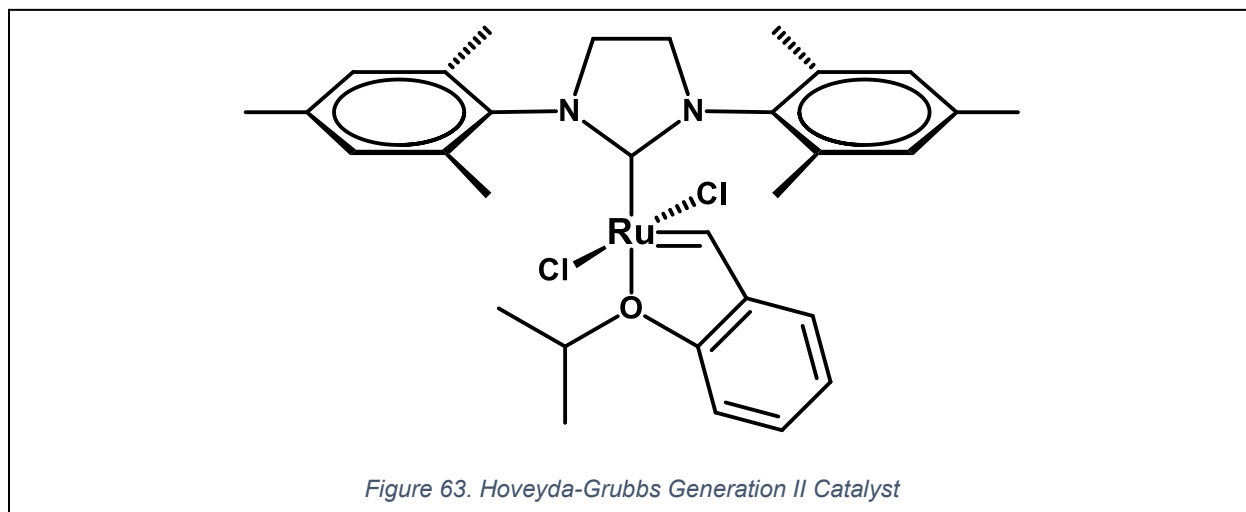
Roberts left over reaction mixtures and characterization data was combined with additional $^1\text{H-NMR}$ and MS spectra that were taken after his graduation. The data was analyzed to determine if he had been making trace amounts of the metathesis product. Unfortunately, all the data led to the conclusion that the desired product was not present.

Olefin cross metathesis, sometimes referred to as the Grubbs reaction or Grubbs metathesis, uses a molybdenum or ruthenium catalyst to “stitch” together two terminal olefins through a fragmentation and regeneration of two new olefins.⁹⁶ If the two olefins are monosubstituted, the byproduct would be ethylene. The catalyst starts as a metal carbene and forms a metallacyclobutane ring via a [2+2] cycloaddition reaction mediated by the metals available d-orbitals. A reverse cycloaddition generates the olefin by product leaving the substrates on the metal as a carbene. A second [2+2] cycloaddition then occurs to give the intermediate shown in **Figure 62**. This intermediate then fragments through a second reverse cycloaddition to give the cross metathesis product regenerating the catalyst.⁹⁷



Robert Grubbs, Yves Chauvin, and Richard Schrock were awarded the Nobel Prize in chemistry in 2005 for their work elucidating the mechanism and developing various catalyst capable of performing olefin cross metathesis reactions. The second-

generation Hoveyda-Grubbs metathesis catalyst (HGII, **Figure 63**) is one of the most popular catalyst because of its extreme stability in the presence of air and water.^{96,97}

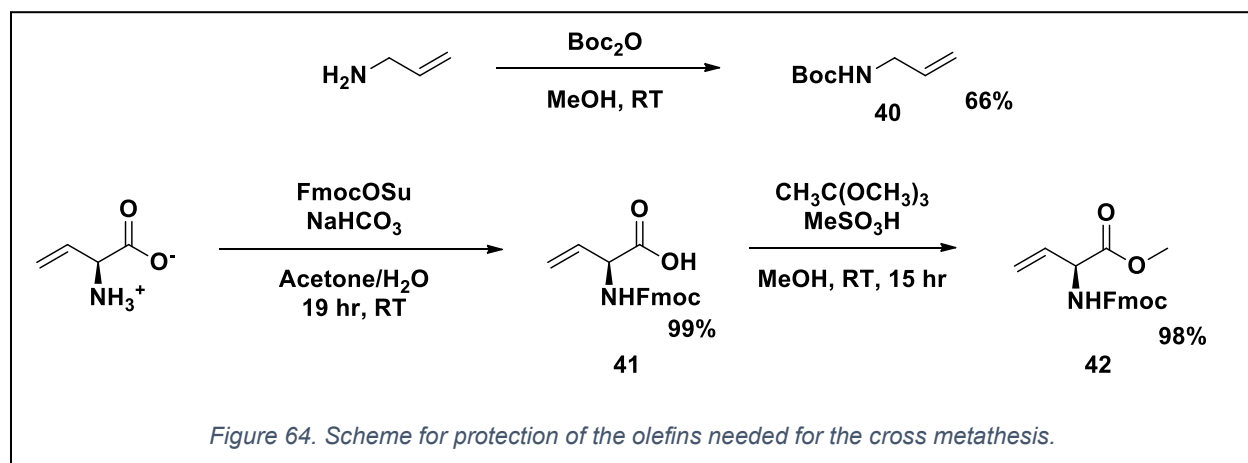


As Robert was unable to obtain the product, the catalyst was first assessed for catalytic activity. Allyl alcohol and HGII were refluxed in dichloromethane. After 5 hours, the starting material was still present by TLC (10% acetonitrile in dichloromethane; $R_f = 0.7$). Reaction was left stirring at room temperature for an additional 2 days before the reaction mixture was concentrated and analyzed by ^1H NMR spectroscopy. The proton spectrum showed some product had formed but it was still incomplete. As this reaction is known to be complete within 24 hours in refluxing CH_2Cl_2 ⁹⁸, the metathesis catalyst was deemed unusable and a new batch was ordered. The same experiment was performed with the new catalyst. This time the starting material was gone by TLC after 18 hours in refluxing CH_2Cl_2 and the ^1H NMR spectrum of the crude reaction mixture showed no trace of allyl alcohol.

The new catalyst was used to repeat some of the metathesis reaction attempted by Robert but were still unsuccessful. An example of the desired metathesis was found in the literature using Boc-N-L-(vinyl glycine) *t*-butyl ester and Fmoc-N-allyl amine. The

reported procedure used 2 equivalents of Fmoc-N-allylamine with 20 mol% HGII and gave a 36% yield after stirring for 14 hours at room temperature.⁹⁹ Encouraged by this report, a *t*-butyl ester was installed on the Boc-N-(vinyl glycine) by activating the carboxylic acid with N,N'-diisopropylcarbodiimide and catalytic N,N-dimethyl-4-aminopyridine in the presence of *t*-butanol. The crude mixture wasn't fully purified and only briefly characterized to ensure it was the desired product and was free of base. Using the impure Boc-N-L-(vinyl glycine) *t*-butyl ester, a microscale reaction was performed finally giving TLC, ¹H NMR, and MS evidence of the desired protected β,γ-dehydro-L-ornithine.

Due to the propensity of the protected vinyl glycine to isomerize in the presence of base, an ester had to be installed via an acid catalyzed reaction. Although it was unknown whether or not the fully protected β,γ-dehydro-L-ornathine would have the same isomerization potential as the protected vinyl glycine, it was assumed it would as a precaution. The scheme was altered to remove the ester using acidic conditions. As the Boc protecting group is acid labile, the protecting groups were switched so the side chain amine would be deprotected using the same reaction leaving the α-amine Fmoc



protected. The guanidinyl group could be installed and the final product would be obtained after complete deprotection.

Boc protection of allyl amine was done via di-*t*-butyl dicarbonate in methanol to give Boc-N-allyl amine **40**. The crude reaction mixture showed nearly 100% conversion by NMR integration. Purification is done by sublimation and product was lost during this product to give the subpar yield of 66%. As the reagents were cheap this was not a huge concern. L-(vinyl glycine) was dissolved in an acetone water mixture with solid sodium bicarbonate followed by the addition of N-(9-Fmoc) succinimide (Fmoc-OSu). Once the reaction was found to be complete by TLC (10% CH₃CN in CH₂Cl₂; SM: baseline, Product R_f: 0.2), the reaction mixture was brought to pH 1 with 12 M HCl and extracted with dichloromethane to give Fmoc-N-L-(vinyl glycine) **41** in a near quantitative yield. Further purification was not performed as the product would be more easily isolatable after installation of the ester. A methyl ester was installed using trimethylorthoformate and catalytic methanesulfonic acid. After refluxing in methanol for 15 hours the crude mixture was diluted in ether and washed with saturated sodium bicarbonate and brine to give the crude Fmoc-N-L-(vinyl glycine) methyl ester **42** in 98% yield. While there was no obvious contamination by ¹H NMR analysis, the product was recrystallized from a mixture of ether in hexanes (~ 3:1 by vol; bp 43 °C) to give an isolated yield of 63% from one crop. Although the ¹H NMR of each appeared to be of the same quality material the recrystallized product had a 10 °C higher melting point (108-109 °C).

Once the olefins were properly protected, the cross metathesis was performed using the Hoveyda-Grubbs II catalyst (HGII). The TLC analysis showed new spots not previously observed. A drop of the reaction mixture was diluted into CDCl₃ and analyzed by ¹H NMR spectroscopy. The spectrum obtained showed a doublet of triplets at 5.76 ppm and a doublet of doublets at 5.66 ppm. This was consistent with the literature values⁹⁹ indicating the production of the desired cross metathesis product **43**. After two additions of catalyst (5% by mol each addition) spread out over the course of two days the reaction mixture was separated via column chromatography and the protected β,γ-dehydro-L-ornithine **43** was isolated with a 40% yield. Heating the protected β,γ-dehydro-L-ornithine **43** uncovered at 60 °C in 12 M HCl for 1 hour successfully removed both the Boc protecting group and the methyl ester. Installation of the guanidyl group on **44** was accomplished with N,N'-di-boc-1H-pyrazole-1-

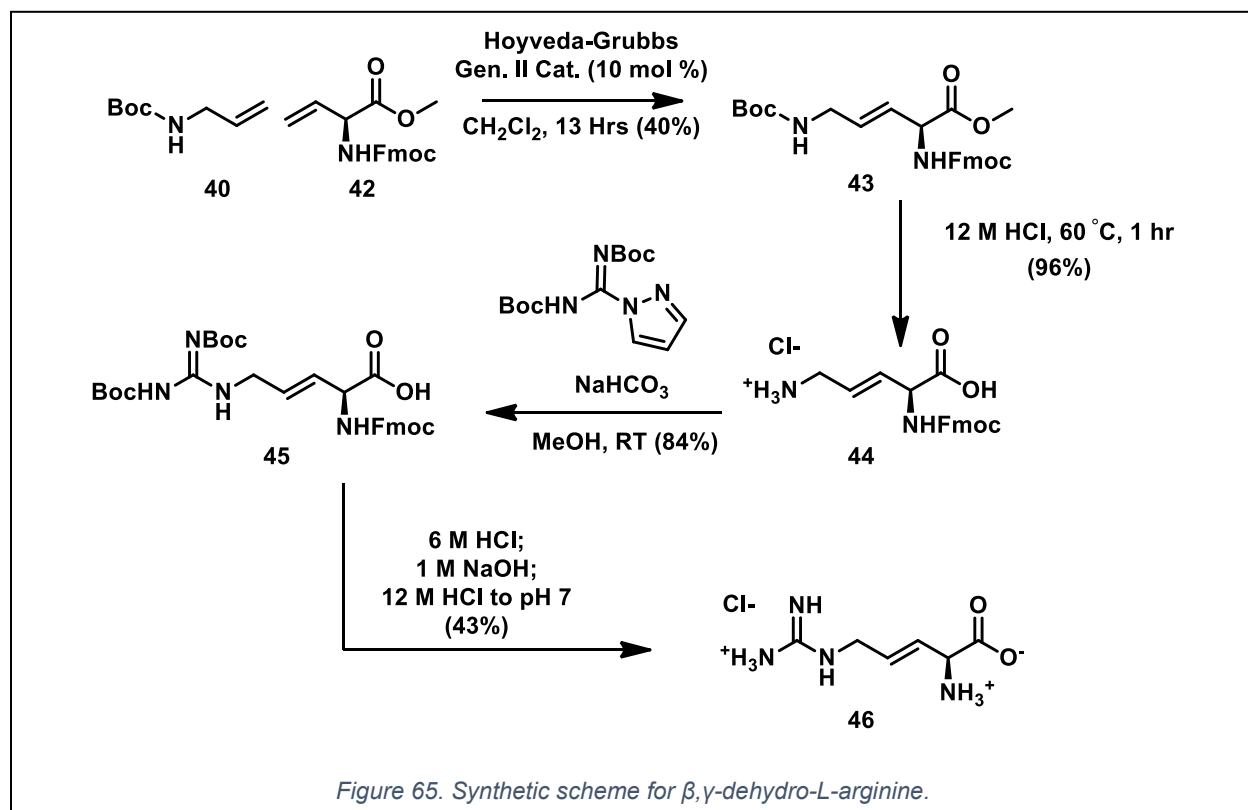


Figure 65. Synthetic scheme for β,γ-dehydro-L-arginine.

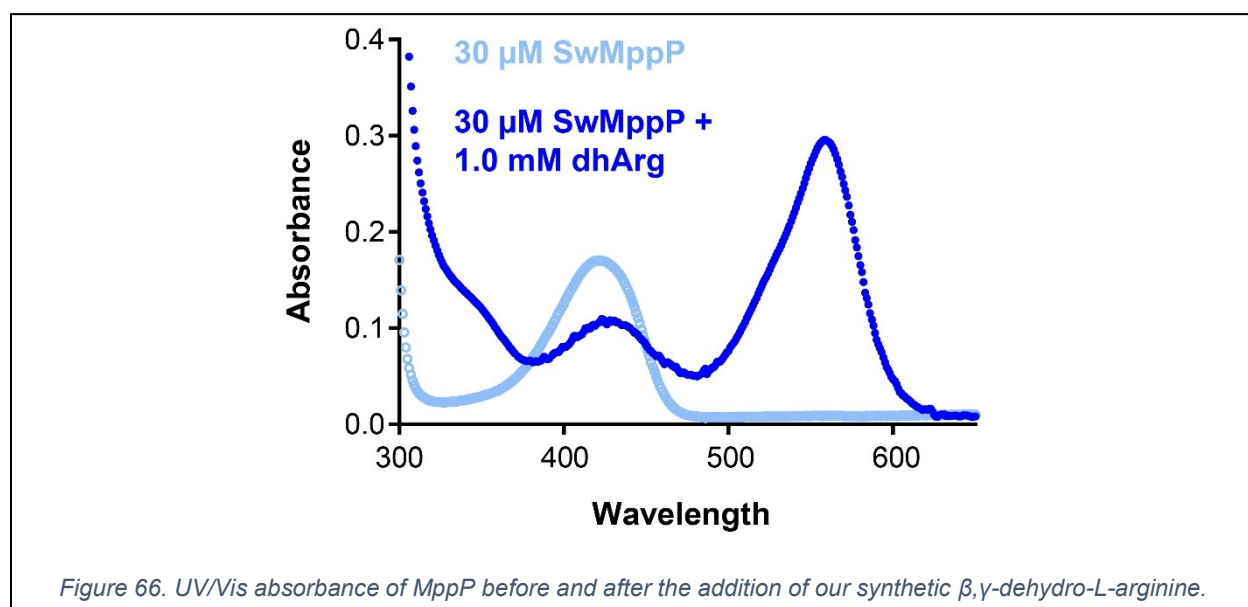
carboxamidine and sodium bicarbonate in methanol to give N,N'-diboc-N''-Fmoc- β,γ -dehydro-L-arginine **45** with an 84% yield.

The final product was obtained by suspending **45** in 12M HCl. The solid was treated with 2 portions of acid each of which was removed under reduced pressure leaving behind a off white solid. Removal of the Fmoc group was achieved by stirring this crude residue with minimal 1M NaOH and extracting the fluorene adduct with ethyl acetate. Neutralizing the solution with 12M HCl gave β,γ -dehydro-L-arginine **46** contaminated with NaCl. Using a known amount of *t*-butanol as an internal standard, a yield of 43% was calculated from ¹H NMR integration values.

Isolation of **46** was still of interest and alternative methods were explored to obtain it free of excess salt. Pyrrolidine is sufficiently basic enough to remove Fmoc groups and it's volatile enough that it can be removed under reduced pressure. Protected dehydroarginine **45** was combined with excess pyrrolidine in acetonitrile to facilitate the Fmoc removal. The mixture was concentrated until a constant mass was achieved giving the intermediate as a pyrrolidinium salt and the pyrrolidine fluorene adduct. The crude mass was triturated with ethanol multiple times and then treated with 6 M HCl in 50% aq. CH₃CN. This allowed the solid to be soluble for the Boc deprotection. The solution was concentrated again and dissolved in water, brought to pH 7 with LiOH and concentrated to giving a crude mass containing **46**, LiCl, and pyrrolidine. The crude mass was triturated with THF to remove the LiCl. Analysis of this product showed a small amount of **46** present but was still very impure and the yield was not any better. Work will continue in the Schwabacher group to improve these

procedures. The salt contaminated product was handed off to the Silvaggi group from MppP studies.

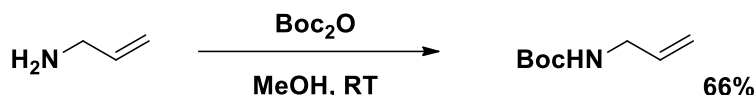
Preliminary studies by the Silvaggi group shows that when this product was given to MppP under anaerobic conditions, the enzyme showed a strong absorbance at 560 nm that quickly disappeared when exposed to O₂ giving strong evidence that our proposal was correct (**Figure 66**).



Experimental Details: Compounds 40-46

All characterization spectra can be found in the appendix to this dissertation.

N-Boc-allyl amine **40**



To a solution of di-tert-butyl dicarbonate (10.3177g, 47.3 mmol) in 40 mL methanol, allyl amine (4.0 mL, 53.4 mmol) was added and stirred for 20 minutes at room temperature. Reaction mixture was then concentrated to dryness under reduced pressure. Caution: The product is volatile, and yield can be reduced in placed under reduced pressure for a prolonged period of time. Product was sublimed under reduced pressure to give 4.955g (**67%**). MP: 28-34 °C (Sublimes).

¹H NMR (500 MHz, DMSO) δ 6.97 (s, 1H), 5.76 (dtd, *J* = 10.5, 5.3, 17.0 Hz, 1H), 5.08 (qd, *J* = 1.7, 17.2 Hz, 1H), 5.01 (qd, *J* = 1.7, 10.5 Hz, 1H), 3.54 (t, *J* = 5.2 Hz, 2H), 1.38 (s, 9H). ¹³C NMR (126 MHz, DMSO) δ 155.47 (s, 1C), 135.90 (s, 1C), 114.58 (s, 1C), 77.57 (s, 1C), 42.21 (s, 1C), 28.22 (s, 1C).

Fmoc Vinyl Glycine **41**

Fmoc-N-(L-Vinyl Glycine)-OH



To a suspension of vinyl glycine (0.9780g, 9.67 mmol) and sodium bicarbonate (1.6797g, 20.0 mmol) in a 40% acetone in water (50 mL) was added Fmoc-OSu (2.9364g, 8.71 mmol) and stirred under nitrogen. After stirring for 20 hours, TLC

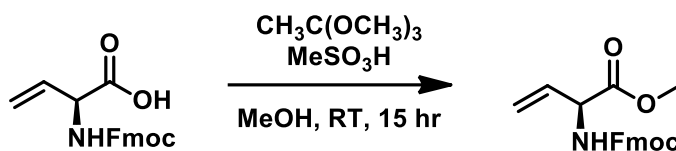
indicated the reaction was complete (10% CH₃CN/CH₂Cl₂). Reaction mixture was acidified to pH 1 with 12 M HCl and extracted with CH₂Cl₂ (3x100 mL). Organic layers were combined and washed with 1 M HCl (1x50 mL), dried over Na₂SO₄ and concentrated under reduced pressure to yield 2.8142g of a fluffy white solid (99.9%).

M.P. 154-156 °C

¹H NMR (500 MHz, DMSO) δ 12.82 (s, 1H), 7.93 (d, *J* = 8.2 Hz, 1H), 7.90 (d, *J* = 7.6 Hz, 2H), 7.74 (dd, *J* = 7.3, 4.3 Hz, 2H), 7.42 (t, *J* = 7.4 Hz, 2H), 7.33 (t, *J* = 7.3 Hz, 2H), 5.93 (ddd, *J* = 10.6, 6.3, 17.1 Hz, 1H), 5.34 (d, *J* = 17.3 Hz, 1H), 5.22 (d, *J* = 10.4 Hz, 1H), 4.62 (t, *J* = 7.2 Hz, 1H), 4.29 (d, *J* = 7.2 Hz, 2H), 4.23 (t, *J* = 7.3 Hz, 1H). ¹³C NMR (126 MHz, DMSO) δ 171.77, 155.86, 143.81, 143.77, 140.71, 132.94, 127.65, 127.07, 125.32, 120.11, 117.40, 65.80, 56.46, 46.60. ESI-MS Calculated for C₁₉H₁₇NO₄ [M+Na⁺] 346.10, Found 346.25

Fmoc Vinyl Glycine Methyl Ester **42**

Fmoc-N-(L-Vinyl Glycine)-OCH₃

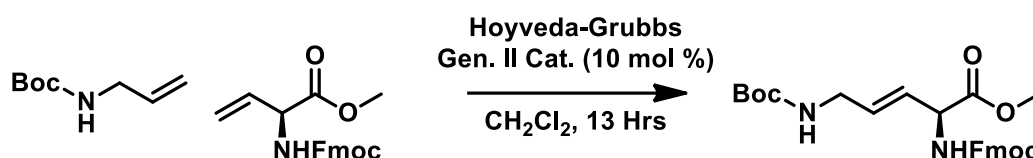


To a solution of Fmoc-(vinyl glycine)-OH (2.8142g, 8.70 mmol) and trimethyl orthoacetate (1.20 mL, 9.43 mmol) in methanol (50 mL) was added methanesulfonic acid (0.10 mL, 1.54 mmol) and stirred at room temperature for 15 hours. Methanol removed by rotary evaporation and crude residue dissolved in ether (50 mL). Ether was washed with sat. NaHCO₃ (2x25 mL) and brine (25 mL), dried over Na₂SO₄,

concentrated by rotary evaporation and dried under reduced pressure to give 2.8835g (98%) of fluffy white solid. M.P. 100-102 °C

¹H NMR (500 MHz, DMSO) δ 8.08 (d, *J* = 7.8 Hz, 1H), 7.91 (d, *J* = 7.5 Hz, 2H), 7.74 (dd, *J* = 6.9, 5.6 Hz, 2H), 7.43 (t, *J* = 7.4 Hz, 2H), 7.34 (t, *J* = 7.4 Hz, 2H), 5.92 (ddd, *J* = 10.6, 6.7, 17.2 Hz, 1H), 5.36 (d, *J* = 17.2 Hz, 1H), 5.26 (d, *J* = 10.4 Hz, 1H), 4.71 (t, *J* = 7.1 Hz, 1H), 4.32 (td, *J* = 6.8, 2.5 Hz, 2H), 4.24 (t, *J* = 6.9 Hz, 1H), 3.66 (s, 3H). ¹³C NMR (126 MHz, DMSO) δ 170.93, 155.83, 143.73, 140.72, 132.28, 127.65, 127.07, 125.26, 120.12, 118.26, 65.82, 56.45, 52.18, 46.58. ESI-MS Calculated for C₂₀H₁₉NO₄ [M+Na⁺] 360.12, Found 360.25.

N_δ-Boc-N_α-Fmoc-β,γ-dehydro-L-ornithine methyl ester **43**

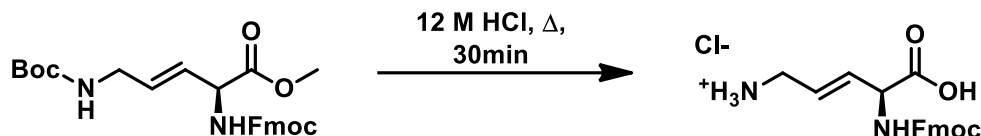


To a solution of Boc-N-allyl amine (0.7281g, 4.63 mmol) and Fmoc-N-(vinyl glycine)-OCH₃ (0.6468g, 1.92 mmol) in CH₂Cl₂ (25 mL) was added Hoveyda Grubbs generation II catalyst (HGII) (62.3 mg, 0.100 mmol) and stirred under N₂ for 4 hours. A 2nd addition of HGII was added (59.5 mg, 0.095 mmol) and stirred for an additional 12 hours before solvent was removed by rotary evaporation. The crude residue was separated via column chromatography (50% ether in hexanes, Product R_f = 0.17) to give 361.3 mg (40%) as a white solid. M.P. 88-91 °C

¹H NMR (500 MHz, DMSO) δ 8.06 (d, *J* = 7.8 Hz, 1H), 7.89 (d, *J* = 7.6 Hz, 2H), 7.73 (dd, *J* = 7.1, 4.4 Hz, 2H), 7.42 (t, *J* = 7.4 Hz, 2H), 7.33 (t, *J* = 7.4 Hz, 2H), 5.72 (td, *J* = 5.0, 15.4 Hz, 1H), 5.61 (dd, *J* = 6.6, 15.6 Hz, 1H), 4.67 (t, *J* = 7.1 Hz, 1H), 4.28 (d, *J* =

6.0 Hz, 2H), 4.22 (t, $J = 7.0$ Hz, 1H), 3.63 (s, 3H), 1.37 (s, 9H). ^{13}C NMR (126 MHz, DMSO) δ 171.64, 156.27, 155.91, 144.26, 144.21, 141.19, 137.17, 131.94, 128.12, 127.55, 125.76, 120.59, 78.19, 66.31, 52.62, 47.06, 28.71, 25.97. ESI-MS Calculated for $\text{C}_{26}\text{H}_{30}\text{N}_2\text{O}_6$ $[\text{M}+\text{Na}^+]$ 489.20, Found 489.40.

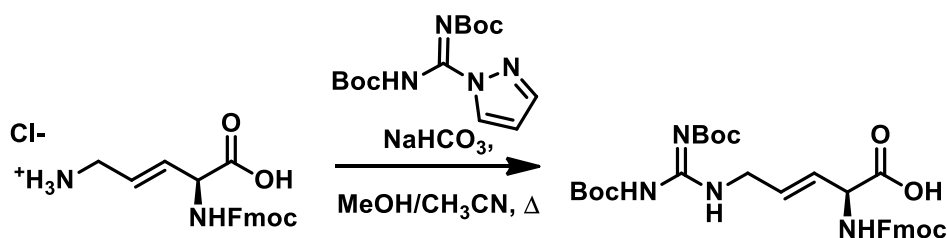
N_α -Fmoc-(β,γ -dehydro-L-ornithine)-OH HCl **44**



Metathesis product **43** (268.5 mg, 0.576 mmol) was boiled in 12 M HCl for 30 minutes before solvent was removed by rotary evaporation and dried azeotropically with toluene (3x25 mL) to give 215.6 mg (96%) of an off-white solid.

^1H NMR (500 MHz, DMSO) δ 8.06 (br-s, 3H), 8.02 (d, $J = 8.5$ Hz, 1H), 7.91 (d, $J = 7.5$ Hz, 2H), 7.75 (dd, $J = 7.2, 4.7$ Hz, 2H), 7.43 (t, $J = 7.4$ Hz, 2H), 7.34 (t, $J = 7.5$ Hz, 2H), 5.97 (dd, $J = 6.2, 15.7$ Hz, 1H), 5.81 (td, $J = 6.5, 15.2$ Hz, 1H), 4.69 (t, $J = 7.1$ Hz, 1H), 4.30 (m, 2H), 4.24 (m, 1H), 3.47 (br-s, 3H). ^{13}C NMR (126 MHz, DMSO) δ 171.46, 155.87, 143.80, 140.74, 130.43, 128.03, 127.69, 127.12, 125.33, 125.07, 120.16, 65.89, 55.29, 46.60. ESI-MS Calculated for $\text{C}_{20}\text{H}_{20}\text{N}_2\text{O}_4$ $[\text{M}+\text{H}^+]$ 353.15, Found 353.30.

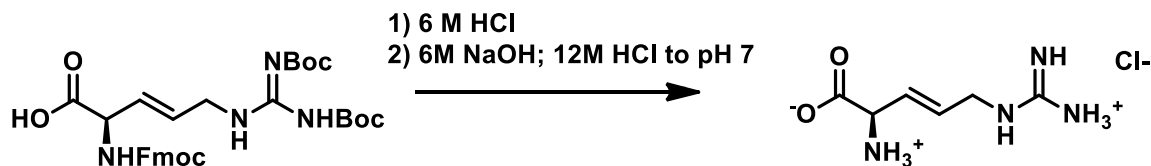
N_α -Fmoc- N_δ -(N,N' -dibocguanyl)-(β,γ -dehydro-L-ornithine)-OH **45**



To a suspension of Fmoc-N^α-(β,γ-dehydroornithine)-OH HCl (181.8 mg, 0.395 mmol) and NaHCO₃ (74.5 mg, 0.887 mmol) in methanol (20 mL) was added N,N'-di-boc-1H-pyrazole-1-carboximidine (149.6 mg, 0.482 mmol) and heated at reflux for 4 days. Reaction mixture was concentrated by rotary evaporation and reconstituted in ethyl acetate (75 mL), extracted with water (30 mL), acidified to pH 3 with conc. H₃PO₄, extracted with ethyl acetate (2x20 mL), dried over Na₂SO₄, concentrated by rotary evaporation and dried under reduced pressure to give 266.6 mg as a crude product. Crude mass was triturated with 50% ether in hexanes (10 mL) and solution decanted and concentrated to give 189.0 mg (81%) as a white solid.

¹H NMR (500 MHz, H₂O+D₂O) δ 7.75 (d, J = 7.2 Hz, 2H), 7.61 (t, J = 6.1 Hz, 2H), 7.39 (t, J = 6.5 Hz, 2H), 7.31 (t, J = 7.4 Hz, 2H), 5.80 (mul, 1H), 5.66 (d, J = 8.0 Hz, 1H), 4.97 (t, J = 5.3 Hz, 1H), 4.46 (d, J = 7.2 Hz, 2H), 4.40 (t, J = 7.4 Hz, 1H), 4.23 (t, J = 6.9 Hz, 2H), 4.07 (s, 1H), 1.49 (s, 18H). ESI-MS Calculated for C₃₁H₃₈N₄O₈ [M+H] 595.28, Found 595.20.

β,γ-dehydro-L-arginine HCl **46**



A suspension of β,γ-dehydroornithine **45** (122.1 mg, 0.205 mmol) in 6 M HCl was heated (60 °C) for 30 minutes before decanting off solvent and drying under reduced pressure. The crude residue was combined with 1M NaOH (10 mL) and stirred for 30 minutes, washed with ethyl acetate (2x25 mL) and acidified with to pH 7 with 12M HCl, concentrated by rotary evaporation and dried under reduced pressure to give 493.7 mg

of solid. ~5% pure by NMR integrations (against known tBuOH added). 43% yield by NMR.

^1H NMR (500 MHz, MeOD) δ 5.98 (dtd, $J = 0.9, 4.7, 15.7$ Hz, 1H), 5.75 (tdd, $J = 1.8, 8.1, 15.8$ Hz, 1H), 4.41 (d, $J = 7.9$ Hz, 1H), 3.87 (d, $J = 4.9$ Hz, 2H). ESI-MS Calculated for $\text{C}_6\text{H}_{12}\text{N}_4\text{O}_2$ $[\text{M}+\text{H}^+]$ 173.10, Found 174.10

References

- (1) Paolieri, M. Ferdinand Munz: EDTA and 40 Years of Inventions. *Bull. Hist. Chem.* **2017**, 2 (42), 133–140.
- (2) Pedersen, C. J. The Discovery of Crown Ethers. In *Nobel Lectures, Chemistry 1981-1990*; Frängsmyr, T., Malmström, B. G., Eds.; World Scientific Publishing Co.: Singapore, 1992; pp 495–511.
- (3) Crini, G. Review: A History of Cyclodextrins. *Chem. Rev.* **2014**, 114, 10940–10975.
- (4) Tiwari, G.; Tiwari, R.; Rai, A. Cyclodextrins in Delivery Systems: Applications. *J. Pharm. Bioallied Sci.* **2010**, 2 (2), 72.
- (5) Kralova, J.; Synytsya, A.; Pouckova, P.; Koc, M.; Dvorak, M.; Kral, V. Novel Porphyrin Conjugates with a Potent Photodynamic Antitumor Effect: Differential Efficacy of Mono- and Bis- β -Cyclodextrin Derivatives In Vitro and In Vivo. *Photochem. Photobiol.* **2006**, 82 (2), 432.
- (6) Gil, E. S.; Wu, L.; Xu, L.; Lowe, T. L. B-Cyclodextrin-Poly(B-Amino Ester) Nanoparticles for Sustained Drug Delivery Across the Blood-Brain Barrier. *Biomacromolecules* **2012**, 13 (11), 3533–3541.
- (7) Davis, M. E. Design and Development of IT-101, a Cyclodextrin-Containing Polymer Conjugate of Camptothecin. *Adv. Drug Deliv. Rev.* **2009**, 61 (13), 1189–1192.
- (8) Ma, J. C.; Dougherty, D. A.; Beckman, M. *The Cation- π Interaction*; 1997; Vol. 97, pp 1303–1324.

- (9) Dougherty, D. A. The Cation- π Interaction. *Acc. Chem. Res.* **2013**, *46* (4), 885–893.
- (10) Petsko, G. A.; Ringe, D. *Protein Structure and Function*; Lawrence, E., Robertson, M., Freeland, K., Eds.; New Science Press Ltd: London, 2004.
- (11) Nowick, J. S. Exploring Beta-Sheet Structure and Interactions with Chemical Model Systems. *Acc. Chem. Res.* **2008**, *41* (10), 1319–1330.
- (12) Nowick, J. S.; Pairish, M.; Lee, I. Q.; Holmes, D. L.; Ziller, J. W. An Extended B-Strand Mimic for a Larger Artificial β -Sheet. *J. Am. Chem. Soc.* **1997**, *7863* (2), 5413–5424.
- (13) Kirsten, C. N.; Schrader, T. H. *Intermolecular-Sheet Stabilization with Aminopyrazoles*; 1997; Vol. 119, pp 12061–12068.
- (14) Liu, C.; Sawaya, M. R.; Cheng, P.-N.; Zheng, J.; Nowick, J. S.; Eisenberg, D. Characteristics of Amyloid-Related Oligomers Revealed by Crystal Structures of Macrocyclic β -Sheet Mimics. *J. Am. Chem. Soc.* **2011**, *133*, 6736–6744.
- (15) Kemp, D. S.; Bowen, B. R.; Muendel, C. C. Synthesis and Conformational Analysis of Epindolidione-Derived Peptide Models for β -Sheet Formation. *J. Org. Chem.* **1990**, *55*, 4650–4657.
- (16) Tsang, K. Y.; Diaz, H.; Graciani, N.; Kelly, J. W.; Gellman, S. H.; Seebach, D.; Matthews, J. L.; Smith, E. M.; Holmes, D. L.; Shaka, A. J.; et al. A Triply Templated Artificial-Sheet⁴ (*A. Bioorg. Med. Chem.* **1990**, *55* (5), 23.
- (17) Nowick, J. S.; Lam, K. S.; Khasanova, T. V; Kemnitzer, W. E.; Maitra, S.; Mee, H.

- T.; Liu, R. An Unnatural Amino Acid That Induces Beta-Sheet Folding and Interaction in Peptides. *J. Am. Chem. Soc.* **2002**, *124*, 4972–4973.
- (18) Nowick, J. S. Exploring-Sheet Structure and Interactions with Chemical Model Systems. *Acc. Chem. Res.* **2008**, *41* (10), 1319–1330.
- (19) Nowick, J. S.; Chung, D. M.; Maitra, K.; Maitra, S.; Stigers, K. D.; Sun, Y. An Unnatural Amino Acid That Mimics a Tripeptide-Strand and Forms-Sheetlike Hydrogen-Bonded Dimers. *J. Am. Chem. Soc.* **2000**, *122*, 7654–7661.
- (20) Salvaggio, F.; Hodgkinson, J. T.; Carro, L.; Geddis, S. M.; Galloway, W. R. J. D.; Welch, M.; Spring, D. R. The Synthesis of Quinolone Natural Products from *Pseudonocardia* Sp. *European J. Org. Chem.* **2016**, *2016* (3), 434–437.
- (21) Xu, X.; Sun, R.; Zhang, S.; Zhang, X.; Yi, W. Divergent Synthesis of Quinolones and Dihydroepindolidiones via Cu(I)-Catalyzed Cyclization of Anilines with Alkynes. *Org. Lett* **2018**, *20*, 1893–1897.
- (22) Mashaly, M. M.; El-gogary, S. R.; Kosbar, T. R. Enaminones in Heterocyclic Syntheses: Part 4. A New One-Step Synthetic Route to Pyrrolo[3,4-b]Pyridine and Convenient Syntheses of 1,4-Dihydropyridines and 1,10-(1,4-Phenylene)Bis(1,4-Dihydropyridine). *J. Heterocycl. Chem* **2014**, *51*, 1078–1085.
- (23) Horchler, C. L.; Mccauley, J. P.; Hall, J. E.; Snyder, D. H.; Moore, W. C.; Hudzik, T. J.; Chapdelaine, M. J. Synthesis of Novel Quinolone and Quinoline-2-Carboxylic Acid (4-Morpholin-4-YI-Phenyl)Amides: A Late-Stage Diversification Approach to Potent 5HT 1B Antagonists. *Bioorg. Med. Chem.* **2007**, *15*, 939–950.

- (24) Zewge, D.; Chen, C.; Deer, C.; Domer, P.; Hughes, D. A Mild and Efficient Synthesis of 4-Quinolones and Quinolone Heterocycles. *JOC Note* **2007**, *72*, 4276–4279.
- (25) Pollock, B. J.; Sikes, C. A.; Louw, R. P. Ter; Hawken, S. R.; Speelman, A. L.; Lynch, E. J.; Stanford, D. J.; Wheeler, K. A.; Gillmore, J. G. Synthesis and Structural Investigation of an "Oxazinoquinolinespirohexadienone" That Only Exists as Its Long-Wavelength Ring-Opened Quinonimine Isomer. *J. Org. Chem.* **2012**, *77*, 8689–8695.
- (26) Tan, E.; Konovalov, A. I.; Fernándezfernández, G. A.; Dorel, R.; Echavarren, A. M.; Domingo, M.; Spain, T. Ruthenium-Catalyzed Peri-and Ortho-Alkynylation with Bromoalkynes via Insertion and Elimination. *Org. Lett.* **2017**, *19*, 5561–5564.
- (27) Hall, C. M.; Wright, J. B.; Johnson, H. G.; Taylor, A. J. Quinoline Derivatives as Antiallergy Agents. 2. Fused-Ring Quinaldic Acids. *J. Med. Chem.* **1977**, *20*, 1337–1343.
- (28) Markofsky, S.; Olney, M. Process for the Preparation of Nitroacetate. 5162572, 1992.
- (29) Bendz, G.; Culvenor, C. C. J.; Goldsworthy, L. J.; Kirby, K. S.; Robinson, R. Quinamine. Part IV. Sulphobenzeneazoquinumine and Nitration and Oxidation of Quinamine to 3:6:8-Trinitro-4-Hydroxyquinoline. *J. Chem. Soc* **1950**, 1130–1138.
- (30) Tiwari, K. Synthesis of a Versatile Building Block for Binding Site Preparation, UW - Milwaukee.

- (31) Sun, B.; Liu, K.; Han, J.; Zhao, L.-Y.; Su, X.; Lin, B.; Zhao, D.-M.; Cheng, M.-S. Design, Synthesis, and Biological Evaluation of Amide Imidazole Derivatives as Novel Metabolic Enzyme CYP26A1 Inhibitors. *Bioorg. Med. Chem.* **2015**, *23*, 6763–6773.
- (32) Weiner, W.; Hamilton, A. Synthesis and Binding Studies of a 1-Alkyl-3,6-Diamino-4-Quinolone Based Receptor for N-Acylated Dipeptides. *Bioorg. Med. Chem. Lett.* **1997**, *8* (6), 681–686.
- (33) Cecchetti, V.; Parolin, C.; Moro, S.; Pecere, T.; Filipponi, E.; Calistri, A.; Tabarrini, O.; Gatto, B.; Palumbo, M.; Fravolini, A.; et al. 6-Aminoquinolones as New Potential Anti-HIV Agents. *J. Med. Chem.* **2000**, *43*, 3799–3802.
- (34) Malvacio, I.; Laura Moyano, E.; Mariano, D.; Vera, A. Gas-Phase Synthesis of 3-Carboethoxy-Quinolin-4-Ones. A Comprehensive Computational Mechanistic Study to Uncover the Dark Side of the Gould-Jacobs Reaction †. *RCS Adv.* **2016**, *6*, 83973–83981.
- (35) Comparison of AAS, ICP-AES, PSA, and XRF in Determining Lead and Cadmium in Soil. *Environ. Sci. Technol.* **1995**, *30*, 204–213.
- (36) Mezohegyi, G.; Fabregat, A.; Font, J.; Bengoa, C.; Stuber, F.; Fortuny, A. Advanced Bioreduction of Commercially Important Azo Dyes: Modeling and Correlation with Electrochemical Characteristics. *Ind. Eng. Chem. Res.* **2009**, *48*, 7054–7059.
- (37) Eggeling, C.; Widengren, J.; Rigler, R.; Seidel, C. A. M. Photobleaching of Fluorescent Dyes under Conditions Used for Single-Molecule Detection: Evidence

- of Two-Step Photolysis. *Anal. Chem.* **1998**, *70*, 2651–2659.
- (38) Karlsson, J. K. G.; Woodford, O. J.; Al-Aqar, R.; Harriman, A. Effects of Temperature and Concentration on the Rate of Photobleaching of Erythrosine in Water. *J. Phys. Chem. A* **2017**, *121*, 8569–8576.
- (39) Tian, Y.; Shumway, B. R.; Meldrum, D. R. A New Cross-Linkable Oxygen Sensor Covalently Bonded into Poly(2-Hydroxyethyl Methacrylate)-Co-Polyacrylamide Thin Film for Dissolved Oxygen Sensing. *Chem. Mater.* **2010**, *22* (6), 2069–2078.
- (40) Tierney, S.; Hasle Falch, B. M.; Hjelme, D. R.; Stokke, B. T. Determination of Glucose Levels Using a Functionalized Hydrogel-Optical Fiber Biosensor: Toward Continuous Monitoring of Blood Glucose in Vivo. *Anal. Chem.* **2009**, *81* (9), 3630–3636.
- (41) Gogoi, N.; Barooah, M.; Majumdar, G.; Chowdhury, D. Carbon Dots Rooted Agarose Hydrogel Hybrid Platform for Optical Detection and Separation of Heavy Metal Ions. *ACS Appl. Mater. Interfaces* **2015**, *7* (5), 3058–3067.
- (42) Zhang, X.; Guan, Y.; Zhang, Y. Ultrathin Hydrogel Films for Rapid Optical Biosensing. *Biomacromolecules* **2012**, *13* (1), 92–97.
- (43) Püntener, A.; Page, C. *European Ban on Certain Azo Dyes*; 2004.
- (44) Kocyła, A.; Pomorski, A.; Krężel, A.; Krężel, A.; Krężel, A.; Krężel, A. Molar Absorption Coefficients and Stability Constants of Metal Complexes of 4-(2-Pyridylazo)Resorcinol (PAR): Revisiting Common Chelating Probe for the Study of Metalloproteins. *J. Inorg. Biochem.* **2015**, *152*, 82–92.

- (45) Vyshcherevich, I. V.; Kalinichenko, I. E. Photometric Determination in Drinking Water of Cobalt and Nickel with 4-(2-Pyridylazo)-Resorcinol. *J. Water Chem. Technol.* **2010**, *32* (1), 33–38.
- (46) Oehm, S. A. Studies in Molecular Recognition: Non-Proteogenic Amino Acids for Antibiotic Studies and Chemosensors for Recognition and Reporting of Metal-Ions, University of Wisconsin - Milwaukee, 2018.
- (47) Maity, D.; Govindaraju, T. Highly Selective Colorimetric Chemosensor for Co²⁺. *Inorg. Chem* **2011**, *50*, 11282–11284.
- (48) Chen, C.-T.; Huang, W.-P. A Highly Selective Fluorescent Chemosensor for Lead Ions. *J. Am. Chem. Soc.* **2002**, *124*, 6246–6247.
- (49) Wang, J.-N.; Qi, Q.; Zhang, L.; Li, S.-H. Turn-On Luminescent Sensing of Metal Cations via Quencher Displacement: Rational Design of a Highly Selective Chemosensor for Chromium(III). *Inorg. Chem* **2012**, *51*, 13103–13107.
- (50) Hee Lee, M.; Wu, J.-S.; Won Lee, J.; Hwa Jung, J.; Seung Kim, J.; Org Lett, J. Highly Sensitive and Selective Chemosensor for Hg²⁺ Based on the Rhodamine Fluorophore. *Org. Lett.* **2007**, *9* (13), 2501–2504.
- (51) Hierlemann, A.; Gutierrez-Osuna, R. Higher-Order Chemical Sensing. *Chem. Rev.* **2008**, *108*, 563–613.
- (52) Palacios, M. A.; Wang, Z.; Montes, V. A.; Zyryanov, G. V; Anzenbacher, P. Rational Design of a Minimal Size Sensor Array for Metal Ion Detection. *J. Am. Chem. Soc.* **2008**, *130* (10307–10314).

- (53) Xu, W.; Ren, C.; Lean Teoh, C.; Peng, J.; Haribhau Gadre, S.; Rhee, H.-W.; Ken Lee, C.-L.; Chang, Y.-T. An Artificial Tongue Fluorescent Sensor Array for Identification and Quantitation of Various Heavy Metal Ions. *Anal. Chem* **2014**, *86*, 8763–8769.
- (54) Labeets, J. A REAL-TIME APPROACH TO PROCESS MONITORING OF HEAVY METALS: SPECTROPHOTOMETRIC CHARACTERIZATION AND APPLICATION OF NOVEL AZO DYES No Title, UW - Milwaukee, 2019.
- (55) BRANDRUP, J.; IMMERGUT, E. H.; GRULKE, E. A. *Polymer Handbook*, 4th ed.; ABE, A., BLOCH, D. R., Eds.; JOHN WILEY & SONS, INC.: New York, NY, 1999.
- (56) Chen, J.-J.; Struk, K. N.; Brennan, A. B. Surface Modification of Silicate Glass Using 3-(Mercaptopropyl)Trimethoxysilane for Thiol–Ene Polymerization. *Langmuir* **2011**, *27* (22), 13754–13761.
- (57) Liu, J.; Lu, X.; Xin, Z.; Zhou, C. Synthesis and Surface Properties of Low Surface Free Energy Silane-Functional Polybenzoxazine Films. *Langmuir* **2013**, *29* (1), 411–416.
- (58) Zeng, X.; Xu, G.; Gao, Y.; An, Y. Surface Wettability of (3-Aminopropyl)Triethoxysilane Self-Assembled Monolayers. *J. Phys. Chem. B* **2011**, *115* (3), 450–454.
- (59) Chen, Y.-H.; He, Y.-C.; Yaung, J.-F. Exploring PH-Sensitive Hydrogels Using an Ionic Soft Contact Lens: An Activity Using Common Household Materials. *J. Chem. Ed* **2014**, *91*, 1671–1674.

- (60) MCGOVERN, M. E.; KALLURY, K. M. R.; THOMPSON, M. Role of Solvent on the Silanization of Glass with Octadecyltrichlorosilane. *Langmuir* **1994**, *10*, 3607–3614.
- (61) AHMED, E. M. Hydrogel: Preparation, Characterization, and Applications: A Review. *J. Adv. Res.* **2015**, *6* (2), 105–121.
- (62) WICHTERLE, O.; LÍM, D. Hydrophilic Gels for Biological Use. *Nature* **1960**, *185* (4706), 117–118.
- (63) SCHWABACHER, A. W.; LANE, J. W.; SCHIESHER, M. W.; LEIGH, K. M.; JOHNSON, C. W. Desymmetrization Reactions: Efficient Preparation of Unsymmetrically Substituted Linker Molecules. *J. Org. Chem.* **1998**, *63* (5), 1727–1729.
- (64) ACRES, R. G.; ELLIS, A. V.; ALVINO, J.; LENAHAN, C. E.; KHODAKOV, D. A.; METHA, G. F.; ANDERSSON, G. G. Molecular Structure of 3-Aminopropyltriethoxysilane Layers Formed on Silanol-Terminated Silicon Surfaces. *J. Phys. Chem. C* **2012**, *116*, 6289–6297.
- (65) ZHU, M.; LERUM, M. Z.; CHEN, W. How to Prepare Reproducible, Homogeneous, and Hydrolytically Stable Aminosilane-Derived Layers on Silica. *Langmuir* **2012**, *10* (28), 416–423.
- (66) MUNIEF, W.-M.; HEIB, F.; HEMPEL, F.; LU, X.; SCHWARTZ, M.; PACHAURI, V.; HEMPELMANN, R.; SCHMITT, M.; INGEBRANDT, S. Silane Deposition via Gas-Phase Evaporation and High-Resolution Surface Characterization of the Ultrathin Siloxane Coatings. *Langmuir* **2018**, *34*, 10217–10229.

- (67) Ek, S.; Iiskola, E. I.; Niinistö, L. Gas-Phase Deposition of Aminopropylalkoxysilanes on Porous Silica. *Langmuir* **2003**, *19*, 3461–3471.
- (68) Cras, J. J.; Rowe-Taitt, C. A.; Nivens, D. A.; Ligler, F. S. Comparison of Chemical Cleaning Methods of Glass in Preparation for Silanization. *Biosens. Bioelectron.* **1999**, *14* (8), 683–688.
- (69) Ek, S.; Iiskola, E. I.; Niinistö, L. Atomic Layer Deposition of Amino-Functionalized Silica Surfaces Using N-(2-Aminoethyl)-3-Aminopropyltrimethoxysilane as a Silylating Agent. *J. Phys. Chem. B* **2004**, *108*, 9650–9655.
- (70) Kiihler, T. C.; Lindsten, G. R. Preparative Reversed-Phase Flash Chromatography, a Convenient Method for the Workup of Reaction Mixtures. *J. Org. Chem.* **1983**, *48* (20), 3589–3591.
- (71) Baggott, J. E.; Frey, M.; Lightfoot, P. D.; Walsh, R. Reactions of the Formyl Radical with Alkyl Radicals. *J. Phys. Chem* **1987**, *91*, 3386–3393.
- (72) Lange, K. M.; Hodeck, K. F.; Schade, U.; Aziz, E. F. Nature of the Hydrogen Bond of Water in Solvents of Different Polarities. *J. Phys. Chem. B* **2010**, *114*, 16997–17001.
- (73) Zielkiewicz, J. Solvation of DMF in the N,N-Dimethylformamide+Alcohol+Water Mixtures Investigated by Means of the Kirkwood-Buff Integrals. *J. Phys. Chem* **1995**, *99*, 4787–4793.
- (74) Fenske, M. R.; Fisher, E. K.; Hersh, R. E. Viscosity of Petroleum Products Viscosity-Temperature Characteristics of Pennsylvania Lubricating Oils. *Ind. Eng.*

- Chem* **1935**, 27 (12), 1441–1446.
- (75) Li, W.; Chung, H.; Daeffler, C.; Johnson, J. A.; Grubbs, R. H.; Arnold, T.; Beckman, M. Application of ¹H DOSY for Facile Measurement of Polymer Molecular Weights. *Macromolecules* **2012**, 45, 9595–9603.
- (76) Li, D.; Kagan, G.; Hopson, R.; Williard, P. G. Formula Weight Prediction by Internal Reference Diffusion-Ordered NMR Spectroscopy (DOSY). *J. Am. Chem. Soc.* **2009**, 131, 5627–5634.
- (77) Plummer, R.; Hill, D. J. T.; Whittaker, A. K. DOSY NMR Studies of Chemical Exchange Behavior of Poly(2-Hydroxyethyl Methacrylate). *Macromolecules* **2006**, 39, 3878–3889.
- (78) Phane Viel, S.; Capitani, D.; Mannina, L.; Segre, A. Diffusion-Ordered NMR Spectroscopy: A Versatile Tool for the Molecular Weight Determination of Uncharged Polysaccharides. *Biomacromolecules* **2003**, 4, 1843–1847.
- (79) Einstein, A. *Investigations on the Theory of the Brownian Movement*; Dover Books on Physics Series; Dover Publications, 1956.
- (80) Chen, A.; Wu, D.; Johnson, C. S. Determination of Molecular Weight Distributions for Polymers by Diffusion-Ordered NMR. *J. Am. Chem. Soc.* **1995**, 117, 7965–7970.
- (81) Gu, K.; Onorato, J.; Xiao, S. S.; Luscombe, C. K.; Loo, Y.-L. Determination of the Molecular Weight of Conjugated Polymers with Diffusion-Ordered NMR Spectroscopy. *Chem. Mater* **2018**, 30, 570–576.

- (82) Kasten, K.; Slawin, A. M. Z.; Smith, A. D. Enantioselective Synthesis of β -Fluoro- β -Aryl- α -Aminopentenamides by Organocatalytic [2,3]-Sigmatropic Rearrangement. *Org. Lett.* **2017**, *19* (19), 5182–5185.
- (83) Good, N. E.; Douglas Winget, G.; Winter, W.; Connolly, T. N.; Izawa, S.; Singh, R. M. Hydrogen Ion Buffers for Biological Research. *Biochemistry* **1966**, *5* (2), 467–477.
- (84) Giltrap, A. M.; Dowman, L. J.; Nagalingam, G.; Ochoa, J. L.; Linington, R. G.; Warwick, II; Britton, J.; Payne, R. J. Total Synthesis of Teixobactin. *Org. Lett.* **2016**, *18*, 2788–2791.
- (85) Han, L.; Schwabacher, A. W.; Moran, G. R.; Silvaggi, N. R. Streptomyces Wadayamensis MppP Is a Pyridoxal 5'-Phosphate-Dependent L-Arginine α -Deaminase, γ -Hydroxylase in the Enduracididine Biosynthetic Pathway. *Biochemistry* **2015**, *54* (47), 7029–7040.
- (86) Fang, X.; Tiyanont, K.; Zhang, Y.; Wanner, J.; Boger, D.; Walker, S. The Mechanism of Action of Ramoplanin and Enduracidin. *Mol. BioSyst.* **2006**, *2* (1), 69–76.
- (87) Yin, X.; Chen, Y.; Zhang, L.; Wang, Y.; Zabriskie, T. M. Enduracidin Analogues with Altered Halogenation Patterns Produced by Genetically Engineered Strains of Streptomyces Fungicidicus. *J. Nat. Prod.* **2010**, *73*, 583–589.
- (88) Haltli, B.; Tan, Y.; Magarvey, N. A.; Wagenaar, M.; Yin, X.; Greenstein, M.; Hucul, J. A.; Zabriskie, T. M. Investigating B-Hydroxyenduracididine Formation in the Biosynthesis of the Mannopeptimycins. *Chem. Biol.* **2005**, *12*, 1163–1168.

- (89) He, H.; Williamson, R. T.; Shen, B.; Graziani, E. I.; Yang, H. Y.; Sakya, S. M.; Petersen, P. J.; Carter, G. T. Mannopectimycins, Novel Antibacterial Glycopeptides from *Streptomyces Hygroscopicus*, LL-AC98. *J. Am. Chem. Soc.* **2002**, *124*, 9729–9736.
- (90) Wang, B.; Liu, Y.; Jiao, R.; Feng, Y.; Li, Q.; Chen, C.; Liu, L.; He, G.; Chen, G. Total Synthesis of Mannopectimycins α and β . *J. Am. Chem. Soc.* **2016**, *138*, 3926–39–32.
- (91) Yang, H.; Chen, K. H.; Nowick, J. S. Elucidation of the Teixobactin Pharmacophore. *ACS Chem. Biol.* **2016**, *11*, 1823–1826.
- (92) Jad, Y. E.; Acosta, G. A.; Naicker, T.; Ramtahal, M.; El-Faham, A.; Govender, T.; Kruger, H. G.; De La Torre, B. G.; Albericio, F. Synthesis and Biological Evaluation of a Teixobactin Analogue. *Org. Lett.* **2015**, *17* (24), 6182–6185.
- (93) Burroughs, A. M.; Hoppe, R. W.; Goebel, N. C.; Sayyed, B. H.; Voegtline, T. J.; Schwabacher, A. W.; Zabriskie, T. M.; Silvaggi, N. R. Structural and Functional Characterization of MppR, an Enduracididine Biosynthetic Enzyme from *Streptomyces Hygroscopicus*: Functional Diversity in the Acetoacetate Decarboxylase-like Superfamily. *Biochemistry* **2013**, *52* (26), 4492–4506.
- (94) Han, L.; Vuksanovic, N.; Oehm, S. A.; Fenske, T. G.; Schwabacher, A. W.; Silvaggi, N. R. *Streptomyces Wadayamensis* MppP Is a PLP-Dependent Oxidase, Not an Oxygenase. *Biochemistry* **2018**, *57*, 3252–3264.
- (95) Hoppe, R. Molecular Recognition in Water: Design, Synthesis, and Characterization of Rigid Molecular Receptors and Enzymatic Mechanistic

Probes, UW - Milwaukee, 2016.

- (96) Scholl, M.; Trnka, T. M.; Morgan, J. P.; Grubbs, R. H. Increased Ring Closing Metathesis Activity of Ruthenium-Based Olefin Metathesis Catalysts Coordinated with Imidazolin-2-Ylidene Ligands. *Tetrahedron Lett.* **1999**, *40* (12), 2247–2250.
- (97) Vougioukalakis, G. C.; Grubbs, R. H. Ruthenium-Based Heterocyclic Carbene-Coordinated Olefin Metathesis Catalysts. *Chem. Rev.* **2010**, *110*, 1746–1787.
- (98) Edwards, G. A.; Culp, P. A.; Chalker, J. M. Allyl Sulphides in Olefin Metathesis: Catalyst Considerations and Traceless Promotion of Ring-Closing Metathesis. *Chem. Commun.* **2015**, *51* (3), 515–518.
- (99) Masuda, Y.; Maruyama, C.; Kawabata, K.; Hamano, Y. Synthesis of (2S,3R,4R)-3,4-Dihydroxyarginine and Its Inhibitory Activity against Nitric Oxide Synthase. *Tetrahedron* **2016**, *72* (36), 5602–5611.

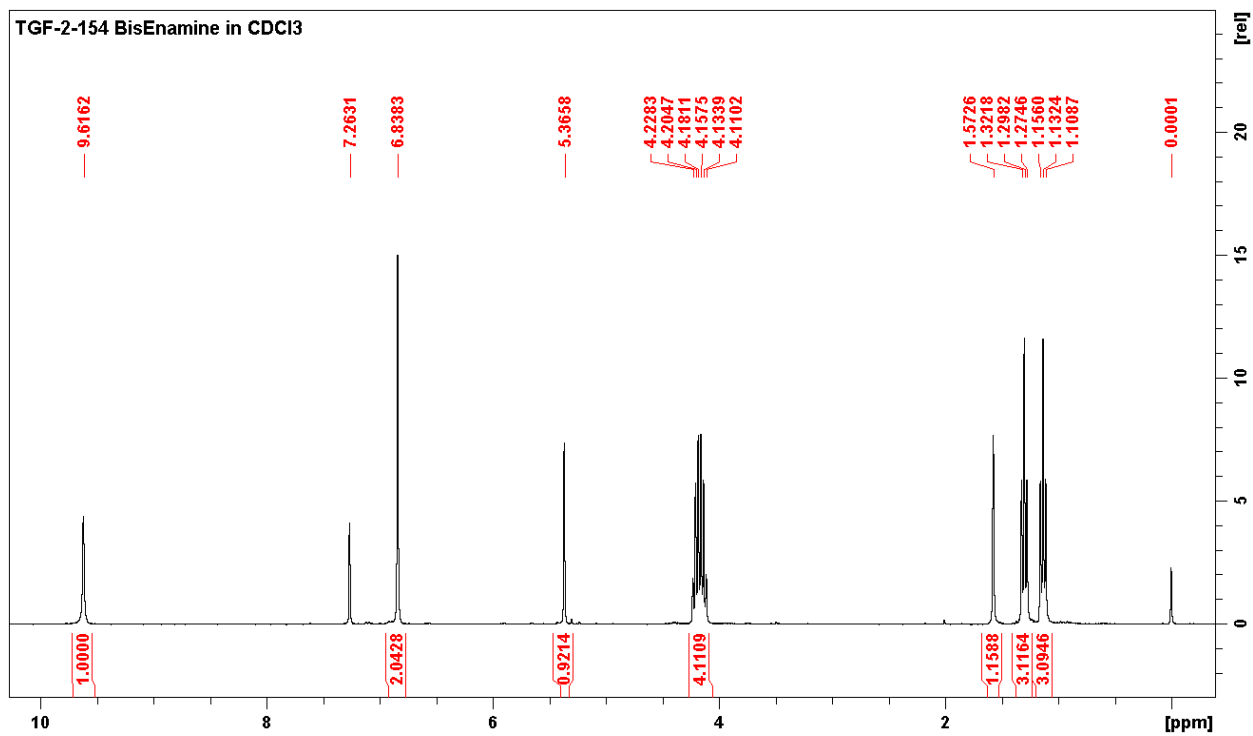
APPENDIX: COMPOUND CHARACTERIZATION SPECTRA

<i>Spectrum 1. ¹H NMR - Bisenamine 2</i>	132
<i>Spectrum 2. ¹³C NMR - Bisenamine 2</i>	132
<i>Spectrum 3. ESI-MS - Bisenamine 2</i>	133
<i>Spectrum 4. ¹H NMR - Phenanthroline 3a</i>	133
<i>Spectrum 5. ESI-MS - Phenanthroline 3a</i>	134
<i>Spectrum 6. ¹H NMR - Enamine 4</i>	134
<i>Spectrum 7. ESI-MS - Enamine 4</i>	135
<i>Spectrum 8. ¹H NMR - Nitroquinolone 5</i>	135
<i>Spectrum 9. ESI-MS - Nitroquinolone 5</i>	136
<i>Spectrum 10. ¹H NMR - Aminoquinolone 6</i>	136
<i>Spectrum 11. ¹H NMR - Aminobromoquinolone 7</i>	137
<i>Spectrum 12. ESI-MS - Aminobromoquinolone 7</i>	137
<i>Spectrum 13. ¹H NMR - Nitroenamine 8</i>	138
<i>Spectrum 14. ¹H NMR - Ethyl nitroacetate 11</i>	138
<i>Spectrum 15. ¹H NMR - Nitroenol ether 12</i>	139
<i>Spectrum 16. ¹H NMR - Diol 17</i>	139
<i>Spectrum 17. ¹³C NMR - Diol 17</i>	140
<i>Spectrum 18. ESI-MS - Diol 17</i>	140
<i>Spectrum 19. ¹H NMR - Enamine 19</i>	141
<i>Spectrum 20. ¹³C NMR - Enamine 19</i>	141
<i>Spectrum 21. ¹H NMR - Nitroquinolone 20</i>	142
<i>Spectrum 22. ESI-MS - Nitroquinolone 20</i>	142

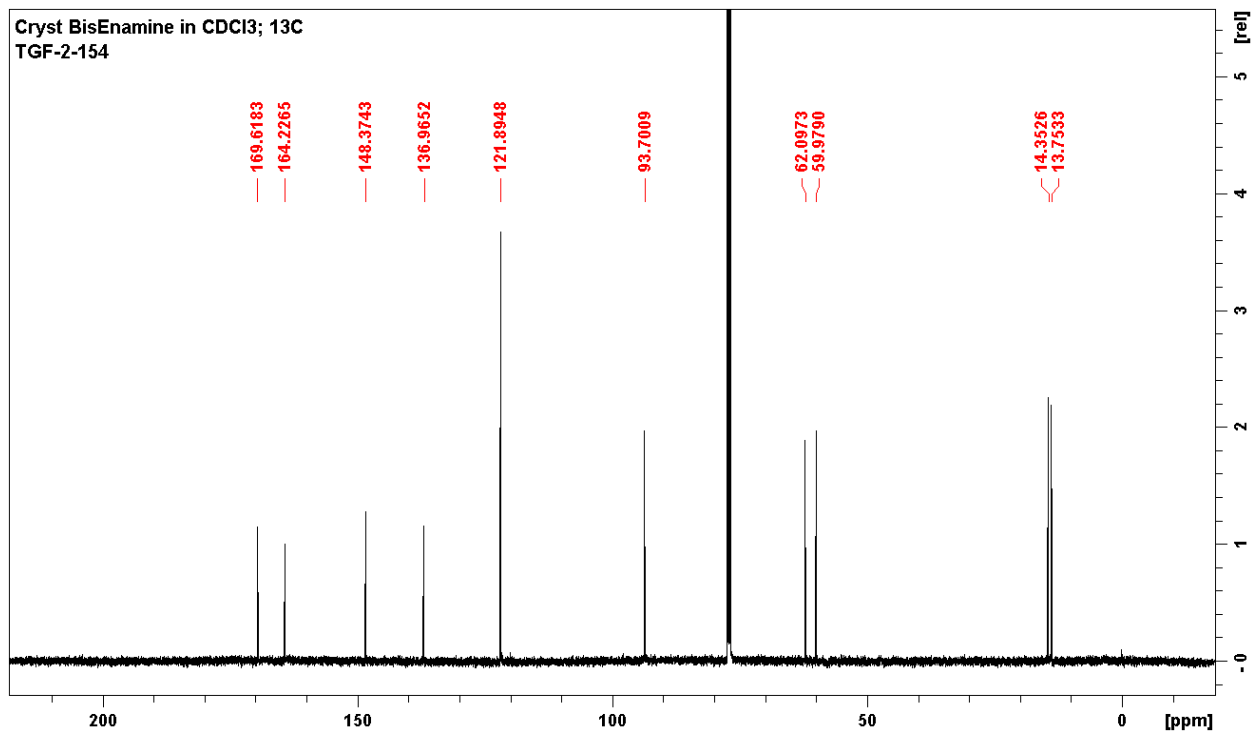
Spectrum 23. ^1H NMR - AllylQuinolone 21a	143
Spectrum 24. ^{13}C NMR - AllylQuinolone 21a	143
Spectrum 25. ^1H NMR - AllylQuinolone 21b	144
Spectrum 26. ^{13}C NMR - AllylQuinolone 21b	144
Spectrum 27. ESI-MS - Nitroquinolone 21b	145
Spectrum 28. ^1H NMR - Boc-N-aminoquinolone 22	145
Spectrum 29. ^{13}C NMR - Boc-N-aminoquinolone 22	146
Spectrum 30. ESI-MS - Boc-N-aminonitroquinolone 22	146
Spectrum 31. ^1H NMR - Boc-N-diaminoquinolone 23	147
Spectrum 32. ^{13}C NMR - Boc-N-diaminoquinolone 23	147
Spectrum 33. ESI-MS - Boc-N-diaminoquinolone 23	148
Spectrum 34. ^1H NMR - Aminonitroquinolone 25	148
Spectrum 35. ^{13}C NMR - Aminonitroquinolone 25	149
Spectrum 36. ESI-MS - Aminonitroquinolone 25	149
Spectrum 37. ^1H NMR - NO_2 -AllylQuin-Ala-Fmoc 26	150
Spectrum 38. ^{13}C NMR - NO_2 -AllylQuin-Ala-Fmoc 26	150
Spectrum 39. ^1H NMR - PAR_2Zn 28b	151
Spectrum 40. ESI-MS - PAR_2Zn 28b	151
Spectrum 41. ^1H NMR - QAR_2Zn 29b	152
Spectrum 42. ^1H NMR - PAR-CMS 30	152
Spectrum 43. ^1H NMR - Diazido(tetraethylene glycol) 31	153
Spectrum 44. ^1H NMR - BocAminoAzide 32	153
Spectrum 45. ^{13}C NMR - BocAminoAzide 32	154

Spectrum 46. ESI-MS - BocAminoAzide 32	154
Spectrum 47. ¹ H NMR - MonoBocDiamineTEG 33	155
Spectrum 48. ¹³ C NMR - MonoBocDiamineTEG 33	155
Spectrum 49. ESI-MS - MonoBocDiAmineTEG 33	156
Spectrum 50. ¹ H NMR - MABA-TEG 34	156
Spectrum 51. ¹³ C NMR - MABA-TEG 34	157
Spectrum 52. ¹ H NMR - N-piperidiniumpropylsulfonate 35	157
Spectrum 53. ¹³ C NMR - N-piperidiniumpropylsulfonate 35	158
Spectrum 54. ESI-MS - N-piperidiniumpropylsulfonate 35	158
Spectrum 55. ¹ H NMR - p-nitrophenyl bromoacetate 36	159
Spectrum 56. ¹³ C NMR - p-nitrophenyl bromoacetate 36	159
Spectrum 57. ¹ H NMR - p-nitrophenyl triethylammoniumacetate bromide 37a	160
Spectrum 58. ¹³ C NMR - p-nitrophenyl triethylammoniumacetate bromide 37a	160
Spectrum 59. ¹ H NMR – p-nitrophenyl zwitterionic acetate 37b	161
Spectrum 60. ¹ H NMR - PAR ₂ Zn (AlkEst) 38	161
Spectrum 61. ¹³ C NMR - PAR ₂ Zn (AlkEst) 38	162
Spectrum 62. ESI-MS - PAR ₂ Zn (AlkEst) 38	162
Spectrum 63. ¹ H NMR - PAR ₂ Zn(AlkAcid) 39	163
Spectrum 64. ¹³ C NMR - PAR ₂ Zn(AlkAcid) 39	163
Spectrum 65. ESI-MS - PAR ₂ Zn (AlkEst) 38	164
Spectrum 66. ¹ H NMR - Boc-N-Allyl Amine 40	164
Spectrum 67. ¹³ C NMR - Boc-N-Allyl Amine 40	165
Spectrum 68. ¹ H NMR - Fmoc-N-(Vinyl Glycine)-OH 41	165

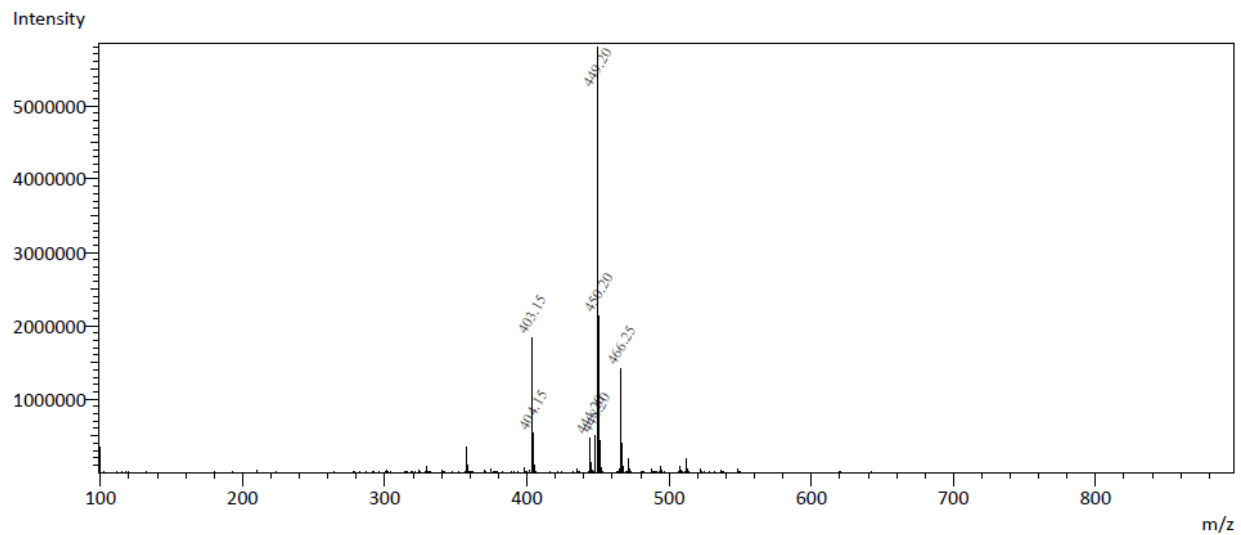
Spectrum 69. ¹³ C - NMR Fmoc-N-(Vinyl Glycine)-OH 41	166
Spectrum 70. ESI-MS - Fmoc-N-(Vinyl Glycine)-OH [M+Na+] 41	166
Spectrum 71 ¹ H NMR - Fmoc-N-(Vinyl Glycine)-OCH ₃ 42	167
Spectrum 72. ¹³ C NMR - Fmoc-N-(Vinyl Glycine)-OCH ₃ 42	167
Spectrum 73. ESI-MS - Fmoc-N-(Vinyl Glycine)-OCH ₃ [M+Na+] 42	168
Spectrum 74. ¹ H NMR - N _δ -Boc--N _α -Fmoc-(β,γ-dehydro-L-ornithine)-OCH ₃ 43	168
Spectrum 75. ¹³ C NMR - N _δ -Boc--N _α -Fmoc-(β,γ-dehydro-L-ornithine)-OCH ₃ 43	169
Spectrum 76. ESI-MS - N _δ -Boc--N _α -Fmoc-(β,γ-dehydro-L-ornithine)-OCH ₃ 43	169
Spectrum 77. ¹ H NMR - N _α -Fmoc-(β,γ-dehydro-L-ornithine)-OH HCl 44	170
Spectrum 78. ¹³ C NMR - N _α -Fmoc-(β,γ-dehydro-L-ornithine)-OH HCl 44	170
Spectrum 79. ESI-MS - N _α -Fmoc-(β,γ-dehydro-L-ornithine)-OH HCl 44	171
Spectrum 80. ¹ H NMR - Protected β,γ-dehydro-L-arginine 45	171
Spectrum 81. ESI-MS - Protected β,γ-dehydro-L-arginine 45	172
Spectrum 82. ¹ H NMR – β,γ-dehydro-L-arginine 46	172
Spectrum 83.ESI-MS - β,γ-dehydro-L-arginine 46	173



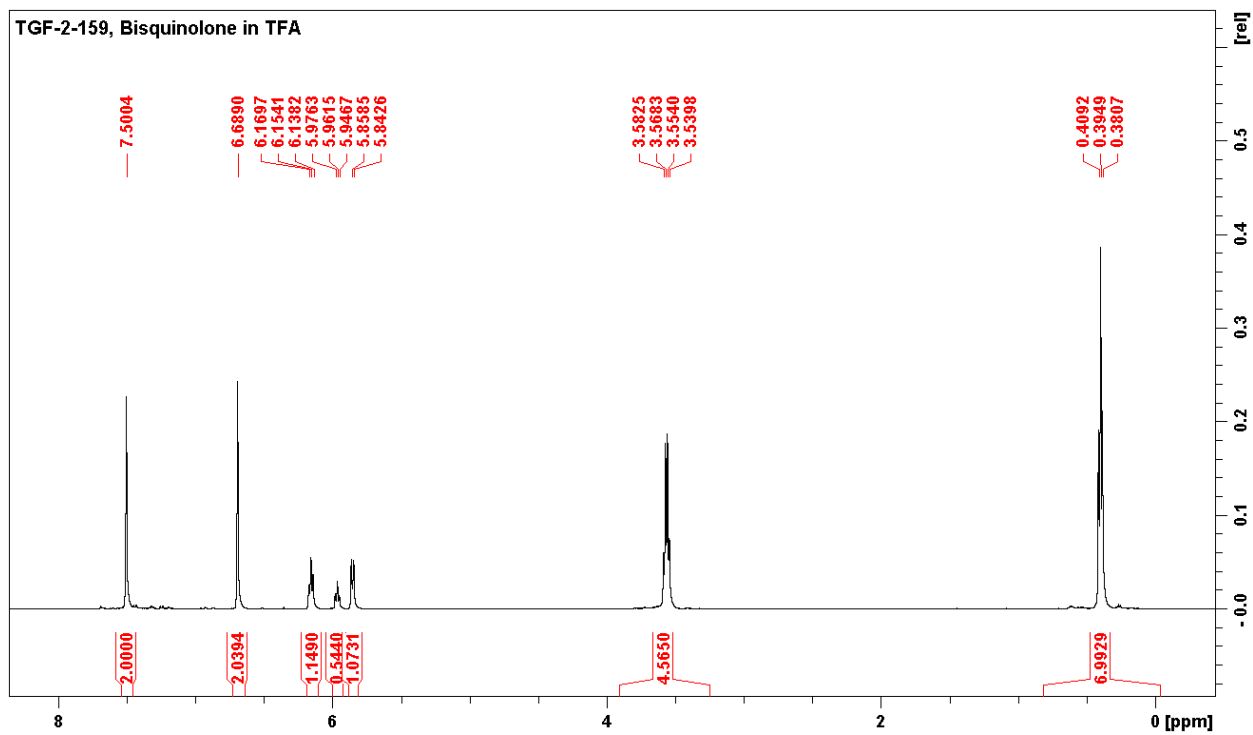
Spectrum 1. ¹H NMR - Bisenamine 2



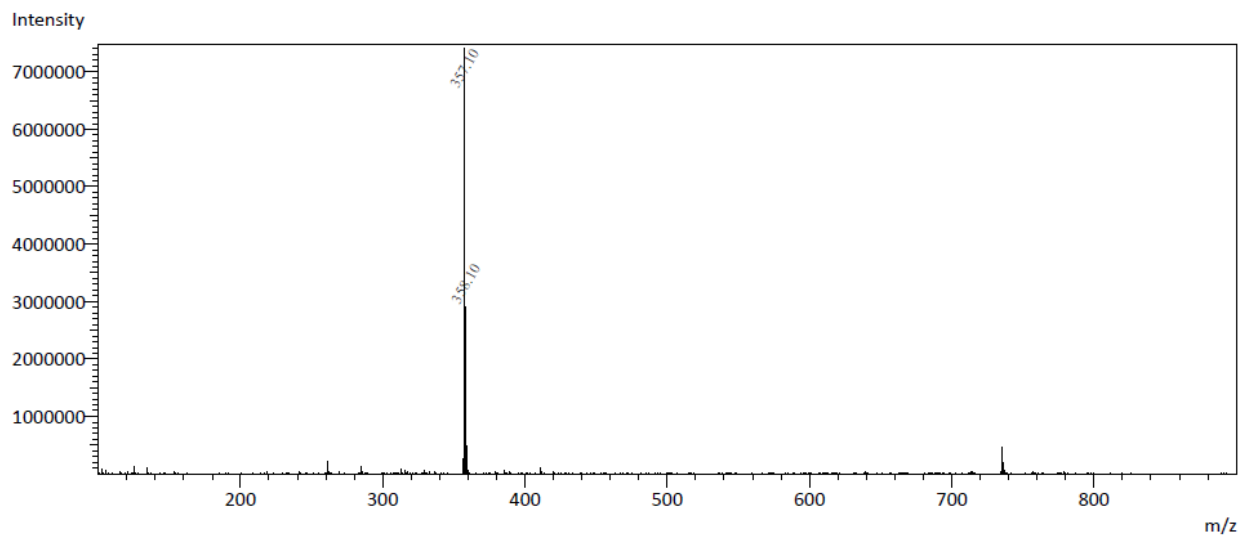
Spectrum 2. ¹³C NMR - Bisenamine 2



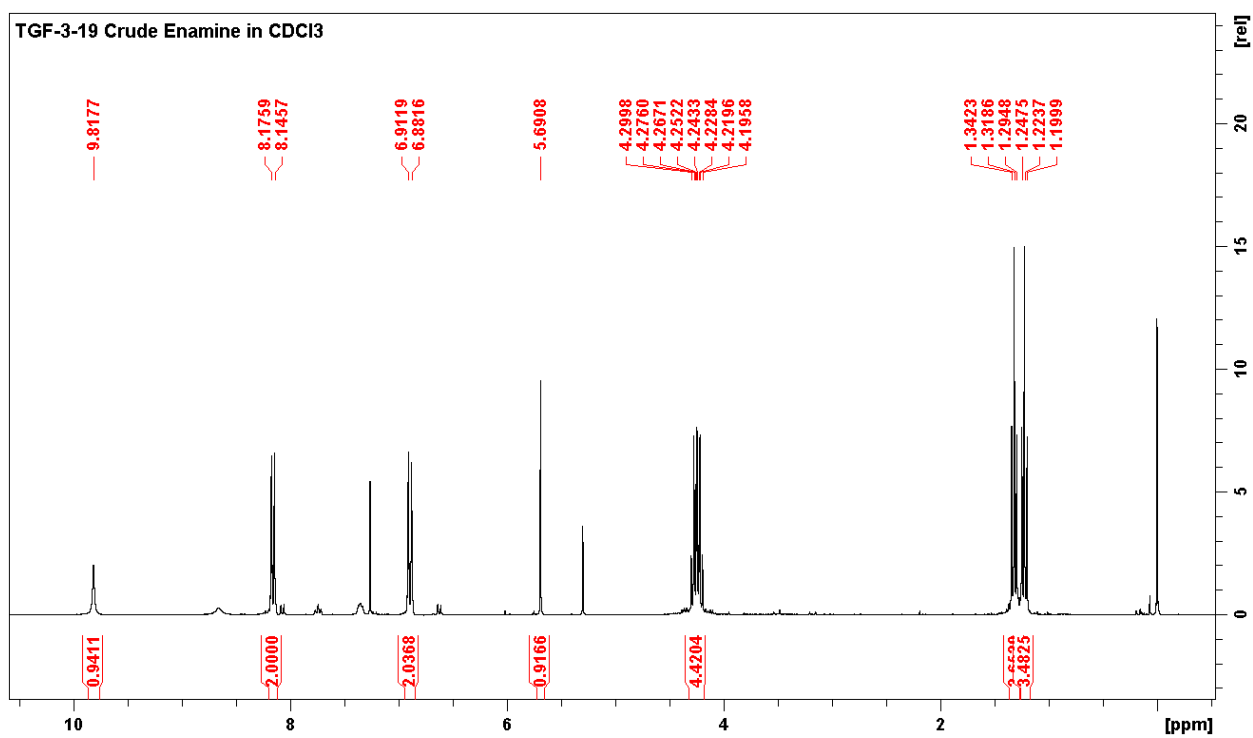
Spectrum 3. ESI-MS -: Bisenamine 2



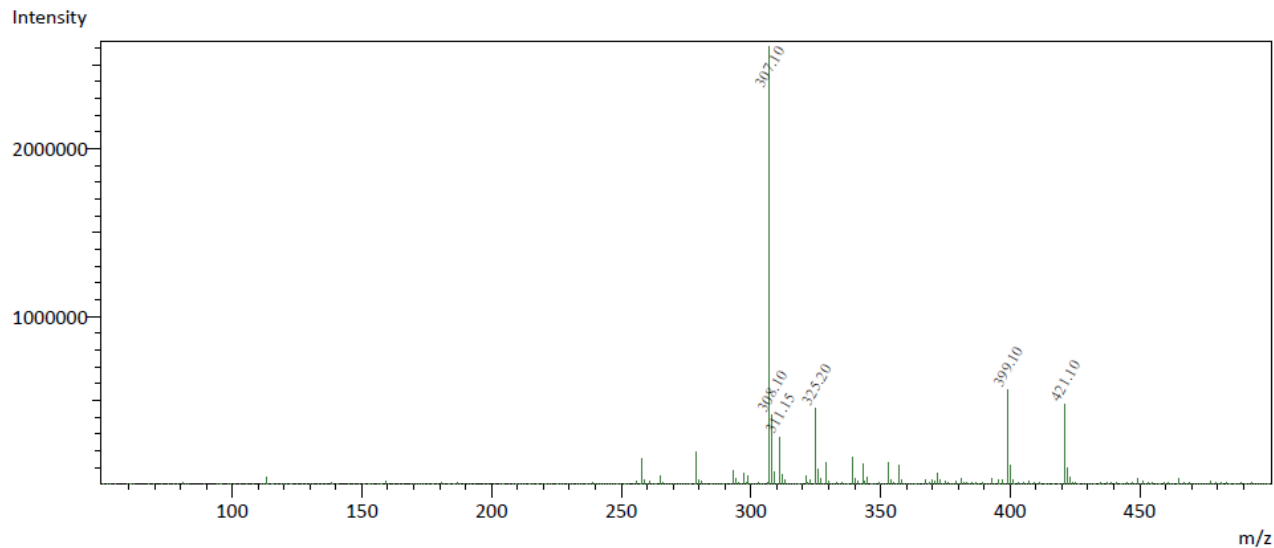
Spectrum 4. ¹H NMR - Phenanthroline 3a



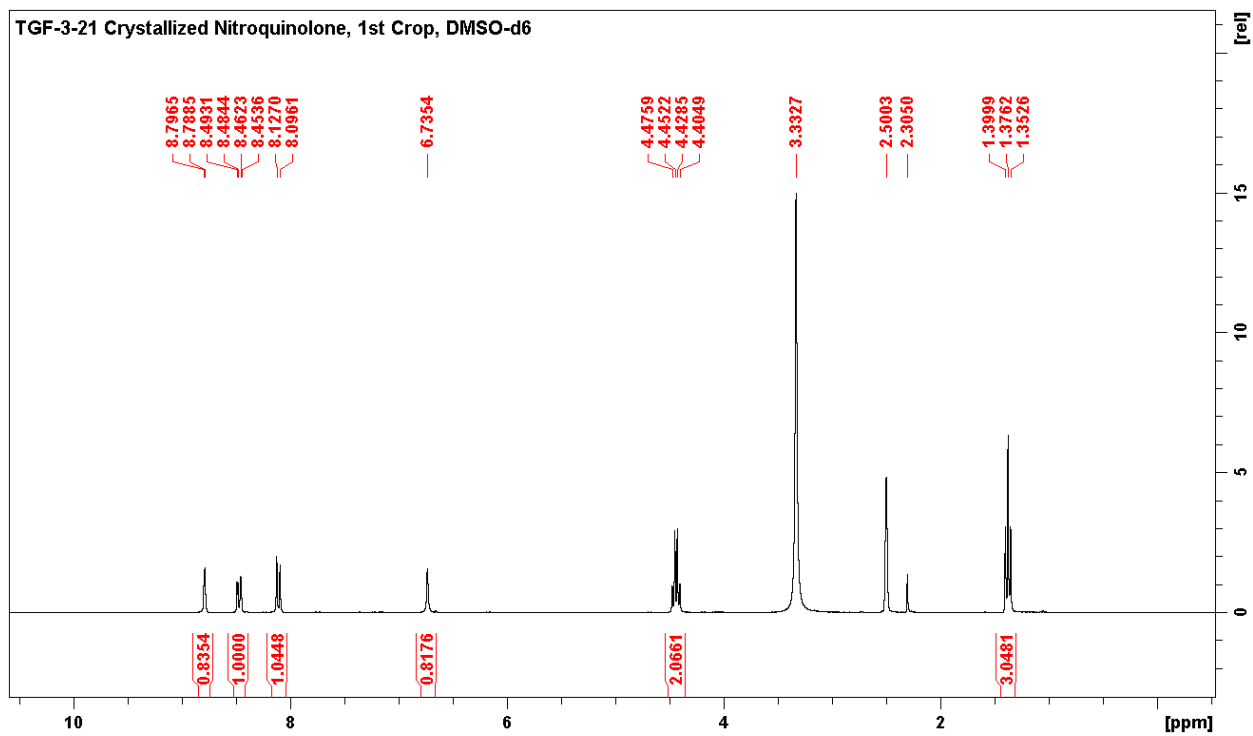
Spectrum 5. ESI-MS - Phenanthroline 3a



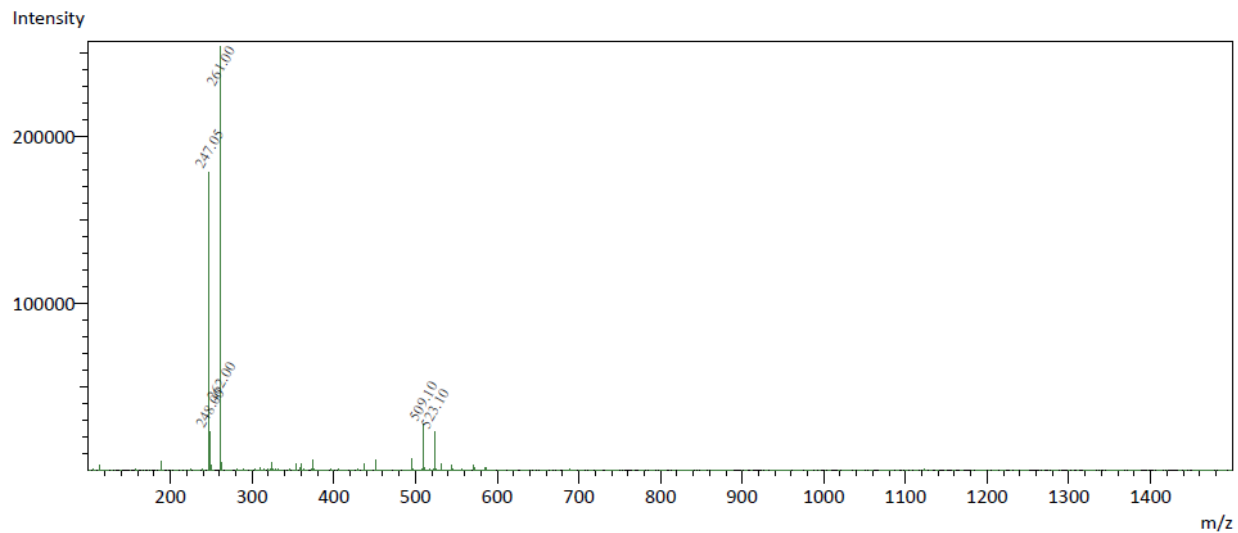
Spectrum 6. ¹H NMR - Enamine 4



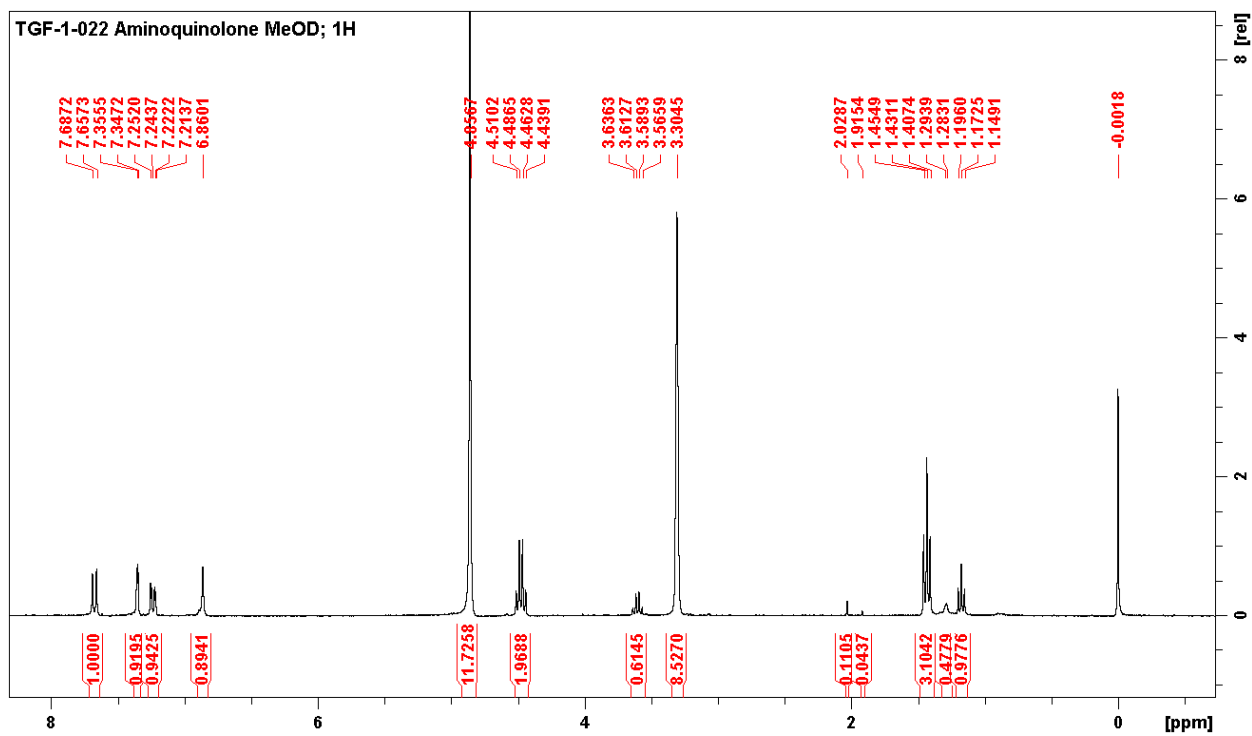
Spectrum 7. ESI-MS - Enamine 4



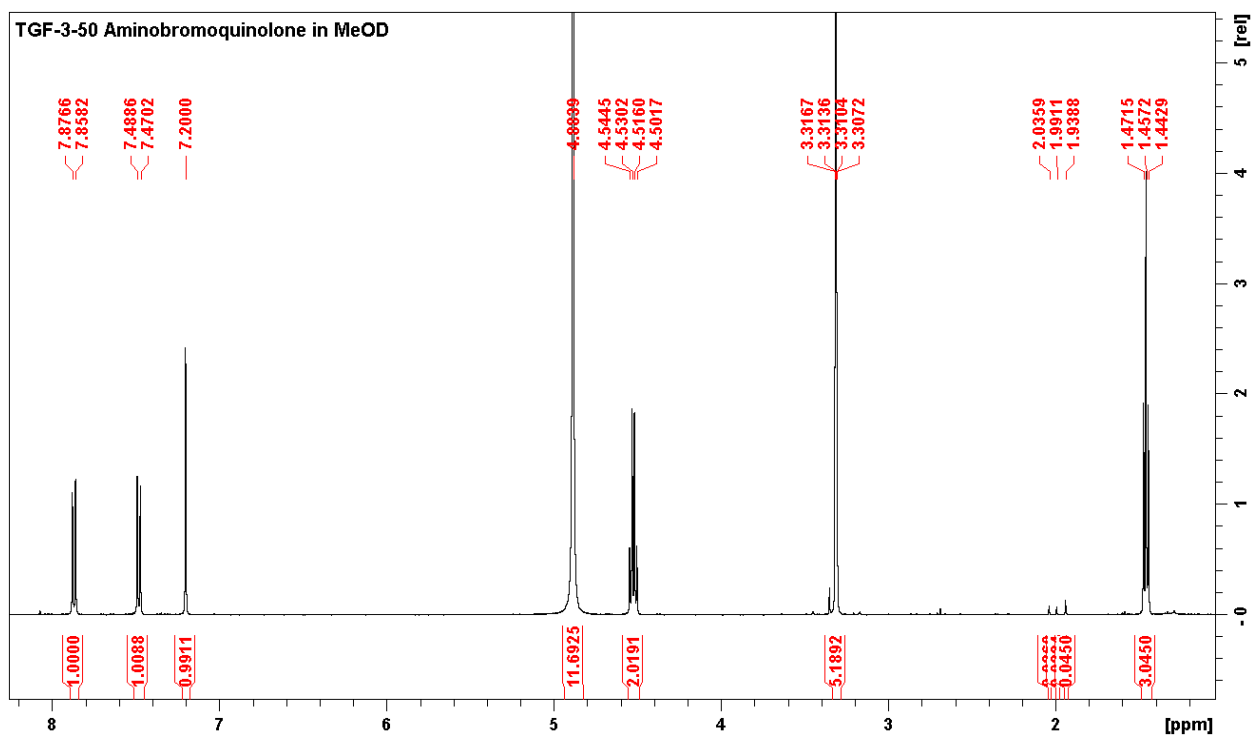
Spectrum 8. ¹H NMR - Nitroquinolone 5.



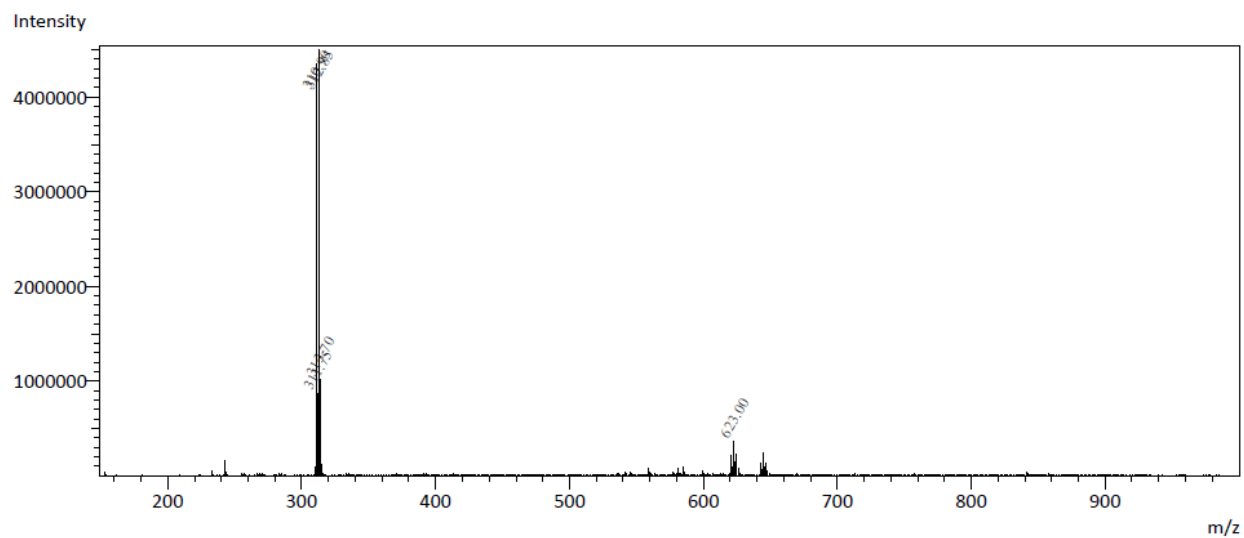
Spectrum 9. ESI-MS - Nitroquinolone 5



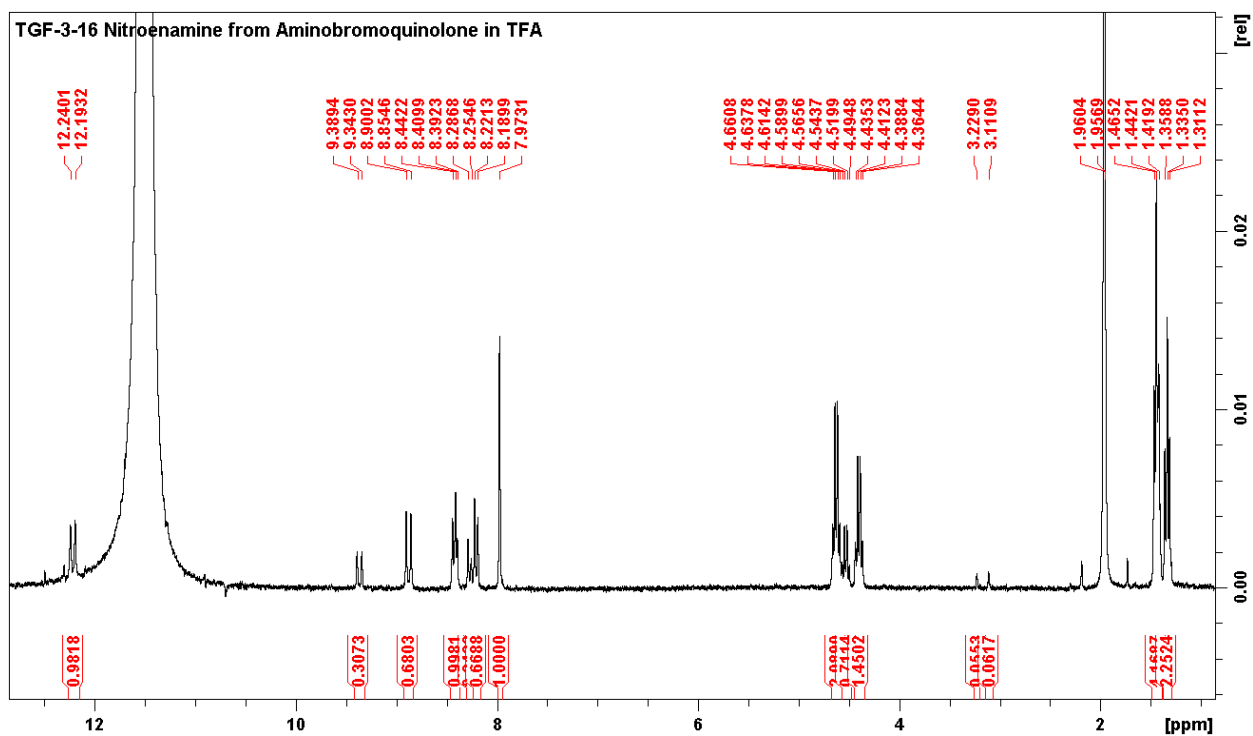
Spectrum 10. ¹H NMR - Aminoquinolone 6



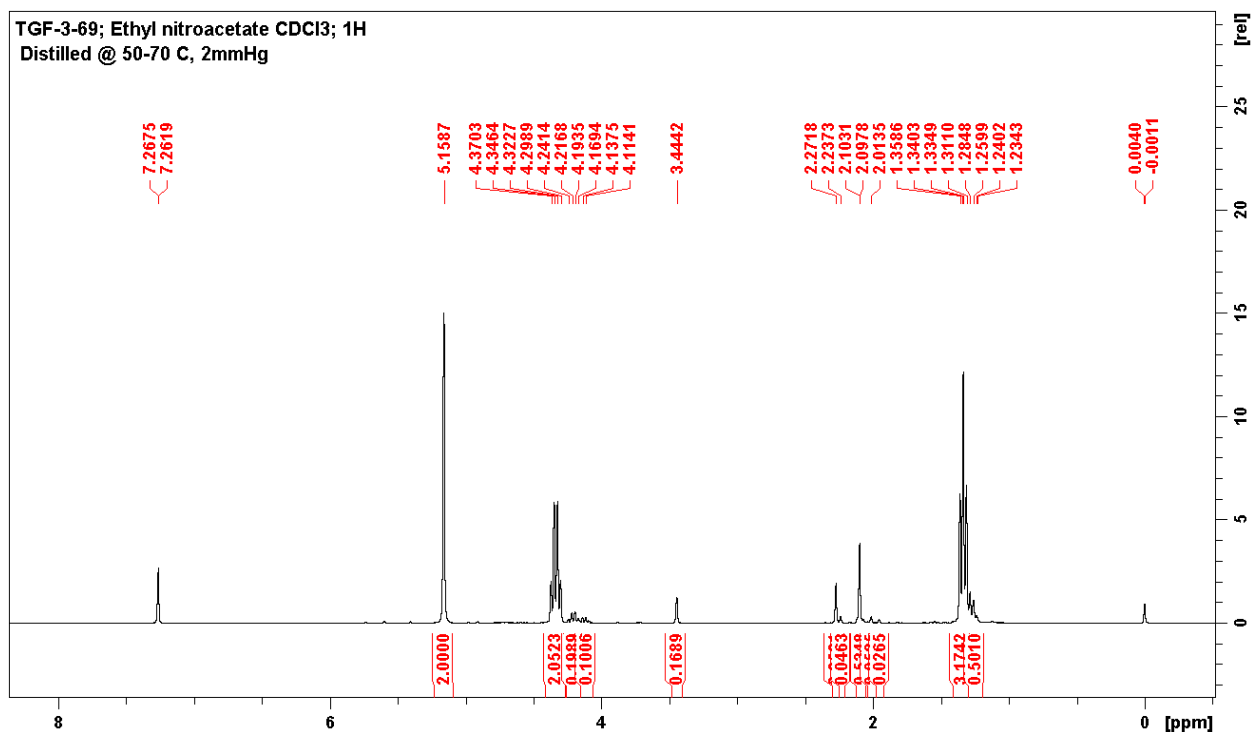
Spectrum 11. ¹H NMR - Aminobromoquinolone 7



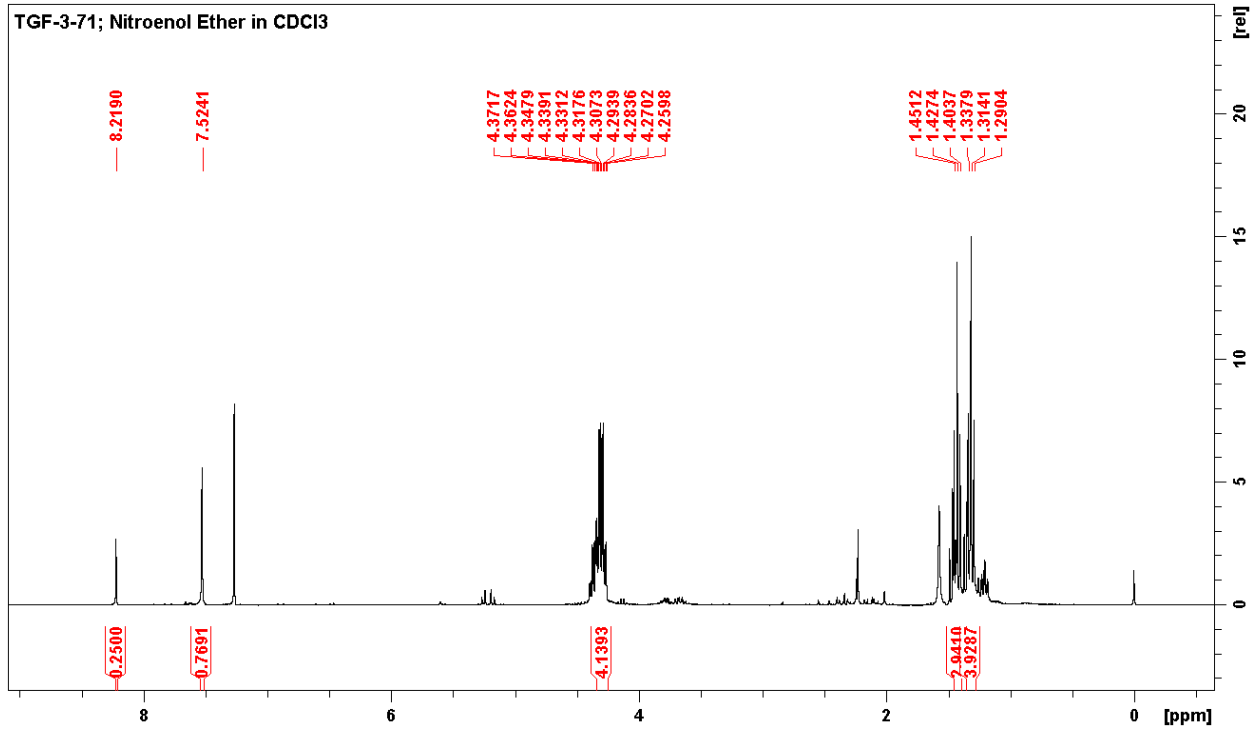
Spectrum 12. ESI-MS - Aminobromoquinolone 7



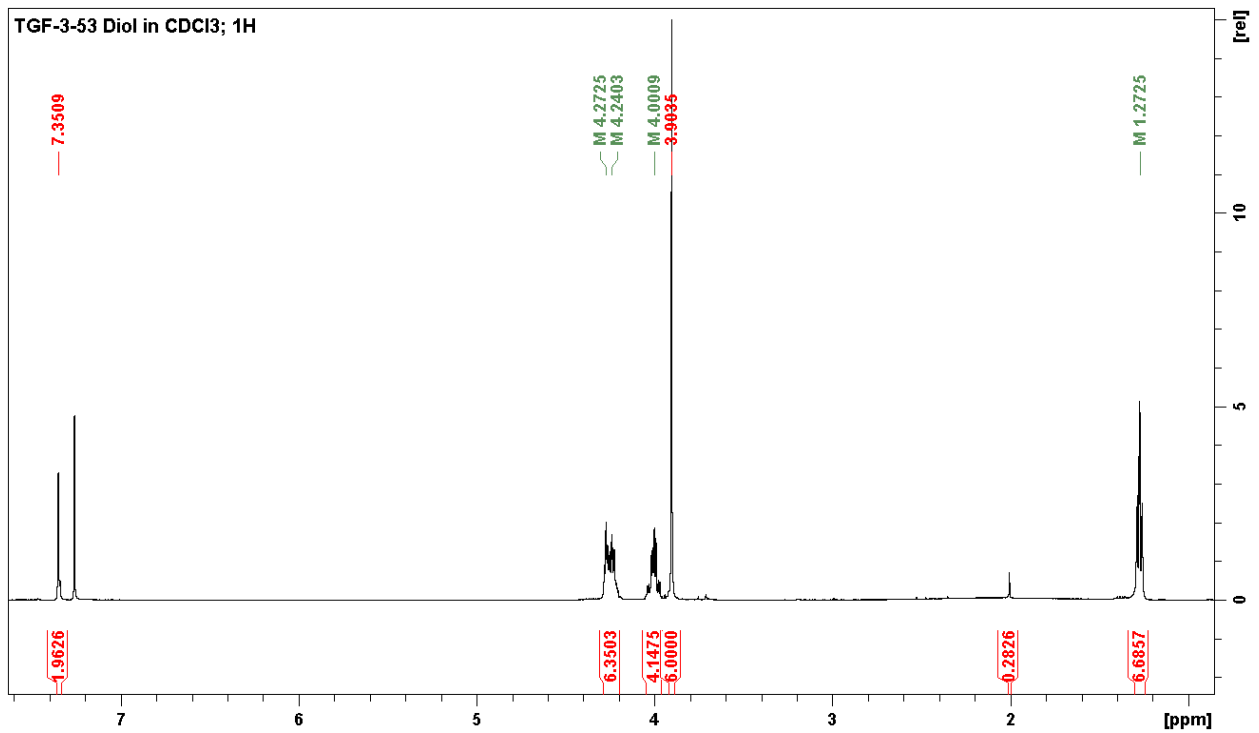
Spectrum 13. ¹H NMR - Nitroenamine 8



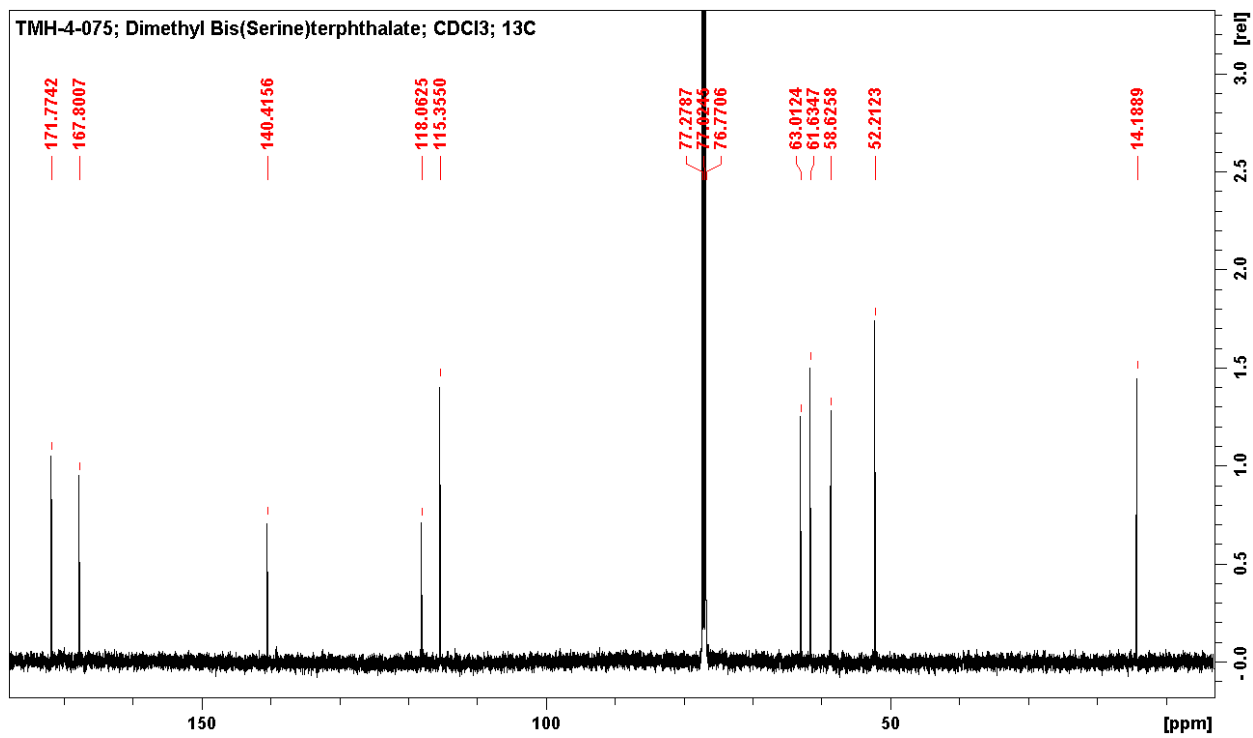
Spectrum 14. ¹H NMR - Ethyl nitroacetate 11



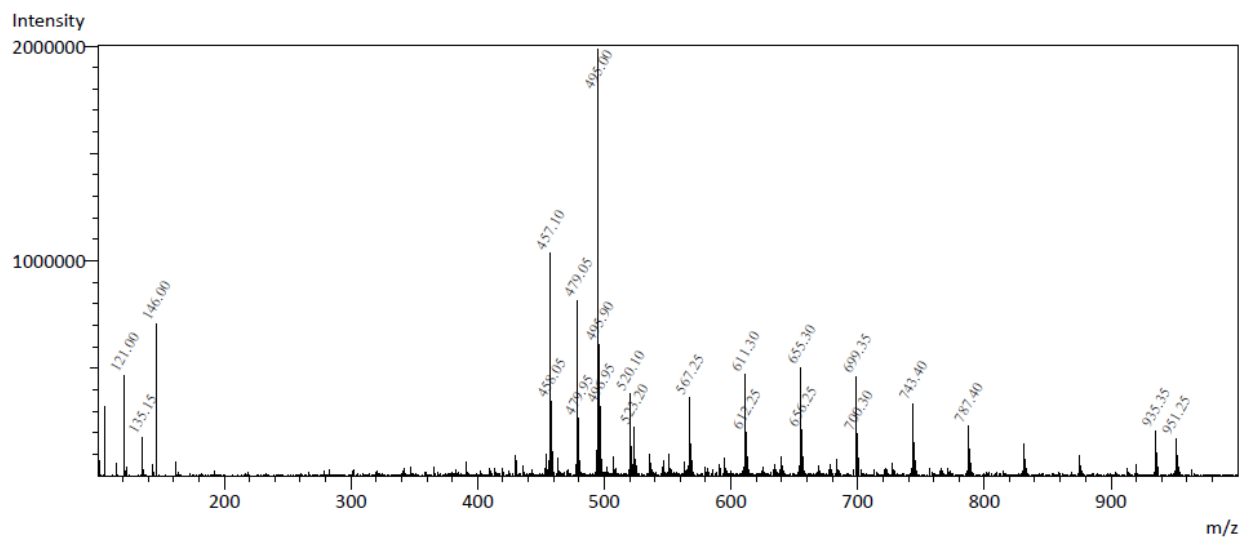
Spectrum 15. ¹H NMR - Nitroenol ether 12



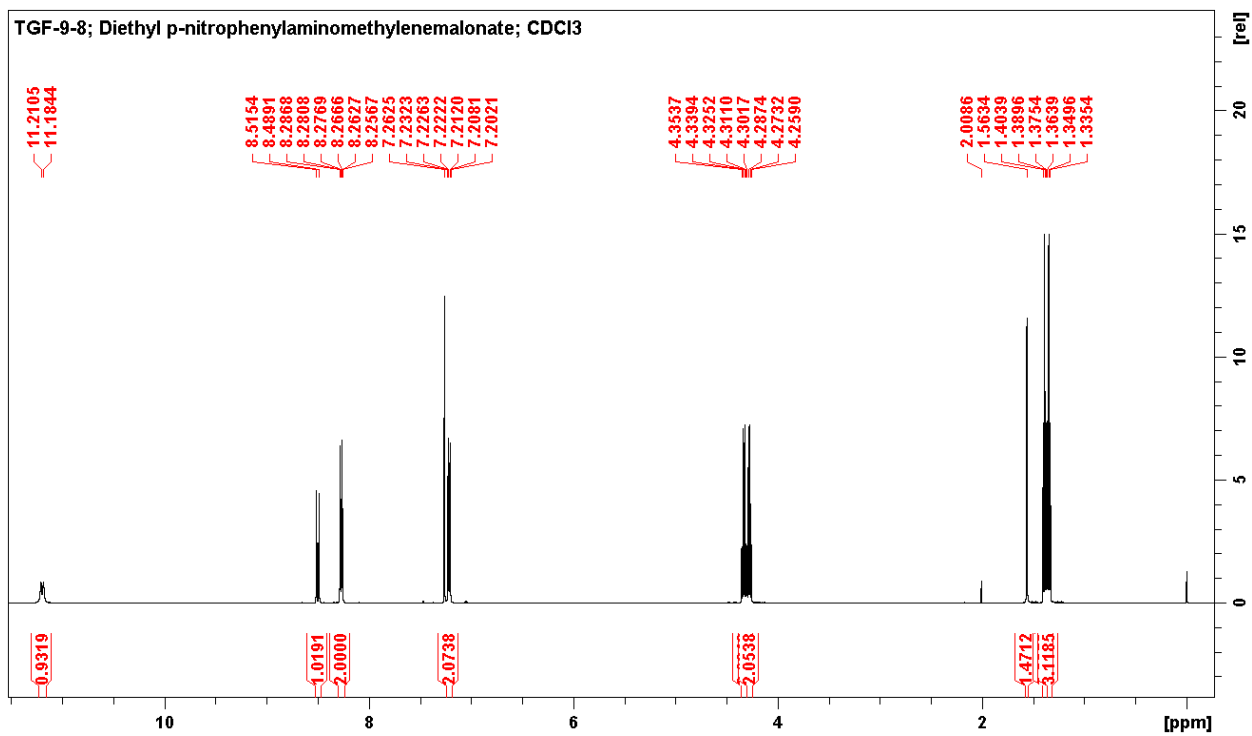
Spectrum 16. ¹H NMR - Diol 17



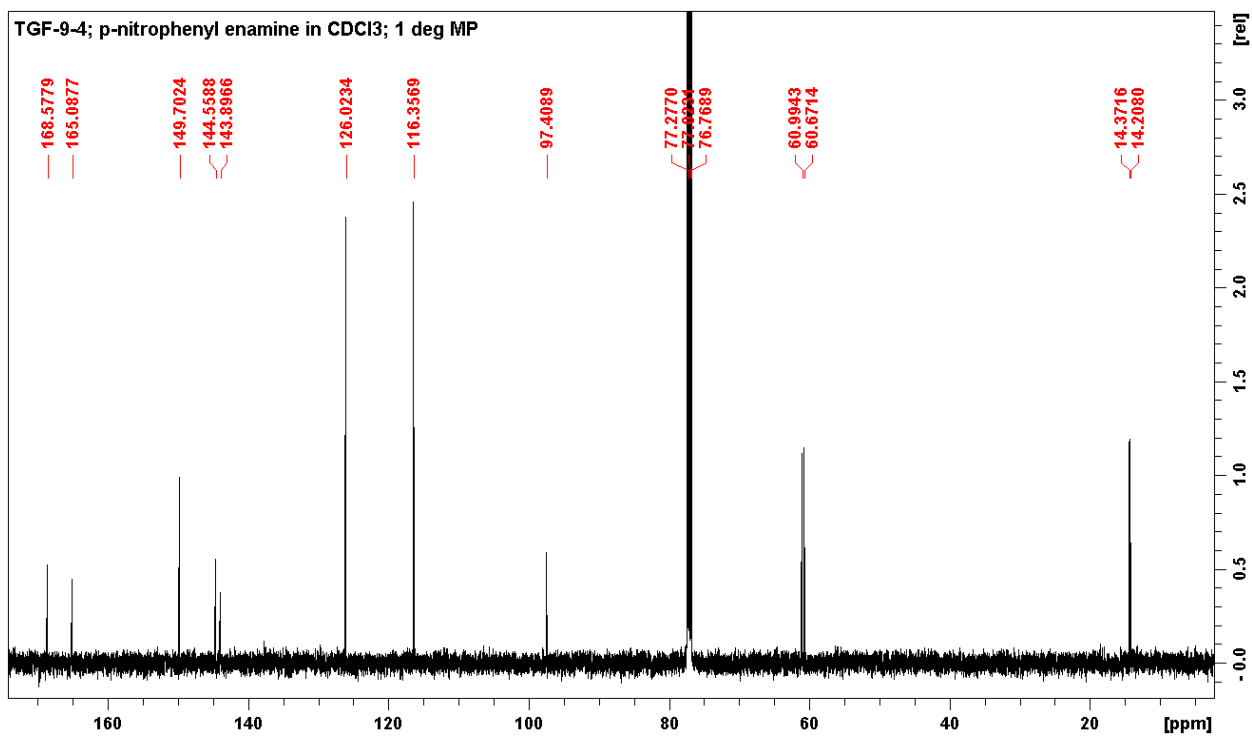
Spectrum 17. ¹³C NMR - Diol 17



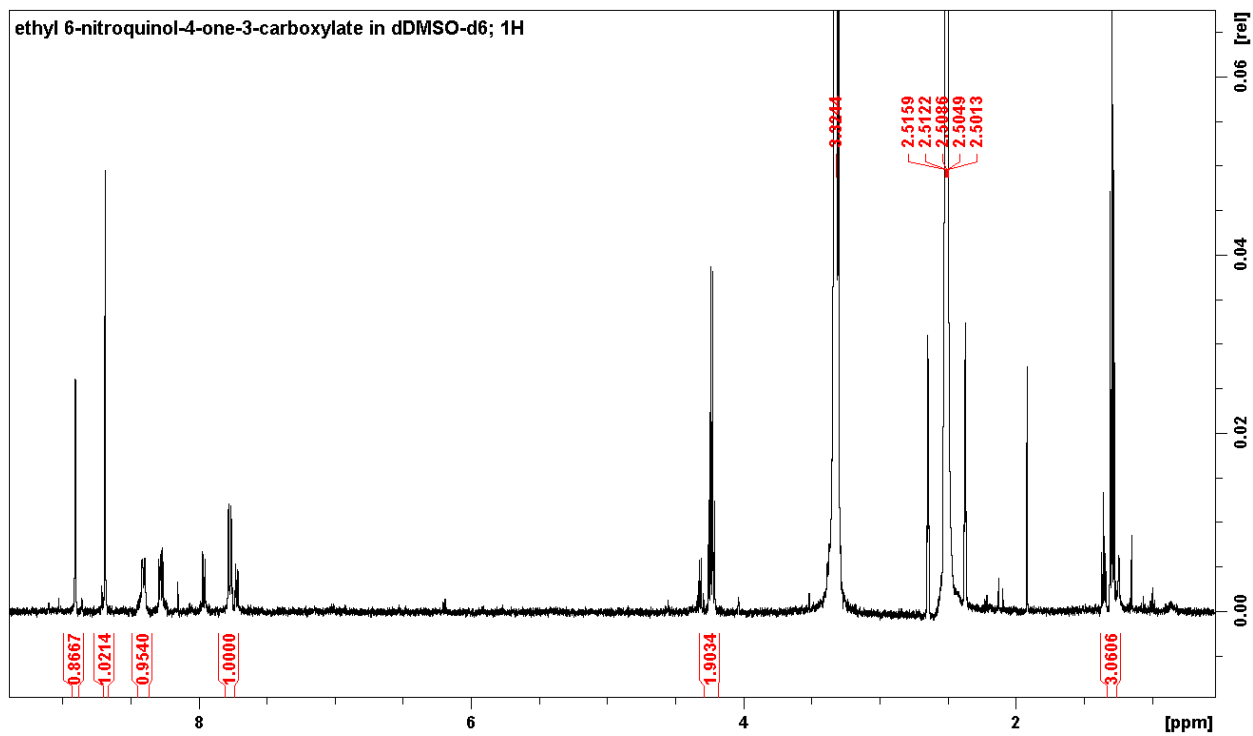
Spectrum 18. ESI-MS - Diol 17



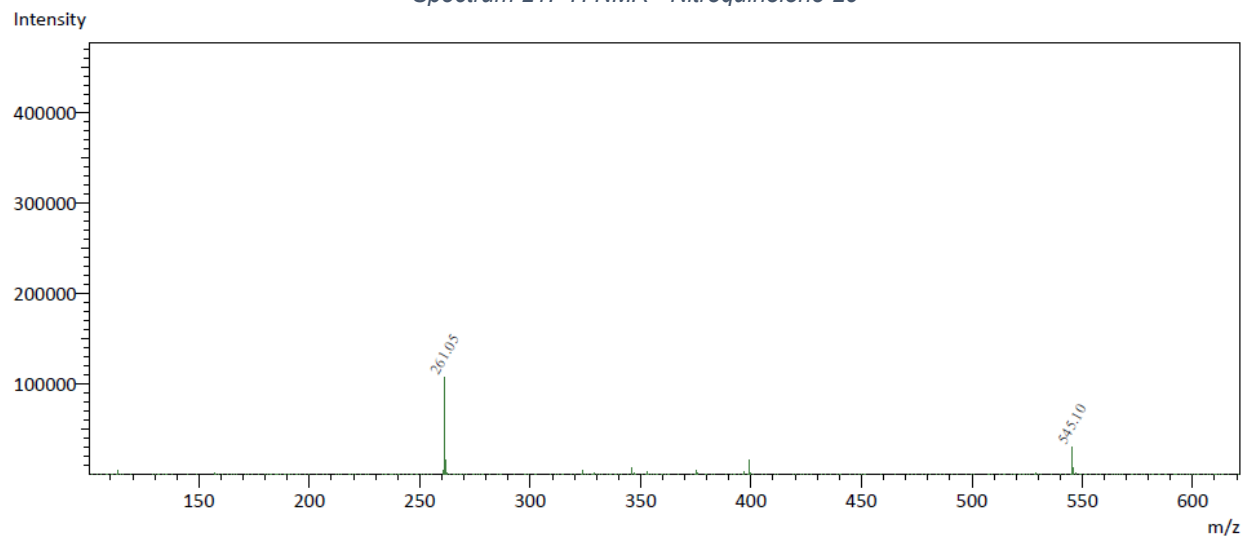
Spectrum 19. ¹H NMR - Enamine 19



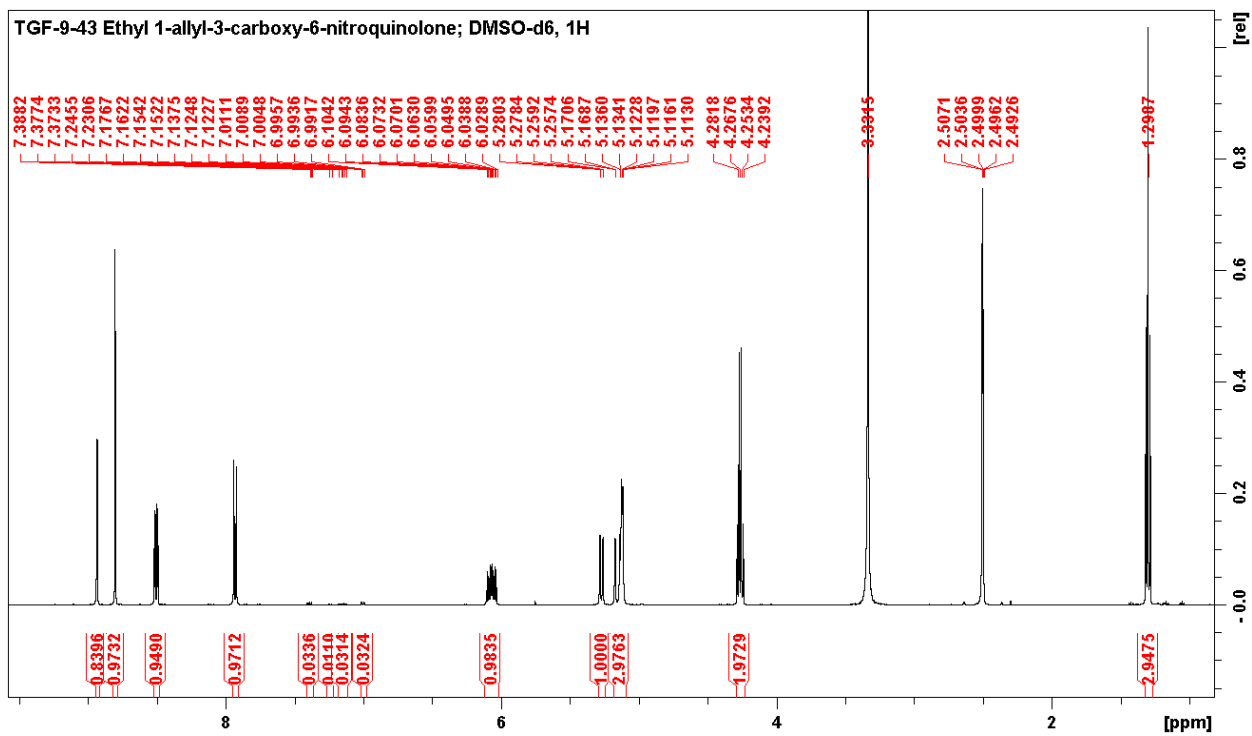
Spectrum 20. ¹³C NMR - Enamine 19



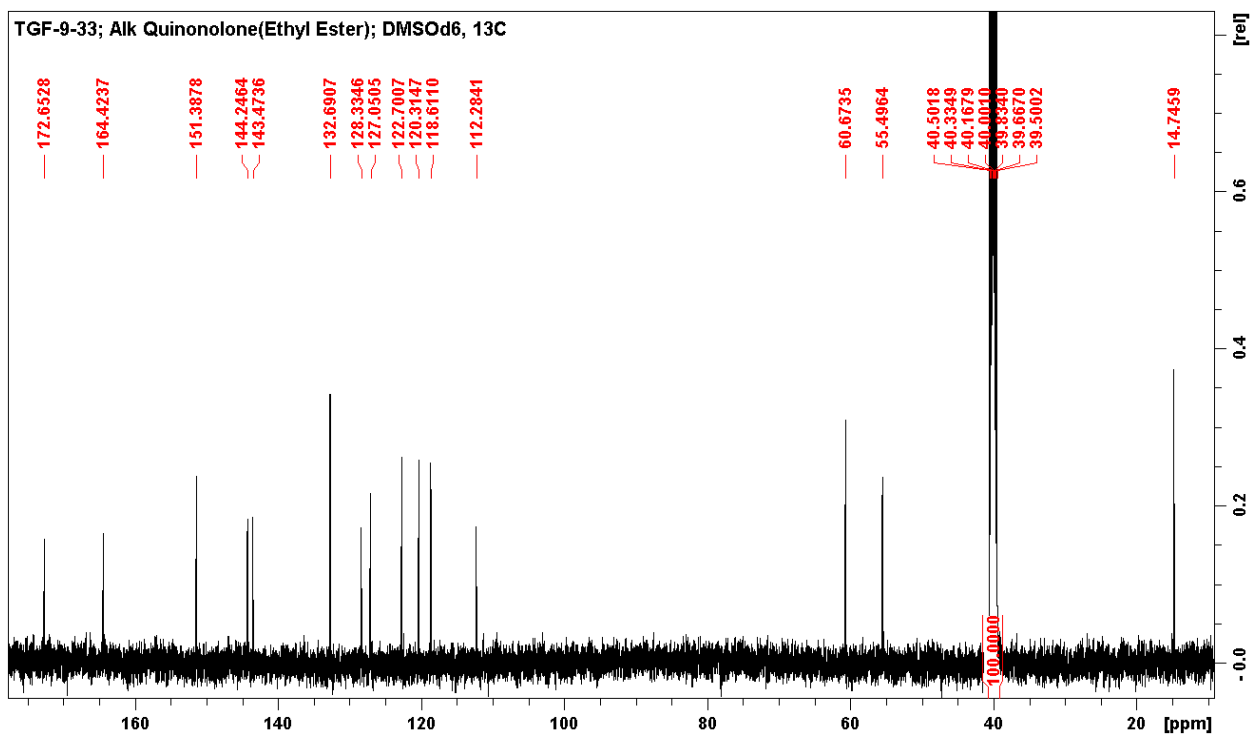
Spectrum 21. ¹H NMR - Nitroquinolone 20



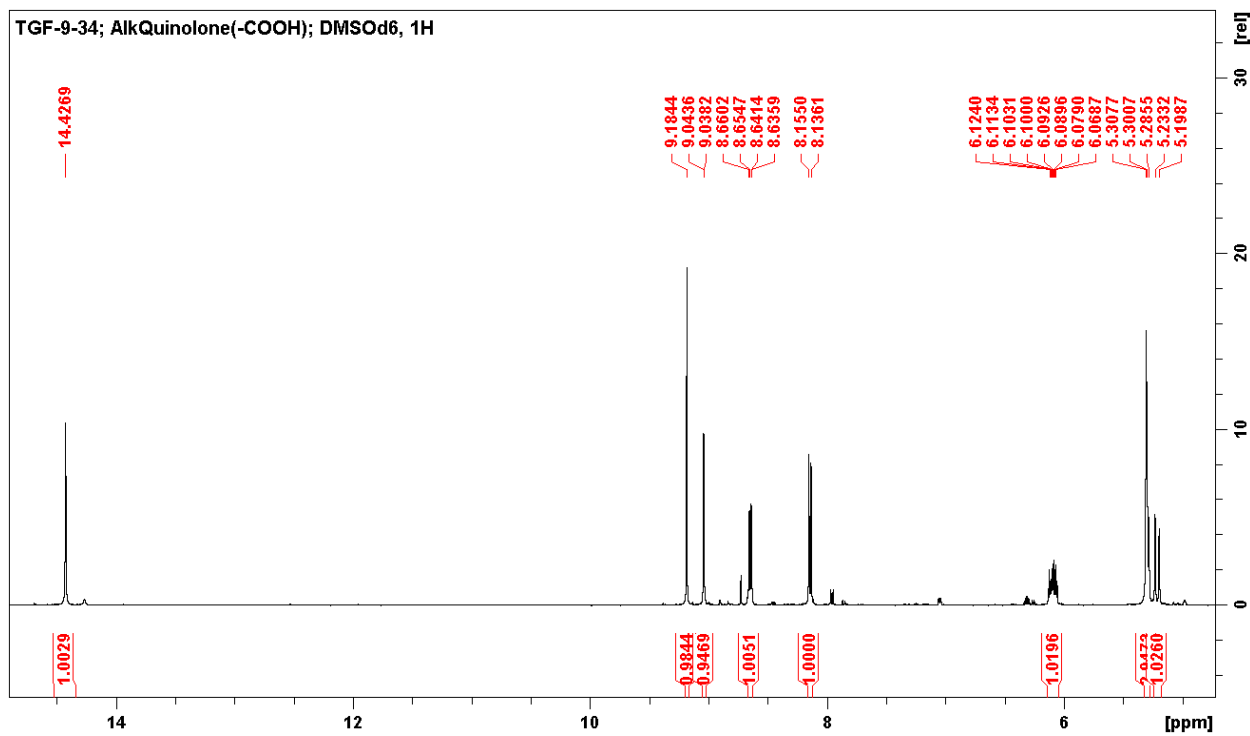
Spectrum 22. ESI-MS - Nitroquinolone 20



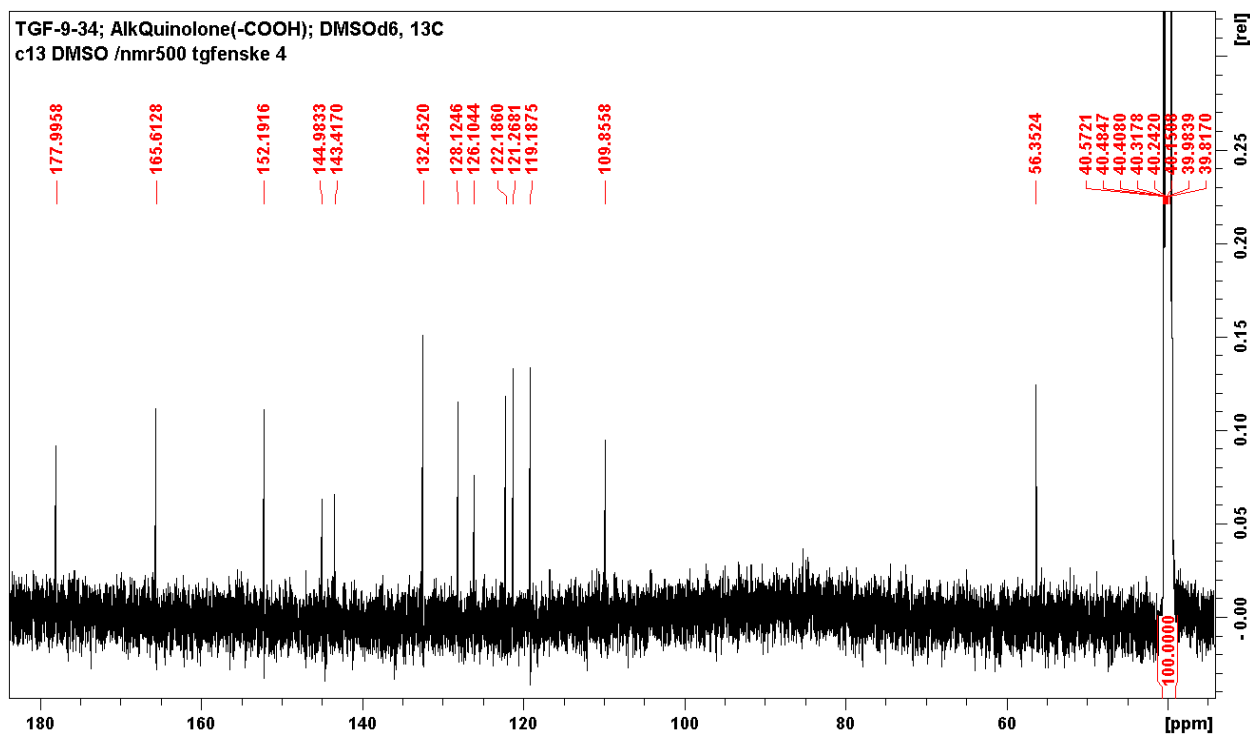
Spectrum 23. ¹H NMR - AllylQuinolone 21a



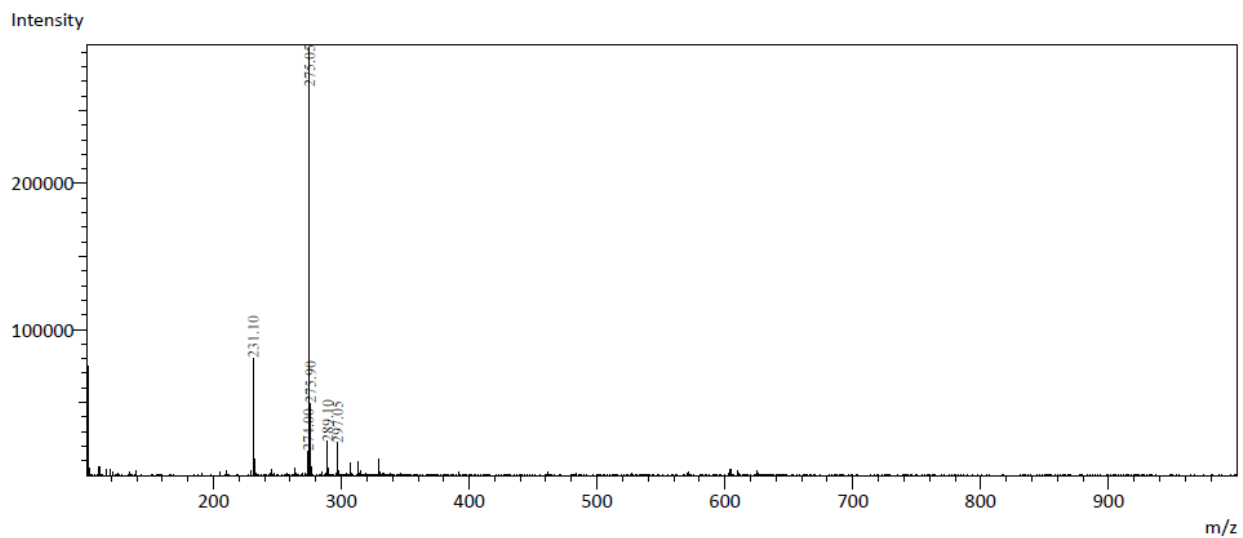
Spectrum 24. ¹³C NMR - AllylQuinolone 21a



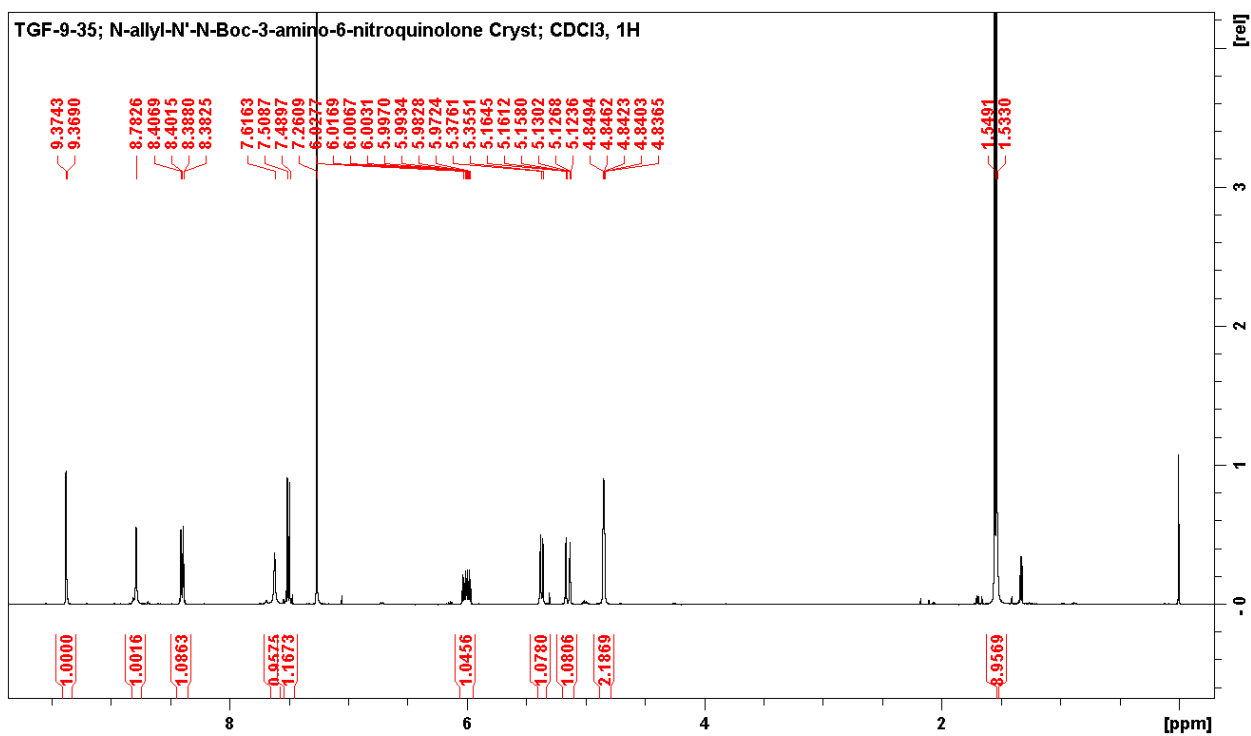
Spectrum 25. ¹H NMR - AllylQuinolone **21b**



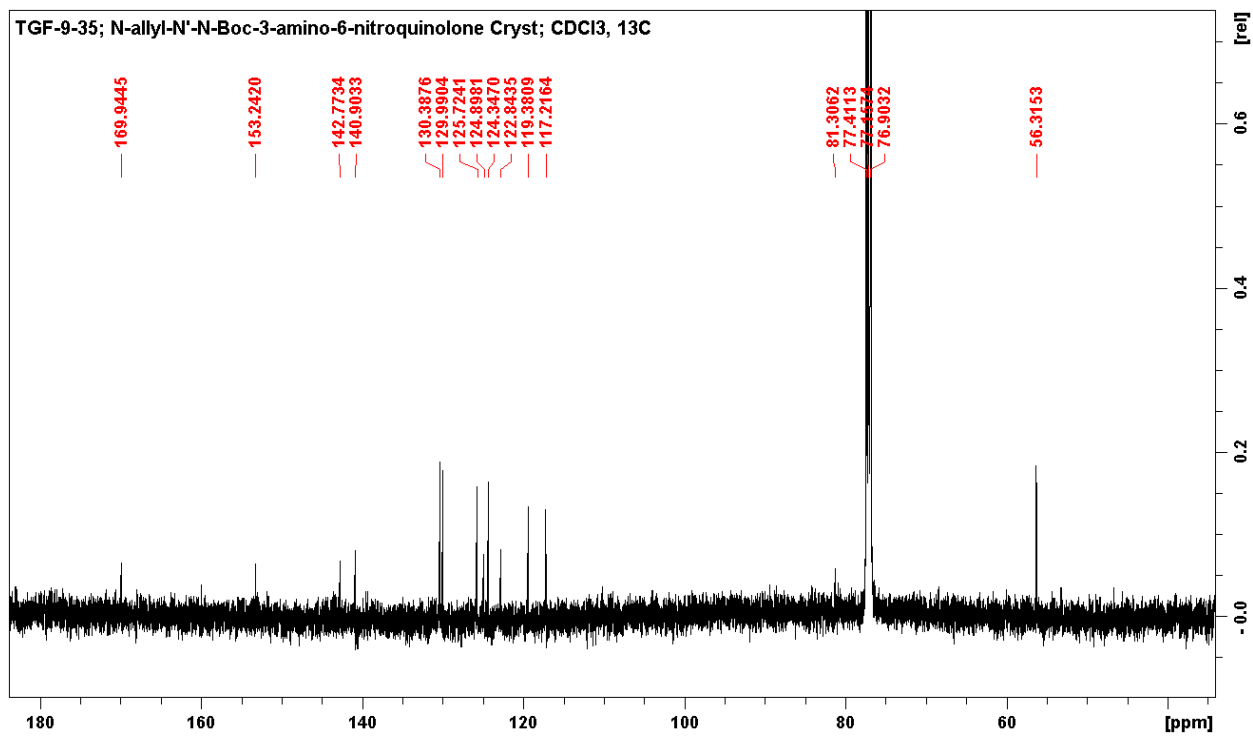
Spectrum 26. ¹³C NMR - AllylQuinolone **21b**



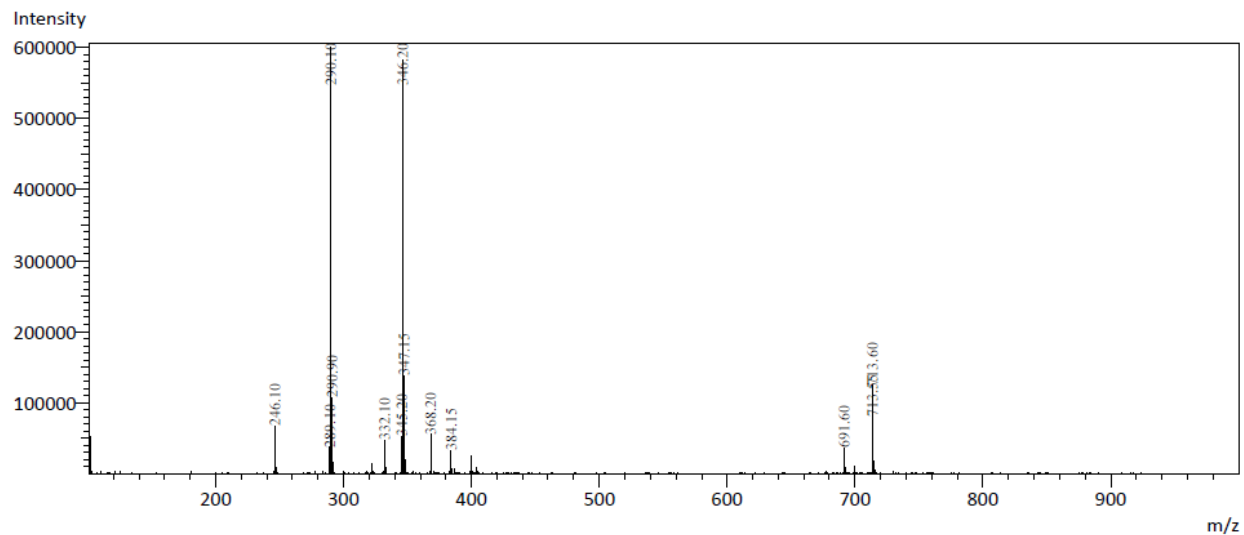
Spectrum 27. ESI-MS - Nitroquinolone **21b**



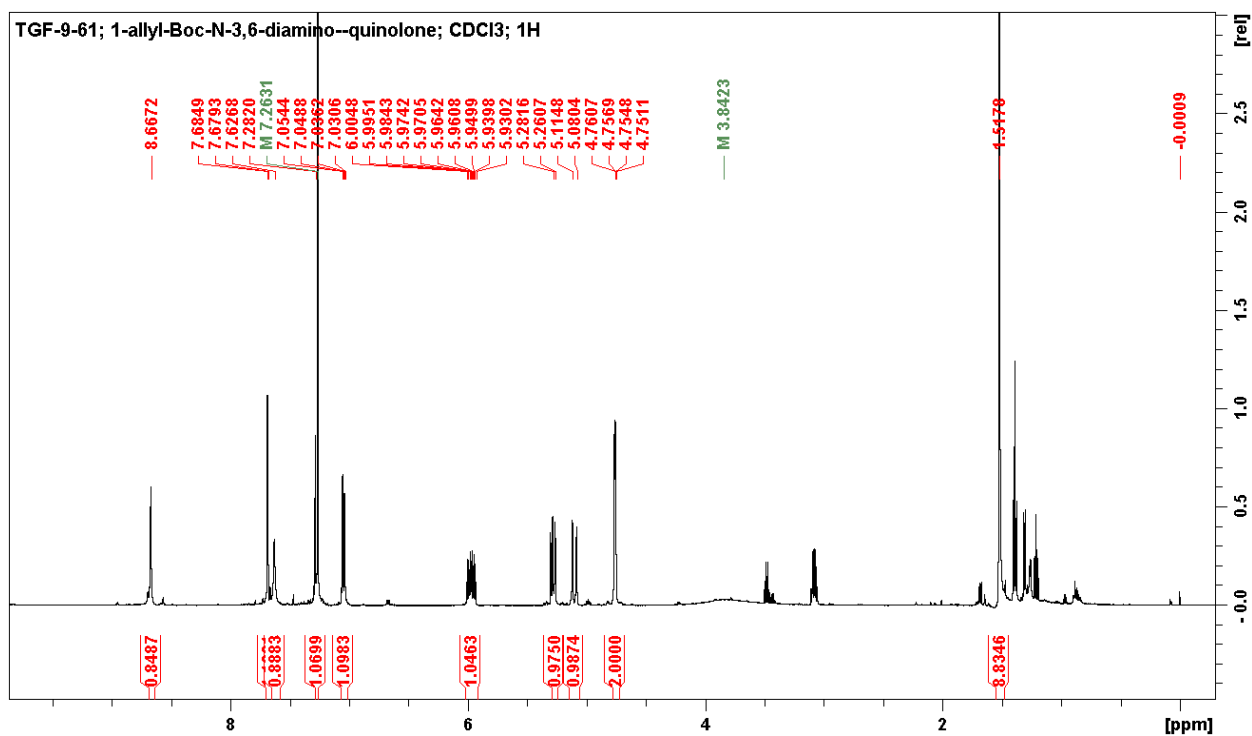
Spectrum 28. ¹H NMR - Boc-N-allylquinolone **22**



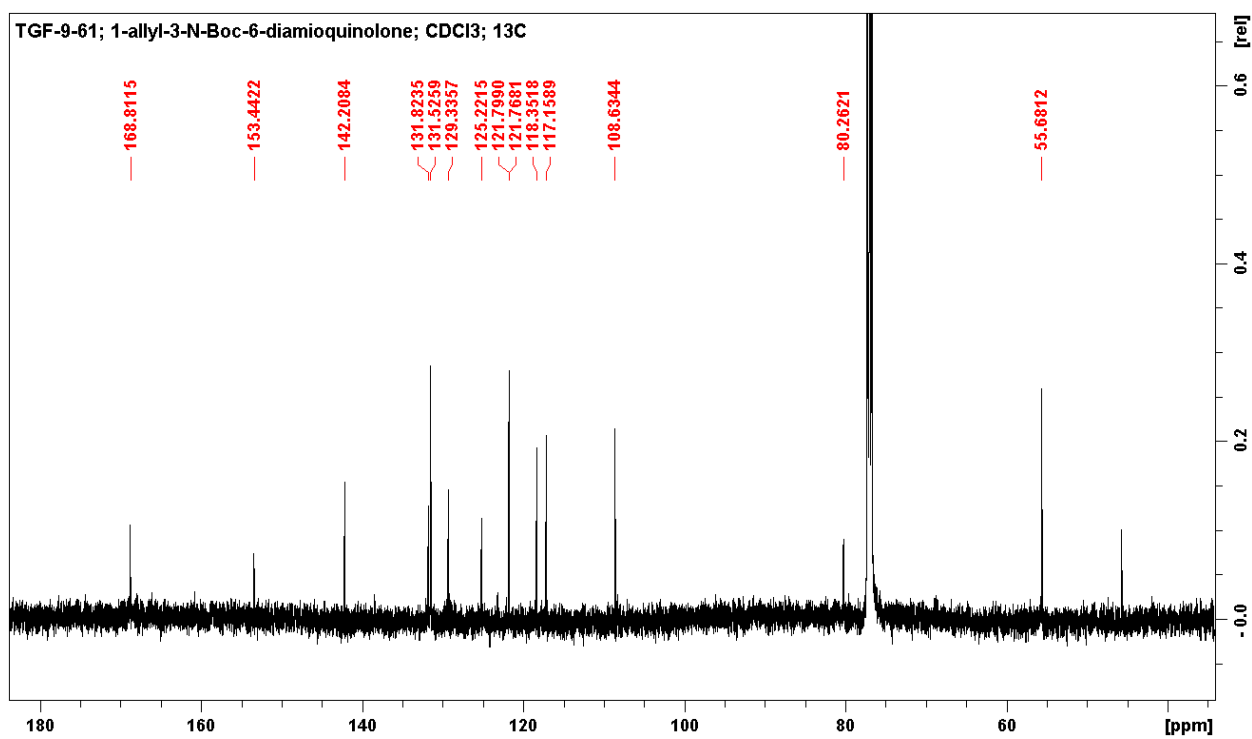
Spectrum 29. ¹³C NMR - Boc-N-aminonitroquinolone 22



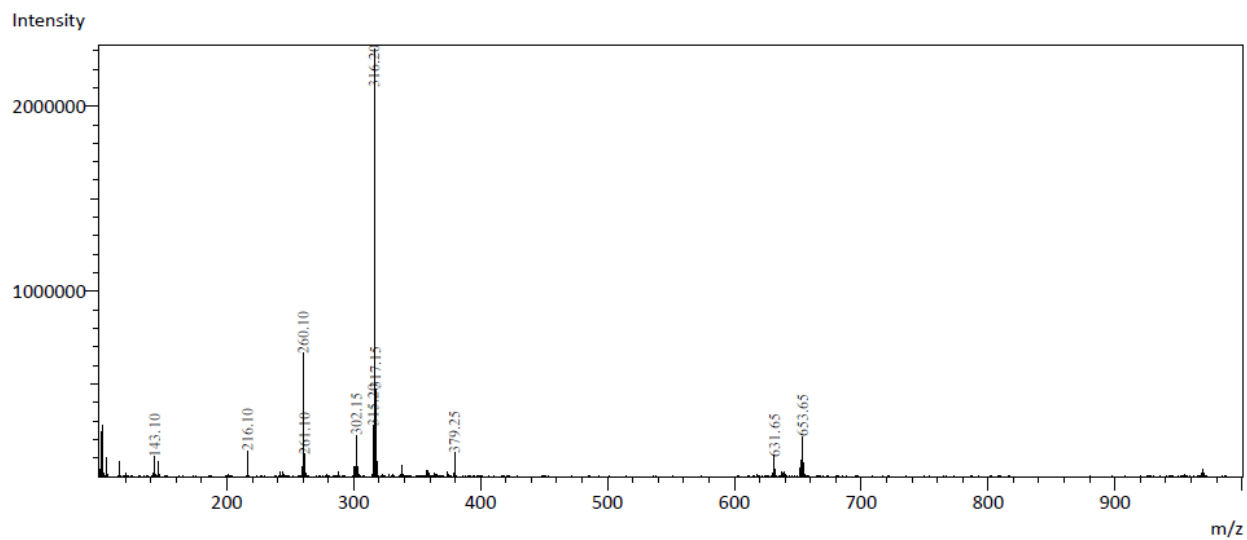
Spectrum 30. ESI-MS - Boc-N-aminonitroquinolone 22



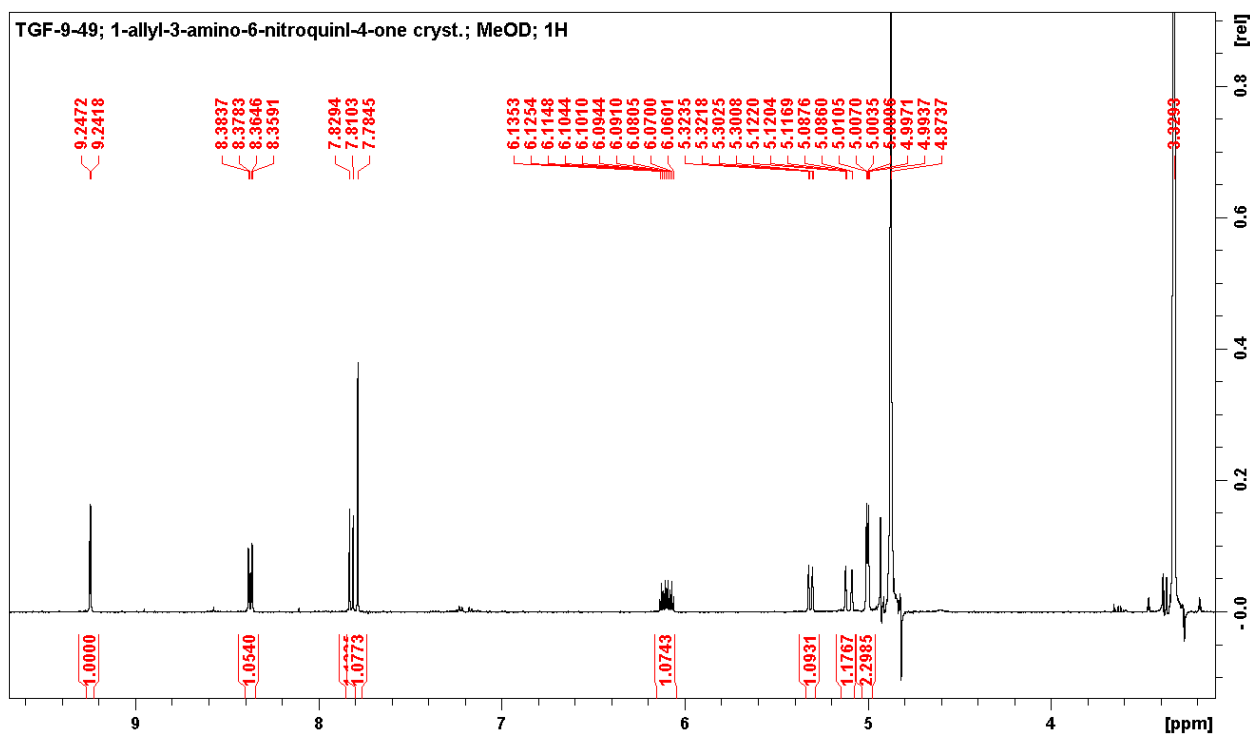
Spectrum 31. ¹H NMR - Boc-N-diaminoquinolone 23



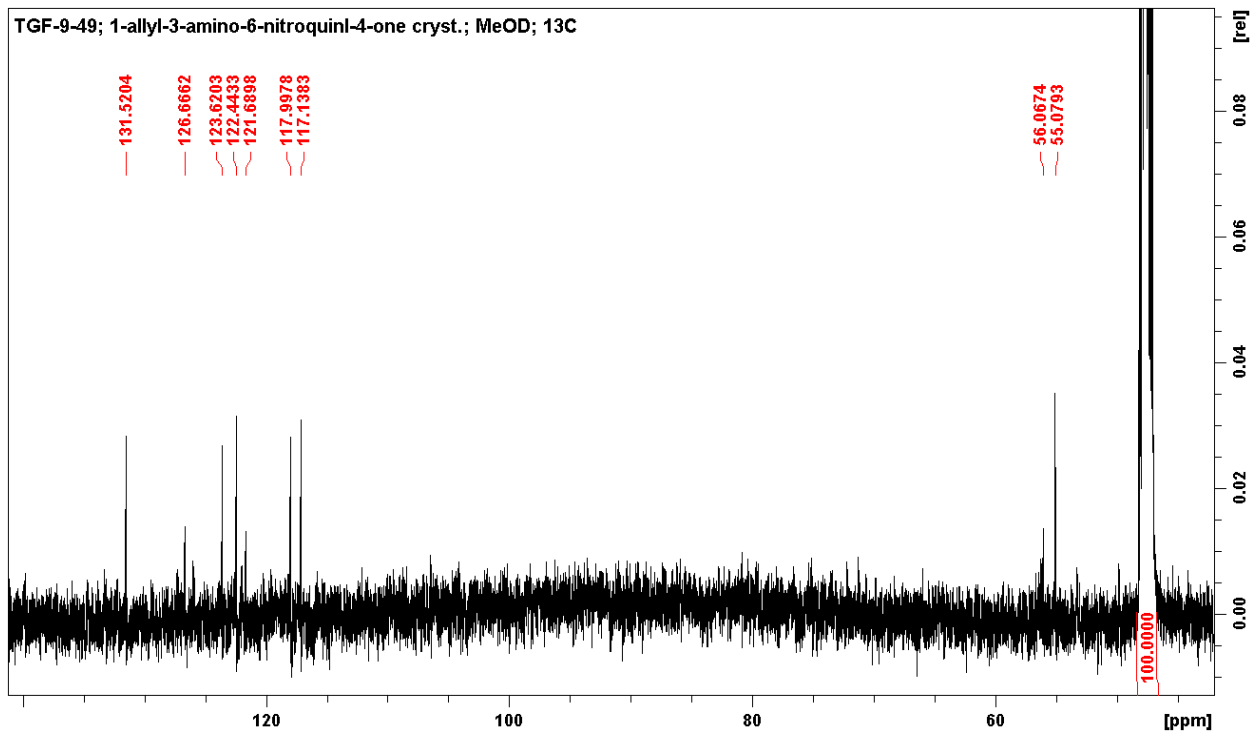
Spectrum 32. ¹³C NMR - Boc-N-diaminoquinolone 23



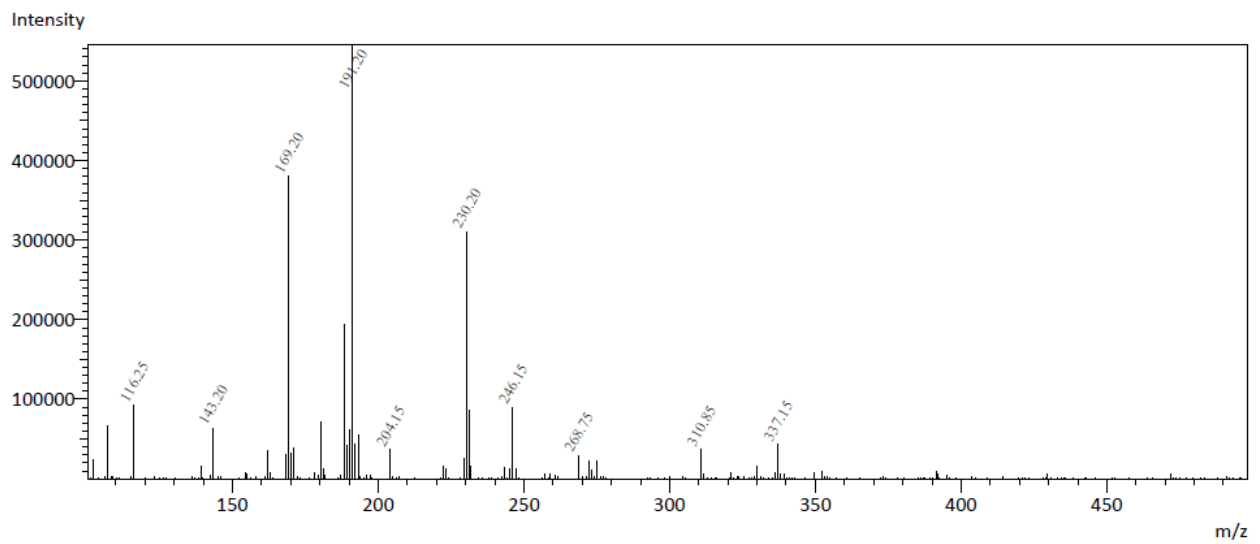
Spectrum 33. ESI-MS - Boc-N-diaminoquinolone 23



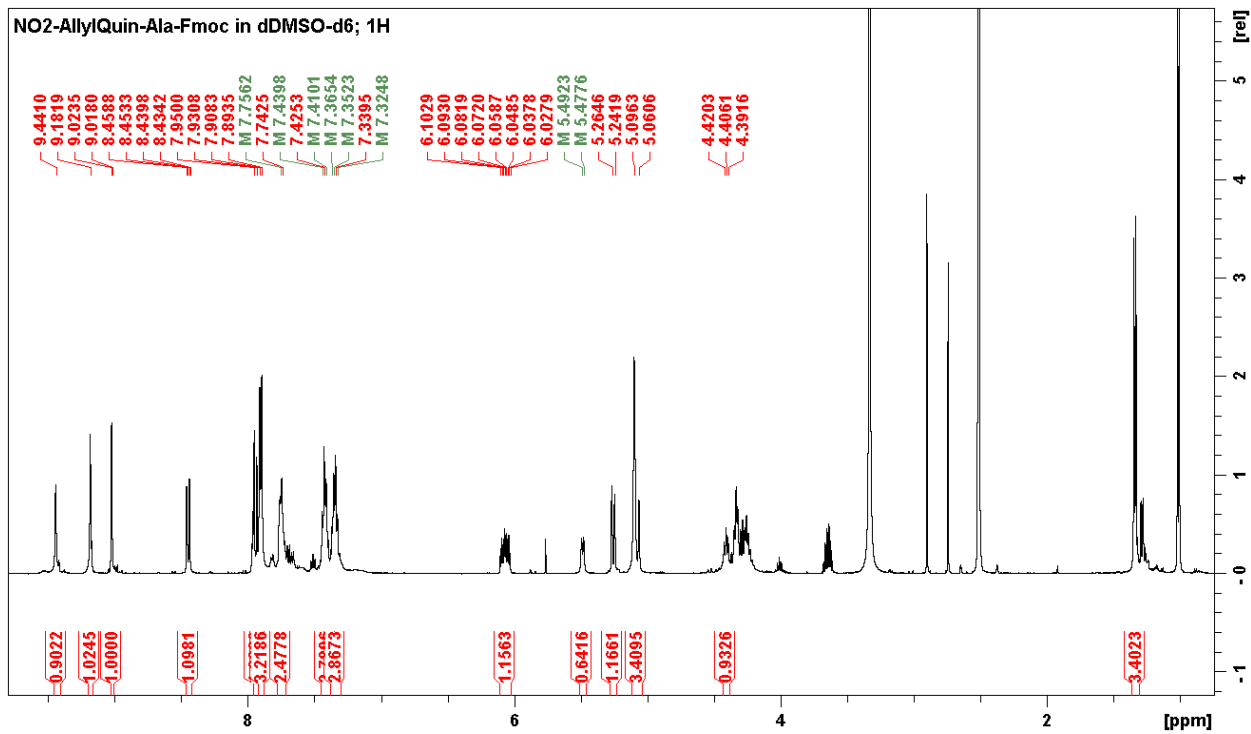
Spectrum 34. ¹H NMR - Aminonitroquinolone 25



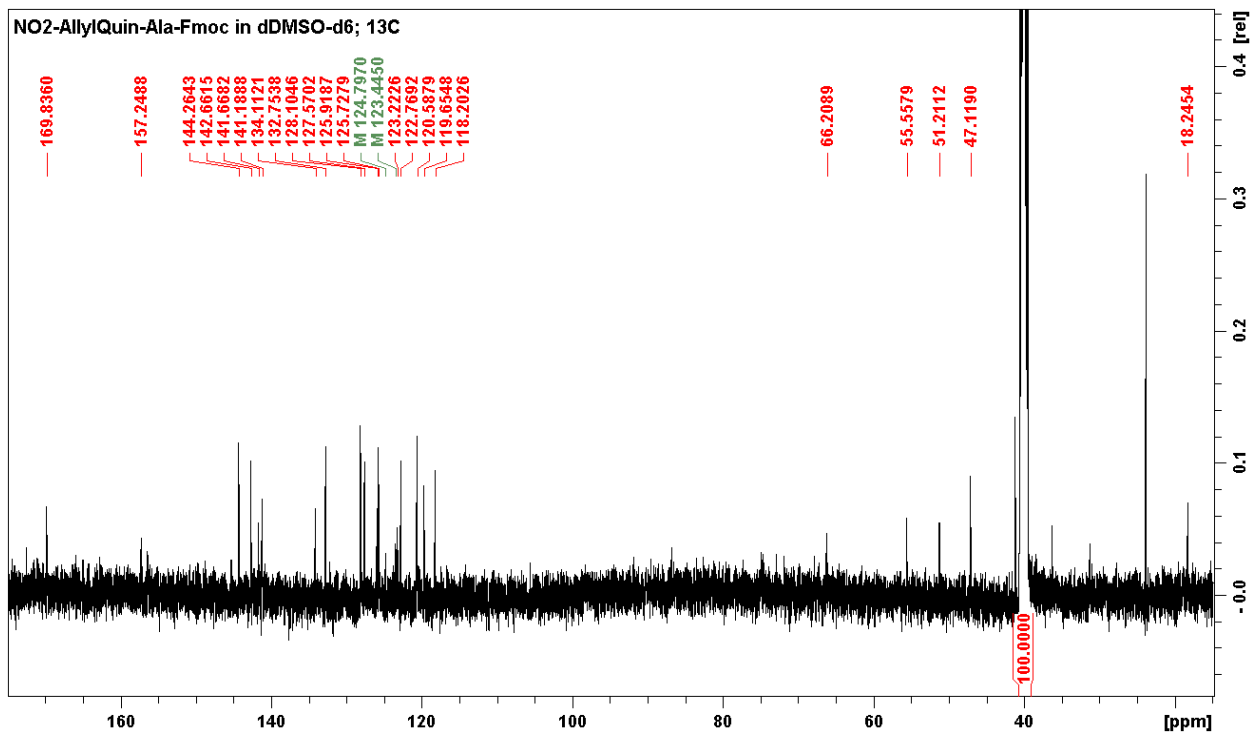
Spectrum 35. ^{13}C NMR - Aminonitroquinolone 25



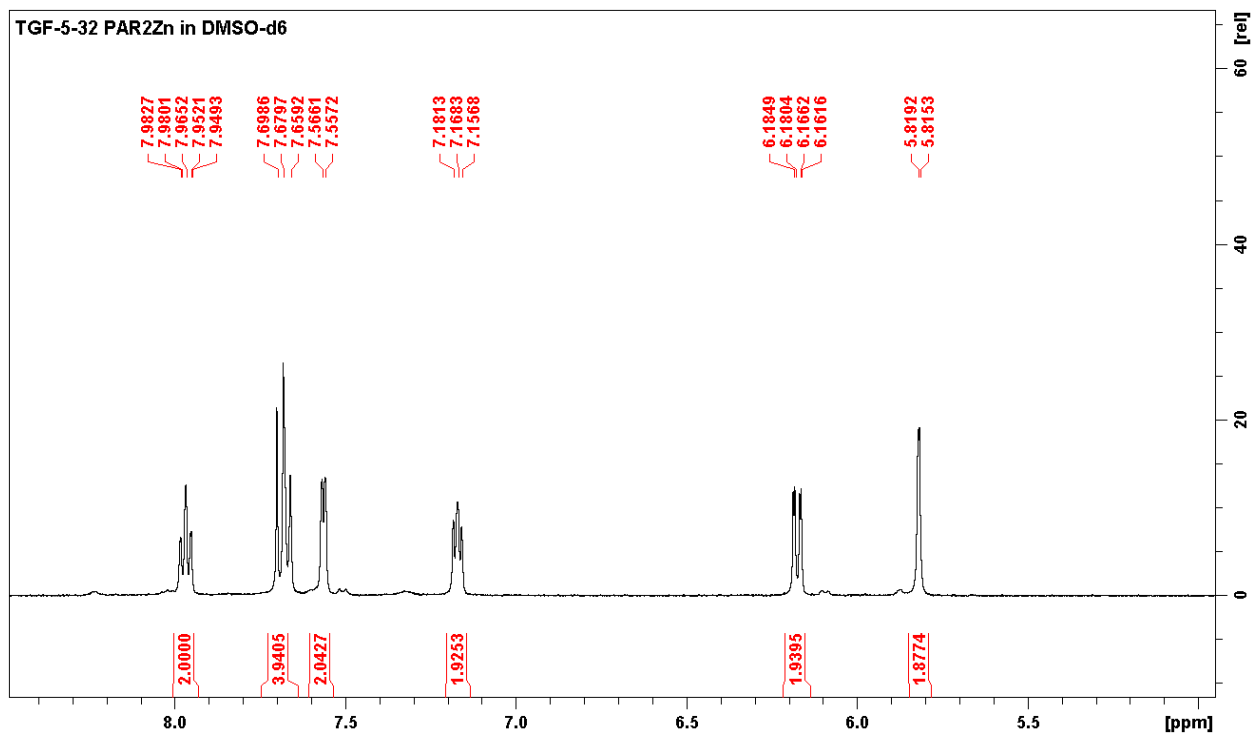
Spectrum 36. ESI-MS - Aminonitroquinolone 25



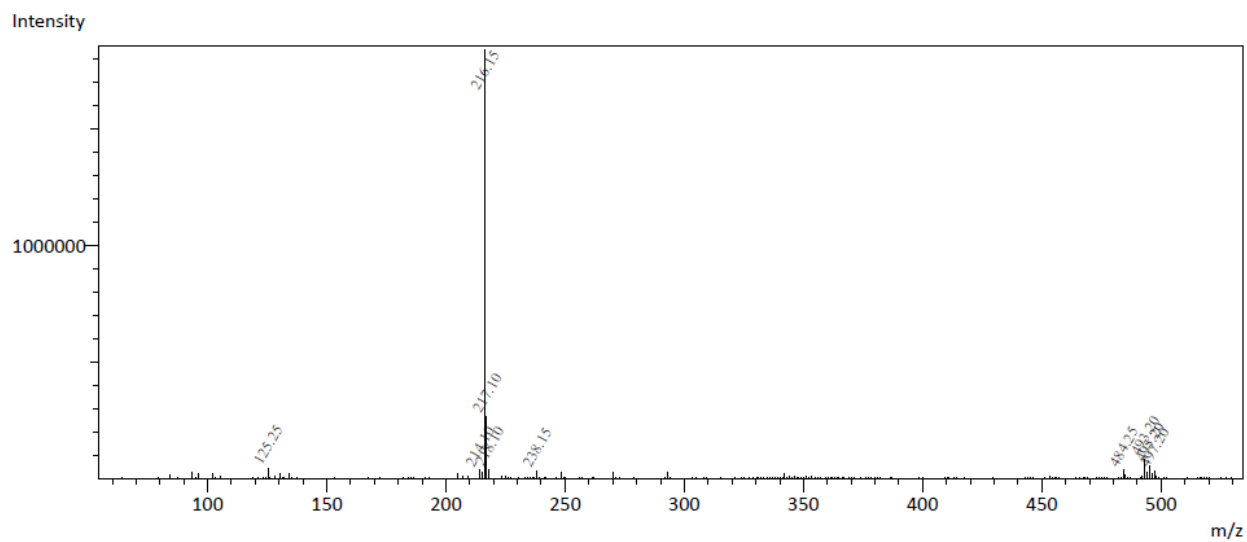
Spectrum 37. ¹H NMR - NO₂-AllylQuin-Ala-Fmoc 26



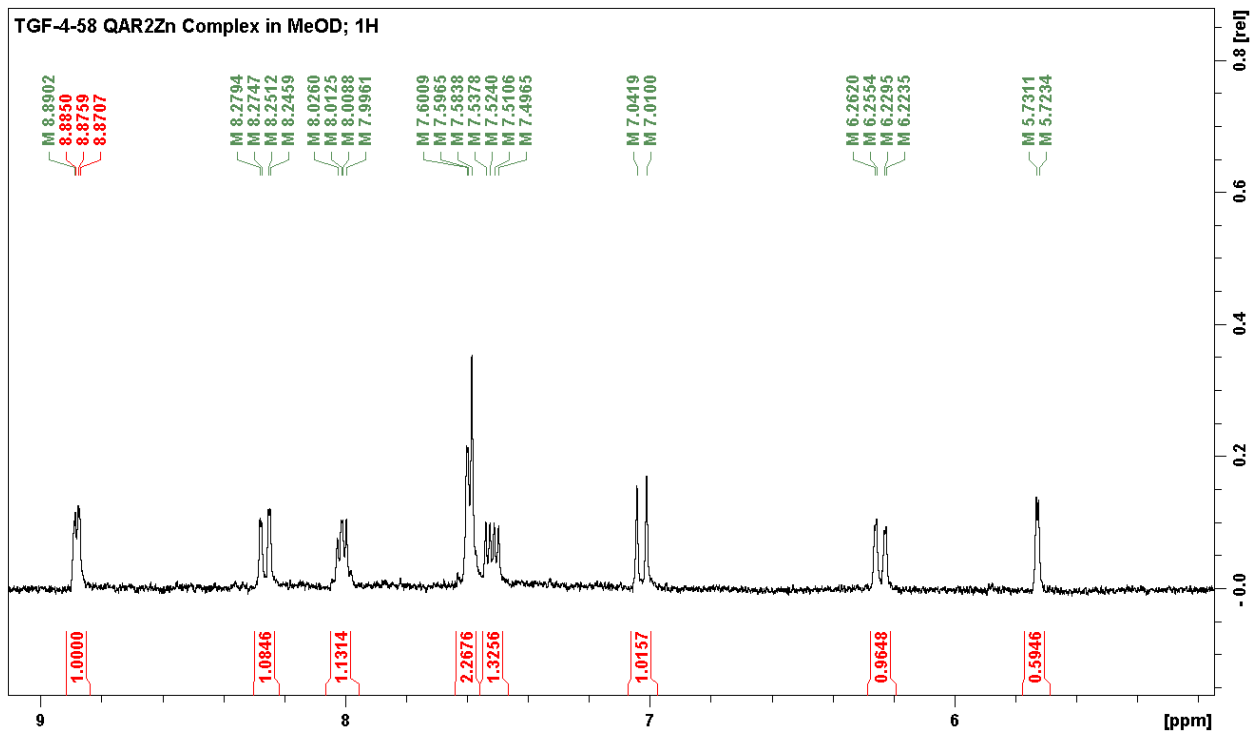
Spectrum 38. ¹³C NMR - NO₂-AllylQuin-Ala-Fmoc 26



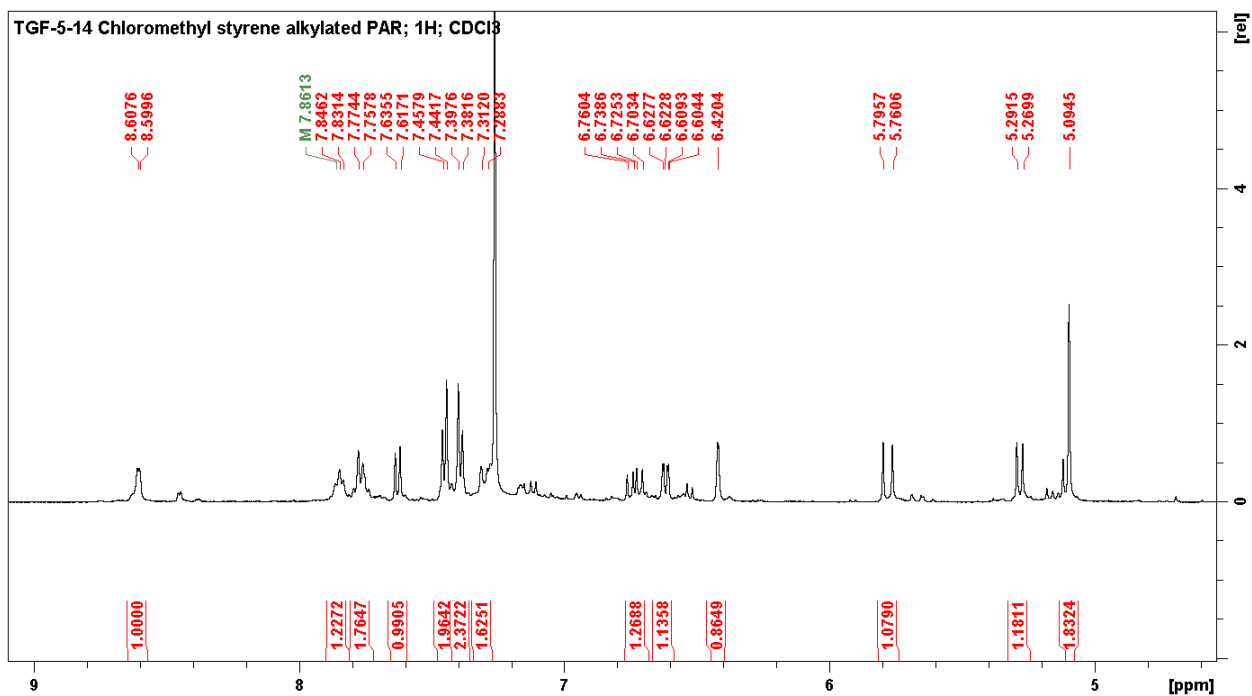
Spectrum 39. ¹H NMR - PAR₂Zn **28b**



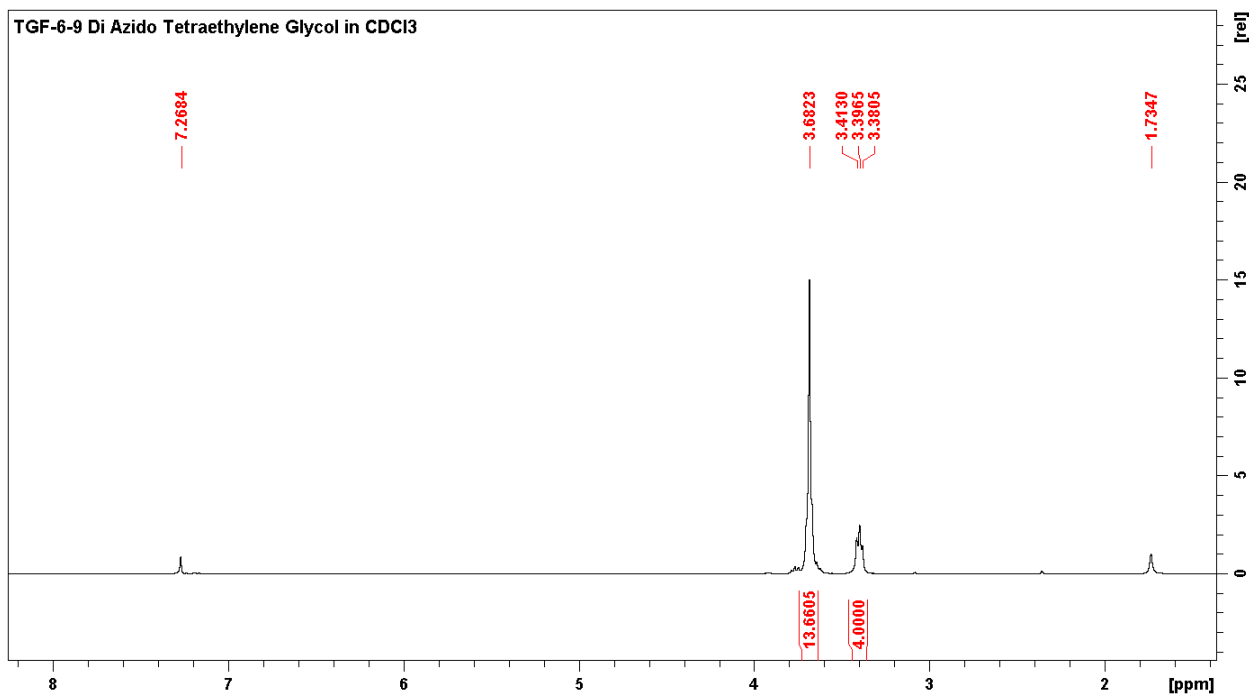
Spectrum 40. ESI-MS - PAR₂Zn **28b**



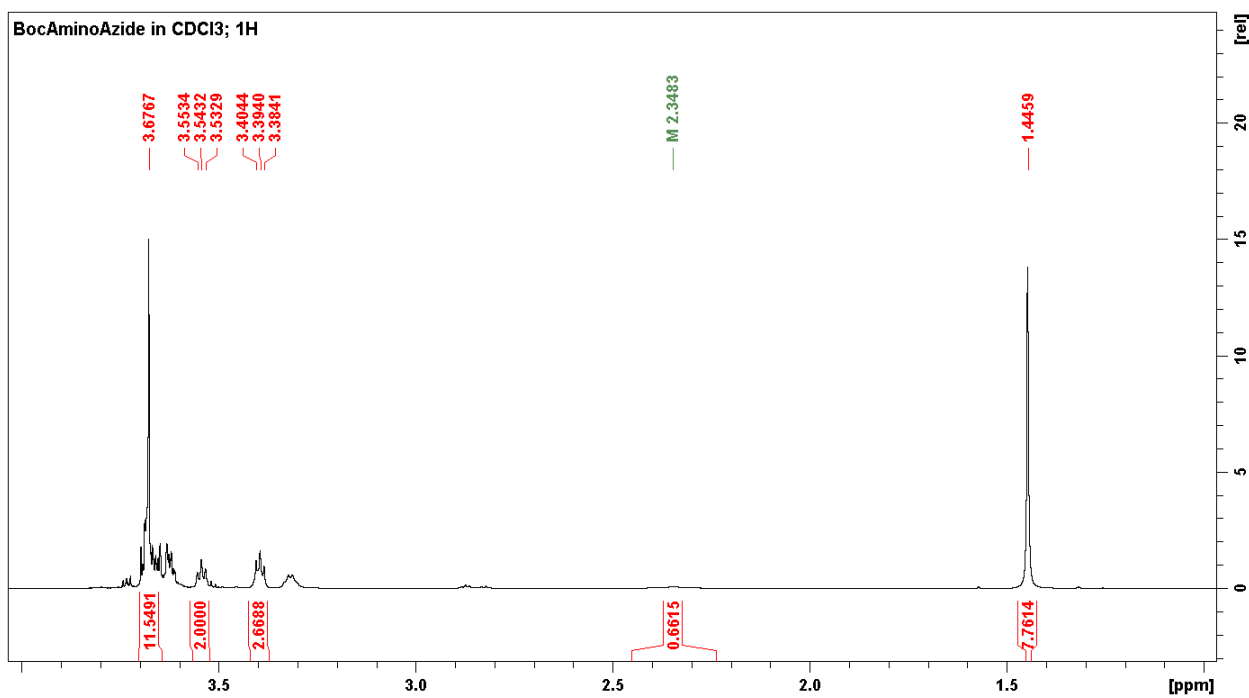
Spectrum 41. ¹H NMR - QAR₂Zn 29b



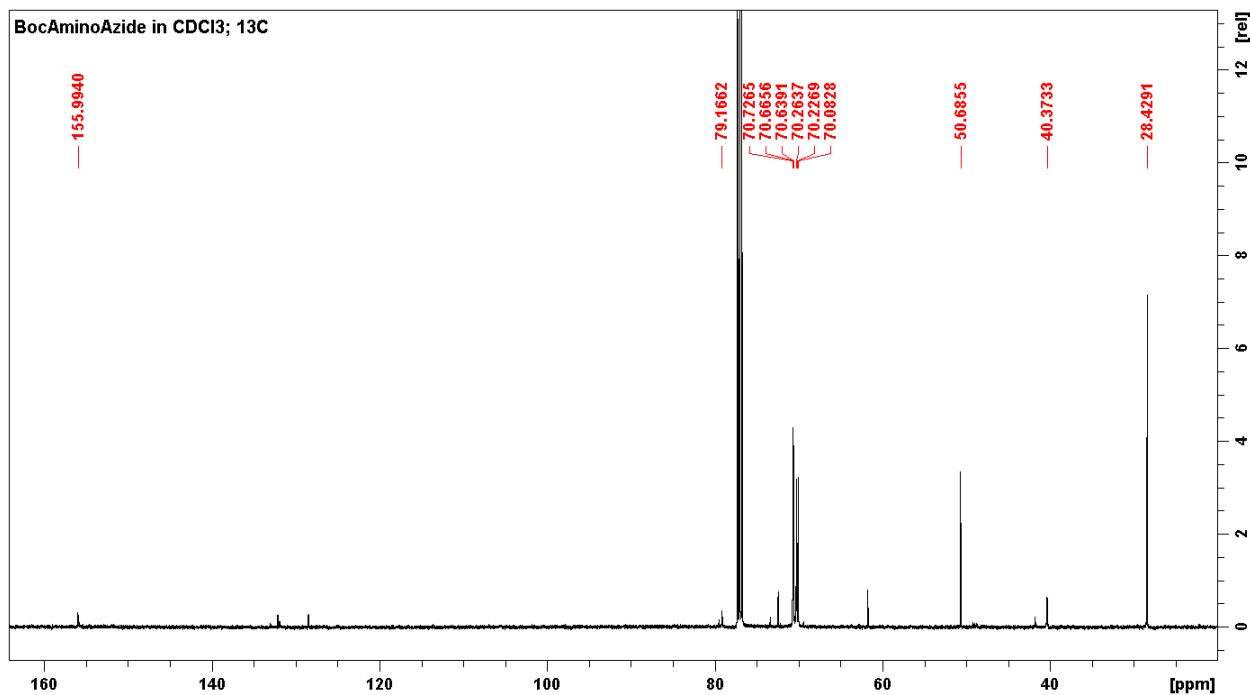
Spectrum 42. ¹H NMR - PAR-CMS 30



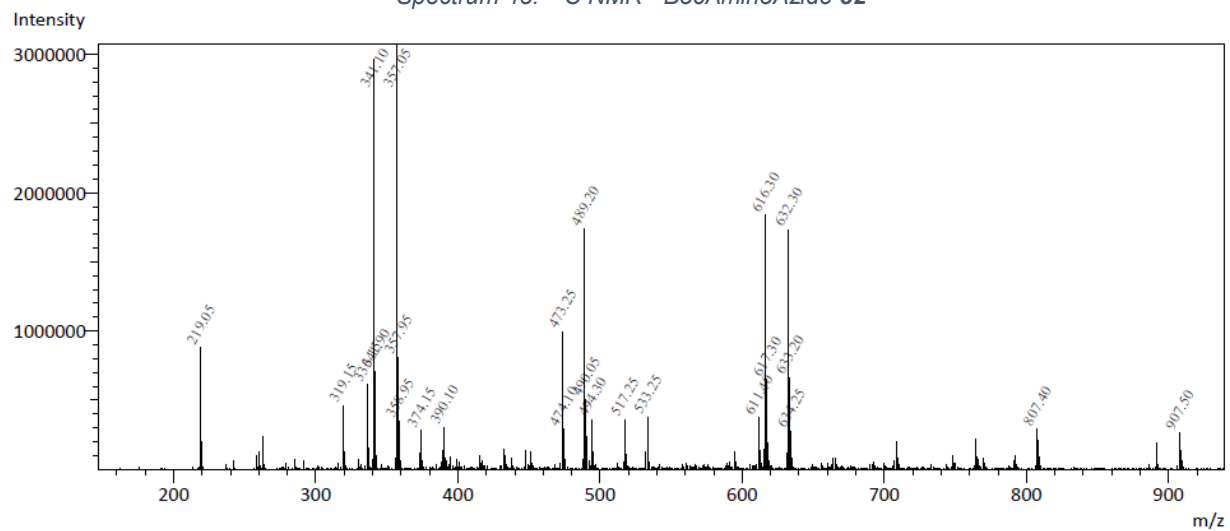
Spectrum 43. ¹H NMR - Diazido(tetraethylene glycol) 31



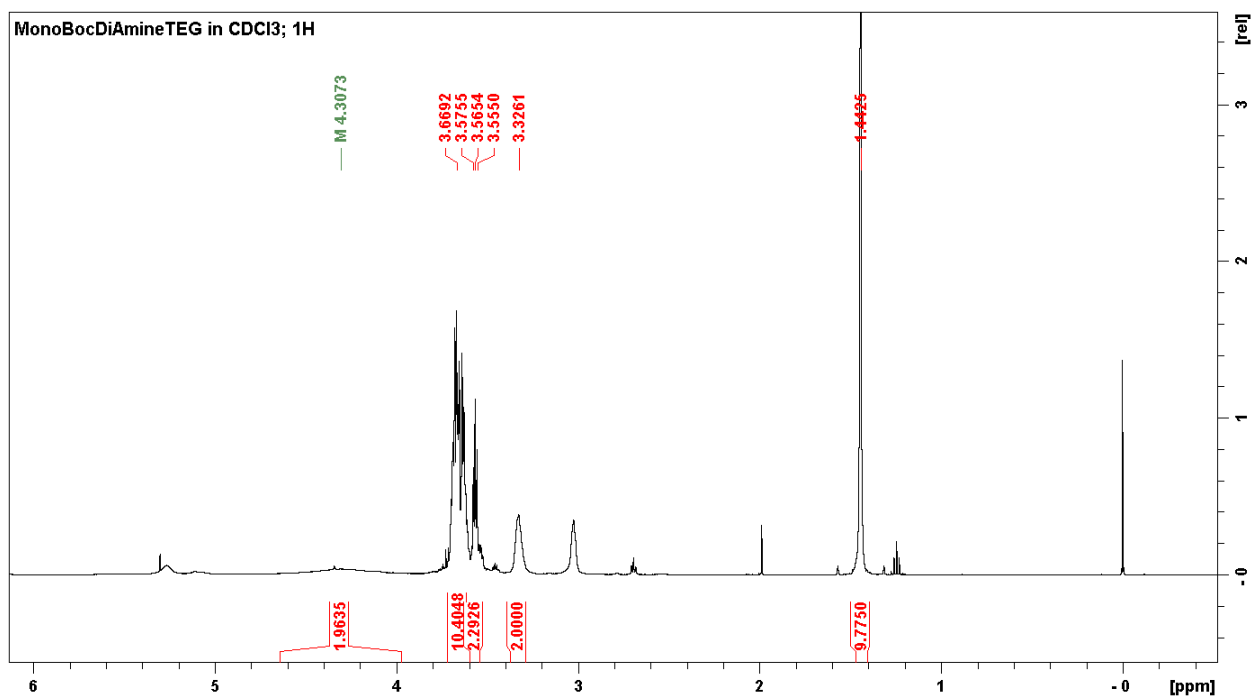
Spectrum 44. ¹H NMR - BocAminoAzide 32



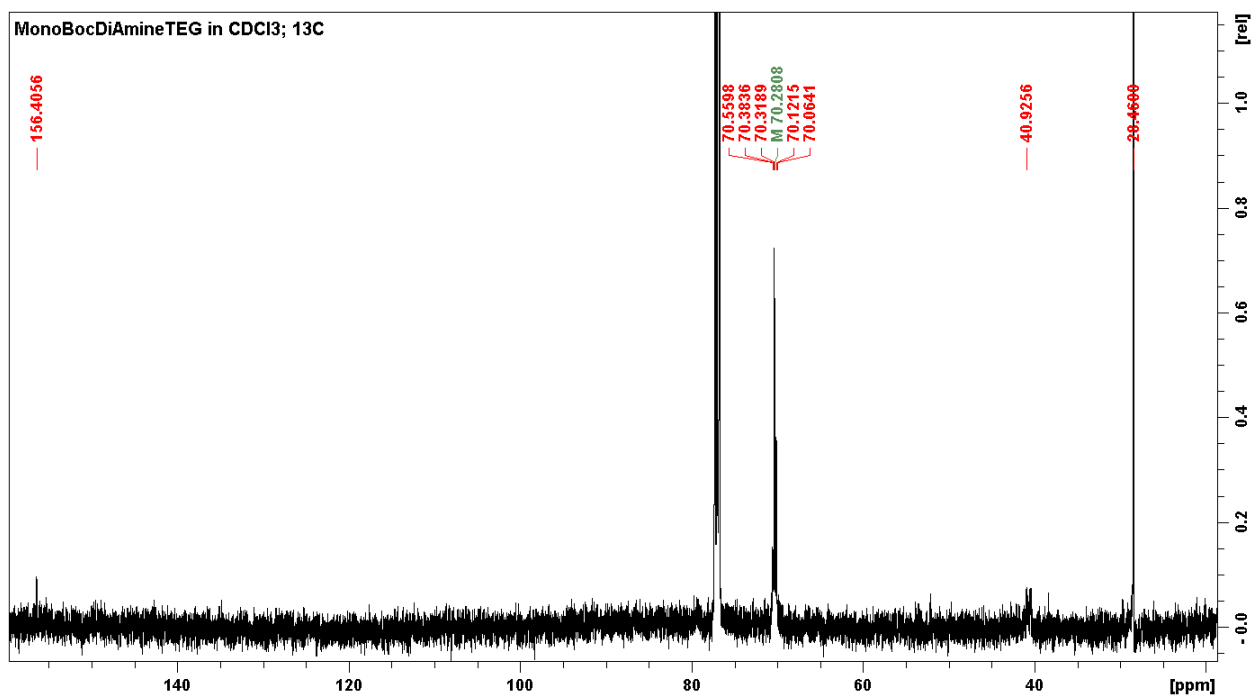
Spectrum 45. ¹³C NMR - BocAminoAzide 32



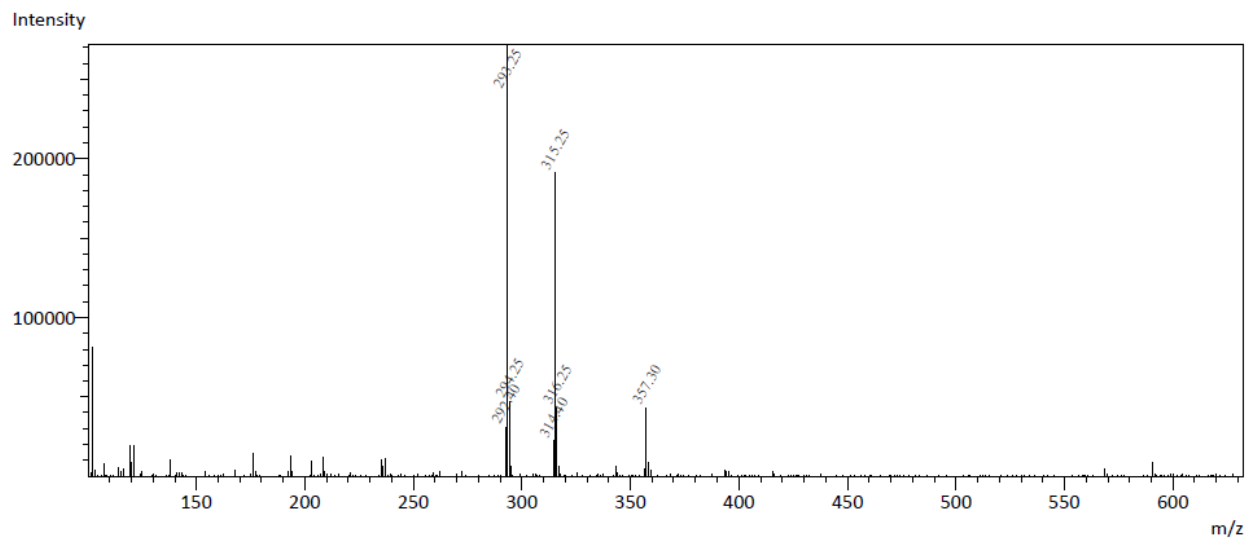
Spectrum 46. ESI-MS - BocAminoAzide 32.



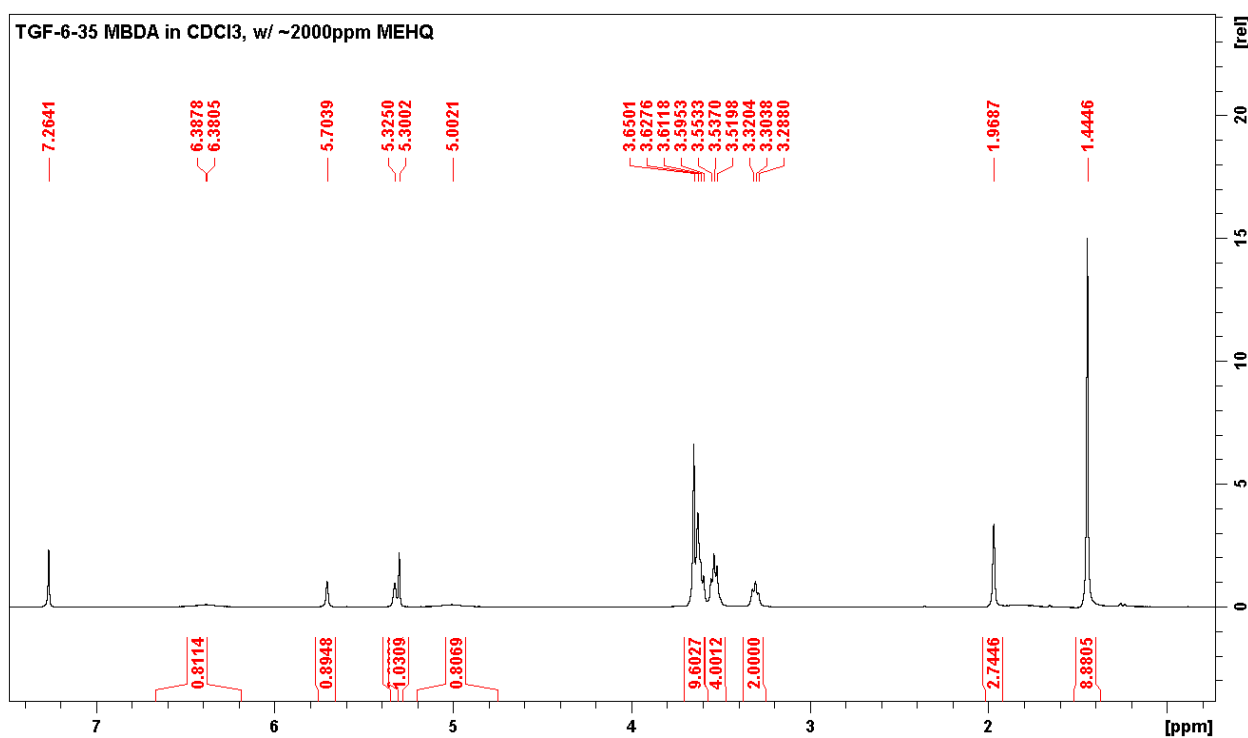
Spectrum 47. ¹H NMR - MonoBocDiamineTEG 33



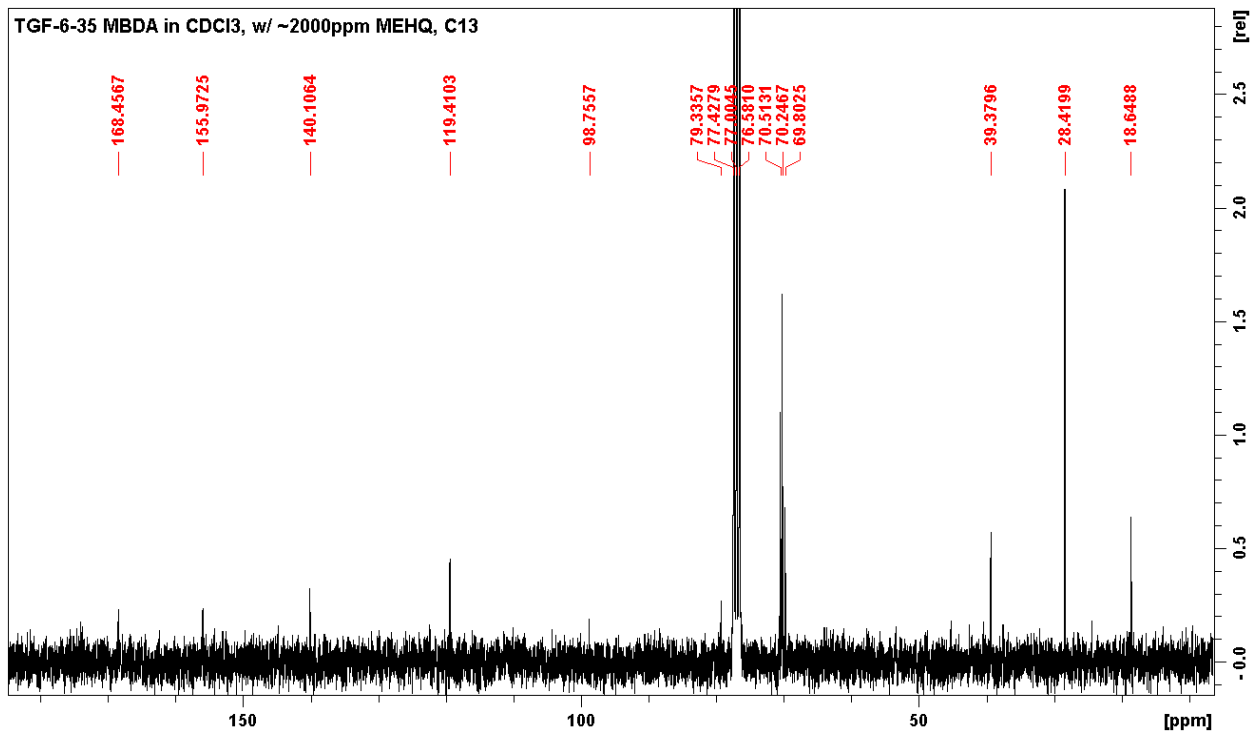
Spectrum 48. ¹³C NMR - MonoBocDiamineTEG 33



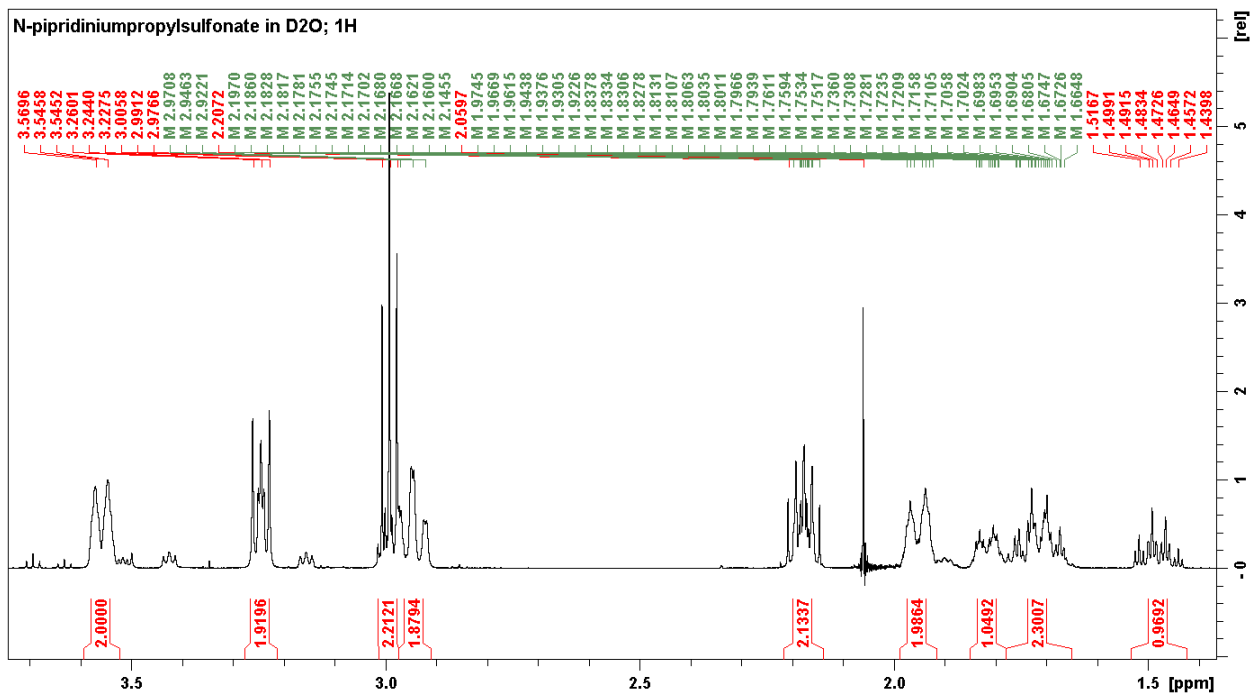
Spectrum 49. ESI-MS - MonoBocDiAmineTEG 33



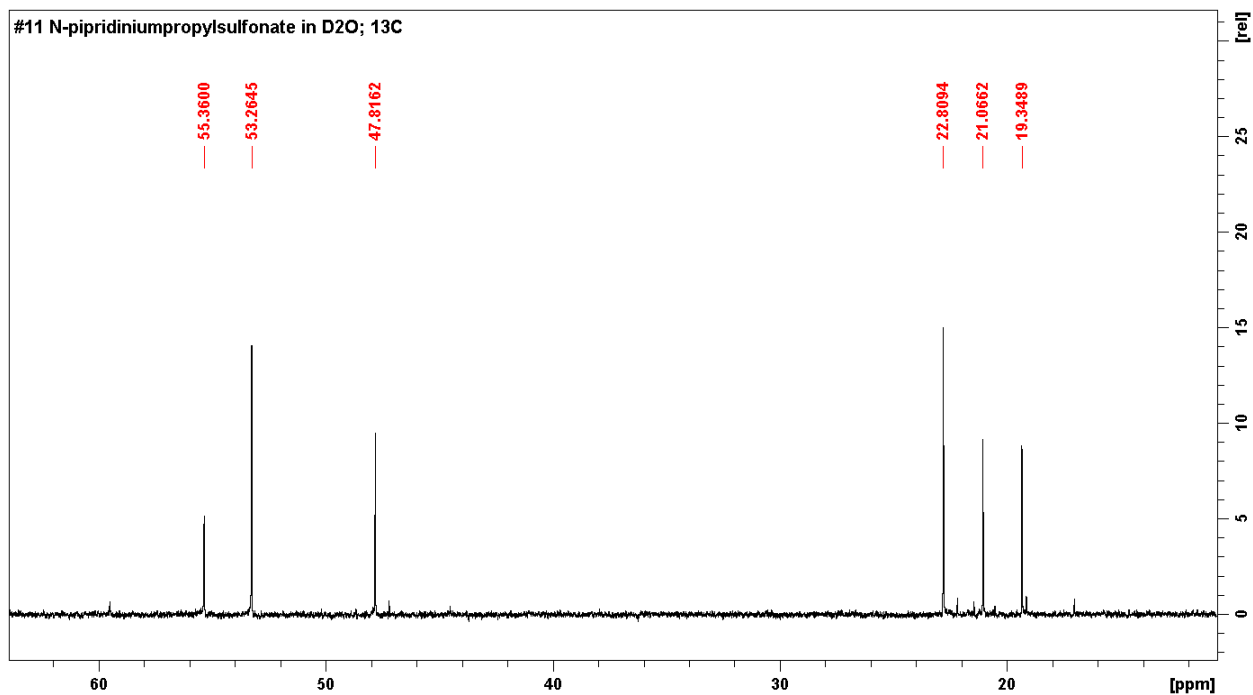
Spectrum 50. ¹H NMR - MABA-TEG 34



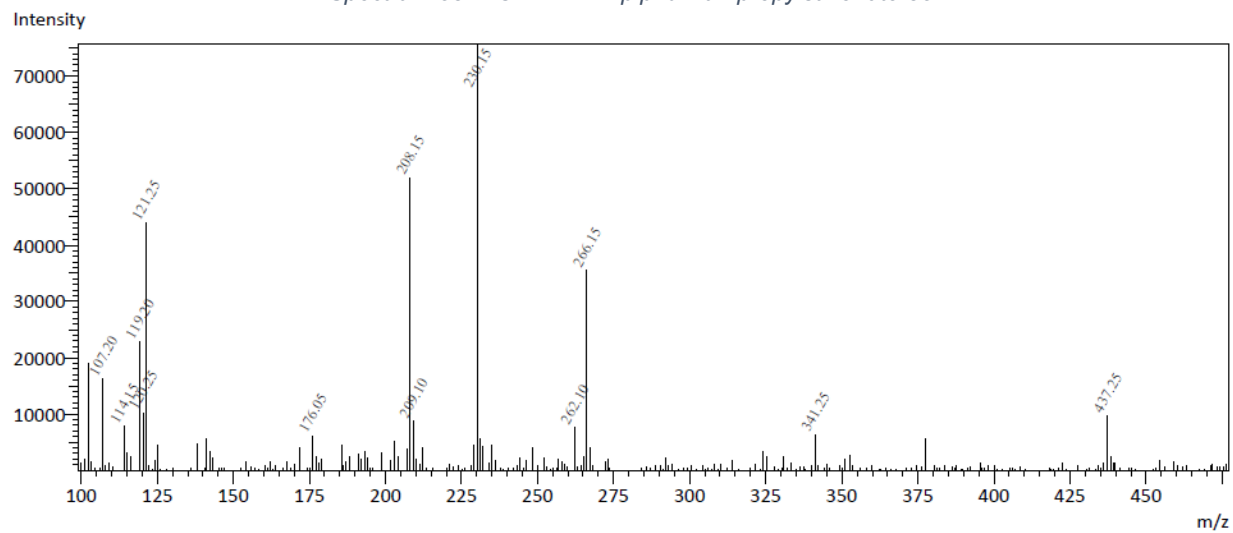
Spectrum 51. ¹³C NMR - MABA-TEG 34



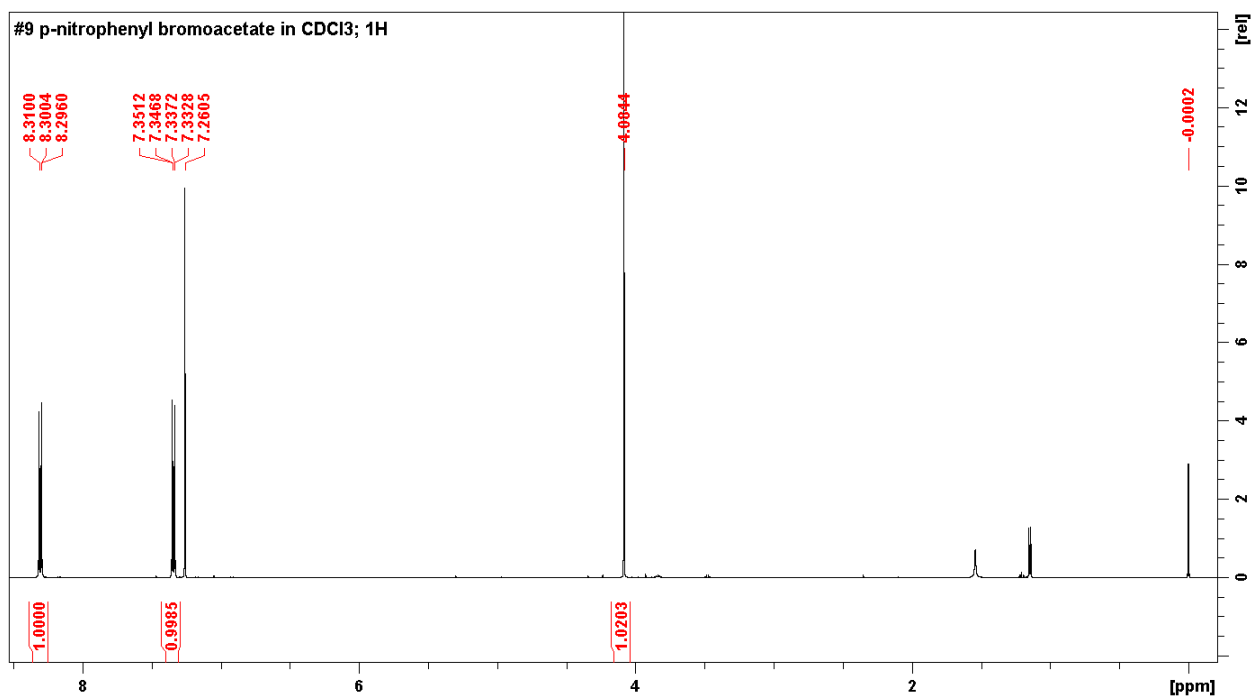
Spectrum 52. ¹H NMR - N-piperidiniumpropylsulfonate 35



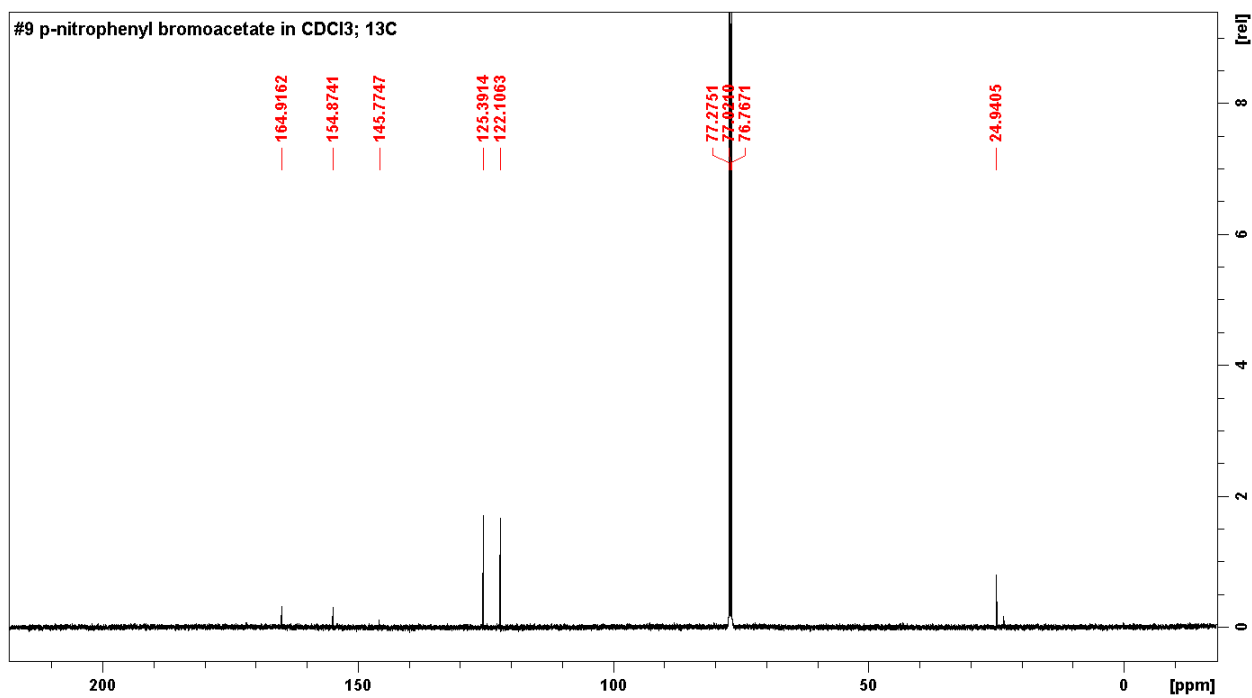
Spectrum 53. ¹³C NMR - N-piperidiniumpropylsulfonate 35



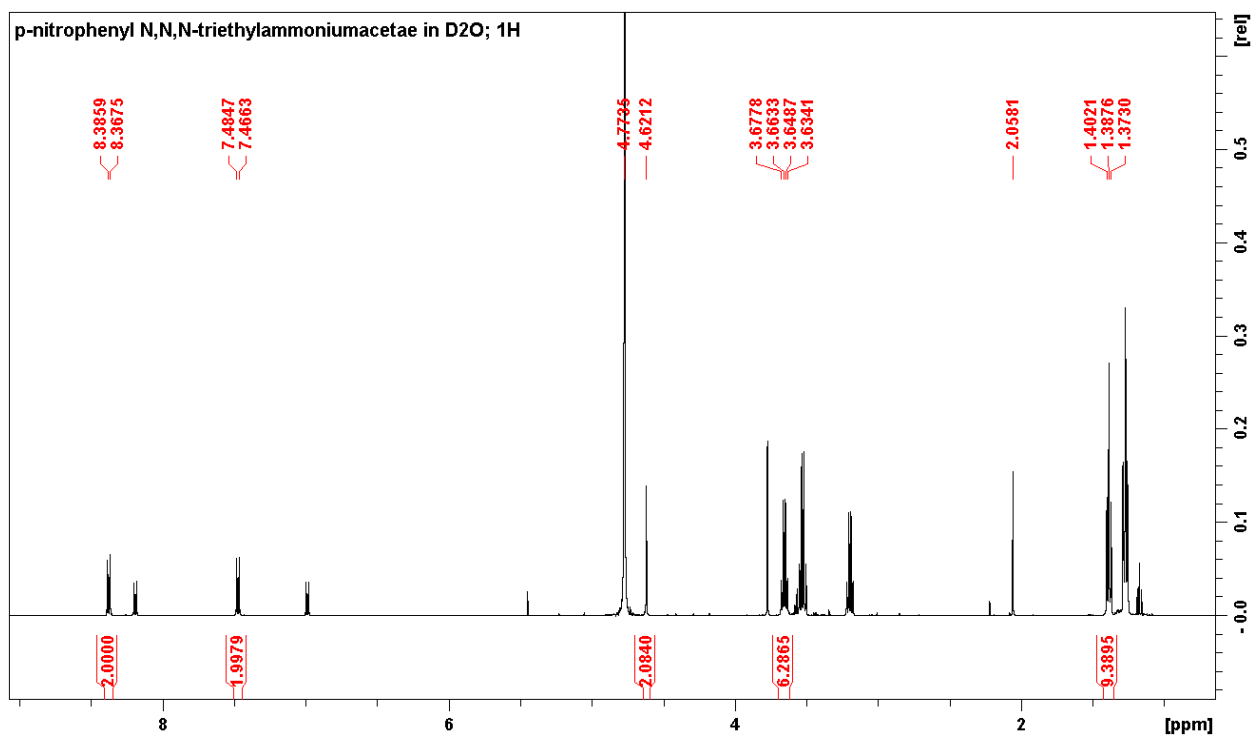
Spectrum 54. ESI-MS - N-piperidiniumpropylsulfonate 35



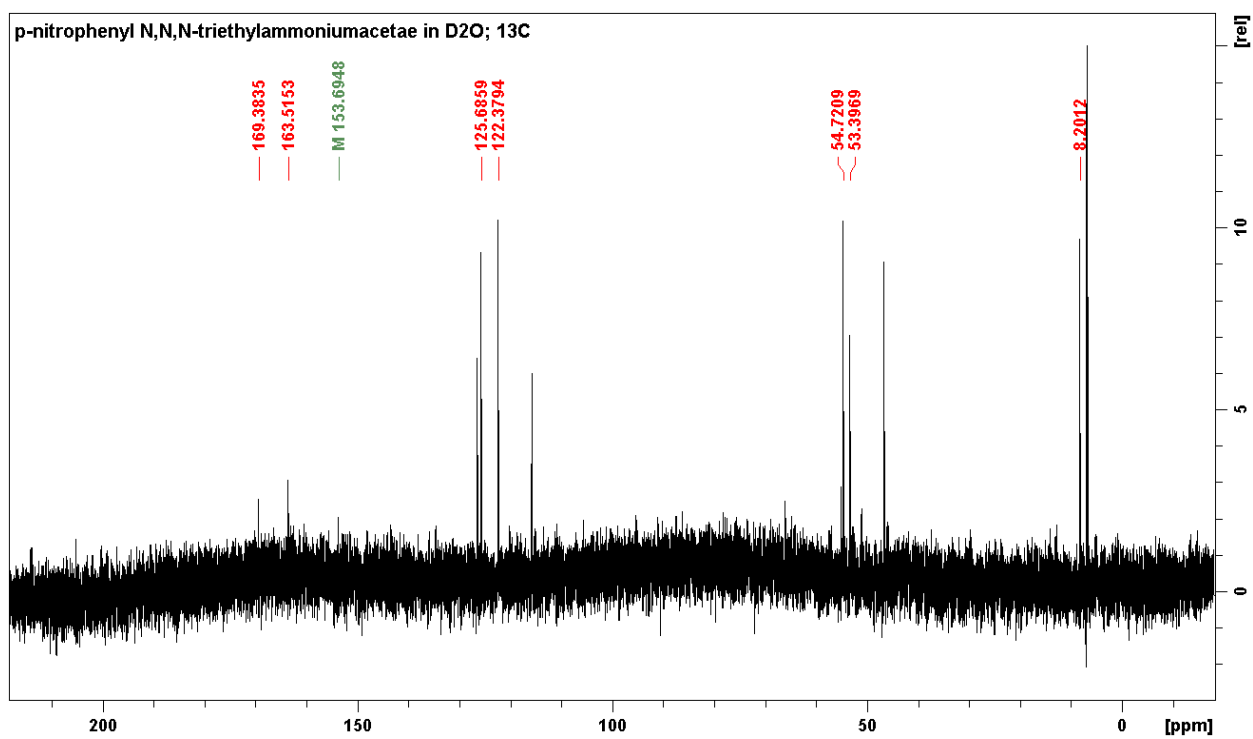
Spectrum 55. ¹H NMR - p-nitrophenyl bromoacetate 36



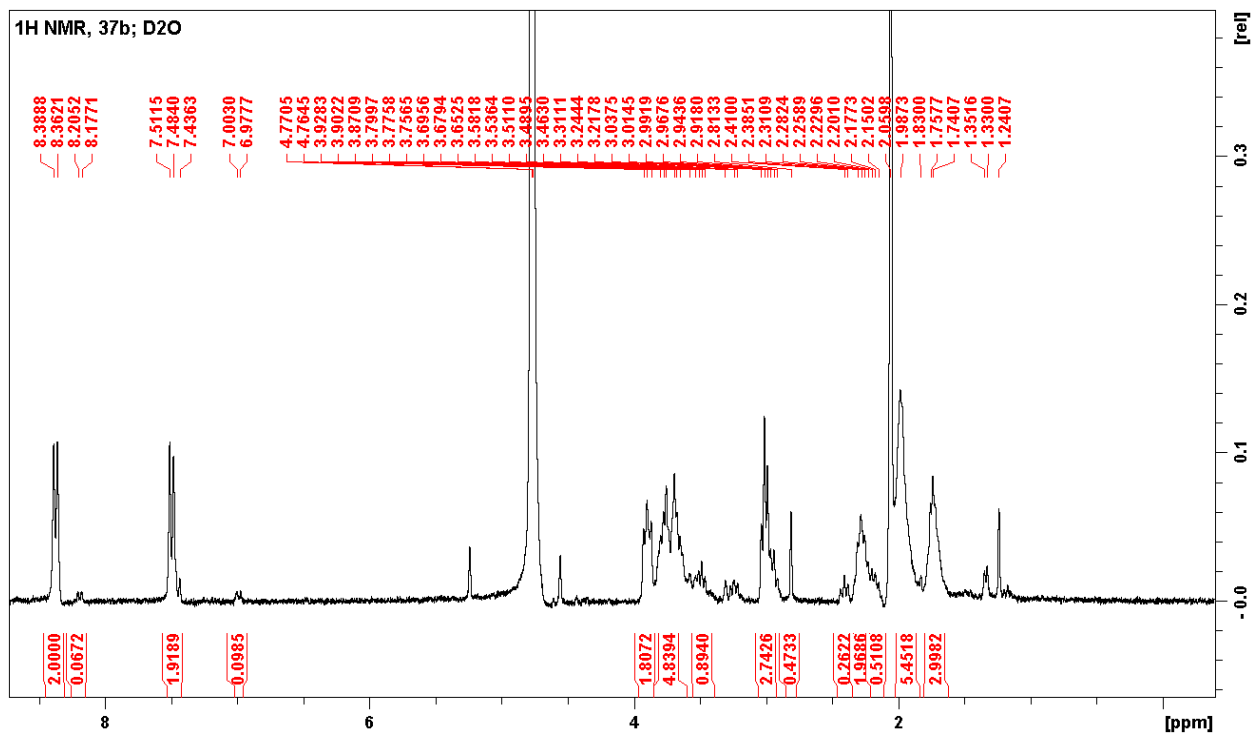
Spectrum 56. ¹³C NMR - p-nitrophenyl bromoacetate 36



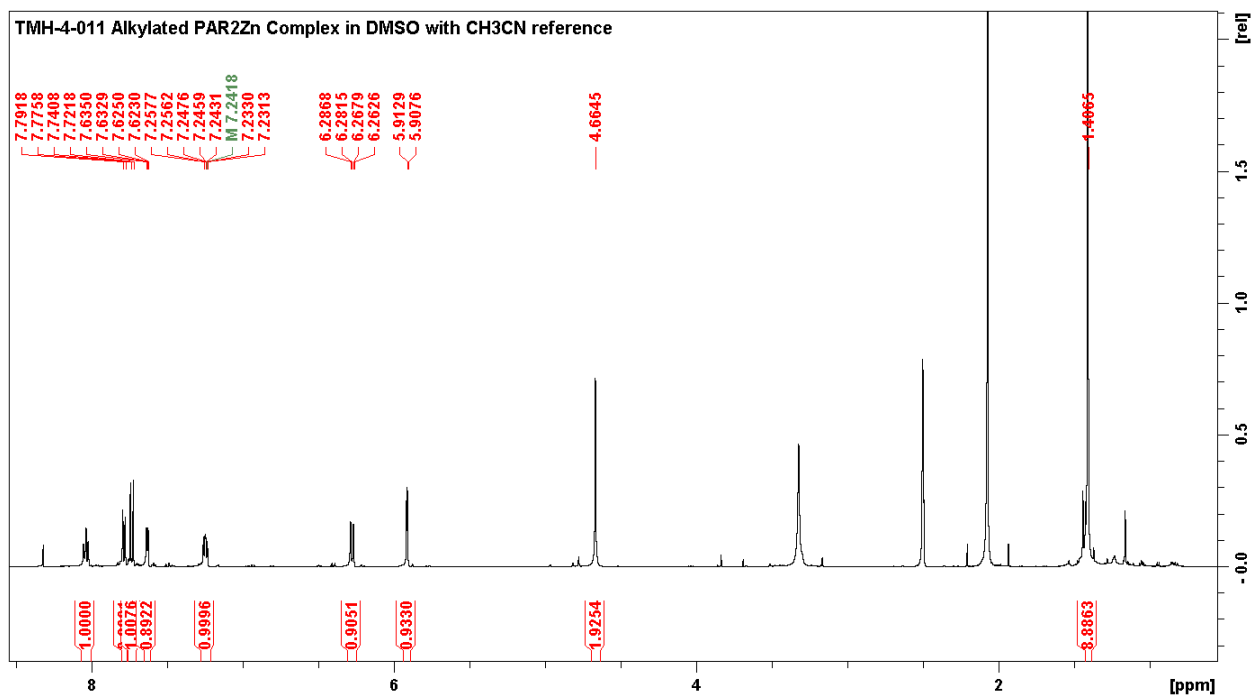
Spectrum 57. ¹H NMR - p-nitrophenyl triethylammoniumacetate bromide 37a



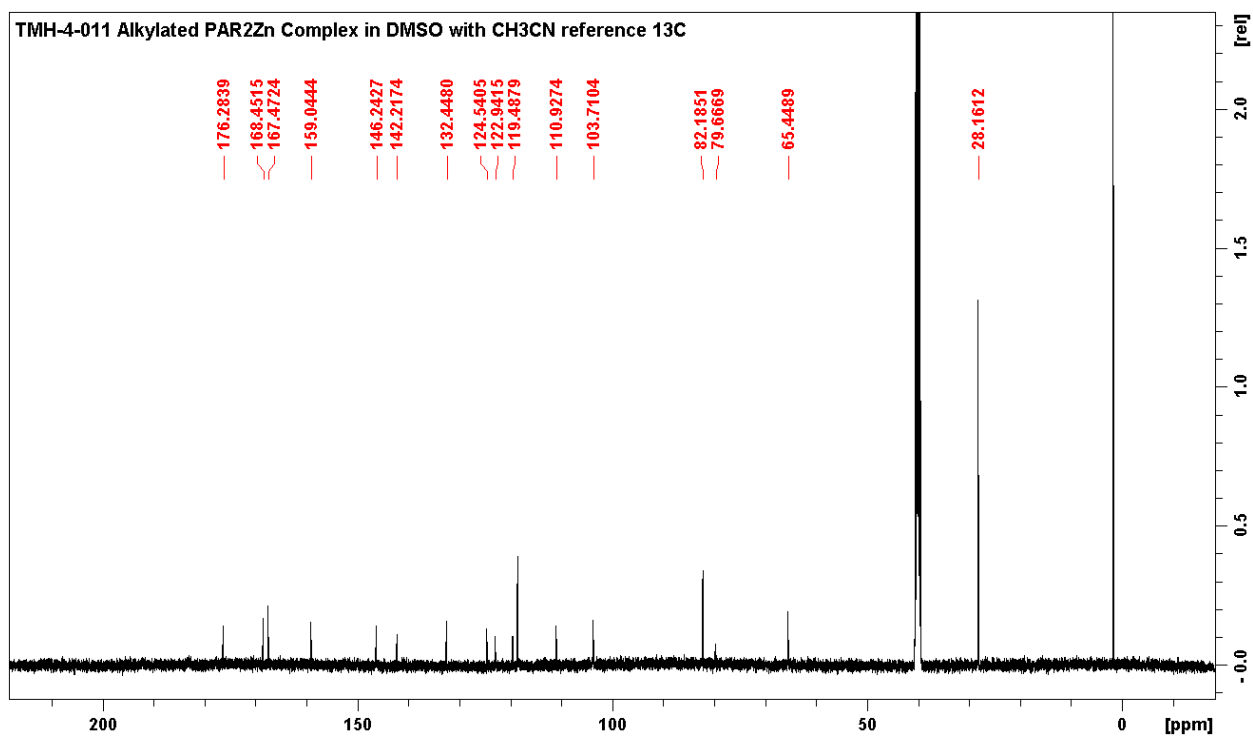
Spectrum 58. ¹³C NMR - p-nitrophenyl triethylammoniumacetate bromide 37a



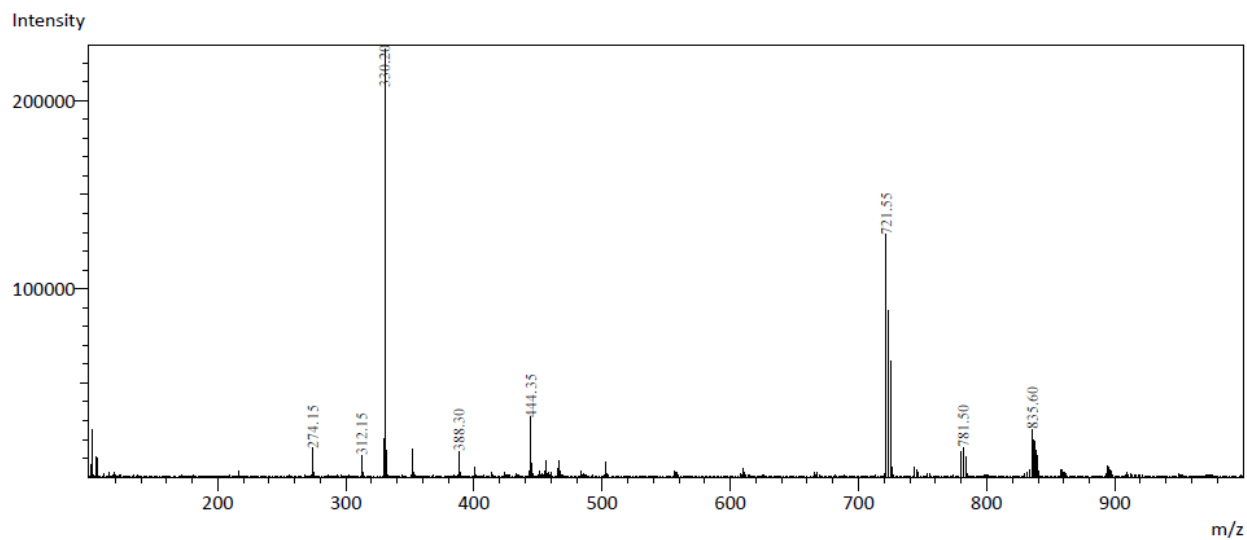
Spectrum 59. ¹H NMR – *p*-nitrophenyl zwitterionic acetate **37b**



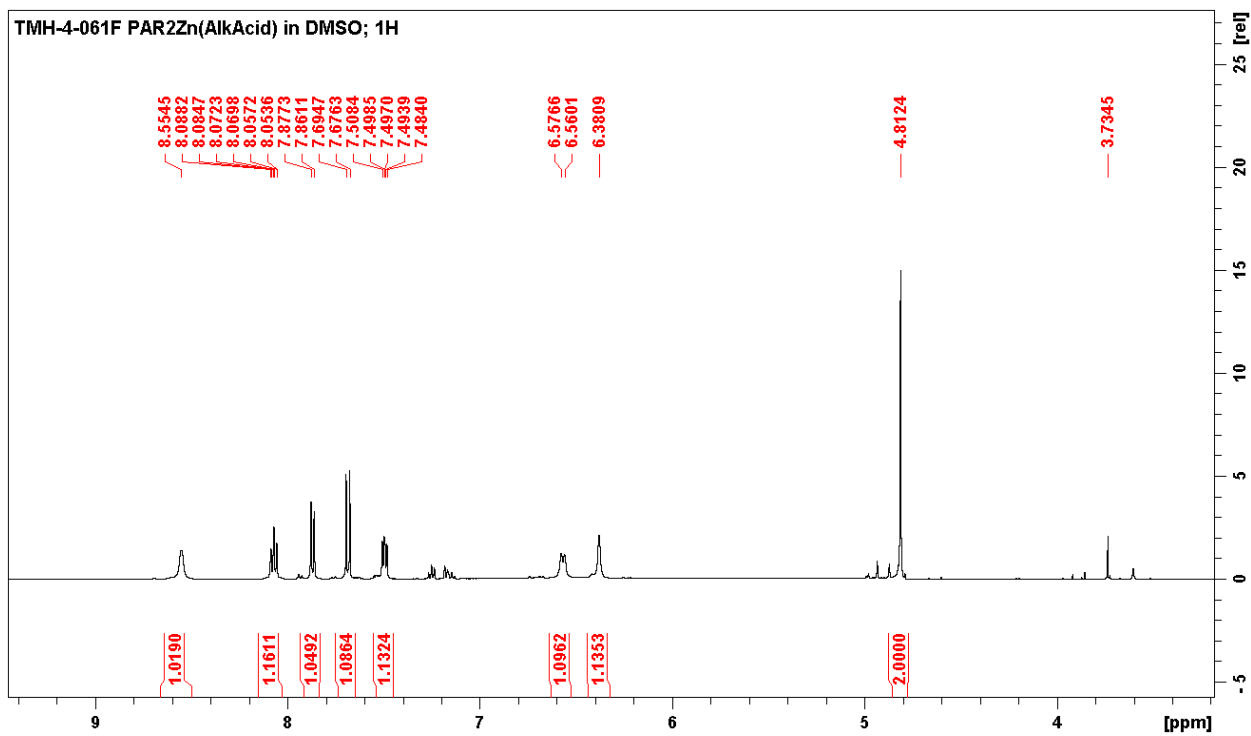
Spectrum 60. ¹H NMR - PAR₂Zn (AlkEst) **38**



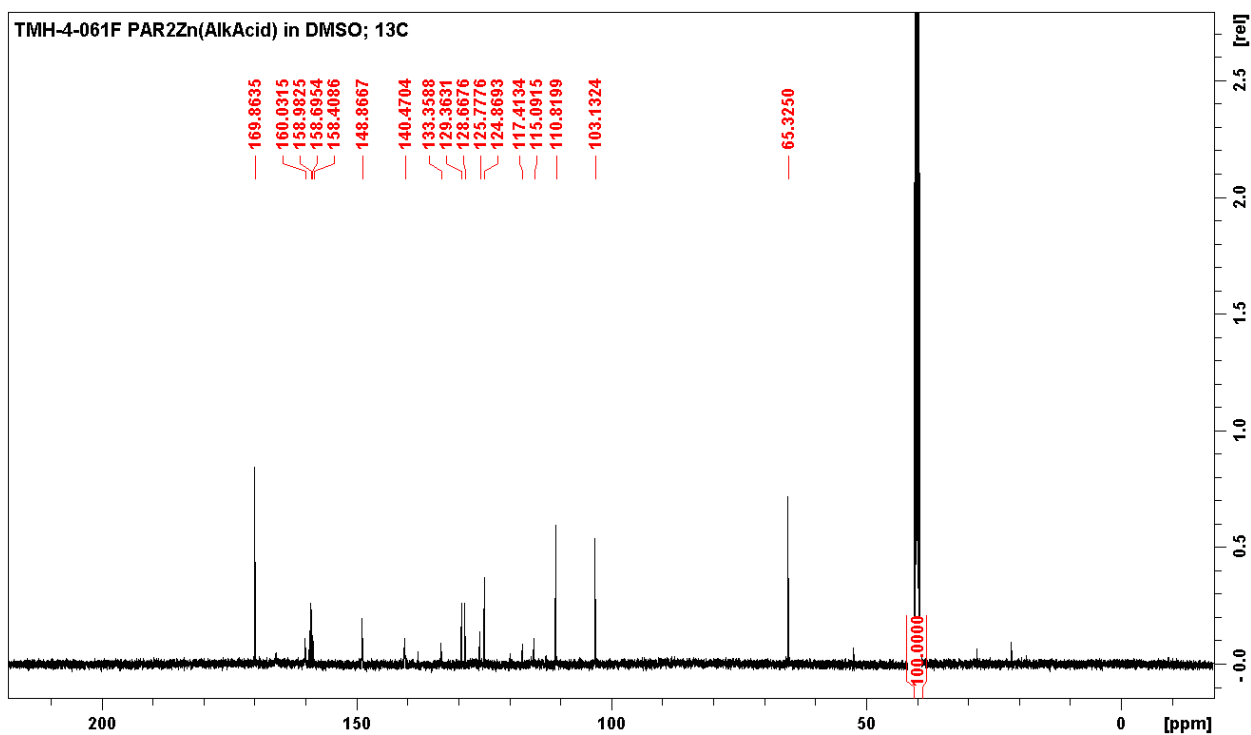
Spectrum 61. ¹³C NMR - PAR₂Zn (AlkEst) 38



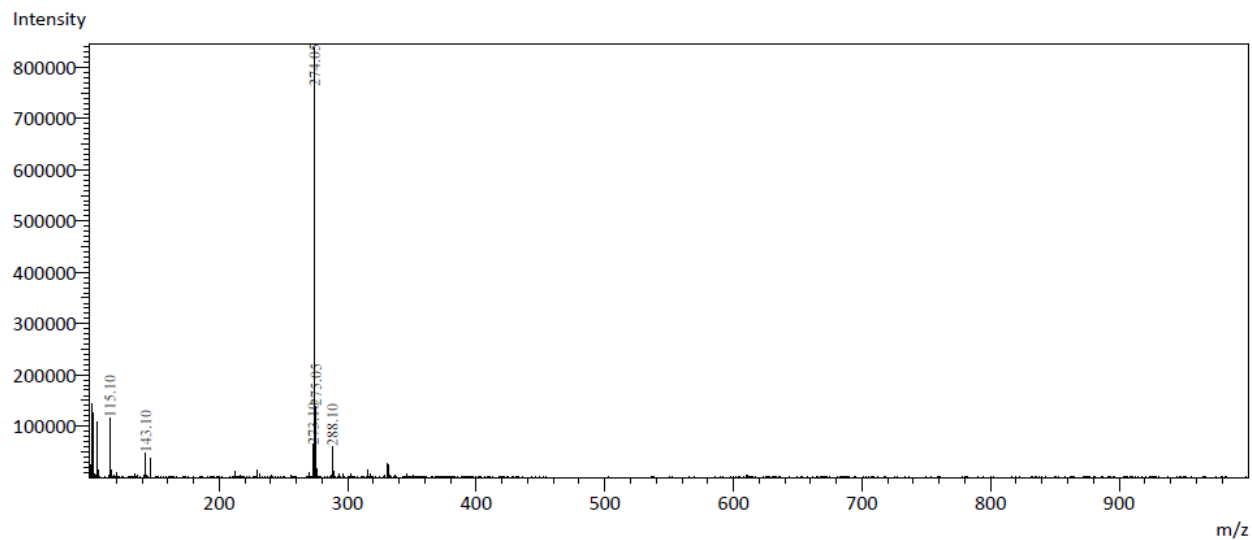
Spectrum 62. ESI-MS - PAR₂Zn (AlkEst) 38



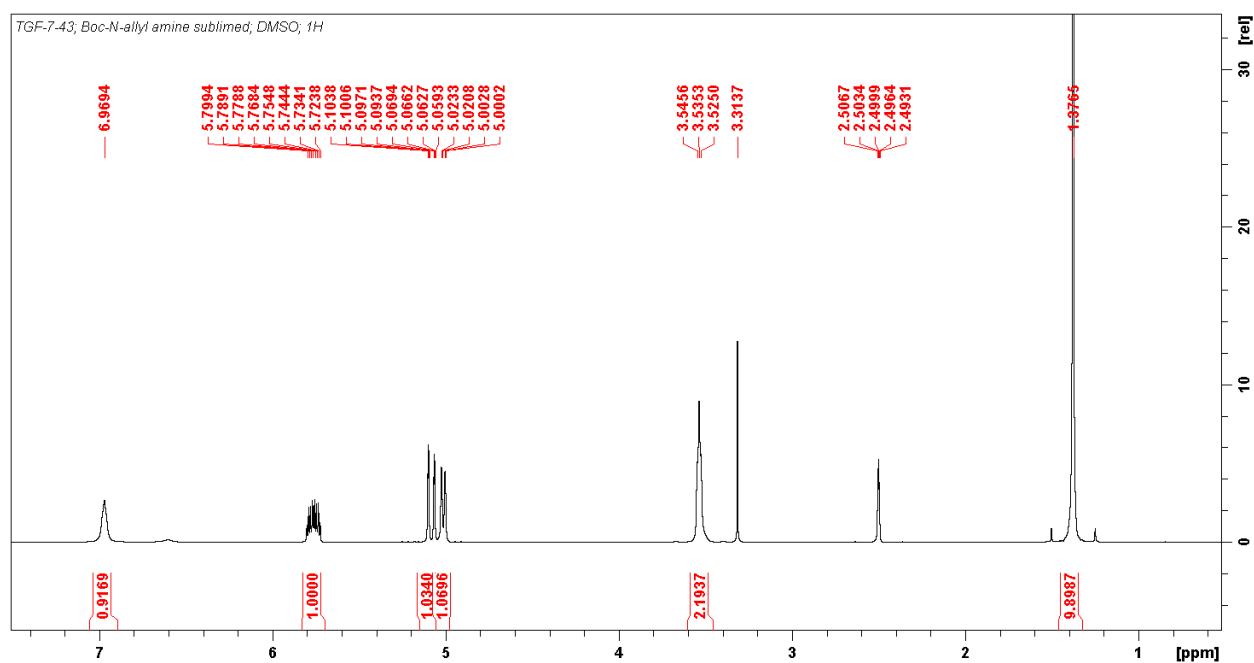
Spectrum 63. ¹H NMR - PAR₂Zn(AlkAcid) 39



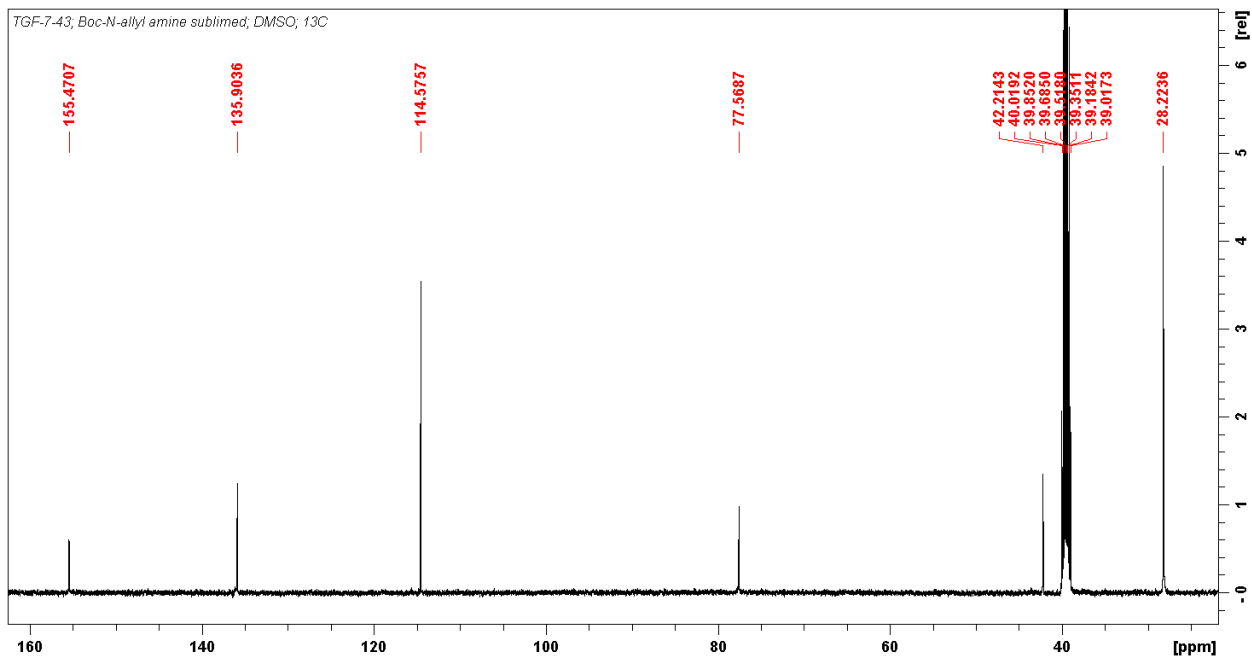
Spectrum 64. ¹³C NMR - PAR₂Zn(AlkAcid) 39



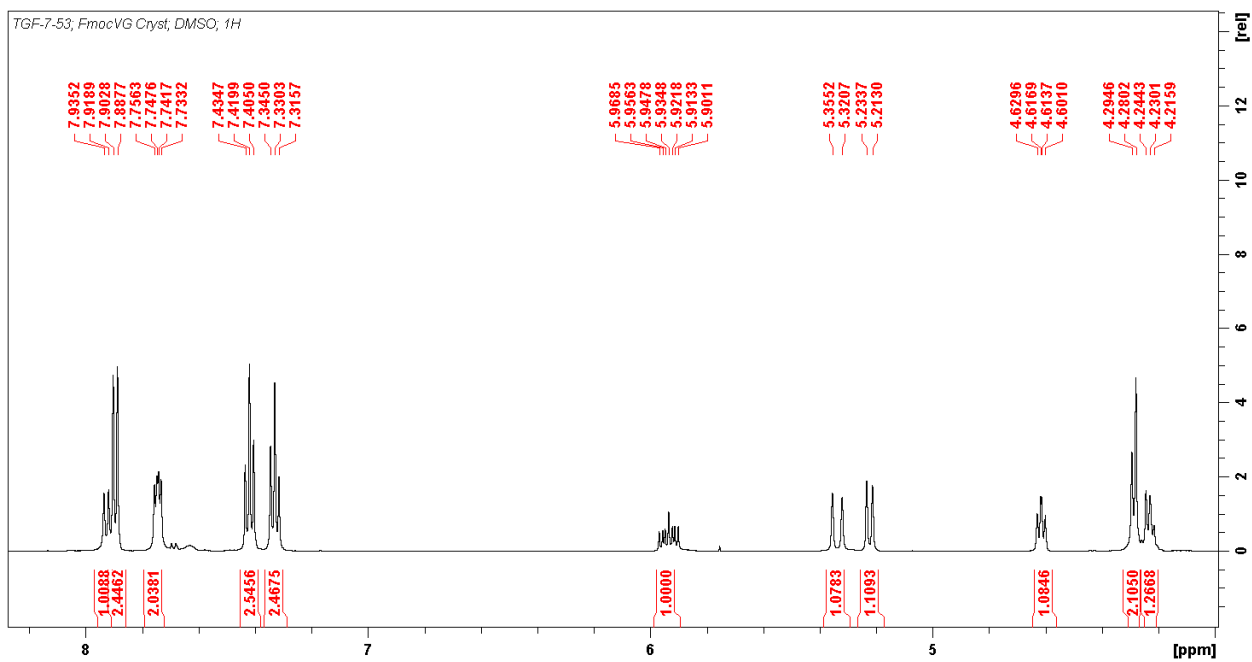
Spectrum 65. ESI-MS - PAR₂Zn (AlkEst) 38



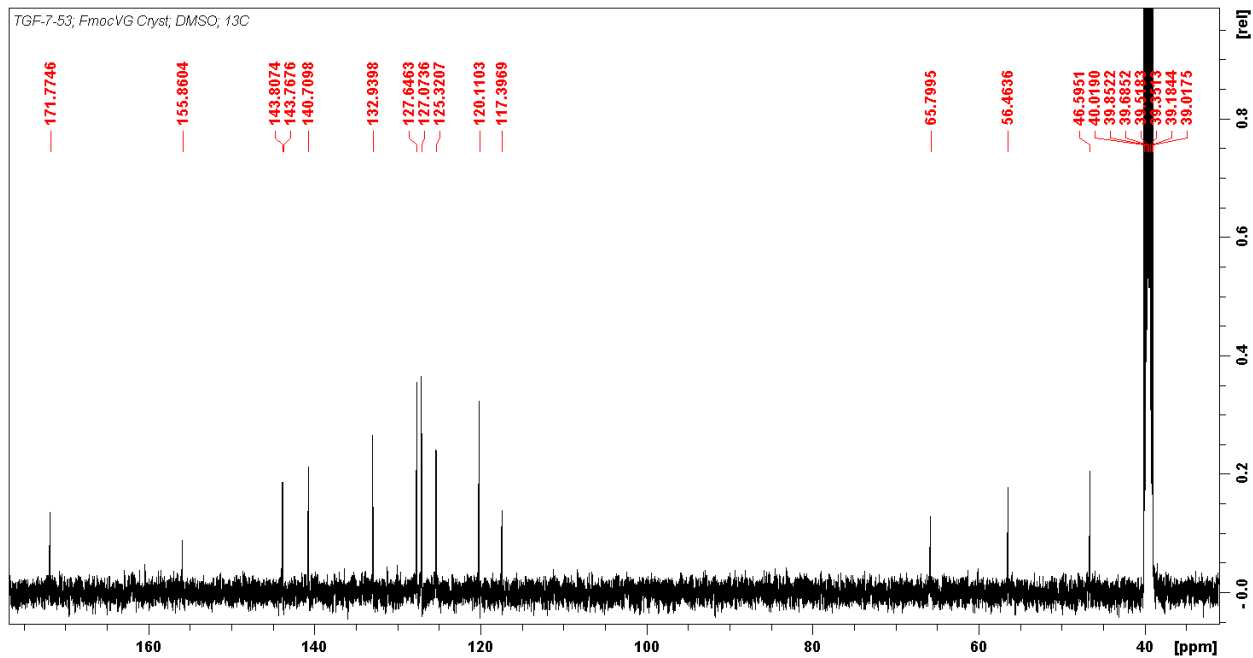
Spectrum 66. ¹H NMR - Boc-N-Allyl Amine 40



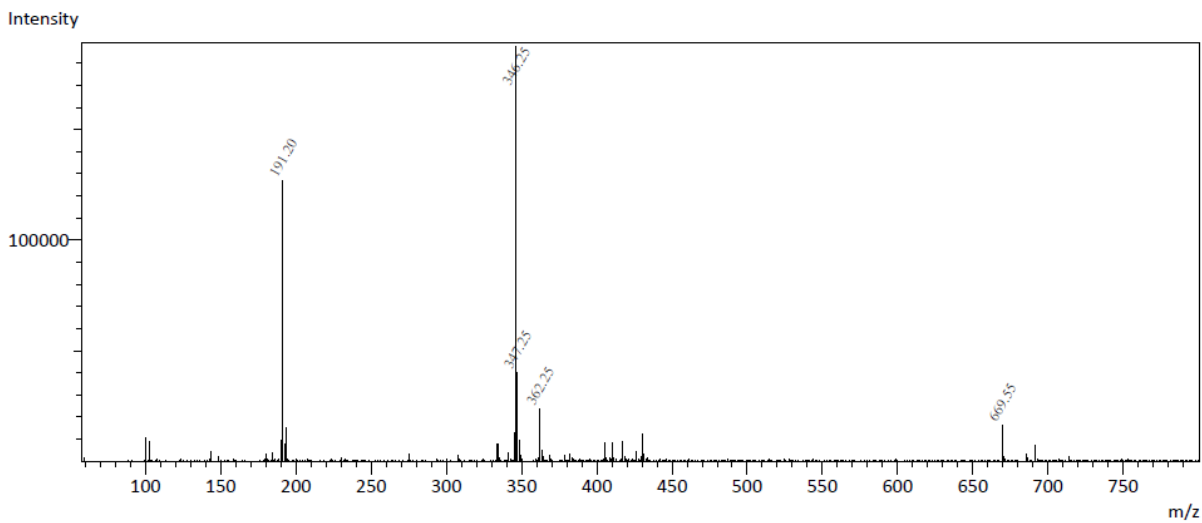
Spectrum 67. ^{13}C NMR - Boc-N-Allyl Amine 40



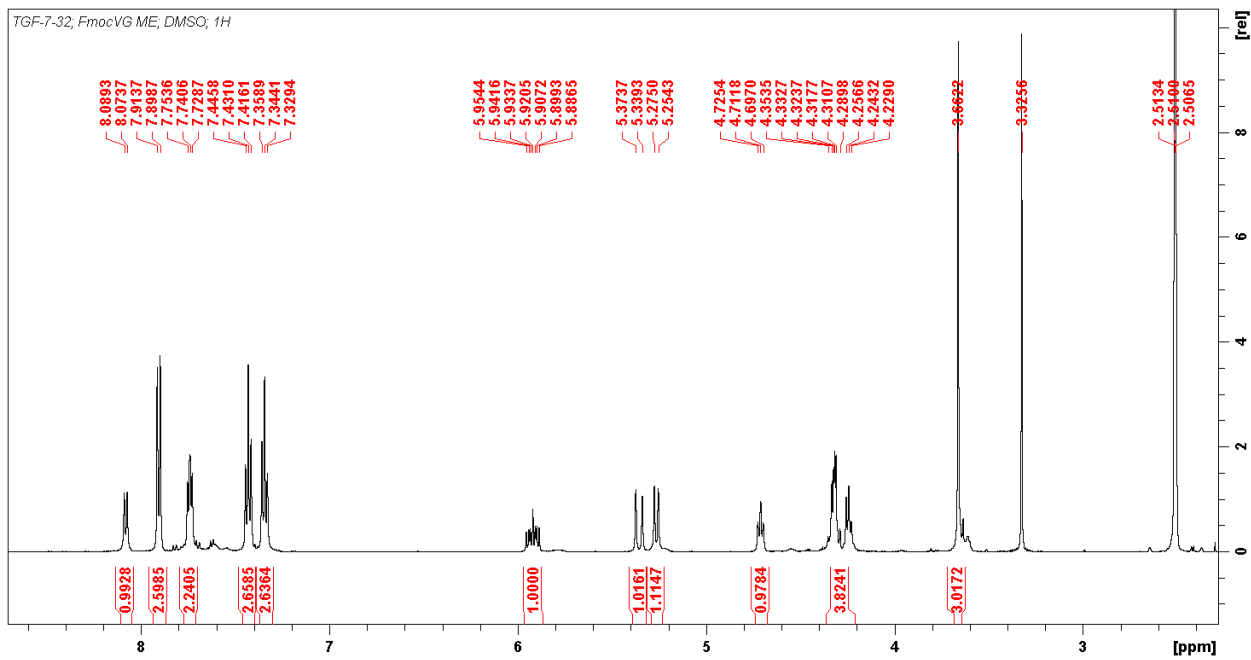
Spectrum 68. ^1H NMR - Fmoc-N-(Vinyl Glycine)-OH 41



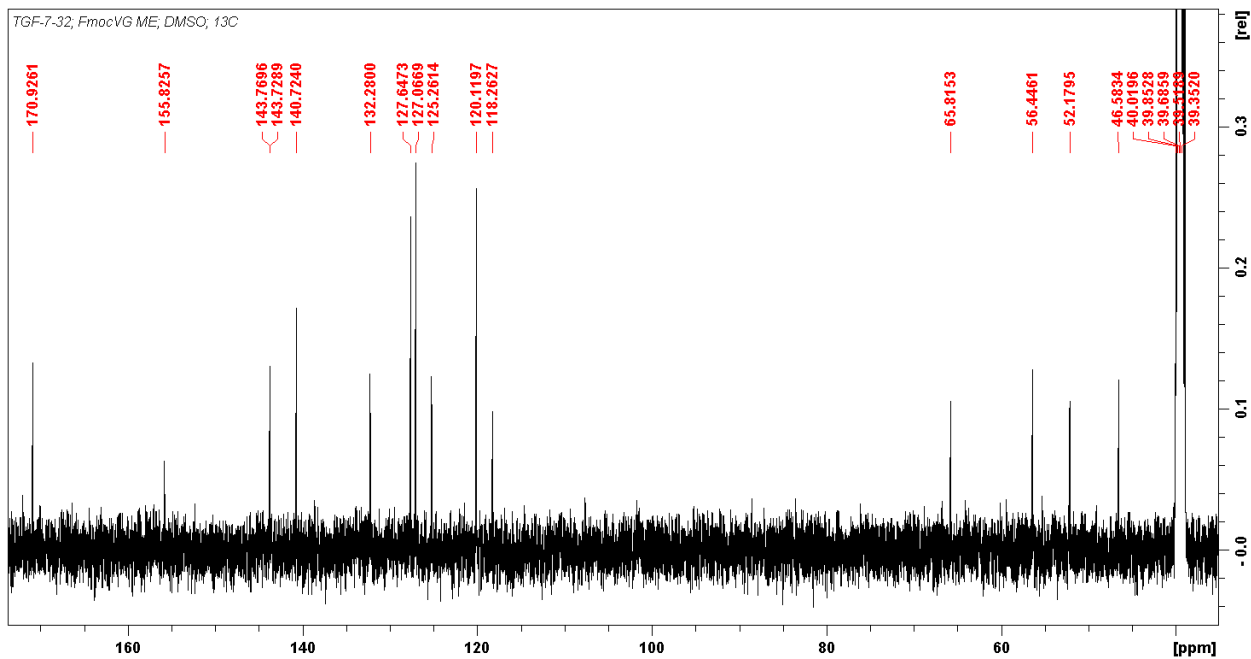
Spectrum 69. ^{13}C - NMR Fmoc-N-(Vinyl Glycine)-OH **41**



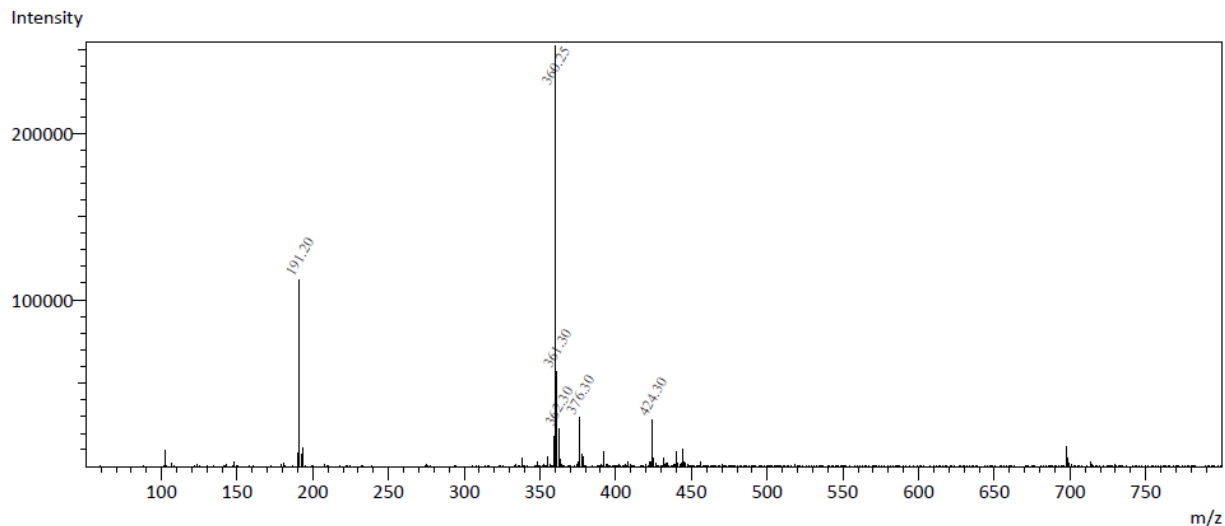
Spectrum 70. ESI-MS - Fmoc-N-(Vinyl Glycine)-OH $[M+\text{Na}]^+$ **41**



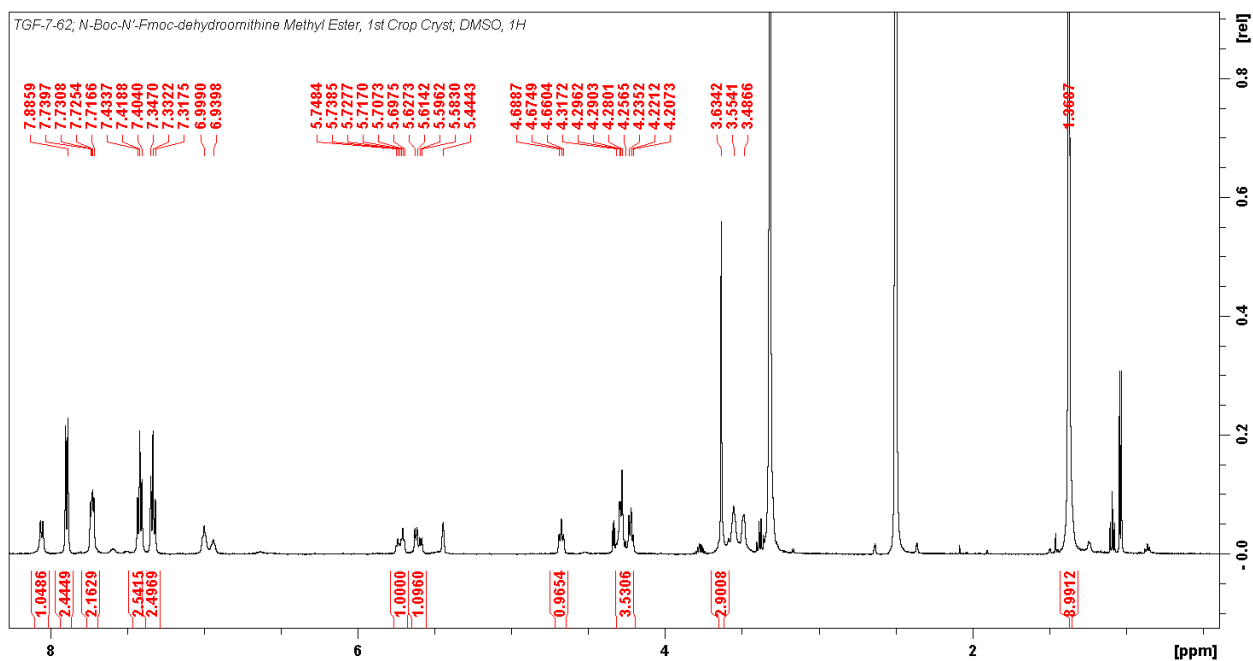
Spectrum 71 ¹H NMR - Fmoc-N-(Vinyl Glycine)-OCH₃ 42



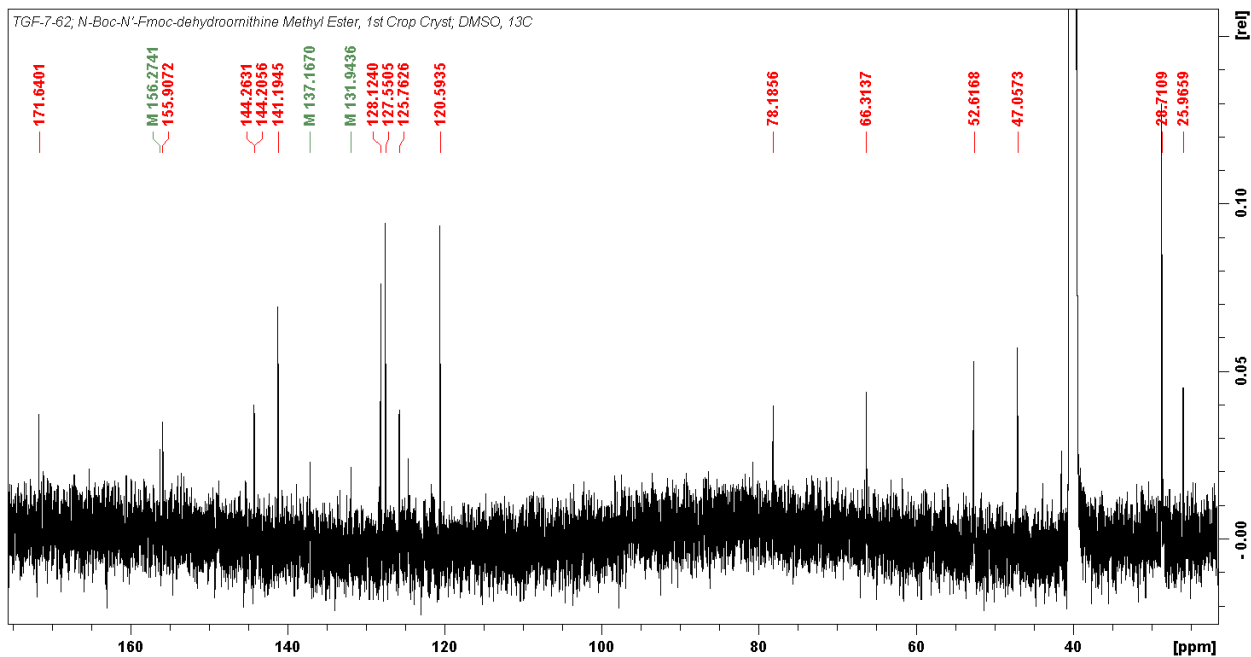
Spectrum 72. ¹³C NMR - Fmoc-N-(Vinyl Glycine)-OCH₃ 42



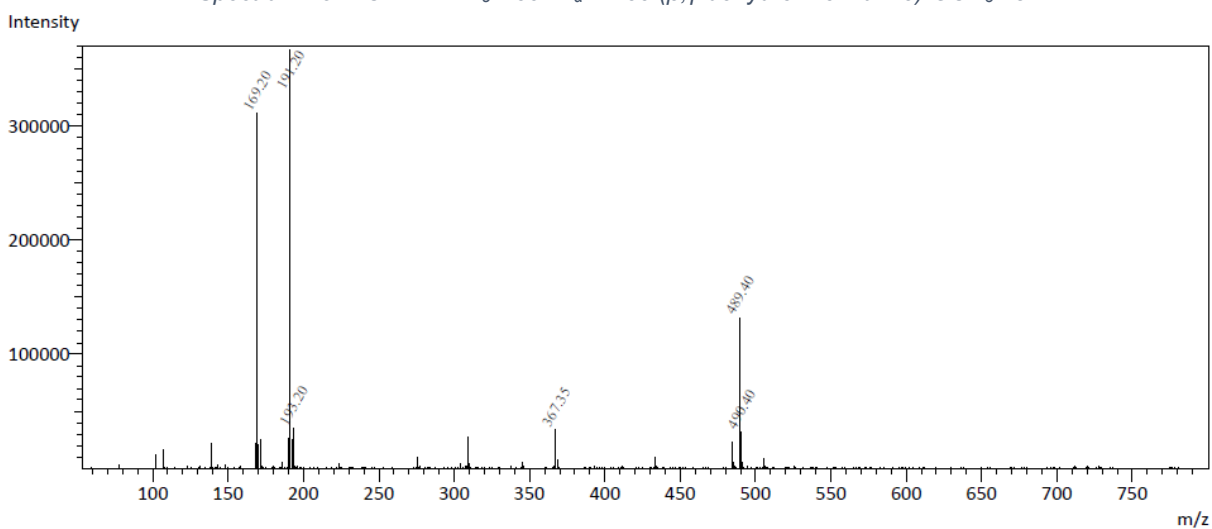
Spectrum 73. ESI-MS - Fmoc-N-(Vinyl Glycine)-OCH₃ [M+Na⁺] 42



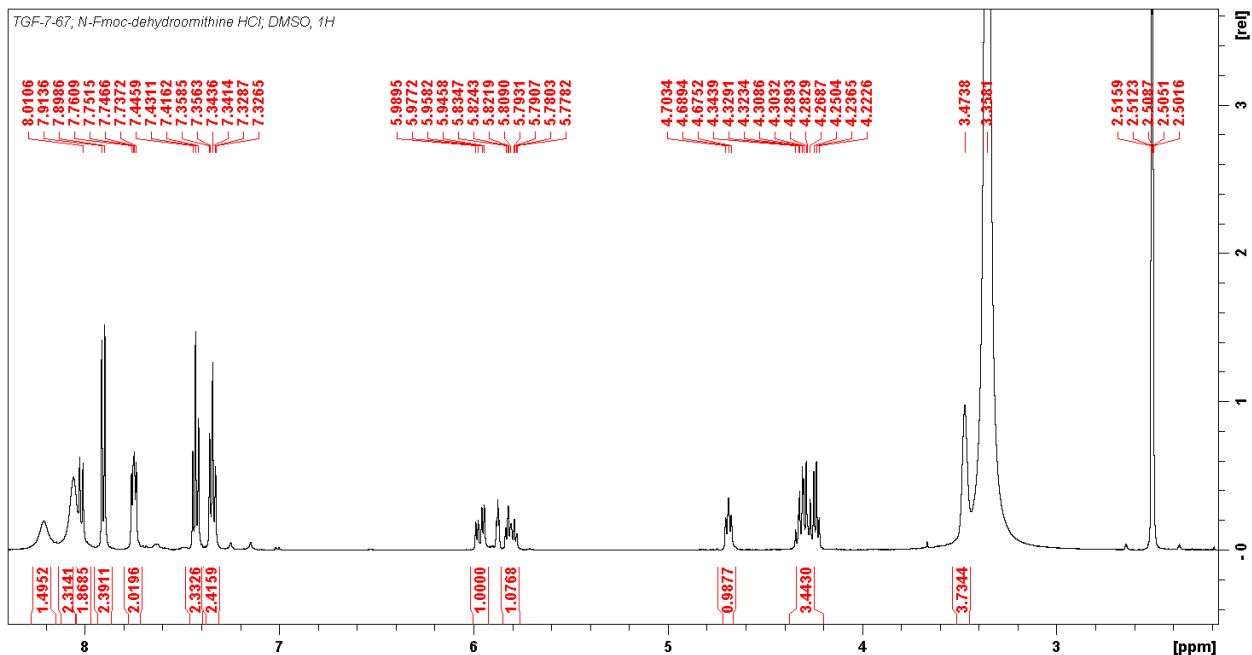
Spectrum 74. ¹H NMR - N₆-Boc--N_α-Fmoc-(β,γ-dehydro-L-ornithine)-OCH₃ 43



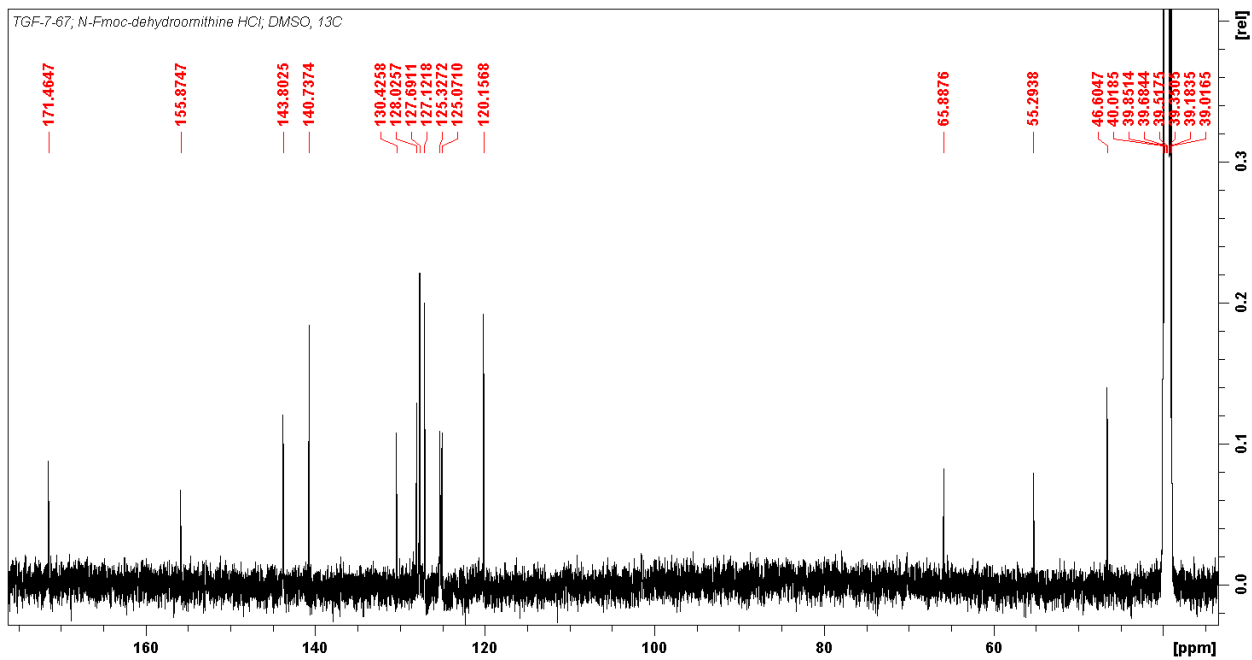
Spectrum 75. ^{13}C NMR - N_δ -Boc-- N_α -Fmoc-(β,γ -dehydro-L-ornithine)- OCH_3 **43**



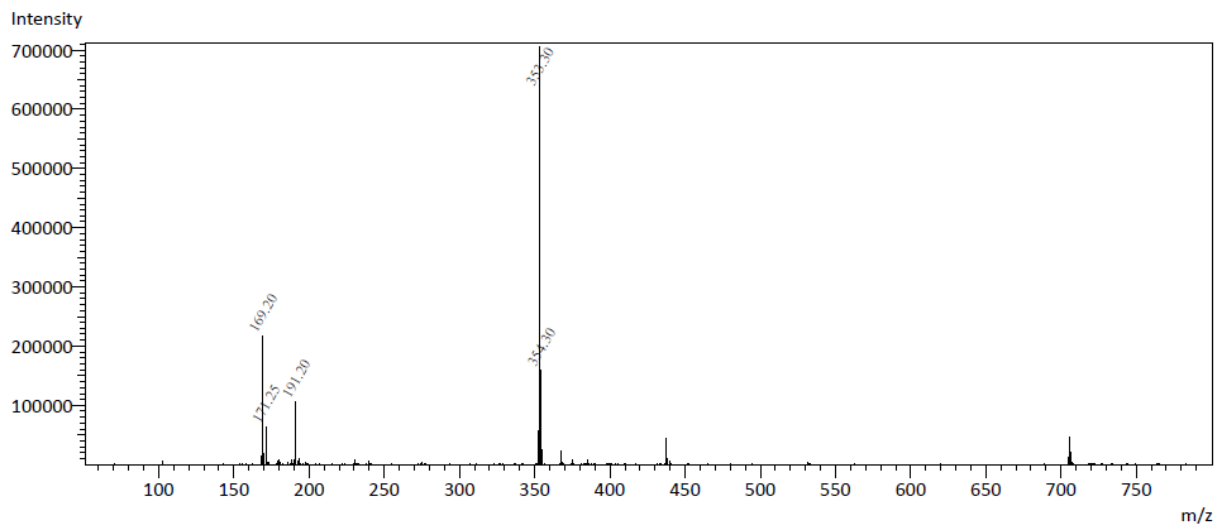
Spectrum 76. ESI-MS - N_δ -Boc-- N_α -Fmoc-(β,γ -dehydro-L-ornithine)- OCH_3 **43**



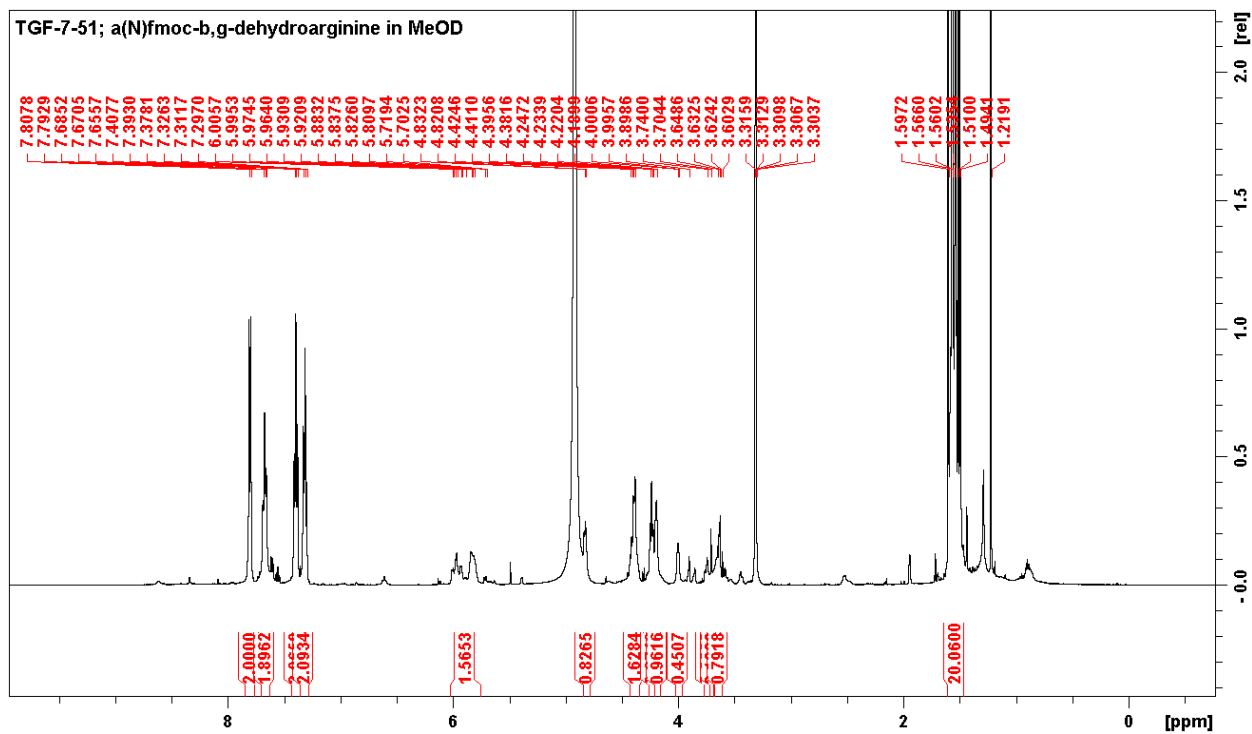
Spectrum 77. ^1H NMR - N_α -Fmoc-(β,γ -dehydro-L-ornithine)-OH HCl 44



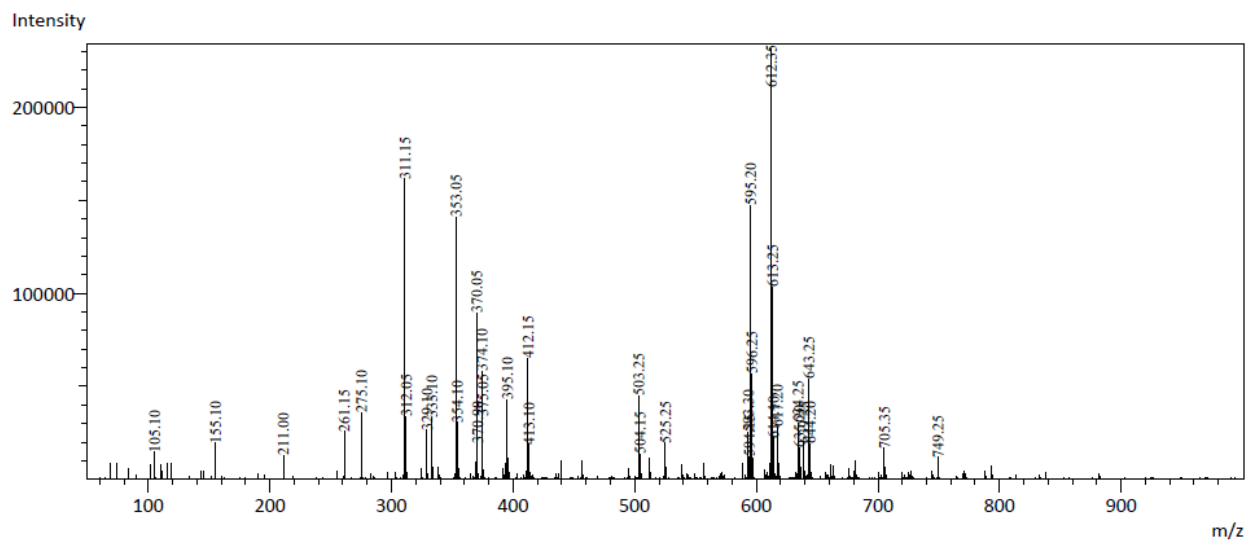
Spectrum 78. ^{13}C NMR - N_α -Fmoc-(β,γ -dehydro-L-ornithine)-OH HCl 44



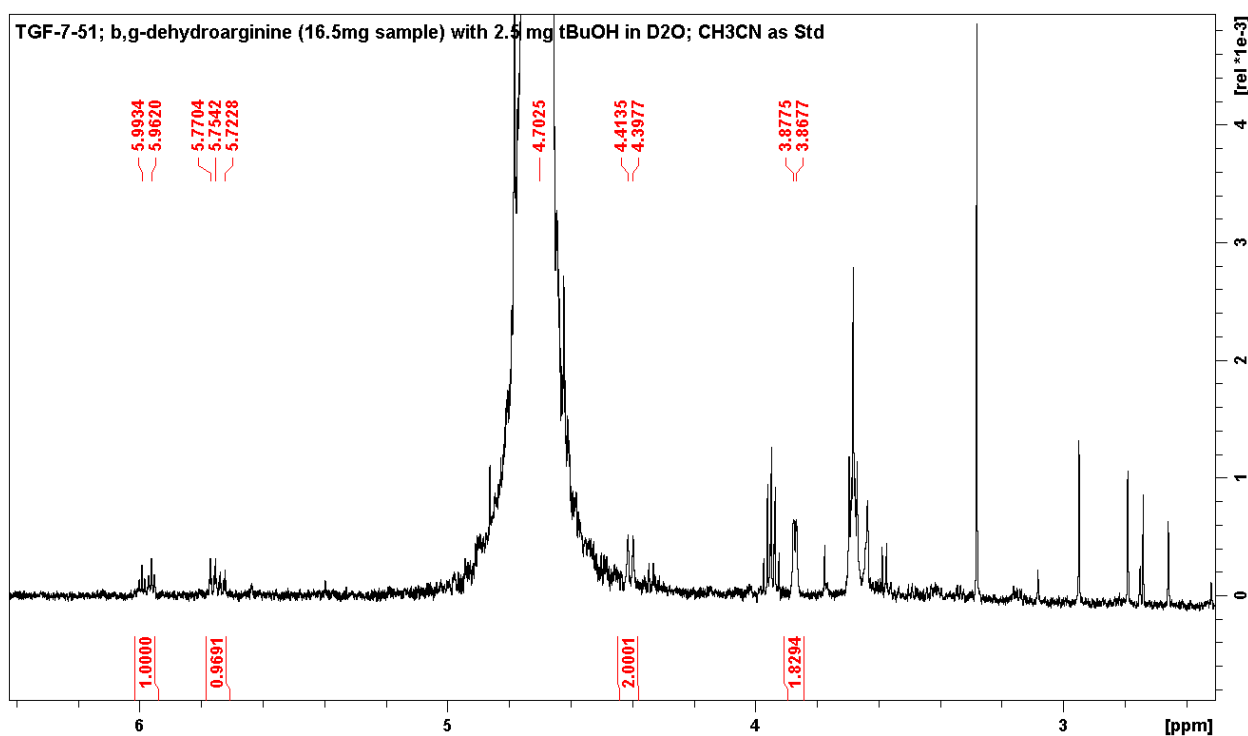
Spectrum 79. ESI-MS - *N_c*-Fmoc-(β,γ -dehydro-L-ornithine)-OH HCl 44



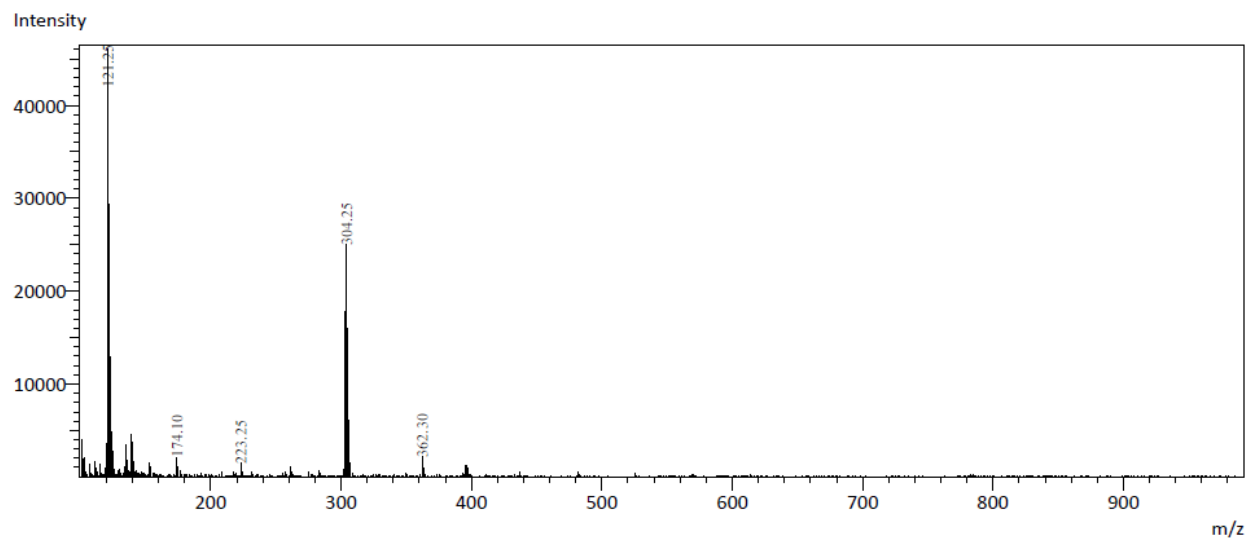
Spectrum 80. ^1H NMR - Protected β,γ -dehydro-L-arginine 45



Spectrum 81. ESI-MS - Protected β,γ -dehydro-L-arginine 45



Spectrum 82. ¹H NMR – β,γ -dehydro-L-arginine 46



Spectrum 83.ESI-MS - β,γ -dehydro-L-arginine 46

CURRICULUM VITAE

Tyler G. Fenske, Ph.D.

Education

Doctor of Philosophy in Chemistry

Conferred August 2019

University of Wisconsin - Milwaukee

Dissertation Title: "A Study in Molecular Recognition: Design, Synthesis and Binding of a Fluorescent β -Sheet Mimic & Quantitation of Metal Ions in Aqueous Solutions Through Solid Supported Semi-Selective Chemosensors"

Principal Investigator: Alan W. Schwabacher

Bachelor of Science in Chemistry

December 2013

University of Wisconsin – Milwaukee

Professional Experience

Research Scientist

September 2018 – February 2019

Aquametals LLC. – Milwaukee, Wisconsin

- Laboratory development for commercial production of azo-dyes and hydrogels.
- Transferring of technology from academic labs to an industrial environment.
- SOP documentation for laboratory operations.

Research Experience

Graduate Research Assistant

August 2014 – May 2019

Department of Chemistry and Biochemistry – University of Wisconsin – Milwaukee

- Design and synthesis of organic compounds for studies in self assembly on surfaces, antibiotics, and enzyme kinetics.
- Optimization of hydrogel polymer with covalently attached chemosensors for the detection and quantitation of metal ions.
- Analysis of organic compounds with Nuclear Magnetic Spectroscopy, Mass Spectrometry, UV/Vis Spectroscopy, IR spectroscopy and Thin Layer Chromatography.
- Collaborations with various research groups within the department and a local company for the commercialization of developed technology.

Undergraduate Research Experience

January 2013 – December 2013

Department of Chemistry and Biochemistry – University of Wisconsin – Milwaukee

- Synthesis of organic compounds towards the development of a “molecular tweezer” for studies in molecular recognition.

Teaching and Mentoring Experience

Graduate Mentor

August 2015 – May 2019

Schwabacher Research Group – University of Wisconsin Milwaukee

- Directly mentored six undergraduate researchers during my graduate student education.
- Trained students in standard organic laboratory techniques including laboratory safety, planning reactions, monitoring reaction, isolating compounds and analysis of experiments.
- Guided students through literature research and presentation of obtained results.

Teaching Assistant, Chemistry Supplemental Instruction – Organic Chemistry

Summer 2017

Department of Chemistry and Biochemistry – University of Wisconsin - Milwaukee

- Provided supplemental instruction to the Organic Chemistry lecture by leading students through various concepts and problems.
- Daily lessons prepared for students, but altered daily topics based on the students' needs and questions.

Teaching Assistant, Organic Chemistry Laboratory

Fall 2015, Spring 2016, Spring 2019

Department of Chemistry and Biochemistry – University of Wisconsin - Milwaukee

- Prepared students for experiments by preparing short pre-lab lectures.
- Led students through various organic experiments demonstrating a wide range of reaction types and analytical techniques.
- Monitored students for technical understanding of physical manipulations, chemical understanding, and safety considerations.
- Worked closely with staff to improve class protocols for better student comprehension.

Teaching Assistant, General Chemistry

Fall 2014

Department of Chemistry and Biochemistry – University of Wisconsin - Milwaukee

- Instructed students in 2 separate laboratory sections and 2 classroom discussion sections.
- Provided insight to lecture material by working with students to understand and complete challenging example problems.

Honor and Awards

1st Place Keith Hall Award for Excellence in Graduate Research

May 2018

University of Wisconsin – Milwaukee – Department of Chemistry and Biochemistry - Awards Day and Symposium

- Awarded to the best Poster Presentation amongst Graduate Students

4th Place Chemistry Alumni Award for Graduate Research

May 2016

University of Wisconsin – Milwaukee – Department of Chemistry and Biochemistry - Awards Day and Symposium

- Award to the 4th best Poster Presentation amongst Graduate Students

Publications

Biochemistry 2018. 57(23), 3252-3264

Streptomyces wadayamensis MppP is a PLP-Dependent Oxidase, Not an Oxygenase

Lanlan Han, Nemanja Vuksanovic, Sarah A. Oehm, Tyler G. Fenske, Alan W. Schwabacher, and Nicholas R. Silvaggi

Acta Crystallographica Section F 2017. 73, 672-681

Swit_4259 an acetoacetate decarboxylase-like enzyme from *Sphingomonas wittichii* RW1

L. Mydy, Z. Mashhadi, T. Knight, T. Fenske, T. Hagemann, R. Hoppe, L. Han, T. Miller, A. Schwabacher, N. Silvaggi

US Patent PCT/US2016/057182

Sensor dyes for real-time sensing of metal ions in aqueous environments

Tyler G. Fenske, Bruce Bathurst, Alan Schwabacher, Peter Geissinger, Trevor Hagemann, Sarah Oehm, Paul Henning

Manuscript in Progress

Hydrogel polymers with covalently attached chemosensors for the detection of zinc in aqueous solutions.

Tyler G. Fenske, Sarah A. Oehm, Trevor Hagemann, Alan W. Schwabacher

Manuscript in Progress

Synthesis, design and binding of a fluorescent β -Sheet mimic.

Tyler G. Fenske, Alex Vincent, Alan W. Schwabacher

University Services

Graduate Student Council Member

August 2015 – July 2016

University of Wisconsin – Milwaukee – Department of Chemistry and Biochemistry

- Relayed concerns from fellow students to faculty and administrators.
- Participated in the welcoming of new graduate students by providing advice for their success.
- Planned and organized the annual department symposium and other events for the benefit of fellow graduate students.

Technical Skills (Non-Chemistry)

- Various proficiencies in computer skills applicable to data organization and work-load optimization.
- General mechanical and handy-man knowledge. Proficient and fixing and troubleshooting simple problems with pumps, motors, instruments, etc.